



HAL
open science

Modelling and simulation of acoustic-thermomechanical coupling of complex fluids

Louis Bouthier

► **To cite this version:**

Louis Bouthier. Modelling and simulation of acoustic-thermomechanical coupling of complex fluids. Mathematical Physics [math-ph]. Université Paris sciences et lettres, 2023. English. NNT : 2023UPSLM057 . tel-04547051

HAL Id: tel-04547051

<https://pastel.hal.science/tel-04547051>

Submitted on 15 Apr 2024

HAL is a multi-disciplinary open access archive for the deposit and dissemination of scientific research documents, whether they are published or not. The documents may come from teaching and research institutions in France or abroad, or from public or private research centers.

L'archive ouverte pluridisciplinaire **HAL**, est destinée au dépôt et à la diffusion de documents scientifiques de niveau recherche, publiés ou non, émanant des établissements d'enseignement et de recherche français ou étrangers, des laboratoires publics ou privés.



THÈSE DE DOCTORAT
DE L'UNIVERSITÉ PSL

Préparée à Mines Paris PSL

**Modelling and simulation of acoustic-thermomechanical
coupling of complex fluids**

Modélisation et simulation du couplage thermo-acoustique dans les fluides complexes

Soutenue par

Louis-Vincent Bouthier

Le Vendredi 1^{er} Décembre 2023

École doctorale n°364

**Sciences Fondamentales
et Appliquées**

Spécialité

**Mathématiques
numériques, Calcul
intensif et Données**

Composition du jury :

Michel CLOITRE École Supérieure de Physique et de Chimie Industrielles de la ville de Paris	<i>Président du jury</i>
Alessio ZACCONE Université de Milan	<i>Rapporteur</i>
Xavier CHATEAU Ecole des Ponts	<i>Rapporteur</i>
Romain CASTELLANI Mines Paris	<i>Examineur</i>
Sébastien MANNEVILLE Ecole Normale Supérieure de Lyon	<i>Examineur</i>
Arnaud POULESQUEN Commissariat à l'Énergie Atomique et aux énergies alternatives	<i>Examineur</i>
Elie HACHEM Mines Paris	<i>Directeur de thèse</i>
Rudy VALETTE Mines Paris	<i>Directeur de thèse</i>

Acknowledgements

I am deeply thankful to Elie Hachem, the seed of the whole project and the first leader of it. I cannot describe exhaustively how rich our relationship is from our first coffee at the cafeteria in Paris to this PhD defense. He has been a trustworthy, supportive, kind and welcoming advisor. While his responsibilities have never stopped to grow over the years, he has succeeded to stay humble and open to the others. For that experience and future adventures, I am warmly grateful.

I would like to show great gratitude towards Rudy Valette, who has been a great complementary advisor. With his meticulous mind, his profound kindness and his daily joy, I have learnt many things about becoming a scientific researcher. I remember our times blackening a white board to understand all the intricate relationships in these complex media.

I am additionally indebted towards Romain Castellani. Coming from different backgrounds, we have progressed to discuss between each other on complex problems needing this broader perspectives. I am happy to have shared the tutoring experience with him about a specific experimental protocol and generally all the discussions while thinking and writing our mutual work.

My appreciation goes also to Sébastien Manneville who has brought his deep knowledge about this field. I remember the couple of days discussing in September 2021 and September 2022 about the progression of the overall work. I was happy to write together an article trying to assess the different difficulties underlying.

I must also show courtesy to Arnaud Poulesquen. Thank him for having hosted me for a couple of months in Marcoule. I was glad to see the actual background of our PhDs with Sébastien Castel. I have liked our discussions about models where I tried my best to explain big mathematical formulation in words and hands.

My obligation needs to go then to Thomas Gibaud with whom we tried to build an experimentalist-theoretician relationship. From our first meeting, we have tried to torture the carbon black particles and bring most of the darkest secret to light. I am happy to have met him and produce so much together.

My acknowledgements must continue with Marion Isambert and Rémy Martinez. They showed great conviction and meticulous devotion to the complex topic they were working on. It was a wonderful opportunity for me to explain what I was doing at the time both to progress in the overall problem and to transmit to them some elements about scientific research. I hope they

bring with them afterwards some valuable skills for their future.

My gratitude will go now to Julien Bauland. We shared some interesting discussions about relating his experiments to models. Thank him for his astonishing work done during a short period to make our collaboration happen.

I thank Emanuela Del Gado for having hosted me in her lab for six months, allowed me to teach and shared her knowledge about molecular dynamics.

I acknowledge Sébastien Castel who works on the same problem as me but on the experimental side. I am warmly grateful for having helped discover the actual materials I was dealing with from a modelling perspective.

I want to thank the 2022 promotion of Corps des Mines. We shared so many experiences together during our training. We have tried to cultivate our relationships to create the community needed to expect the most satisfying career for everyone.

I am additionally indebted towards my family who raised me and continues to make me progress in life and overcome all the difficulties I have faced and will face in my future life.

I want also to show my obligation to my closest friends. I have spent so many good times with you and wish all the best for them in their future to share again the best moments we can have.

Finally, last but not least, I show my profound gratitude and love to my wife, Léa Fontaine-Bouthier. She has motivated, supported, helped and made me grow during our years together and will continue with certainty. She is the unbreakable pillar in my life with whom I will spend the rest of my life.

Miscellanea

General context

This PhD was carried out in parallel of the *Corps des Mines* curriculum starting from september 2020. This curriculum aims to train future administrator of the French public administration in institution like Nuclear Safety Authorities (*ASN*) or Regional Directorates for the Environment, Planning and Housing (*DREAL*) or Regional Directorates for the Economy, Employment, Labor and Solidarity (*DREETS*) or other economic institutions. It is composed of three years of training where the first year is splitted between two months of scientific courses and general courses (law, accounting, ...) and ten months of mission in a company in France. Personally, I worked for *TotalEnergies* as a strategy prospector for the offshore wind team on a ten years horizon. Then, the second year is splitted again between one month of courses, similar to the first year, and eleven months of mission in a company or an institution abroad outside Europe. In my case, as prepared in agreement with the PhD supervision and the *Corps des Mines* supervision, I stayed as a visiting reasearcher for six months in Georgetown University to work on molecular dynamics of gels. Then, to complete the mission period, I worked four months at *CEA Marcoule* on the topic of the sludge rheology. Finally, the last year is dedicated to courses for business and public administration during eight months approximately.

Most of this manuscript is a compilation of papers published or prepared for publications. Hence, some transitions or details will be added with colored background to create an overall story context but the readers will recognise without any difficulty texts which are available online.

In an objective of concision, there will not be an extensive introduction to physical and mechanical concepts in this manuscript. In order to have a reasonable basis to tackle the content of this PhD, I would recommend any reader to understand properly elements of solid mechanics, fluid mechanics, statistical physics, acoustics, and a bit of applied mathematics. For each field, I recommend to read [Landau, 1959; Landau, 1987; Pierce, 2019; Allen, 2017; Bird, 2002].

Personal conclusion

This PhD has been a great experience on many aspects. First of all, I did not intend to do a PhD at first. This

PhD experience is then issued from a set of circumstances which has allowed several people to meet and work together. Starting from the training director of *Corps des Mines*, I met first my PhD advisor who introduced me to the whole team I interacted with during my research. Actually, I think this is how most of professional projects and even careers can be considered: the crossing point of people's paths is the ignition point of potential outcomes. It is afterwards the role of everyone to catch these opportunities and breed them according to everyone's will. Consequently, I am profoundly grateful to all the people I have interacted with who have built this project and have cooperated dynamically. This once a life chance has been a great opportunity for me and I would try to take all the relevant feedbacks to improve myself in my future professional career.

Résumé & Abstract

Résumé

Les suspensions colloïdales, le couplage entre l'environnement, la structure microscopique et la rhéologie sont étudiées dans ce manuscrit. Ce travail utilisera majoritairement un point de vue théorique mais fera intervenir aussi des approches expérimentales et numériques. Caractérisées par des agrégats de particules formés grâce à un potentiel d'interaction attractif, ces suspensions peuvent être soumises à une sollicitation externe sous forme d'ultrasons, de cisaillement ou tout autre forme mécanique. Les agrégats répondent à cette sollicitation en adaptant leur microstructure, notamment en taille.

Par ailleurs, cette même microstructure est la brique élémentaire transmettant les efforts de part et d'autre d'un gel colloïdal, ce qui peut se traduire par des lois d'échelles entre la microstructure et la rhéologie macroscopique.

Par conséquent, on observe un couplage fort entre l'échelle macroscopique, composée de l'environnement extérieur et la réponse rhéologique, et l'échelle microscopique, avec la structure microscopique s'adaptant et influençant l'échelle précédente. C'est ainsi qu'il est possible de construire un outil d'application industriel incorporant cette description physique afin de prédire les effets d'une sollicitation externe sur un matériau la vérifiant.

Abstract

Colloidal suspensions, the coupling between environment, microscopic structure and rheology are studied in this manuscript. This work will mainly use a theoretical point of view but will also involve experimental and numerical approaches. Characterized by aggregates of particles formed thanks to an attractive interaction potential, these suspensions can be subjected to an external solicitation in the form of ultrasound, shear or any other mechanical form. The aggregates respond to this solicitation by adapting their microstructure, especially in size.

Moreover, this same microstructure is the elementary brick transmitting the efforts on both sides of a colloidal gel, which can be recovered by laws of scale between the microstructure and the macroscopic rheology.

Therefore, we observe a strong coupling between the macroscopic scale, composed of the external environment and the rheological response, and the microscopic scale, with the microscopic structure adapting and influencing the previous scale. It is thus possible to build an industrial application tool incorporating this physical description in order to predict the effects of an external stress on a material verifying it.

Mots clés : Suspension colloïdale, Rhéologie, Aggrégats fractales

Keywords : Colloidal suspension, Rheology, Fractal clusters

Notations

α	Exponent of transition between the strong-link and the weak-link regime	λ	Thermal conductivity or first Lamé coefficient
Ad	Adhesion number	$\mathbf{L} = \nabla \mathbf{u}$	Velocity gradient
a	Particle size	L	Macroscopic system size
$\beta = 1/k_B T$		ℓ	Cluster size
Bm	Bingham number	μ	Second Lamé coefficient
c_p	Heat capacity per unit mass	Mn	Mason number
δ	Distance of interaction between particles	ν	Kinematic viscosity
D, \mathfrak{D}	Fractal dimension	\mathbf{N}	Nominal stress tensor
De	Deborah number	n	Power index of strain rate
d, \mathfrak{d}	Chemical dimension or dimension of the elastic back-bone	n_k	Number of cluster with k particles inside
dim	Dimension of the Euclidean space	Ω	System considered, subset of \mathbb{R}^3
$\frac{d^\alpha}{dt^\alpha}$	Fractional derivative with $\alpha \in [0, 1]$	ω	Pulsation
$\frac{d}{dt}$	Material derivative	ψ	Stream function
$\boldsymbol{\varepsilon}$	Linear strain tensor	\mathbf{P}	First Piola-Kirchhoff stress tensor
$\dot{\boldsymbol{\varepsilon}}$	Strain rate tensor	Pe	Peclet number
ϵ	Exponent of transition between stretching and bending	p	Thermodynamic pressure
E	Elastic/Young modulus	q	Wave vector number
\mathcal{E}	Energy functional in the aggregation-disaggregation processes	\mathbf{q}	Heat flux vector
\mathbf{e}	Green-Lagrange strain tensor	ρ	Density
e	Internal energy per unit mass	\mathbf{R}	Rotation tensor in the polar decomposition of the deformation gradient
erf	Error function	Re	Reynolds number
ϕ	Volume fraction	r	Distance from the origin
\mathbf{F}	Deformation gradient	r_0	Particle size
F	Fragmentation kernel or point force	$\boldsymbol{\sigma}$	Cauchy Stress tensor
\mathcal{F}	Fourier transform	σ_y	Yield stress
f	Probability density function with different types of variables	\mathbf{S}	Second Piola-Kirchhoff stress tensor
Γ	Gamma function	s	Entropy per unit mass
γ	1D Shear strain	Θ	Heaviside function
γ_{NL}	Limit of linearity strain	τ	Time constant
γ_y	Yield strain	θ	Polar angle
$\dot{\gamma}$	1D Shear strain rate	T	Temperature
G^*, G', G''	Complex, Storage and Loss moduli respectively	Ta	Taylor number
η	Dynamic viscosity	t	Time
\mathbf{I}	Identity tensor	$\boldsymbol{\nu}$	Vorticity vector
I	Scattering intensity	U	Depth of the interparticle potential
$J = \det(\mathbf{F})$	Local volume variation of the transformation	\mathbf{U}	Right stretch tensor
J^*, J', J''	Complex, storage and loss compliances respectively	\mathbf{u}	Velocity or displacement
κ	Bulk or volume viscosity	Wi	Weissenberg number
K	Aggregation kernel	Ξ	Grand canonical partition function
k	Number of particles in a cluster or wave number	ξ	Cluster size
k_B	Boltzmann constant	\mathbf{x}	Space variable
		\cdot^T	Transpose of a tensor/matrix
		\propto	Proportional to
		\approx	Approximately equals to
		\sim	Equivalent to, in a certain limit
		$:$	Double contracted tensor product
		\otimes	Tensor product
		\times	Vector product
		tr	Trace of a tensor
		$\text{\textcircled{a}}$	Text originally written for the manuscript

Contents

Acknowledgements	i
Miscellanea	iii
Résumé & Abstract	v
Notations	vii
Table of Contents	viii
1 General introduction	1
1.1 Context	1
1.2 State of the art [Bouthier,]	4
1.3 Problematic	27
1.4 Contents	27
2 From the macroenvironment to the microscopic structure	29
2.1 Introduction	30
2.2 Aggregation-disaggregation phenomena [Bouthier, 2023a]	30
2.3 Interpenetration of clusters of carbon-black particles [Dagès, 2022]	41
2.4 Conclusion	48
3 From the microscopic structure to the rheology	49
3.1 Introduction	50
3.2 Interpenetration of clusters [Dagès, 2022]	50
3.3 Multiple fractal [Bouthier, 2022]	53
3.4 The clusters of clusters <i>vs</i> the interpenetrating clusters approach [Bouthier, 2023b]	58
3.5 Conclusion	69
4 Application of ultrasound on materials	71
4.1 Introduction	71
4.2 Analytical description	71
4.3 Numerical case	73
4.4 Describing the phenomenology on radioactive sludges	75
4.5 Conclusion	76
5 General conclusion and perspectives	77
5.1 Conclusion of the study	77
5.2 Perspectives	78
Appendices	80
A Interpenetration of clusters for chapter 2 and according to [Dagès, 2022]	83

A.1	Carbon black particles	83
A.2	Flow properties of Carbon black gels	84
A.3	Evolution of the viscoelastic moduli during rest	84
A.4	$\tan(\delta)$ representation of the viscoelastic spectrum	85
A.5	Model for the normalized viscoelastic spectrum of carbon black gels	85
A.6	Influence of the concentration c_w	86
A.7	Analysis of the rheo-SAXS data	87
B	Other tools to develop and perspectives for future work	89
B.1	Extension of Sequence of Physical Processes relating the second Piola-Kirchhoff stress tensor to the Green-Lagrange strain tensor	89
B.2	Multi-phase problem : Level-Set methods	95
B.3	Use of the canonical framework for the aggregation-disaggregation formulation	97
C	Testing latest artificial intelligence tools	101
C.1	Introduction	101
C.2	Questions about chapter 1	101
C.3	Questions about chapter 2	105
C.4	Questions about chapter 3	107
C.5	Conclusion	110
	List of Figures	111
	List of Tables	117
	Publications list	119
	Bibliography	121

Chapter 1

General introduction

Objectives

This PhD work is focused on issues related to the nuclear industry ; in this chapter, a brief overview of the industry is given and the definition of the problems to solve is proposed : to work on the flow of radioactive sludges and the methods to implement processes like geological storage.

Objectifs

Ce travail de doctorat porte sur des questions liées à l'industrie nucléaire ; dans ce chapitre, un bref aperçu de l'industrie est donné et la définition des problèmes à résoudre est proposée : travailler sur le flux des boues radioactives et les méthodes pour mettre en œuvre des processus tels que le stockage géologique.

Contents

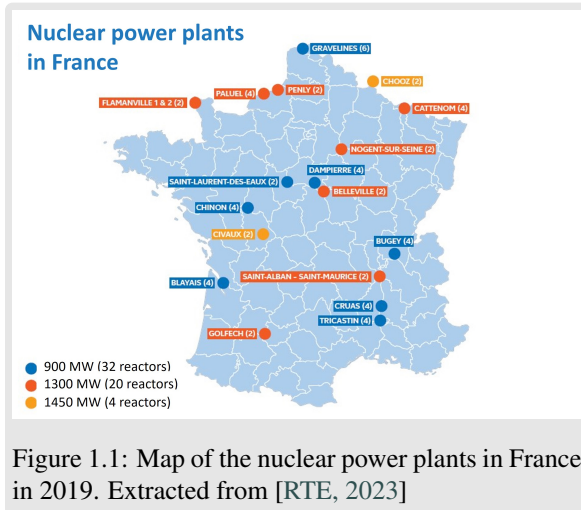
1.1	Context	1
1.2	State of the art [Bouthier,]	4
1.2.1	Abstract of the section	4
1.2.2	Content of the section	4
1.2.3	Generalities about rheological model	4
1.2.4	How clusters influence the rheology	11
1.2.5	How the clusters are influenced externally	20
1.2.6	About dimensionality	24
1.2.7	Open remaining questions	26
1.3	Problematic	27
1.4	Contents	27

Due to the subsequent amount of content coming directly from already published or work in progress papers, each part of the text originally created for this manuscript solely will be colored as in this paragraph. Hence, the reader will be aware of what is coming only from the manuscript and what is already found in the published papers in the context of this PhD.

1.1 Context

France produced, in 2022, 62.7% of its electricity through nuclear power plants[RTE, 2023]. They cover a large part of the country: their distribution is displayed on [figure 1.1](#). Nuclear energy has several advantages like the amount of energy produced per unit mass of fuel, the low carbon footprint compared to fossil fuels and the industrial environment created by such technology. There are also some drawbacks or point of attention like the safety and the security of the installations, the dependance on certain producers of uranium and the waste management.

Precisely, the processing of radioactive waste is an important part of the whole nuclear cycle to ensure safety, efficiency and clean energy production. In France, radioactive waste are treated in factory in La Hague or in *CEA Marcoule*. [Figure 1.2](#) shows the main locations of radioactive materials and warehousing and geological storage sites for radioactive waste. In these installations, the radioactive waste undergo several chemical and physical treatments in order to separate the reusable combustible which will be transported to nuclear power-plants to be consumed and the actual radioactive waste which need to be warehoused or geologically stored. The latter waste come out of the factory in the form of "sludge", in the sense of a suspension of solids in an aqueous solution. These sludges aim to concentrate the radioactive waste and the precipitates coming from the treatment process of liquid effluents. These sludges are



rather viscous materials due to the chemical composition produced by the treatments in the factory of La Hague or in *CEA Marcoule*. To give a broader perspective of nuclear industry, waste which will be geologically stored will be managed by the *Cigeo* project. The latter project aims to store the waste produced from the beginning of French nuclear industry to year 2150 approximately when current power-plants will be totally dismantled and to avoid future generations to take care of burdens brought by the previous ones. The nuclear waste are split into two axes, according to their main characteristics, defined by *Andra*, the National Agency for the management of radioactive waste: the intensity of the activity and waste lifetime (see table 1.1). To give some orders of magnitude, High Activity-Long Life waste, which are the most dangerous waste to manage, represent 2 olympic swimming pools in volume with more than 95% of the radioactivity but account for 2.5% of the volume of all radioactive waste which have been produced from the beginning. This whole project started in 1991 with the Bataille law mentioning three solutions to study: transmutation, geological storage and long time warehousing. The site was then chosen in 1998 in Meuse/Haute-Marne. In 2005-2006, the first public debate occurred and French Parliament chose to geologically store High Activity and Medium Activity-Long Life waste with a reversibility of the storage during 100 years. The *Cigeo* project, Industrial Centre for geological storage, was presented in 2012 after some studies. A second public debate about *Cigeo* in 2013 gave rise to the modalities law of *Cigeo* in 2016. From 2016 and 2018, the Nuclear Safety Authority studied the project to finally conclude with a favourable opinion. In 2022, the Public utility declaration and the National interest operation were created.

Coming back to the topic of this PhD, in order to ensure the most relevant warehousing environment, it may be interesting to transport the sludges from one container to another. Nevertheless, the sludges are too viscous or rheologically complex to allow regular pumps to do the transportation. It is then necessary to find a method to allow pumping them.

Recent studies like [Gibaud, 2020a; Dagès, 2021] demonstrated that the use of ultrasound may have an influence on the behaviour of a suspension, more specifically its rheology. These studies showed that applying an external solicitation on certain suspensions may create a decrease of the storage modulus which helps the material to flow.

Hence, the basis of this PhD is to focus on a theoretical and numerical framework in order to understand how applying an external solicitation on these sludges may help to pump. The understanding may also allow to predict the conditions needed to make the sludges flow without meeting some dangerous boundaries like a violent increase in temperature, due to the dissipation in such viscous materials, or an enormous amount of energy needed for the operation.

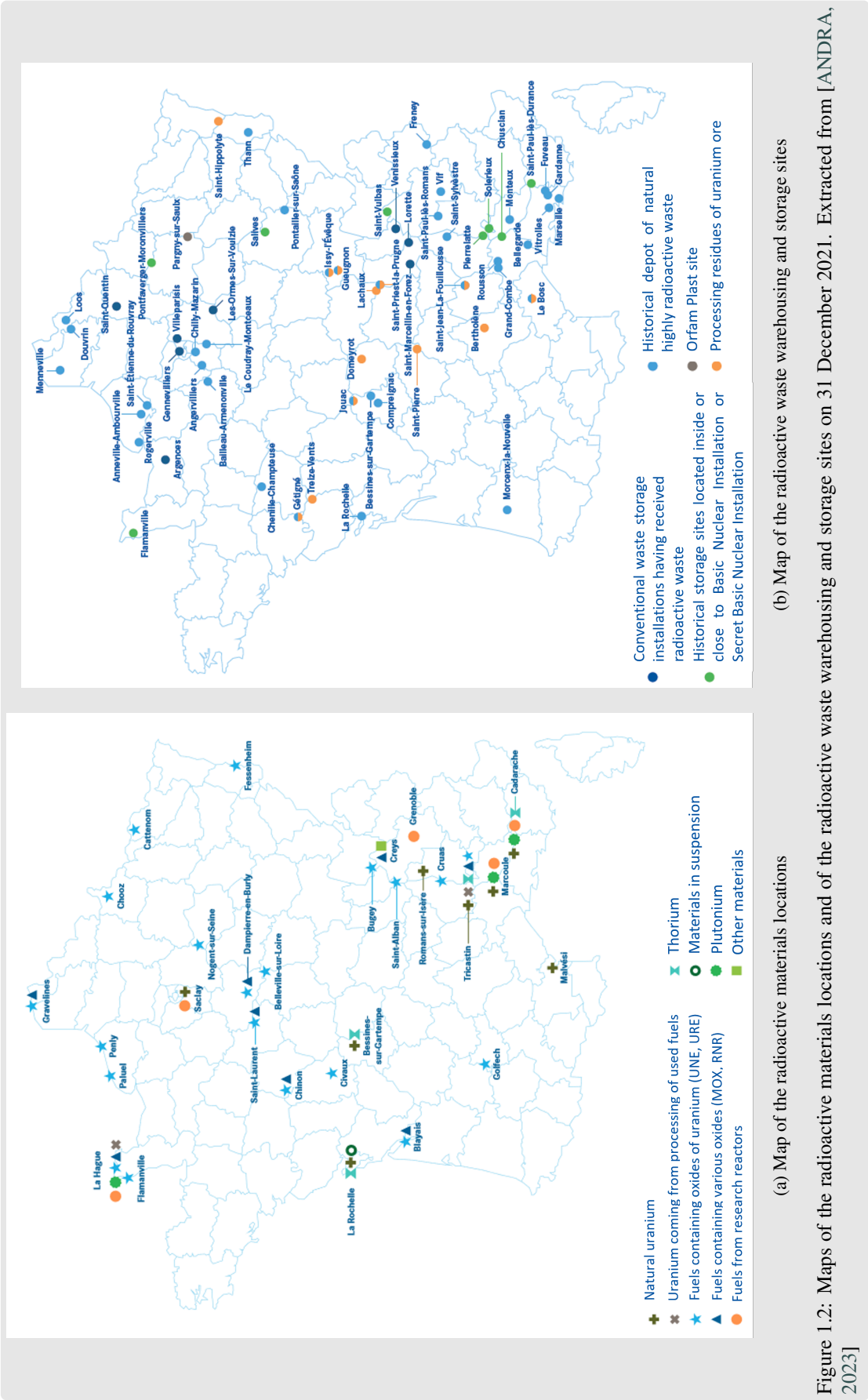


Figure 1.2: Maps of the radioactive materials locations and of the radioactive waste warehousing and storage sites on 31 December 2021. Extracted from [ANDRA, 2023]

		Radioactive period		
		Very short lifetime	Short lifetime	Long lifetime
Activity	Very low activity (< 100Bq/g)	Very short lifetime waste managed by radioactive decreasing	Very low activity waste warehoused in surface (Industrial center for gathering, warehousing and storage)	
	Low activity (> 100Bq/g and < 1MBq/g)		Low and Medium short lifetime warehoused at the surface in the warehouse center in <i>Aube</i> and <i>Manche</i>	Low activity long lifetime geologically stored at low depth understudy
	Medium activity (> 1MBq/g and < 1GBq/g)			Medium activity long lifetime deeply geologically stored in <i>Cigeo</i> project
	High activity (> 1GBq/g)	Not applicable	High activity deeply geologically stored in <i>Cigeo</i> project	

Table 1.1: Waste management matrix according to *Andra*. Extracted from [ANDRA, 2023].

1.2 State of the art [Bouthier,]

To give a more accurate view of the scientific background, I will describe in the following section the state of the art for rheology and structural analysis of colloidal suspensions.

1.2.1 Abstract of the section

The coupling between the microstructure and the external environment has been of great interest in recent rheological or mechanical studies. It can be tackled through phenomenological approaches, or trying to disentangle the reciprocal relationships between the components of the system. In this article, we present, after a brief overview of different rheological model, how microscopic structure influences the rheology, then, how microstructure is constrained by the external environment. The range of applications is humongous and should invite many others to study the strong coupling in industrial fields and numerical simulations.

1.2.2 Content of the section

Some generalities about rheology will be tackled in [section 1.2.3](#). Then, a particular focus will be taken to understand the influence of microscopic structures like clusters of particles on the rheology in [section 1.2.4](#)¹. Afterwards, in [section 1.2.5](#), the reciprocal dependence of cluster of particles according to external solicitation will be addressed². Furthermore, some additional insights about dimensionality will be studied in [sec-](#)

¹This will be the basis of my published work in [Bouthier, 2022; Dagès, 2022; Bouthier, 2023b] and developed in [chapter 3](#)

²This will be the basis of my published work in [Dagès, 2022; Bouthier, 2023a] and developed in [chapter 2](#)

[tion 1.2.6](#). Finally, in [section 1.2.7](#), some conclusions will be drawn.

1.2.3 Generalities about rheological model

1.2.3.1 Linear models

The word "rheology" comes from the greek $\rho\acute{\epsilon}\omega\lambda\acute{o}\gamma\iota\alpha$ which means literally "the study of the flow". It is a field at the boundaries of mechanics and physics because it is needed by continuum mechanics to solve the flow problems and rely mainly on physical argument to build properly the laws. Taking the angle of continuum mechanics, the equations of motions relate classically density, displacement or velocity and stresses (see [Landau, 1959; Landau, 1987; Barber, 2004]). To be more precise, in the Eulerian framework in the deformed configuration, the equations are according to [Bird, 2002; Bergman, 2011; Bharti, 1987]

$$\frac{\partial \rho}{\partial t} + \text{div}(\rho \mathbf{u}) = 0 \quad (1.1)$$

$$\frac{\partial \rho \mathbf{u}}{\partial t} + \mathbf{div}(\rho \mathbf{u} \otimes \mathbf{u}) = \mathbf{div}(\boldsymbol{\sigma}) + \rho \mathbf{b} \quad (1.2)$$

$$\boldsymbol{\sigma} = \boldsymbol{\sigma}^T \quad (1.3)$$

$$\frac{\partial \rho e}{\partial t} + \text{div}(\rho e \mathbf{u}) = \boldsymbol{\sigma} : \nabla \mathbf{u} - \text{div}(\mathbf{q}) + R \quad (1.4)$$

with ρ the density, \mathbf{u} the velocity, $\boldsymbol{\sigma}$ the Cauchy stress tensor, \mathbf{b} the body forces, e the internal energy per unit mass, R the radiation per unit volume, \mathbf{q} the heat flux vector, $:$ the double contracted product and the differential operators are in the deformed configuration. Then, in the Lagrangian framework, the equations are

$$\rho J = \rho_0 \quad (1.5)$$

$$\rho_0 \frac{\partial^2 \mathbf{x}}{\partial t^2} = \mathbf{DIV}(\mathbf{N}) + \rho_0 \mathbf{b} \quad (1.6)$$

$$\mathbf{FN} = \mathbf{N}^T \mathbf{F}^T \quad (1.7)$$

$$\rho_0 \frac{\partial e}{\partial t} = \mathbf{N} : \frac{\partial \mathbf{F}}{\partial t} - \mathbf{DIV}(\mathbf{q}) + R \quad (1.8)$$

with ρ_0 the density in the reference configuration, \mathbf{N} the nominal stress tensor (see the discussion below), \mathbf{x} the position vector, \mathbf{F} the deformation gradient, $J = \det(\mathbf{F})$ and the differential operators are in the reference configuration. To give some clarifications, equations (1.1) and (1.5) come from the conservation of mass, equations (1.2) and (1.6) comes from the conservation of linear momentum, equations (1.3) and (1.7) comes from the conservation of angular momentum and equations (1.4) and (1.8) comes from the conservation of energy, respectively in the Eulerian framework and the Lagrangian framework. The conservation equations between those quantities are incomplete to properly solve the problem. Therefore, new equations are proposed to relate, most of the time, the stresses with displacements and/or velocities. The pictures given here may be simplistic but other parameters may play a role like temperature, electromagnetism, chemistry or radiation. The most simple relations that can be found between stresses and displacements or velocities are proportional ones namely linear elastic and newtonian viscous. Precisely, for a Cauchy stress tensor $\boldsymbol{\sigma}$, a linear strain tensor $\boldsymbol{\varepsilon}$, a linear strain rate tensor $\dot{\boldsymbol{\varepsilon}}$, one can write

$$\boldsymbol{\sigma} = \lambda \text{tr}(\boldsymbol{\varepsilon}) \mathbf{I} + 2\mu \boldsymbol{\varepsilon} \quad (1.9)$$

$$\boldsymbol{\sigma} = -p \mathbf{I} + \kappa \text{tr}(\dot{\boldsymbol{\varepsilon}}) \mathbf{I} + 2\eta \left(\dot{\boldsymbol{\varepsilon}} - \frac{1}{3} \text{tr}(\dot{\boldsymbol{\varepsilon}}) \mathbf{I} \right) \quad (1.10)$$

with p the thermodynamic pressure, λ , μ , κ and η , the first Lamé coefficient, the second Lamé coefficient, the volume viscosity and the dynamic viscosity respectively (see [Landau, 1959; Landau, 1987]). These simple linear relations allow to recover respectively the Navier equations and the Navier-Stokes equations. Even if these partial derivatives equations may have a certain difficulty of resolution for complex geometry or non-linear properties, they may not represent truly the behaviour of the system.

1.2.3.2 Non-linear and sophisticated models

One of the first refinement that can exist is to create a yielded system. Precisely, in solid mechanics, the concept of plasticity, highlighted in [Tresca, 1864; Mises, 1913; Halphen, 1975], introduces a critical stress point (or yield stress) σ_y above which the behaviour changes. The elastic-perfectly plastic material follows for instance the law

$$\boldsymbol{\sigma} = \min(E\boldsymbol{\varepsilon}, \sigma_y) \quad (1.11)$$

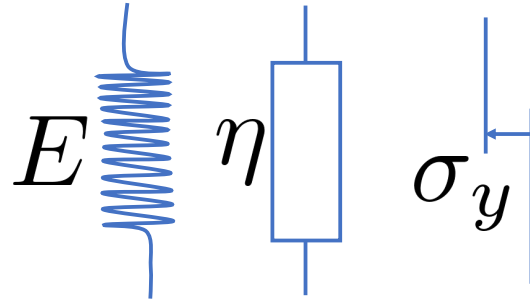


Figure 1.3: Usual rheological elements used to build rheological laws. From left to right, there are a spring of constant E , a dashpot of viscosity η and a friction element of yield stress σ_y

with E the Young modulus of the material. A similar example exists in fluid mechanics with the [Bingham, 1922] fluid reading

$$\boldsymbol{\sigma} = \boldsymbol{\sigma}_y + \eta \dot{\boldsymbol{\varepsilon}}. \quad (1.12)$$

A remark to be noticed is that, in the following part of this manuscript, the pressure p will not appear due to the fact we are considering mostly the non conservative stress contribution in shear. Hence, the pressure contribution should appear when resolving a complete 3D problem but will be omitted in the case of one dimensional shear only problems. From these simple models, others were proposed (see table 1.2). As a general comment, most of the following models are built as combination of elements presented in figure 1.3 either in parallel or in series, like in an electrical circuit. Keeping the similarity with electricity, electrical tension is similar to the strain and the electrical current is similar to the stress. Therefore, elements in series will share the same stress and add the several strains, as if tensions are summed while having the same current, and elements in parallel will share the same strain and add the several stresses, as if currents are summed while having the same tension. The elements presented in figure 1.3 are classical elements in the sense that most of usual models are built from these basic elements and refined non-linear elements are modification starting from the previous ones.

In [Ostwald, 1925], the newtonian behavior is modified by a power-law index which characterises shear-thinning fluid if it is below unity, newtonian behaviour if it is equal to unity and shear-thickening fluid [Madraki, 2017] if it is above unity. In [Herschel, 1926a], the same power-law behaviour is kept but using a yielding criterion as in [Bingham, 1922]. These models describe very well particle suspensions, like carbon black particle suspensions, where the particle volume fraction is low, or chlorine ions flow with blood cells[Mullieux, 2008].

Reference	1D Rheological law
[Landau, 1959]	$\sigma = E\varepsilon$
[Landau, 1987]	$\sigma = \eta\dot{\varepsilon}$
[Mises, 1913; Tresca, 1864; Halphen, 1975]	$\sigma = \min(E\varepsilon, \sigma_y)$
[Bingham, 1922]	$\sigma = \sigma_y + \eta\dot{\varepsilon}$
[Ostwald, 1925]	$\sigma = K\dot{\varepsilon}^n$
[Herschel, 1926a]	$\sigma = \sigma_y + K\dot{\varepsilon}^n$
[Goodeve, 1938; Larson, 2019]	$\sigma = \sigma_y(\lambda) + \eta(\lambda)\dot{\varepsilon}$
[Papanastasiou, 1987]	$\sigma = \sigma_y(1 - e^{-m\dot{\varepsilon}}) + \eta\dot{\varepsilon}$
Carreau [Macosko, 1994]	$\frac{\sigma}{\dot{\varepsilon}} = \eta_\infty + (\eta_0 - \eta_\infty)(1 + (\lambda\dot{\varepsilon})^2)^{\frac{n-1}{2}}$
[Einstein, 1911]	$\frac{\sigma}{\eta\dot{\varepsilon}} = 1 + \frac{5}{2}\phi$
[Krieger, 1959; Krieger, 1972]	$\frac{\sigma}{\eta\dot{\varepsilon}} = \left(1 - \frac{\phi}{\phi_m}\right)^{-[\eta]}$
[Maxwell, 1867]	$\sigma + \tau\dot{\sigma} = \eta\dot{\varepsilon}$
[Kelvin, 1890; Voigt, 1890]	$\sigma = E\varepsilon + \eta\dot{\varepsilon}$
Fractional Kelvin-Voigt [Jaishankar, 2012; Jaishankar, 2014]	$\sigma = \mathbb{U} \frac{d^\alpha \varepsilon}{dt^\alpha} + \mathbb{V} \frac{d^\beta \varepsilon}{dt^\beta}$
[Saramito, 2009]	$\frac{\dot{\sigma}}{E} + \max\left(0, \frac{ \sigma - \sigma_y}{K \sigma ^n}\right)^{\frac{1}{n}} \sigma = \dot{\varepsilon}$
[Saramito, 2007]	$\frac{\dot{\sigma}}{E} + \max\left(0, \frac{ \sigma - \sigma_y}{\eta \sigma }\right) \sigma = \dot{\varepsilon}$
Casson [Bonn, 2017]	$\sqrt{\sigma} = \sqrt{\sigma_y} + \sqrt{\eta\dot{\varepsilon}}$
[Caggioni, 2020]	$\sigma = \sigma_y + \sigma_y \sqrt{\frac{\dot{\varepsilon}}{\dot{\varepsilon}_c}} + \eta\dot{\varepsilon}$
[Snabre, 1996]	$\sigma \left(1 - \left(\frac{\sigma_0}{\sigma}\right)^m\right)^2 = \eta\dot{\varepsilon} \frac{1 - \phi}{(1 - \phi/\phi_0^*)^2} \left(1 - \frac{\phi}{1 - \phi} \left(\frac{\sigma^*}{\sigma}\right)^m\right)$

Table 1.2: Compilation of various rheological models expressed in one dimension with their sources.

In [Kelvin, 1890; Voigt, 1890; Maxwell, 1867], some classical viscoelastic models are presented to represent various phenomenologies depending on the experimental data like frequency sweep, shear start-up or creep. In [Zhang, 2021], prestresses can modify the elasticity of amorphous materials (see also [Nampoothiri, 2020]). In [Bonacci, 2022; Pantina, 2005], yield stress aging is investigated in attractive colloidal suspension. In [Larson, 2019; Mewis, 2009], a review of thixotropy is carried out in order to distinguish it from other phenomena, giving some model fluid examples, some phenomenology and how to model these type of fluids. In [Benzi, 2016; Benzi, 2021a; Benzi, 2021b], there is the use of the fluidity, which can be compared to the inverse of the viscosity, following a partial differential equation involving a cooperativity length and a steady-state solution. This is a coarse-graining model which helps to capture Soft Glassy Material behaviour as described and modelled in [Sollich, 1997; Sollich, 1998; Fielding, 2020; Divoux, 2013]. The Soft Glassy Material model covers a lot of cases and particularly certain particle suspensions. The

latter papers used a local partial differential equation involving the probability to find element in a certain energy depth at a certain time. This model helps to understand some mesoscopic phenomena when integrated at bigger scale. It can also be extended in tensorial form.

In [Saramito, 2007; Saramito, 2009; Ozenda, 2018], viscoelastoplastic rheological laws are considered involving phenomenological parameters starting from a thermodynamical framework to extend some famous forms (i.e. [Bingham, 1922] and [Herschel, 1926a]) into tensorial form. Precisely, as shown in figure 1.4, several elements illustrated in figure 1.3 have been used both in parallel and in series to tackle some more realistic materials. Following the description of the author, such model construction allows to mimic the behaviour of human blood or liquid foams. In this case, the classical yield stress fluid presented by [Bingham, 1922] is supplemented by an elastic contribution which affects the behaviour before yielding. The author investigated the response of such materials in uniaxial elongation, in simple shear flow and in periodic shear flow

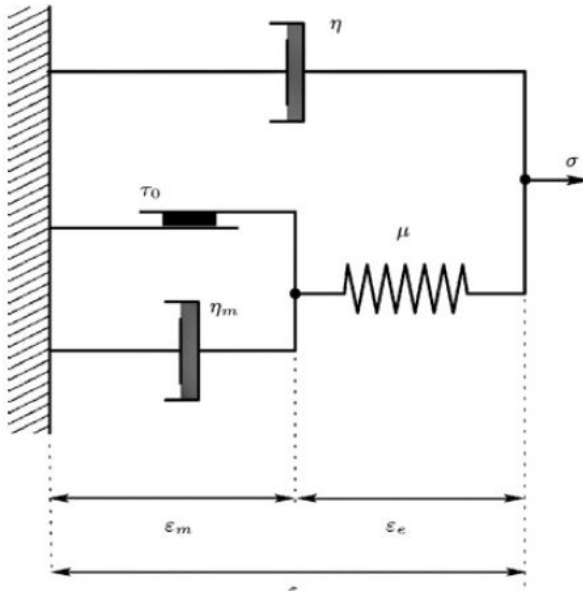


Figure 1.4: Elastoviscoplastic model proposed by [Saramito, 2007] to account for multiple physical processes in some materials taking a thermodynamic framework approach

to emphasize the type of response expected which can agree with some experimental data. An additional value of [Saramito, 2007; Saramito, 2009; Ozenda, 2018] is the use of the generalised standard materials framework [Halphen, 1975] which uses a free energy function and a potential of dissipation to derive the analytical form of the rheological law in one dimension and in tensor form. Therefore, the partition of energy is directly explicit and quick estimate can be made relating storage and dissipation.

To continue the different perspectives, in [Griffith, 1921; Irwin, 1957; Creton, 2016; Webber, 2007; Ducrot, 2014], rupture can be added to the models starting from linear elasticity, incorporating plasticity and investigating toughness of some soft materials. This rupture can be tuned by mixing two different networks [Gong, 2003; Gong, 2010] to increase the toughness. In [Papanastasiou, 1987], the [Bingham, 1922] model is modified to avoid the divergence of viscosity when strain rate tends to zero. The finite limit of such model helps for numerical implementation for simulations. With all these models, one can capture specific complex phenomena on real materials.

Regarding the effect of particle volume fraction on viscosity, in [Einstein, 1911], the effective viscosity of a suspension of solid particles with a certain volume fraction is linearly increased compared to the solvent viscosity. In [Krieger, 1972; Krieger, 1959; Brinkman, 1952], the same approach of suspension of solid particles is taken but increasing the particle volume fraction. The proximity of the particle volume fraction from

the jamming point modifies the effective viscosity in this analytical-phenomenological law.

If some comments are drawn about the specific topic of radioactive sludges in this manuscript, the particle volume fraction usually encountered is between 7% to 14%. Hence, it is possible to discuss which kind of the previous models may be interesting to consider. However, as what will be seen afterwards, the interaction between the particles is not purely hydrodynamic which imposes to complement previous models with some additional characteristics to completely deal with the complexity of the sludges.

In [Jaishankar, 2012; Jaishankar, 2014; Geri, 2017], the classical viscoelastic model presented in [Kelvin, 1890; Voigt, 1890; Maxwell, 1867] are modified incorporating fractional derivatives. These fractional derivatives, as described in [Schiesse, 1993; Schiesse, 1995b; Schiesse, 2000], are non local time integrals which help to capture some non-trivial frequency sweep measurements, such as displaying power-law behaviour which are not purely elastic or purely viscous, and avoids a high number of parameters. There exists multiple types of derivatives such as, for all $\alpha \in \mathbb{R}$ and a function f on an interval $[a, b]$, the Riemann-Liouville derivative with upper and lower variants [Herrmann, 2018],

$$D_{\alpha}^{\text{URL}} f(t) = \frac{d^{[\alpha]}}{dt^{[\alpha]}} \left(\frac{1}{\Gamma([\alpha] - \alpha)} \int_a^t (t - \tau)^{[\alpha] - \alpha - 1} f(\tau) d\tau \right) \quad (1.13)$$

$$D_{\alpha}^{\text{LRL}} f(t) = \frac{d^{[\alpha]}}{dt^{[\alpha]}} \left(\frac{1}{\Gamma([\alpha] - \alpha)} \int_t^b (\tau - t)^{[\alpha] - \alpha - 1} f(\tau) d\tau \right) \quad (1.14)$$

with $[\alpha]$ the smallest integer greater than α , the Caputo derivative [Caputo, 1967],

$$D_{\alpha}^{\text{C}} f(t) = \frac{1}{\Gamma([\alpha] - \alpha)} \int_a^t (t - \tau)^{[\alpha] - \alpha - 1} \frac{d^{[\alpha]} f}{dt^{[\alpha]}}(\tau) d\tau \quad (1.15)$$

the Caputo-Fabrizio derivative [Caputo, 2015],

$$D_{\alpha}^{\text{CF}} f(t) = \frac{1}{1 - \alpha} \int_a^t \frac{df}{dt} \exp\left(-\alpha \frac{t - \tau}{1 - \alpha}\right) d\tau \quad (1.16)$$

for $\alpha \in]0, 1[$, the Atangana-Baleanu derivatives [Alghamdi, 2016; Atangana, 2016]

$$D_{\alpha}^{\text{ABRL}} f(t) = \frac{\text{AB}(\alpha)}{1 - \alpha} \frac{d}{dt} \left(\int_a^t f(\tau) E_{\alpha} \left(-\alpha \frac{(t - \tau)^{\alpha}}{1 - \alpha} \right) d\tau \right) \quad (1.17)$$

$$D_{\alpha}^{\text{ABC}} f(t) = \frac{\text{AB}(\alpha)}{1 - \alpha} \int_a^t \frac{df}{dt}(\tau) E_{\alpha} \left(-\alpha \frac{(t - \tau)^{\alpha}}{1 - \alpha} \right) d\tau \quad (1.18)$$

with E_{α} the Mittag-Leffler function or the Riez deriva-

tive [Ding, 2015; Bayin, 2016],

$$D_a^R f(t) = \mathcal{F}^{-1}(\omega \mapsto -\omega^\alpha \mathcal{F}(s \mapsto f(s)))(t). \quad (1.19)$$

Each definition has its advantages and drawbacks due to the quality of the smoothness of the function f . It is clear that depending on the type of data measured or processed, it will be more or less difficult to handle the different derivatives of f like in equation (1.15) or to derive afterwards as in equations (1.13), (1.14) and (1.17). The numerical implementation of fractional derivative may not be trivial but some directions and helpful paths are presented in [Tavares, 2016; Pooseh, 2012; Atangana, 2017]. The same kind of framework may be considered in [Vilensky, 2012; Kelly, 2009] in the case of sound absorption, which extends discrete models into continuum ones, to reproduce some specific measurements in biological tissues.

About fractional models, they can be used to represent a continuum of time scales in a material which can be approximated through a hierarchical structure of rheological elements. For instance, using figure 1.5 and [Schiessel, 1995a; Schiessel, 1993], let consider a hierarchical structure of springs having spring constants $(E_n)_{n \in \mathbb{N}}$ and dashpots having viscosities $(\eta_n)_{n \in \mathbb{N}}$. In the case of infinite ladder, the viscoelastic modulus can be calculated to give

$$\frac{G^*}{E_0} = \mathbf{K}_{n=1}^{+\infty} \frac{a_n}{1} \quad (1.20)$$

$$\forall n \in \mathbb{N}^*, \quad a_n = \begin{cases} 1 & \text{if } n = 1 \\ \frac{E_{(n-2)/2}}{i\eta_{(n-2)/2}\omega} & \text{if } n \text{ even} \\ \frac{E_{(n-1)/2}}{i\eta_{(n-3)/2}\omega} & \text{if } n > 1 \text{ odd} \end{cases} \quad (1.21)$$

with \mathbf{K} the Carl Friedrich Gauss notation for continued fractions³ and ω the pulsation. If for all $n \in \mathbb{N}$, $E_n = E$ and $\eta_n = \eta$, it can be demonstrated according to [Schiessel, 1995a] that

$$G^* = \frac{i\eta\omega}{2} \left(\sqrt{\frac{4E}{i\eta\omega} + 1} - 1 \right) \quad (1.22)$$

which leads with $\eta\omega/E \rightarrow 0$ to $G^* \underset{\eta\omega/E \rightarrow 0}{\sim} \sqrt{i\eta\omega E}$. Be-

³The Carl Friedrich Gauss notation is used to describe concisely a continued fraction with two sequences $(a_n)_{n \in \mathbb{N}^*}$ and $(b_n)_{n \in \mathbb{N}^*}$ writing

$$\mathbf{K}_{n=1}^{+\infty} \frac{a_n}{b_n} = \frac{a_1}{b_1 + \frac{a_2}{b_2 + \frac{a_3}{b_3 + \ddots}}}$$

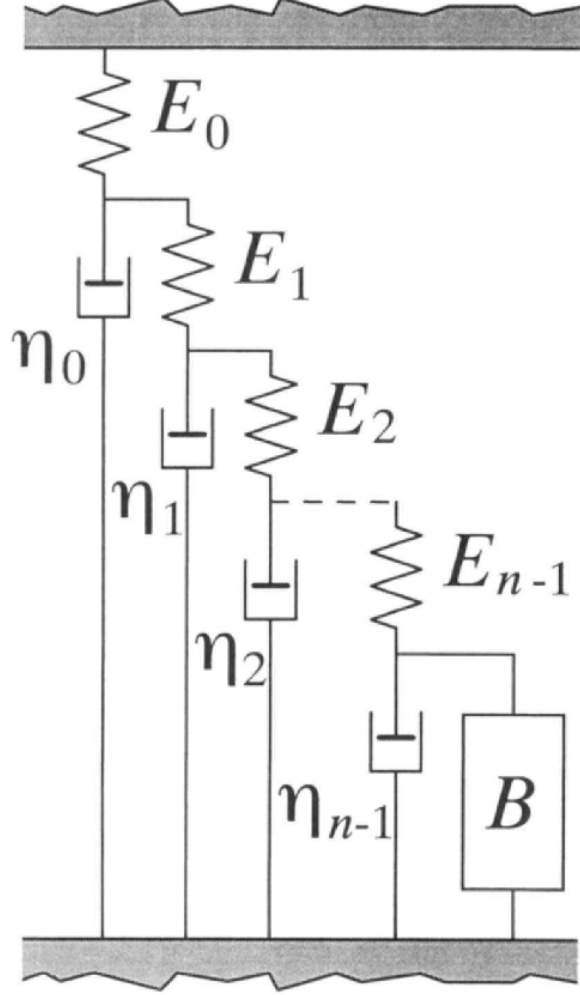


Figure 1.5: Ladder arrangements used to model scaling behaviours. According to the physical regime, the box B represents (a) a Maxwell element (pregel), (b) an infinite ladder (critical gel), and (c) a spring (postgel). Extracted from [Schiessel, 1995a]

sides, if for $n \in \mathbb{N}^*$,

$$\frac{i\eta_0\omega a_n}{E_0} = \begin{cases} 1 & \text{if } n = 1 \\ 1 - \alpha & \text{if } n = 2 \\ \frac{n - 2\alpha}{4(n - 1)} & \text{if } n > 2 \text{ even} \\ \frac{4(n - 1)}{n + 2\alpha - 3} & \text{if } n > 1 \text{ odd} \\ \frac{4(n - 2)}{4(n - 2)} & \end{cases} \quad (1.23)$$

with $\alpha \in [0, 1]$, it can be demonstrated according to [Schiessel, 1993] that

$$\frac{G^*}{E_0} = \left(1 + \frac{E_0}{i\eta_0\omega} \left(1 + \frac{E_0}{i\eta_0\omega} \right)^{\alpha-1} \right)^{-1} \quad (1.24)$$

which leads to $G^*/E_0 \underset{\eta_0\omega/E_0 \rightarrow 0}{\sim} (i\eta_0\omega/E_0)^\alpha$ when $\eta_0\omega/E_0 \rightarrow 0$. Therefore, both cases demonstrate that

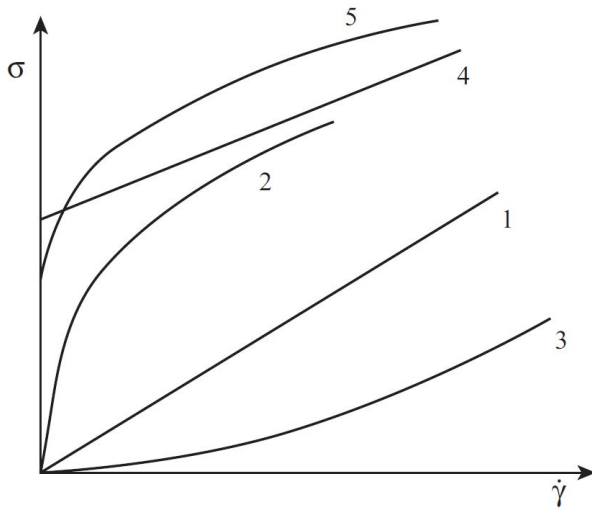


Figure 1.6: General curves of shear stress vs shear rate: (1) Newtonian; (2) shear thinning; (3) shear thickening; (4), (5) materials with yield stress. Extracted from [Mewis, 2012].

an infinite spectrum of time scale may bring power-law relationships in the frequency sweeps which can be easily approximated through fractional derivatives. A question remains about how to relate the exponent with realistic characteristics of materials. I am not a powerful defender of fractional derivatives used in rheological model but I acknowledge the easiness of use of such tools. Waiting for a convincing explanation does not force to forbid these tools to properly study and compare some phenomenologies.

In [Beris, 1994], another thermodynamical framework compared to [Halphen, 1975] is proposed using Poisson brackets and helps to considered rheological laws as general as possible. The reader is invited to take a look in [Macosko, 1994; Bonn, 2017; Mahbubul, 2012; Sugimoto, 2019; Fardin, 2012; Cloitre, 2017a; Cloitre, 2017b; Gibaud, 2020b; Coussot, 2010; Tanner, 2018; Bertram, 2021] to have a broader perspective of rheological law existing in the literature. Different flowing regimes are presented on figure 1.6 to capture all the existing behaviour.

1.2.3.3 Extension to tensor forms

As a general comment, all the previous laws, except a few of them, were originally designed in one dimension. The extension to two and three dimensions can be more or less straightforward. For example, in [Maxwell, 1867], there is a derivative of the stress. In order to extend to higher dimension, a simple partial time derivative ∂_t is not sufficient. Even a total derivative $d_t = \partial_t + \nabla(\cdot)\mathbf{u}$ with \mathbf{u} the velocity is not complete. Objective derivative must be used and are rather diverse. First

of all, the use of Cauchy stress tensor, Kirchhoff stress tensors or other forms must be considered because, depending on the type of transformation happening in the system, referring to the current or the reference configuration for one or both sides is a relevant question to address. Precisely, the different stresses measure are the Cauchy stress tensor $\boldsymbol{\sigma}$, the Kirchhoff stress tensor $\boldsymbol{\tau}$, the Nominal stress tensor \mathbf{N} , the first Piola-Kirchhoff stress tensor \mathbf{P} , the second Piola-Kirchhoff stress tensor \mathbf{S} and the Biot stress tensor \mathbf{T} which are related to each other according to table 1.3. According to [Wikipedia contributors, 2022a; Landau, 1959], the Cauchy stress is a measure of the force acting on an element of area in the deformed configuration, the first Piola-Kirchhoff stress tensor relates forces in the deformed configuration with areas in the reference configuration and the second Piola-Kirchhoff stress tensor relates forces in the reference configuration to areas in the reference configuration. To give an example, in simple shear $\boldsymbol{\varepsilon}$ in the xy plane, one gets

$$\mathbf{F} = \mathbf{I} + \boldsymbol{\varepsilon} \mathbf{e}_x \otimes \mathbf{e}_y \quad (1.25)$$

$$\mathbf{S} = \boldsymbol{\sigma} - \boldsymbol{\varepsilon} \begin{pmatrix} 2\sigma_{xy} - \varepsilon\sigma_{yy} & \sigma_{yy} & \sigma_{yz} \\ \sigma_{yy} & 0 & 0 \\ \sigma_{yz} & 0 & 0 \end{pmatrix} \quad (1.26)$$

$$2\mathbf{e} = \boldsymbol{\varepsilon} (\mathbf{e}_x \otimes \mathbf{e}_y + \mathbf{e}_y \otimes \mathbf{e}_x) + \varepsilon^2 \mathbf{e}_y \otimes \mathbf{e}_y \quad (1.27)$$

with \mathbf{e} the Green-Lagrange strain tensor. Therefore, knowing that \mathbf{S} and \mathbf{e} are energy conjuguate, it is relevant to measure some stresses $\boldsymbol{\sigma}$ in the current configuration, bring them back into the reference configuration with \mathbf{S} and relate \mathbf{e} and \mathbf{S} according to the time derivative, a potential yielding, ... Then, following [Gurtin, 2010], it is possible to identify the Truesdell rate

$$\overset{\circ}{\boldsymbol{\sigma}} = \frac{\partial \boldsymbol{\sigma}}{\partial t} - \mathbf{L}\boldsymbol{\sigma} - \boldsymbol{\sigma}\mathbf{L}^T + \text{tr}(\mathbf{L})\boldsymbol{\sigma} \quad (1.28)$$

where $\mathbf{L} = \partial_t \mathbf{F}\mathbf{F}^{-1}$ is the velocity gradient with \mathbf{F} the displacement gradient, T the transpose of a tensor and tr the trace of a tensor. There is also the Green-Naghdi rate

$$\overset{\square}{\boldsymbol{\sigma}} = \frac{\partial \boldsymbol{\sigma}}{\partial t} + \boldsymbol{\sigma}\boldsymbol{\Omega} - \boldsymbol{\Omega}\boldsymbol{\sigma} \quad (1.29)$$

with $\boldsymbol{\Omega} = \partial_t \mathbf{R}\mathbf{R}^T$ and \mathbf{R} the orthogonal rotation tensor in the polar decomposition of the displacement gradient $\mathbf{F} = \mathbf{R}\mathbf{U}$ with $\mathbf{R}^T = \mathbf{R}^{-1}$ and \mathbf{U} is symmetric, positive definite, right stretch. Moreover, there are the Zaremba-Jaumann rate

$$\overset{\Delta}{\boldsymbol{\sigma}} = \frac{\partial \boldsymbol{\sigma}}{\partial t} + \boldsymbol{\sigma}\mathbf{W} - \mathbf{W}\boldsymbol{\sigma} \quad (1.30)$$

Equation for	σ	τ	P	N	S	T
$\sigma =$	σ	$J^{-1}\tau$	$J^{-1}PF^T$	$J^{-1}N^T F^T$	$J^{-1}FSF^T$	$J^{-1}RTF^T$
$\tau =$	$J\sigma$	τ	PF^T	$N^T F^T$	FSF^T	RTF^T
$P =$	$J\sigma F^{-T}$	τF^{-T}	P	N^T	FS	RT
$N =$	$JF^{-1}\sigma$	$F^{-1}\tau$	P^T	N	SF^T	$T^T R^T$
$S =$	$JF^{-1}\sigma F^{-T}$	$F^{-1}\tau F^{-T}$	$F^{-1}P$	$F^{-1}N^T$	S	$U^{-1}T$
$T =$	$JR^T\sigma F^{-T}$	$R^T\tau F^{-T}$	$R^T P$	$R^T N^T$	US	T

Table 1.3: Conversion formulae between the Cauchy stress tensor σ , the Kirchhoff stress tensor τ , the Nominal stress tensor N , the first Piol-Kirchhoff stress tensor P , the second Piola-Kirchhoff stress tensor S and the Biot stress tensor T . $F = RU$ is the displacement gradient with $R^T = R^{-1}$ and U is symmetric, positive definite, right stretch and $J = \det(F)$. Extracted from [Wikipedia contributors, 2022a] and inspired from [Landau, 1959].

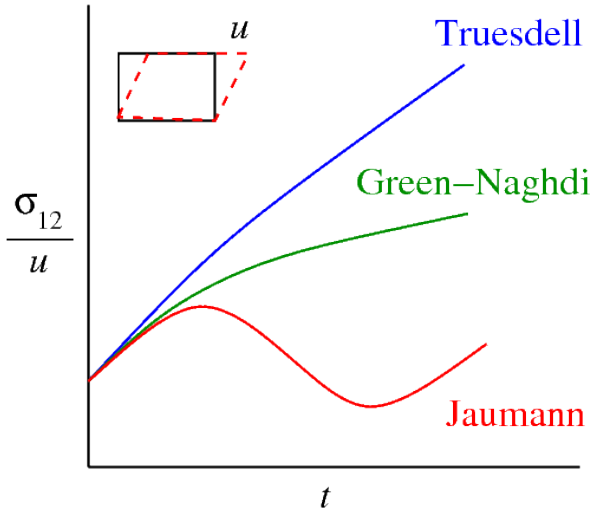


Figure 1.7: Predictions from Truesdell, Green-Naghdi and Jaumann objective stress rates under simple shear test of a hypoelastic material with constant elastic moduli. The ratio of the shear stress to the displacement is plotted as a function of time. The same moduli are used with the three objective stress rates. Extracted from [Wikipedia contributors, 2022b] and inspired from [Dienes, 1979]

with $W = (L - L^T)/2$ the skew part of the velocity gradient, the Oldroyd stress rate

$$\overset{\nabla}{\sigma} = \frac{\partial \sigma}{\partial t} - L\sigma - \sigma L^T, \quad (1.31)$$

which is the most used model in fluid rheology, and the convective stress rate

$$\overset{\circ}{\sigma} = \frac{\partial \sigma}{\partial t} + L\sigma + \sigma L^T. \quad (1.32)$$

Different results of an applied shear as a function of time with the same rheological parameters but with different objective stress rates are presented in figure 1.7. It is then blatant to properly design the objective stress

rate and the rheological parameters to reproduce properly the observed phenomenology. In the same discussion the consideration of Lagrangian or Eulerian framework is a crucial topic when the deformation becomes large. In small deformation, both frameworks are identical but deviates formally from each other while describing the same phenomena. For example, the linear strain rate tensor in Eulerian framework is defined as

$$\dot{\varepsilon} = \frac{1}{2} (\nabla u + \nabla u^T) \quad (1.33)$$

and in the Lagrangian framework as

$$\dot{\varepsilon} = \frac{1}{2} \left(\frac{\partial F}{\partial t} F^{-1} + F^{-T} \frac{\partial F^T}{\partial t} \right). \quad (1.34)$$

It is relevant to recall that, in general, to extend differential forms for the stress tensor in 3D can be very delicate. Indeed, there is no clear extension of equations (1.13) to (1.19) in 3D when we consider the stress tensor. How can we properly account for objectivity with a time integro-differential operator which also has an impact in space due to the transformation of coordinates?

The previous paragraph may seem out of the scope of this chapter but these notions seem to be the next step that would be tackled in the future. Indeed, according to the analysis of the current knowledge in the field, there may be two main outcomes. On the one hand future studies will rely on simple microscopic ingredients of mechanical scaling like those presented in section 1.2.4.2 and should investigate macroscopic heterogeneities and anisotropies in three dimensions. In this case, how to properly extend microlocal laws with a 3D scaling should imply to think about the mechanical bases of dynamic quantities in the relevant framework. Hence, paying attention to the possible discrepancies in the formalism is very important. On the other hand, the other perspective is to build a more robust microscopic approach with probabilistic approach which helps to account for variations in real systems. Nevertheless, this second path may be more difficult to conduct.

1.2.3.4 Some experimental techniques

The experimental techniques to assess parameters present in rheological laws are diverse [Peuvrel-Disdier, 2012]. Due to continuum mechanics, investigating material properties without being overwhelmed by geometrical effects or non-linearities can be a hard task. Therefore, considering simple geometries creating only one desired effect is an absolute need. For instance in usual rheological experiments, the flow is produced with a low Reynolds number in order to avoid any inertial effects and, maybe, some time dependence due to inertia. Without being exhaustive, turbulence effects as described in [Boussinesq, 1868] may create secondary flows and perturb the measurement, instabilities like in [Drazin, 1970] will produce diverging energies which can be dangerous for the machines, phase separation as in [Andreotti, 2013; Nedderman, 1992] can not help to isolate one specific characteristic among others or other phenomena described in [Johnson, 2016] which are detrimental effects and need to be avoided. In the case of radioactive sludges, due to the presence of several phases, the opportunity to create heterogeneous flows is rather important and may cause difficulties to measure properly rheological quantities, that is why phase separation is one of the biggest issues to prevent. Thus, some simple geometries like Taylor-Couette flow or Poiseuille flow are used due to their analytical solution, their simple velocity profiles and their low boundary effects to avoid too much complexities [Çengel, 2006; Tennekes, 1972; Berker, 1936; Berker, 1963]. When looking at equations (1.9) and (1.10), it is straightforward to disentangle the volume effects from the shear effects, as illustrated by the deviatoric part of the tensors. Hence, a common assessment of the rheology of certain materials is done through shear measurements. Particularly, oscillatory shear measurements with a certain amplitude and a fixed frequency allow to extract the viscoelastic modulus G^* or the viscoelastic compliance J^* , depending on the controlled variable, strain ε or stress σ respectively, through

$$G^* = \frac{\mathcal{F}(\sigma)}{\mathcal{F}(\varepsilon)} \quad (1.35)$$

$$J^* = \frac{\mathcal{F}(\varepsilon)}{\mathcal{F}(\sigma)} \quad (1.36)$$

with \mathcal{F} the Fourier transform of the variable, see [Macosko, 1994; Rehage, 1988]. These two previous quantities can be analysed at different amplitudes of controlled variables (namely strain-sweep or stress-sweep respectively) and different frequencies (namely frequency sweep). It is common to separate the real part and the imaginary part to represent respectively the *elastic* behaviour of the material and the *dissipative* behaviour of the material, respectively. Optimal

techniques as presented in [Geri, 2018; Bouzid, 2018b], namely Optimally Windowed Chirps, may help to reduce the time to compute the whole spectrum of frequency sweep. The computations of the previous quantities are mainly done using the first harmonic of the numerical Fourier transform estimation. Some recent methods may also allow to compute a time-resolved viscoelastic modulus through the Sequence of Physical Processes in [Rogers, 2017; Donley, 2019; Rogers, 2011; Rogers, 2012b; Rogers, 2012a]. This framework is based on the Frenet-Serret apparatus to compute local partial derivatives and may be extended to time-resolved viscoelastic compliances. An interesting question for oscillatory shear measurements is that some people are investigating the previous quantities even at large amplitudes, i.e. outside of the non-linear regime of certain materials, without taking into account some potential non-linear geometrical effects. Some future works analysing the deviation of *linear* rheology at large amplitude, in Large Amplitude Oscillation Strain (LAOS) for instance, may be relevant.

When looking at the physical construction of certain rheological laws in suspensions of particles, authors may try extrapolate microscopic properties and structures to the macroscopic level to recover the rheological values measured experimentally. The influence of the microscopic structures on the rheology will be tackled in the next section.

1.2.4 How clusters influence the rheology

1.2.4.1 Construction of the clusters

The types of systems in the colloidal gels class can have particles ranging from nanometer size to micrometer size, and a characteristic time scale ranging from few picoseconds to milliseconds. The different families of suspension of particles can be tackled through a phase diagram as presented in [Sciortino, 2002; Trappe, 2001]. For instance, referring to figure 1.8, the phase diagram often represents the state of suspension of particles, at least, in a temperature-particle volume fraction plane. The temperature can also be compared to the strength of the interaction potential between particles because there is generally a proportional relationship between those two quantities [Gibaud, 2020a; Varga, 2019]. At high volume fraction close to the jamming point, it is possible to find different types of glasses [Schoenholz, 2016; Hwang, 2016; Biroli, 2018] or granular materials [Bassett, 2015; Guazzelli, 2018; Hanotin, 2012; Hanotin, 2015]. Depending on the strength of the interaction potential, it can be either a repulsive material with a rather homogeneous microstructure or an attractive material with a more heterogeneous microstructure [Prasad, 2003; Joshi, 2014]. The microstructure and rheology of concentrated suspensions were addressed

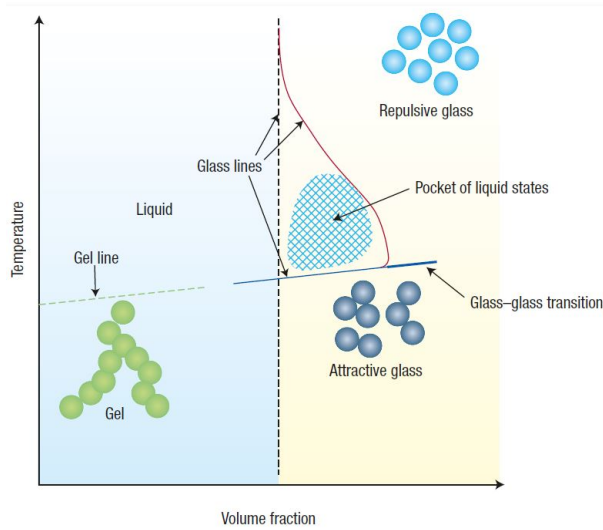


Figure 1.8: Temperature versus volume fraction phase diagram. The glass lines separate the ‘liquid’ regions, where particles are able to diffuse, from the ‘glass’ regions. The vertical black dashed line represents the hard-sphere glass line. In the case of short-range attractive colloids, the re-entrant (non-monotonic) shape of the glass line (solid red and blue lines) creates a pocket of liquid states that are stabilized by the short-range attraction. The location of the theoretical glass–glass transition line (thick blue line) and the proposed connection between the gel-line (at low volume fractions) and the attractive glass line (solid blue line) are also indicated. Equilibrium (and metastable) lines between gas, liquid and solid phases — which in the case of attractive colloids are significantly different from the case of long-range attractions — are not shown. Extracted from [Sciortino, 2002].

by [Blanc, 2011; Blanc, 2013]. When the volume fraction is very low, there are also two cases depending on the interaction potential: a more repulsive interaction potential will just lead to a more fluid-like material, whereas a more attractive potential can bring a gel. The different phase separation were tackled in [Furukawa, 1985; Lu, 2008]. There exist also other types of materials with non-brownian suspensions [Lobry, 2019], frictional suspensions [Tapia, 2019] and colloidal suspensions. The latter category will be our main focus in this paper. Due to the attractive interaction potential and the low particle volume fraction, the microscopic structure is more heterogeneous and sparse than any other materials but keeps its consistency to create soft-solid/fluid materials. To give some orders of magnitude, the typical particle volume fraction encountered in colloidal gels is of few percents and the typical attractive potential energy scale is around tens of $k_B T$ with k_B the Boltzmann constant and T the temperature.

In a suspension of particles with a certain volume fraction, if the particles are only repulsive as in granular media [Bassett, 2015; Guazzelli, 2018; Hanotin, 2012; Hanotin, 2015] some classical laws such as [Einstein, 1911; Krieger, 1959; Krieger, 1972] exist to account for the impact of the particles on the overall rheology. Hard-spheres in general have been of great interest to account for rheological laws coming from colloidal dispersions [Ven, 1977]. Some polydispersity may be considered to modify the viscosity law [Mwasame, 2016]. The particles can be rather diverse in terms of materials like alumina [Nguyen, 2011; Waite, 2001; Schilde, 2011; Sauter, 2008; Mahbulul, 2014], polystyrene [Okubo, 1995], silica [Mondragon, 2012] or titania [Fazio, 2008]. When the particles interact between each other with an attractive potential, they tend to form some bigger sets which can be called clusters, flocs or aggregates depending on the terminology (see figure 1.9) [Lattuada, 2003]. This attractive interaction may be pure Van der Waals attraction like in [Visser, 1972; Hartley, 1985; Klimchitskaya, 2000; Yuan, 2016], Derjaguin, Landau, Verwey and Overbeek interaction like in [Gibaud, 2020a; Dagès, 2021] or capillary attraction like in [Vassileva, 2005; Rahman, 2019; He, 2015; Seemann, 2011; Herminghaus, 2000]. These clusters may have different structures from dense to sparse [Weitz, 1984; Weitz, 1985; Knoll, 2018].

The sparse clusters may have a fractal structure as described in [Mandelbrot, 1983]. Fractal structures are self-similar structures which are usual in percolation theory [Broadbent, 1957] and related to critical exponents [Grassberger, 1985; Grassberger, 1992b; Grassberger, 1992a]. A usual description of a fractal structure is considering elements of size a aggregated in a cluster; if the window size of the analysis is l , the number of elements N in this window is $N \propto (l/a)^D$ with D the exponent called the fractal dimension [Deng, 2010; Wang, 2013; Xu, 2014; Zhou, 2012]. Varying the window size allows to measure the fractal dimension, which is a technique used in a box counting algorithm [Panigrahy, 2019; Zhang, 1996]. As illustrated in [Kantor, 1984a; Kantor, 1984b], the fractal structures are sometimes studied for conductivity problems as well as mechanical problems.

The self-similar structure may be recognized easily through scattering experiment as reviewed in [Sorensen, 2001; Lin, 1989; Zhou, 1991; Galvan-Miyoshi, 2008]. Scattering experiments allows also to capture some sedimentation velocity as in [Xue, 1992], the chord distribution of a network as in [Levitz, 1992] or to characterise blood cells [Monchy, 2016; Monchy, 2018; Franceschini, 2011; Franceschini, 2012; Franceschini, 2010]. The identification of cluster’s characteristic features like its size or its fractal dimension may be done by fitting some model to the scattering intensity spectrum like in [Hammouda, 2010; Burns, 1997; Beaucage, 1995;

Beaucage, 1996] with

$$I(q) = A \left[\exp\left(-\frac{q^2 \ell^2}{3}\right) + \frac{B(D)}{(q\ell)^D} \operatorname{erf}\left(\frac{q\ell}{\sqrt{6}}\right)^{3D} \right] \quad (1.37)$$

$$B(D) = D \left(\frac{6D^2}{(2+D)(2+2D)} \right)^{\frac{D}{2}} \Gamma\left(\frac{D}{2}\right) \quad (1.38)$$

with A a fitting parameter, ℓ the size of the cluster, q the norm of the wave vector, D the fractal dimension, erf the error function and Γ the Gamma function. Other scattering papers may be read like [Burns, 1997; Zhang, 1996; Teixeira, 1988; Freltoft, 1986; Wagner, 1990; Monchy, 2016; Monchy, 2018]. In the case of the colloidal suspensions studied in this PhD, the X-Ray scattering experiments are properly suited to capture the cluster sizes between 1nm and 1 μ m. The typical behaviour of the scattered intensity as a function of the wave vector number for a fractal object is represented on [figure 1.10](#), highlighting the start of the decreasing trend for the cluster size, the power-law decrease with a slope equals to the opposite of the fractal dimension and the final cut-off due to the particle size with a slope equals to -4 in the Porod regime limit.

The construction of the clusters may be tackled through the percolation theory. To recall the basis of this framework, a lattice of dimension \dim has a linear size n with one element on each point of the lattice. There is an imposed probability p that two neighbouring elements of the lattice connect between each other. We are then interested in the smallest probability p_c where it is possible to create a connected path from one side of the network to the other. One of the first investigation was done by [Flory, 1941; Stockmayer, 1944] about the percolation of polymers. An extension called random cluster model [Fortuin, 1972] tried to unify the Ising model, the Potts model and the percolation theory. These models are also closely related to graph theories as described in the Albert-Barabási model [Barabási, 1999; Barabási, 2003; Albert, 2002], the scale free network [Pastor-Satorras, 2001], the force-chain structure [Giusti, 2016], the Erdős-Rényi model [Erdős, 1959] or the Bianconi-Barabási model [Bianconi, 2001a; Bianconi, 2001b].

The construction of the clusters may be also done with other methods. A first example is the coagulation equations [Banasiak, 2020a; Banasiak, 2020b]. In these equations, there exists a probability density function f depending on the number of elements $x \in \mathbb{R}_+$ of the cluster and time $t \in \mathbb{R}_+$. The variation of the probability density function f is determined by an aggregation rate given by an aggregation kernel $K(x, y)$ which gives the probability rate that a cluster of number of elements x and a cluster of number of elements y aggregate together. The coagulation equation is a balance equation

usually written as follows

$$\frac{\partial f}{\partial t}(x, t) = \frac{1}{2} \int_0^x K(x-y, y) f(y, t) f(x-y, t) dy - f(x, t) \int_0^{+\infty} K(x, y) f(y, t) dy \quad (1.39)$$

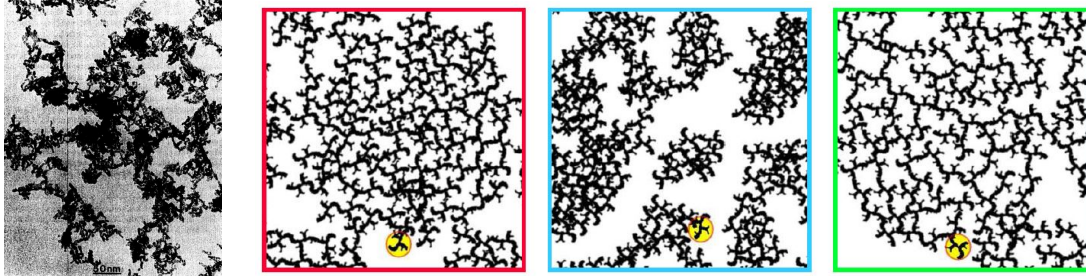
The continuum form has been considered above but a discrete version of the previous equation may also be written. Several solutions have been analytically found for $K(x, y) = 1$, $K(x, y) = x + y$ and $K(x, y) = xy$ for example in [Wattis, 2006]. More complex kernels exist as discussed in [Kryven, 2014] like

$$K(x, y) = \sqrt{\frac{\pi k_B T}{2}} \sqrt{\frac{1}{m(x)} + \frac{1}{m(y)}} (d(x) + d(y))^2 \quad (1.40)$$

$$K(x, y) = \frac{2k_B T}{3\eta} \left(x^{\frac{1}{D_1}} + y^{\frac{1}{D_2}} \right) \left(x^{-\frac{1}{D_1}} + y^{-\frac{1}{D_2}} \right) \quad (1.41)$$

$$K(x, y) = \frac{2k_B T (xy)^\gamma}{3W\eta} \left(x^{\frac{1}{D_1}} + y^{\frac{1}{D_2}} \right) \left(x^{-\frac{1}{D_1}} + y^{-\frac{1}{D_2}} \right) \quad (1.42)$$

with k_B the Boltzmann constant, T the temperature, $m(x)$ the mass of the cluster of number of elements x , $d(x)$ the diameter of the cluster of number of elements x , η the viscosity of the solvent, D_i for $i \in \{1, 2\}$ the fractal dimension of the clusters i , W the Fuchs stability ratio, γ a fitting parameter. [Equation \(1.40\)](#) is the free-molecular kernel which describes collisions in a dilute gas-phase system, [equation \(1.41\)](#) is the kernel which describes the diffusion-limited aggregation (i.e. DLCA), that can be influenced by sedimentation and buoyancy [Wu, 2003], and [equation \(1.42\)](#) is the kernel which describes the reaction-limited aggregation (i.e. RLCA) which can be driven by shear [Zaccone, 2010]. The interest of such modelling is to capture the evolution kinetics for the aggregation of certain systems and the overall distribution of sizes. Indeed, most of cluster populations display polydispersity with a certain range of significant sizes. However, in the scattering models or in the micromechanical models, this polydispersity is omitted to simplify the calculations. As demonstrated by the previous coagulation framework, everything relies on probabilities, hence the different analytical approaches should take into account this perspective to properly analyse and interpret the data. The coagulation framework may be extended to the coagulation-fragmentation case, also known as the population balance model [Puisto, 2012; Lattuada, 2016], where a fragmentation kernel is introduced to represent the disaggregation of clusters due to external solicitation (shear flow, thermal fluctuations, ...) (see [section 1.2.5.2](#)) [Banasiak, 2020a; Banasiak, 2020b; Sorensen, 1987]. The different coagulation-fragmentation processes are illus-



(a) Transmission electron micrograph of part of a colloidal ZrO_2 floc. Extracted from [Shih, 2020a] 1990]. (b) Qualitative views of the gel microstructure before (left), during (middle), and after application of ultrasound (right) as inferred from USAXS data. The yellow circle highlights a carbon black particle of effective diameter 300 nm (scale bar). Extracted from [Gibaud, 1990]

Figure 1.9: Construction of clusters

trated on figure 1.11 with the different phenomena and the expression of the different terms in the equation.

Another probabilistic framework exists and is based on the kinetic of particles: the Boltzmann equation. Precisely, in phase space of time t , space \mathbf{x} , velocity \mathbf{u} , number of elements n , there exists a probability density function f following

$$\frac{\partial f}{\partial t} + \mathbf{u} \cdot \frac{\partial f}{\partial \mathbf{x}} + \frac{\mathbf{F}}{m(n)} \cdot \frac{\partial f}{\partial \mathbf{u}} + N \frac{\partial f}{\partial n} = \mathcal{J}(f) \quad (1.43)$$

where \mathbf{F} is the force applied on clusters at location \mathbf{x} with a velocity \mathbf{u} at time t with a number of elements n , $m(n)$ the mass of a cluster of number of elements n , $N = dn/dt$ the rate of change in the number of elements and \mathcal{J} the collision integral which represents the direct interaction between the clusters. Such framework is generally described in [Alexeev, 2004; Stannichuk, 2015; Tine, 2011] and is applied on the case of droplets and bubbles for combustion and jets. For instance, [Eggers, 2008] studied the physics of liquid jets, [Marmottant, 2004] investigated the spray formation, [Williams, 1985] studied the combustion theory, [Pratsinis, 1998] investigated the flame aerosol synthesis of ceramic powders and [Delichatsios, 1976] studied the effect of coalescence on the average drop size in Liquid-liquid dispersions. Besides the relative complexity of such modelling, some simple solutions may be found in [Williams, 1985] and some simplifications of the collision integral \mathcal{J} may be proposed as in [Bhatnagar, 1954] to have a closed formulation of the Boltzmann equation. For instance, on figure 1.12, the droplet size distribution is showed as an evolution of the different parameters of the coalescence model: the general increase of the average size and the distribution spreading is visible when the parameter $(1 + t_j)/s_j$ is increased. Also, the Boltzmann equation allows to recover general conservation equations of continuum mechanics taking the various moments of the distribution according to each variable

[De Groot, 2013] which is called the Chapman-Enskog expansion. Therefore, solving the Boltzmann equation gives the system general insights if properly modelled. The numerical framework in the Boltzmann equation is the lattice Boltzmann technique which is described in [Jiang, 2020; Cheng, 2010; Yu, 2009]

The aggregation of the clusters may also be tackled by Monte-Carlo Simulation as in [Suarez, 2018; Masoero, 2014; García Daza, 2022]. Other tools may exist [Swope, 1982].

All these descriptions and models are great tools to understand how clusters are formed. The scattering experiments model are perfect to quickly capture some relevant quantities. There can be some critics on the fact that, sometimes, due to the lack of data on a broad range, it is possible to fit several models and to deduce different types of structures afterwards. Indeed, that is the risk but, like other experimental studies, the objective is to draw conclusions from samples and use the principle of induction. It may seem frustrating but it is through the multiplication and the validation of such studies that a common shared knowledge can be built.

About the theoretical tools to describe the particles kinematic of aggregation and disaggregation, the percolation theory, the coagulation equations or the Boltzmann equations try to use an abstract framework to rationalise to the simplest ingredients these really complex phenomena. The percolation theory, even if seducing with simple probabilistic argument, may seem a little bit disconnected from physical aspects like potentials of interaction as the two latter deal with. Nevertheless, these two latter are complex to solve analytically or even numerically which does not help to manage them easily even with some ideal materials. Potential users are suggested to understand the underlying physical problem first before digging deep in these frameworks due to the intrinsic complexities on which they rely. It may be dangerous to focus only on these models which can bring, in the end, not easily explainable outcomes.

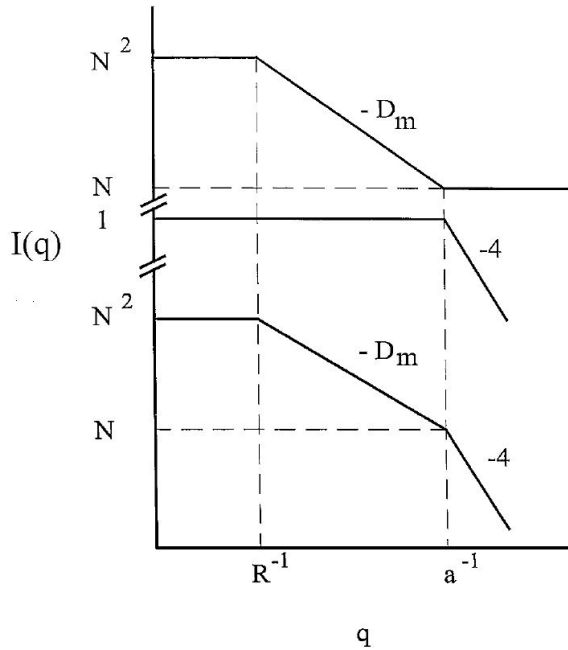


Figure 1.10: Generic depiction of scattering from a mass fractal aggregate of radius R with a fractal dimension D_m made up of spherical, smooth surfaced monomers of radius a . Upper curve is for point particles, second curve is for spherical particles, lowest curve is the product of these. Extracted from [Sorensen, 2001]

1.2.4.2 Clusters and rheology

Once all the previous parameters are identified, some authors tried to relate these microscopic structures to rheological properties. This is a general microscopic to macroscopic approach that is used for various types of fluid systems. For example, in [Palierne, 1990], the dynamic viscoelastic modulus of mixtures of polymers is given according to the dynamic viscoelastic modulus of the matrix, the surface tension between the two phases and the radius of the droplets, or, in [Shah, 2003], the viscoelasticity of the flocculated gels is investigated. Some of the founding paper of these approaches are [Kantor, 1984a; Kantor, 1984b]. They consider the fractal cluster as mechanical structures which can undergo a certain force or bending moment. These papers were followed by a series of models relating the storage modulus to the particle volume fraction through an exponent depending on the fractal dimension, the dimension of the euclidean space and the chemical dimension (see [Herrmann, 1984; Herrmann, 1988]). The starting point is presented by [Shih, 1990] where the relationships are

$$G' \propto \phi^\mu \quad (1.44)$$

$$\gamma_y \propto \phi^\zeta \quad (1.45)$$

$$\mu = \frac{1}{\dim - D} \begin{cases} \dim + d & \text{strong-link regime} \\ \dim - 2 & \text{weak-link regime} \end{cases} \quad (1.46)$$

$$\zeta = \frac{1}{\dim - D} \begin{cases} -1 - d & \text{strong-link regime} \\ 1 & \text{weak-link regime} \end{cases} \quad (1.47)$$

with G' the storage modulus, γ_y the limit of linearity strain, ϕ the particle volume fraction, D the fractal dimension, \dim the dimension of the euclidean space and d the dimension of the elastic back-bone. The typical microstructure used for the construction of the rheological properties is illustrated on figure 1.13 with a certain cluster size composed by particles of a certain size. The reasoning of such demonstrations is to find scaling relations from microscopic mechanical properties to the macroscopic scale. The up-scaling study is carried out with the consideration of springs in series and/or in parallel assuming some distorted path of mechanical stress bearing chain and crystalline-like packing of the clusters in the systems to create the percolated network. The strong-link regime and the weak-link regime, see figure 1.13, refer to two types of mechanical structure where, respectively, the inside of the clusters is weaker than the links between the clusters thus the internal distorted path should appear. Or, the inside of the clusters is stronger than the links between the clusters thus only the connection between the clusters dominates the elastic rheology [Shih, 1990; Wu, 2001]. The common assumptions of all these models is that the particle volume fraction ϕ is related to the cluster size ℓ , the particle size a and the fractal dimension D of the clusters through $\phi = (\ell/a)^{D-\dim}$. This assumption comes from the fact that the effective volume fraction of the clusters in the system is computed and the number of clusters in the system is decomposed by the number of particles divided by the number of particles for each cluster which is equal to $(\ell/a)^D$ due to the fractal nature of the clusters. Hence, the effective volume fraction ϕ_{eff} of the clusters in the system is expressed as

$$\phi_{\text{eff}} = \phi \frac{\ell^{\dim}}{a^{\dim}} \left(\frac{\ell}{a}\right)^{-D} \quad (1.48)$$

with ϕ the particle volume fraction, ℓ^{\dim} the volume of the clusters, a^{\dim} the volume of the particles and $(\ell/a)^{-D}$ the inverse of the number of particles per cluster. Finally, assuming that the fractal clusters fill the space as a spanning network this effective volume fraction is equal to unity and the previous relationship is recovered. Another common assumptions of these papers is that the scaling between the macroscopic stiffness K and the microscopic stiffness of an element of a network k is $K = (L/\ell)^{\dim-2} k$ with L the size of the network, ℓ the size of the element and \dim the dimension of the network. As sketched on figure 1.14, in a crystalline network of dimension \dim solicited according one spe-

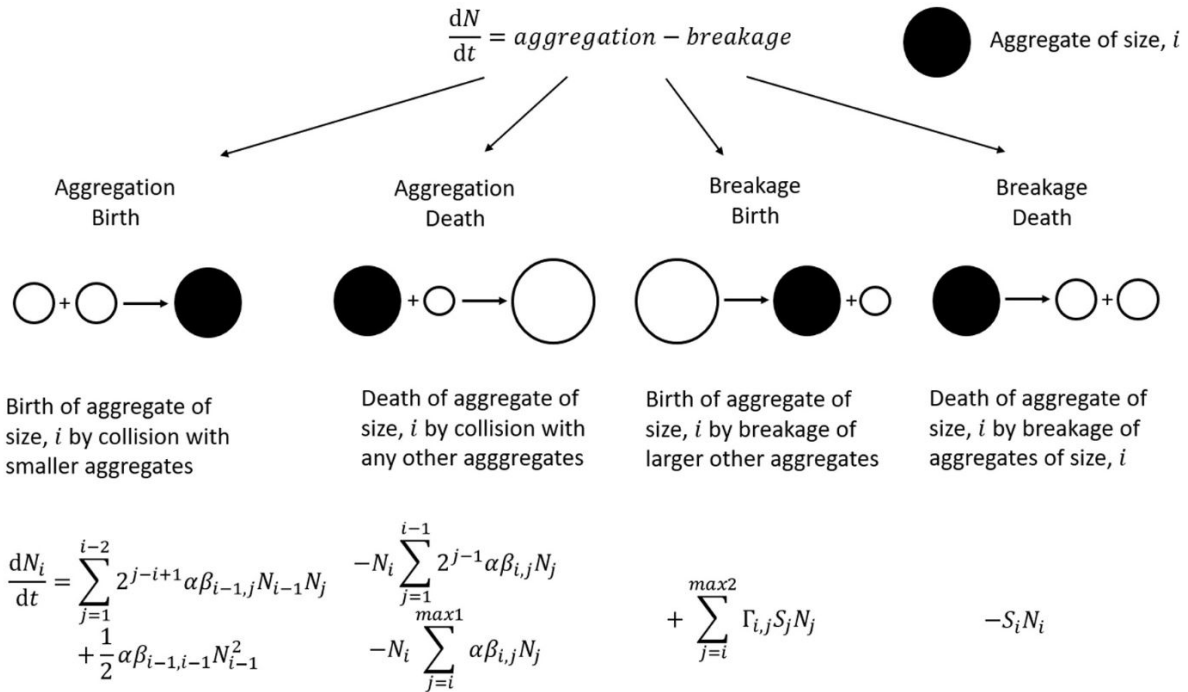


Figure 1.11: Dynamics of aggregation and breakage for discretised population balance, adapted from [Biggs, 2002; Jeldres, 2018]

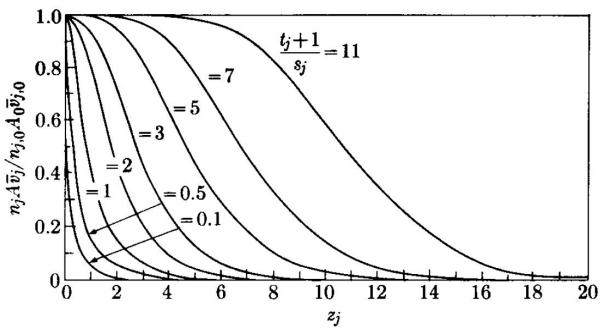


Figure 1.12: The ratio of the number flux of droplets of kind j to its value at $x = 0$ as a function of the dimensionless distance z_j for various values of $(t_j + 1) / s_j$. Extracted from [Williams, 1985]

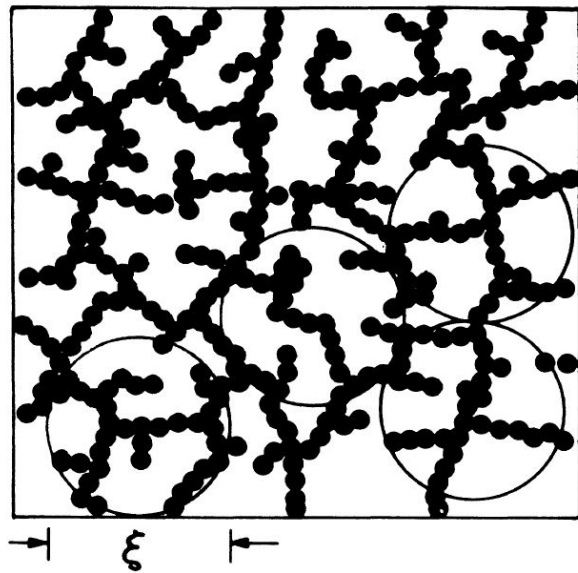


Figure 1.13: Schematic structure of a colloidal gel. The circles indicate fractal clusters of size ξ . The regions between the flocs are regarded as links. Extracted from [Shih, 1990]

cific direction for stretching, along this axis, the springs are summed in series thus the effective stiffness of each chain is the inverse of the sum of the inverse of each element stiffness k , which corresponds to the inner sum of each case on [figure 1.14](#) and is equal to $k\ell/L$. On the other axis, the chains are not aligned to the deformation thus not playing a role. Finally, to get the overall macroscopic stiffness, one needs to sum all the chains aligned to the axis of the deformation which are parallel to each other. There is the same amount of chains in parallel in each direction than the amount of element in each chain, that is to say L/ℓ . Hence, there are $\text{dim} - 1$ directions to sum the stiffnesses of parallel chains, which boils down to $K = (L/\ell)^{\text{dim}-2} k$. Usual results plotting the storage modulus and the linearity limit strain as a function of the particle volume fraction are presented on [figure 1.15](#), which is also used most of the times to measure the fractal dimension and/or the dimension of the elastic back-bone. A limit of this hypothesis is highlighted in [[Gravelle, 2021](#); [Tang, 2008](#); [Bouthier, 2022](#)] where the clusters may not be space-filling as in a crystal but may show some holes and/or heterogeneous distribution in the percolated system. Addressing this issue may help to reconcile theoretical models with experimental and numerical data. Some refinements were proposed by [[Mellema, 2002](#); [Kim, 2018](#); [Kim, 2020](#)] to take into account the difference between stretching and bending, by [[Wu, 2001](#)] to take into account the bridging between the strong-link regime and the weak-link one, by [[Potanin, 1995](#); [Rooij, 1993](#)] to recover also the viscous behaviour of the gel, by [[Marangoni, 2000](#); [Roldughin, 2003](#); [Tang, 2006](#)] to get the multiplicative factor in the proportional relation, by [[Tang, 2008](#); [Gravelle, 2021](#)] using a heterogeneous stress distribution in the system, by [[Bouthier, 2022](#)]⁴ to extend to a double fractal structure or multiple levels fractal structures or, by [[Dagès, 2022](#)] to take into account the interpenetration of clusters. A summary of main existing models with their exponent is reported in [table 1.4](#) to help the reader to navigate amongst those models. A deeper discussion is proposed by [[Mewis, 2012](#); [Wagner, 2021](#)]. Other articles preferred to consider the elasticity arising from a critical phenomenon related to percolation as in [[Stauffer, 2003](#)].

There exist other types of models like proposed by [[Genovese, 2012](#); [Møller, 2008](#)] that modified the model from [[Krieger, 1972](#); [Krieger, 1959](#)] to take into account the effective volume fraction of clusters into a suspension, the one proposed by [[Gisler, 1999](#)] to predict strain hardening from fractal clusters, the concept proposed by [[Whitaker, 2019](#)] to consider locally glassy clusters.

During years, the experimental measurements of both the rheology and the microscopic structure were difficult to carry on. Nevertheless, some recent paper like

[[Gibaud, 2020a](#); [Dagès, 2021](#); [Richards, 2017](#); [Hipp, 2021](#); [Wang, 2022](#)] for carbon-black particle suspensions, [[Keshavarz, 2021](#)] for aluminosilicate gels, [[Ben Messaoud, 2020](#); [Patel, 2022](#)] for hydrogels, [[Räntzsch, 2019](#)] for polymers or [[Kádár, 2021](#)] for liquid crystals tried to carry both measurement simultaneously and may begin to discover disagreement in the previous theories.

Other insights of the same problem have been tackled through numerical experiments. For instance, part of the literature used molecular dynamics, modelling coarse grained suspension of particles, starting from the model in [[Colombo, 2013](#)] assuming the boundary conditions described in [[Lees, 1972](#)]. This model has been studied according to different conditions with load curves in [[Colombo, 2014b](#)], a variation of the volume fraction [[Bouziid, 2018a](#)], assessing efficiently the frequency sweep with a fractional model in [[Bouziid, 2018b](#)], applying thermal fluctuations in [[Bouziid, 2017](#)], covering the whole range of parameters in [[Bantawa, 2021b](#); [Bantawa, 2021a](#)], tuning the preparation protocol in [[Colombo, 2014a](#)], having multiple components in [[Ferreiro-Córdova, 2020](#); [Vereroudakis, 2020](#); [Varrato, 2012](#)], studying the non affine rearrangements in [[Mosayebi, 2014](#)], and at last, investigating disease mutation [[Feng, 2018](#)]. Another part of the literature is using a probabilistic mesoscopic model like proposed by [[Sollich, 1997](#); [Sollich, 1998](#); [Hébraud, 1998](#)]. A simplified refinement of this model is proposed by [[Fielding, 2020](#)] and derivation around this model exists in [[Bocquet, 2009](#); [Mansard, 2011](#)]. In general, soft gels modelling has been addressed in [[Bouziid, 2019](#); [Del Gado, 2021](#); [Allen, 2017](#); [Chandler, 1987](#); [Giordano, 2006](#); [Frenkel, 2002](#); [Press, 2007](#)].

Orientation of the microstructure may also play a role in the rheological response of certain materials as presented in [[MacKintosh, 1991](#); [Lubensky, 1993](#); [Broedersz, 2011](#)] or in [[Shivers, 2020](#); [Picu, 2011](#); [van Dillen, 2008](#); [Vernerey, 2021](#)] with fibers. Some papers also used beam network models [[Hosseini, 2021](#)] to investigate fracture with a hierarchical microstructure.

After having looked at how microstructures influence the rheology, the reciprocal influence of external solicitation on the microstructure is tackled.

To summarise, the relationship between the clusters and the rheology has been addressed multiple times in the literature and in History. The most famous models, which are some of the simplest ones, are based on geometric arguments to scale microscopic mechanical properties to the macroscopic scale in terms of rheological quantities. Even if these demonstrations rely on questionable assumptions, it seems there is no satisfying counter-offer in terms of simplicity and applicability in experiments. The other models rely on complex calculations which need, most of the times, numerical simulations to properly handle the results and compare it to

⁴We will come back to this topic in [section 3.3](#)

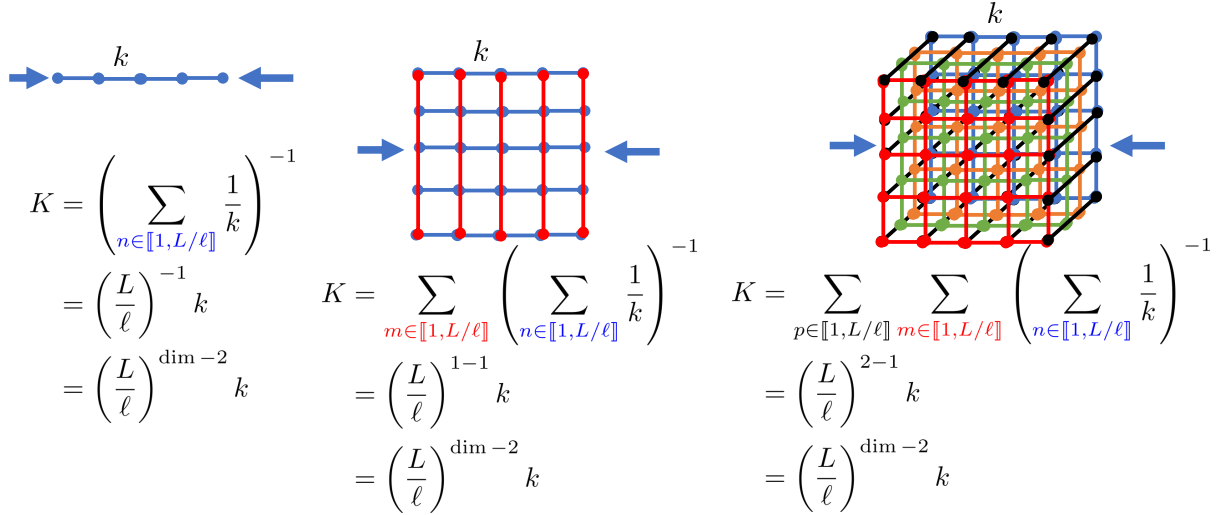
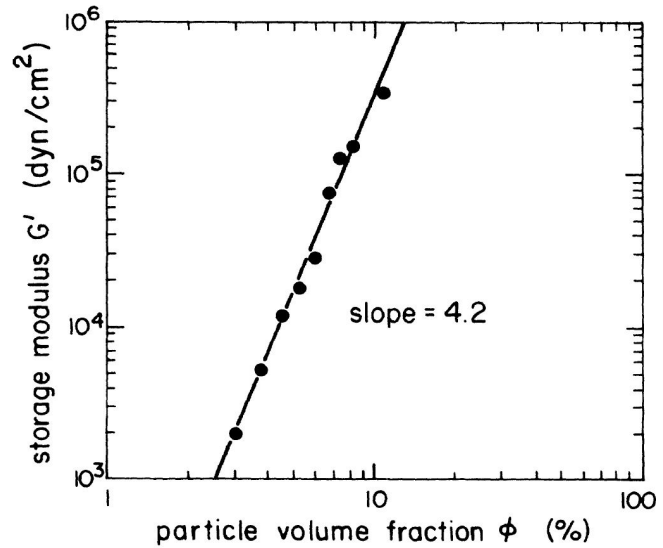
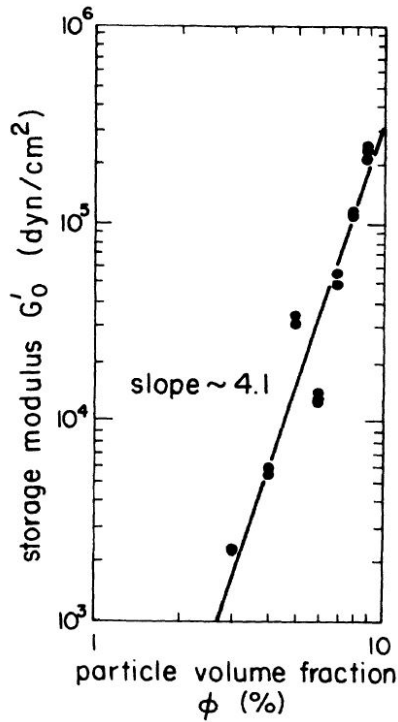


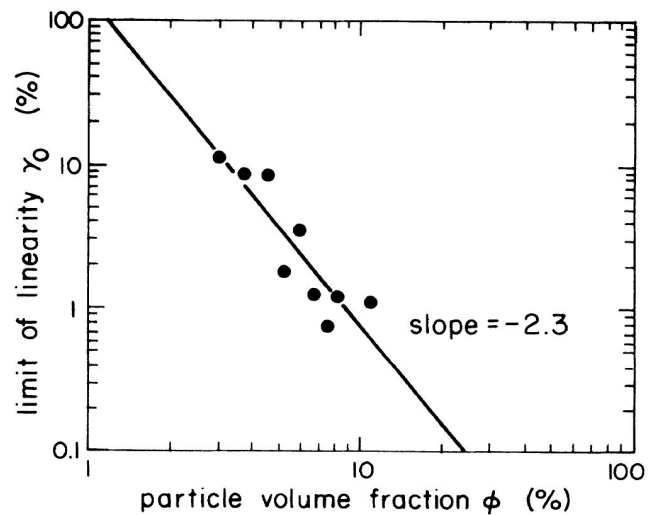
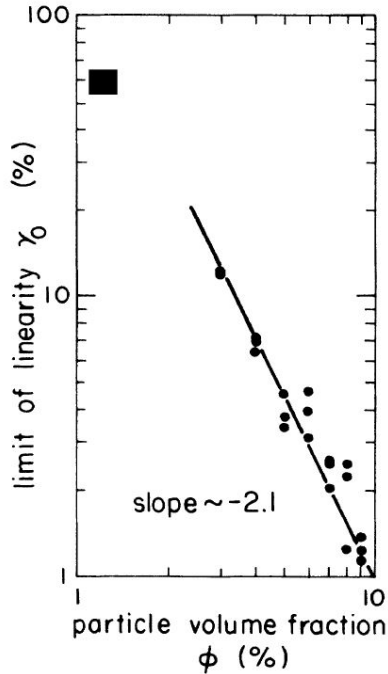
Figure 1.14: Sketch to explain the scaling relationship between the macroscopic stiffness K and the microscopic stiffness k for a network of size L with an element size l and a dimension dim . The arrows represent the stretching/compressing direction.

Source	Condition	Exponent for G'	Exponent for γ_y	Exponent for σ_y
[Shih, 1990]	Weak-link regime	$\text{dim} - 2$	1	$\text{dim} - 1$
[Shih, 1990]	Strong-link regime	$\text{dim} + d$	$-1 - d$	$\text{dim} - 1$
[Mellema, 2002]	Transition between bending and stretching	$\text{dim} - 2 + 2\epsilon + d$	$-2\epsilon - d + 1$	$\text{dim} - 1$
[Wu, 2001]	Transition between strong-link and weak-link regime	$\text{dim} - 2 + \alpha(2 + d)$	$-\alpha(2 + d) + 1$	$\text{dim} - 1$
[Bouthier, 2022]	Transition between all the regimes	$\text{dim} - 2 + \alpha(2\epsilon + d)$	$-\alpha(2\epsilon + d) + 1$	$\text{dim} - 1$

Table 1.4: Comparison of models relating the storage modulus G' , the limit of linearity strain γ_y , and the yield stress σ_y . The exponents reported in the table are the exponent of the $\phi^{\frac{1}{\text{dim}-D}} = \ell/a$ with ϕ the particle volume fraction, dim the dimension of the euclidean space, D the fractal dimension, ℓ the size of the cluster and a the particle size. Here above, $\epsilon \in [0, 1]$ with $\epsilon = 0$ corresponds to the stretching regime and $\epsilon = 1$ corresponds to the bending regime, then, $\alpha \in [0, 1]$ with $\alpha = 0$ corresponds to the weak-link regime and $\alpha = 1$ corresponds to the strong-link regime. Adapted from [Bouthier, 2022].



(a) Storage modulus in the linear region as a function of Catapal particle concentration at pH = 5.5. (b) Storage modulus in the linear region as a function of the Dispal particle concentration at electrolyte concentration 0.244mol.



(c) Limit of linearity as a function of Catapal particle concentration at pH = 5.5. (d) Limit of linearity as a function of Dispal particle concentration at electrolyte concentration 0.244mol.

Figure 1.15: Storage modulus and limit of linearity strain as a function of the particle volume fraction for Catapal and Dispal particles. Extracted from [Shih, 1990]

experiments. In short, the geometrical models are the least worst models to try to understand the scaling of microscopic properties to the macroscopic scale.

1.2.5 How the clusters are influenced externally

1.2.5.1 Generalities about clusters under stress

The evolution of microstructures under external solicitation is at the core of modern rheology to predict consistently the behaviour of a system. Several experimental works have demonstrated this influence. For example, [Gibaud, 2020a; Dagès, 2021] showed that applying ultrasound on carbon-black particle suspensions may change the microstructure (flocs, clusters, ...), [Hengl, 2014] applied ultrasound on colloidal suspension for filtration, [Sehgal, 2019; Lin, 2016] applied ultrasound on shear thickening fluids to tune them, [Koumakis, 2015] used shear to tune the colloidal gel, [Nguyen, 2011; Mondragon, 2012] showed that applying ultrasound on a silica suspension may change the size of the clusters of particles, [Mohraz, 2005; Selomulya, 2001; Selomulya, 2002; Massaro, 2020; Lorenzo, 2022] disaggregated fractal gels in shear flow and [Schilde, 2011; Sauter, 2008] demonstrated that the amount of energy provided to a system may decrease the size of the clusters. Parallel studies even exist with collision cascades involving fractal analysis in [Wallace, 2017]. To have more general insights about the aggregation of particles in fractal structures, the reader is invited to read [Berka, 2005] where Kaolinite aggregates are studied for their aggregation kinetics and their final structure, [Waite, 2001] where alumina particles are studied, [Lin, 1989; Lin, 1990b; Lin, 1990a] where universal behaviour of diffusion-limited aggregated forming fractal clusters are presented, [Wu, 2013] where variation of the fractal dimension according to the particle size is investigated, [Carpinetti, 1990] where aggregation of polystyrene is studied, [Tirado-Miranda, 1999] where finite binding energies are investigated to study the growth mechanism of fractal structures, [Jungblut, 2019] where diffusion limited aggregation and reaction limited aggregation are considered, [Meakin, 1992] where aggregation kinetics is studied, [Gauer, 2009] where surface properties and their effect on coalescence and aggregation kinetics of elastomer colloids is investigated, [Sztucki, 2007] where soot particles produced by flames aggregate in somewhat fractal clusters, [Kim, 2004] where soot fractal superaggregates in laminar diffusion flames seem to rely on a universal phenomenon, [Hurd, 1988] where silica aggregates grow in fractal structures under a flame, [Carpinetti, 1992] where a spinodal-type fractal aggregation is reported, [Kusters, 1991] where particles aggregate under turbulence effects, [Hoekstra, 2003] where a two-dimensional suspension aggregate

anisotropically and reversibly due to the effect of a flow and [Hoekstra, 2005] where a sticky spheres dispersion forms a microstructure induced by shear flow.

To give some comments about the previous paragraph, aggregation of particles is rather universal in the sense that it occurs in many different conditions with various types of materials. Trying to find an abstract universal framework can be a key to properly catch relevant phenomena which can then be applied on several cases like the radioactive sludges of this manuscript.

Also, several papers studied the aggregation of particles on an interface. For instance, [Kralchevsky, 2001b] studied how an undulated contact line of particles with a fluid interface may give some insights about the relationship between capillarity and rheology, [Kralchevsky, 2001a] investigated the construction of layers of colloid particles through capillary interaction, [Kralchevsky, 2001c] reviewed the particles at fluid interfaces with their mutual interaction, [Vassileva, 2005] calculated the forces between spherical particles floating at a liquid-liquid interface, [Knoll, 2018] studied the modifications of crystallisation by particles aggregation and the hierarchical order, [Vella, 2005] investigated the "Cheerios" effect comparing buoyancy effect with capillary interaction, [Madihalla, 2009] studied ellipsoidal particles and their self-assembly at interfaces, [Danov, 2010] studied theoretically the capillary forces between particles at an interface and [Dalbe, 2011] investigated the aggregation of frictional particles through capillary interactions.

As before, the universality of aggregation of particles is a key aspect that invites us to understand further the global relationships that can be extracted to manage other situations where similar conditions are met.

These aggregated structures may be interestingly disaggregated in a 2D geometry. For example, [Barman, 2016] looked at the link between microstructure, capillarity and interfacial viscoelasticity, [Krzysko, 2020] studied the correlation between particles interaction and particles shape in shear induced aggregation and fragmentation and [Bossler, 2018] used interfacial rheology and confocal microscopy to characterise fractal capillary structures. Ramified structures can be identified in [Okubo, 1995]. Some general thoughts about colloidal suspensions in out-of-equilibrium system are presented in [Aranson, 2013]. Some direct visualizations of fractal clusters are proposed by [Masschaele, 2009; Villa, 2018; Stamou, 2000]. For example, the aggregation of particles in fractal clusters is reported on [figure 1.16](#) where the ramified structures grow with time.

The goal of the previous paragraph is to highlight the universality of the approach. The range of energies covers from few units of $k_B T$ in the case of colloidal suspensions to approximately $0.1 \mu\text{J}$ in the case of capillary interactions. It covers many types of systems which shows the interest to focus on this field. In the case of the ra-

dioactive sludges, there is aggregation due to a chemical potential between the particles coming from the chemical composition of the liquid effluents. This aggregation process gives rise to a certain size population distribution in the material which can be influenced according to external solicitation. The investigation of the predominant microscopic behaviour in the constitution of such material is a key to comfortably predict its evolution according to certain conditions.

1.2.5.2 Attempts to model the coupling between aggregation and disaggregation

Several papers have tried to bring an understanding of this influence of the macroscopic conditions on the microstructures. One fundamental article in the field is [Wessel, 1992]. It proposed a relationship between the cluster size and the shear rate applied to the suspension of particles. Other papers like [Snabre, 1996; Barnes, 1999] proposed some phenomenological relations between the cluster's size and an external shear rate or shear stress. Following a review in [Kimbonguila Mannonou, 2014], it has been proposed to understand the equilibrium size of clusters through a balance between disaggregating forces and aggregating forces. Precisely, the consideration of the adhesion number like in [Ruan, 2020; Ruan, 2021; Yao, 2021] or the Mason number in [Jamali, 2020; Jamali, 2019a; Varga, 2019] may bring a power law relationship between the size of the cluster and one of these dimensionless number. An example of relationship is given by

$$\frac{\ell}{a} = \text{Ad}^m \quad (1.49)$$

with ℓ the size of the clusters, a the size of the particles, $\text{Ad} = U/\sigma a \delta^2$ the adhesion number which weights the relative importance of the attractive forces Ua/δ^2 to the disaggregating forces σa^2 and $m \in [0.2, 0.8]$ the exponent. The competition between attractive forces and disaggregating forces is reported on [figure 1.17](#) where starting from an unknown initial distribution of size, the different clusters tend to change theirs to get closer to the most stable size emphasising an equilibrium between aggregating forces and disaggregating forces⁵. This approach can actually be extended to other previous articles which demonstrated this power law relationship. For instance, from an experimental perspective, [Hunter, 1980] studied the flow behavior of colloidal sols, [Sonntag, 1986; Sonntag, 1987a; Sonntag, 1987b] investigated the structure and the breakup of flocs subjected to fluid stresses, [Brakalov, 1987] studied the connection between the orthokinetic coagulation capture efficiency and the maximum size of the aggregates, [Torres, 1991a] investigated the structure and the coagulation of

polystyrene colloids under shear, [Torres, 1991b] simulated the coagulation under viscous flows and [Harshe, 2011] studied the breakage and the restructuring of open and dense aggregates. Then, from a theoretical perspective, [Potanin, 1991] studied the mechanism of aggregation of suspensions in shear flows and [Potanin, 1992] investigated the aggregation of colloids. Also, from a numerical perspective, [Potanin, 1996] simulated a fractal model to consolidate weak aggregates in colloidal suspensions, [Higashitani, 1998] simulated in two dimensions the breakup process of aggregates in shear and elongational flow, [Higashitani, 2001] studied the breakup of large aggregates in viscous flow and [Eggersdorfer, 2010] investigated the fragmentation and the restructuring of soft aggregates under shear. [Zaccone, 2009a; Xie, 2010] even proposed a mixed approach with experiments and theory to break dense colloidal aggregates under hydrodynamic stress giving an expression for m of the form

$$m = \frac{2}{(\text{dim} - D) \left(2(\zeta + 1) + (\text{dim} - D)^{-1} \right)} \quad (1.50)$$

where $\zeta \approx 3.8$ is the exponent relating the mean coordination number to the particle volume fraction in [Alexander, 1998]. Also, [Conchúir, 2013] proposed a similar approach for flow-induced breakup of biomolecular and colloidal aggregates proposing the following form for the exponent m

$$m = \frac{1}{D - 2.06491D - 0.0180344(3 - D)^{-1} + 4.98585} \quad (1.51)$$

The relationship above may be tackled through the adhesion of particles as described in [Marshall, 2014] for the general adhesion of particles with or without interaction, in [Barthel, 2008] for the adhesive elastic constants of the JKR model and others, in [Krijt, 2014] to compute the rolling friction of adhesive microspheres and in [Gilbert, 2021] where contacts in rheology are studied. Other papers tried investigating clusters under shear flow like [Saxena, 2022] in numerical simulation or [Varga, 2019] in experiments with numerical simulations. An example of results is given in [figure 1.18](#) where the cluster size under certain shear flows is estimated according to the adhesion number and highlights the power-law relationship. Moreover, [table 1.5](#) displays the different exponents of the power-law relationship existing in the literature depending on the fractal dimension. There is no clear explanation of the values of exponents depending on the experimental conditions but they fall in the same range.

This power law relationship can also be extracted from different arguments than mechanical balance. For instance, some papers initiated by [Sorensen, 1987] proposed the use of a coagulation-fragmentation equation

⁵We will come back to that topic in [section 2.2](#)

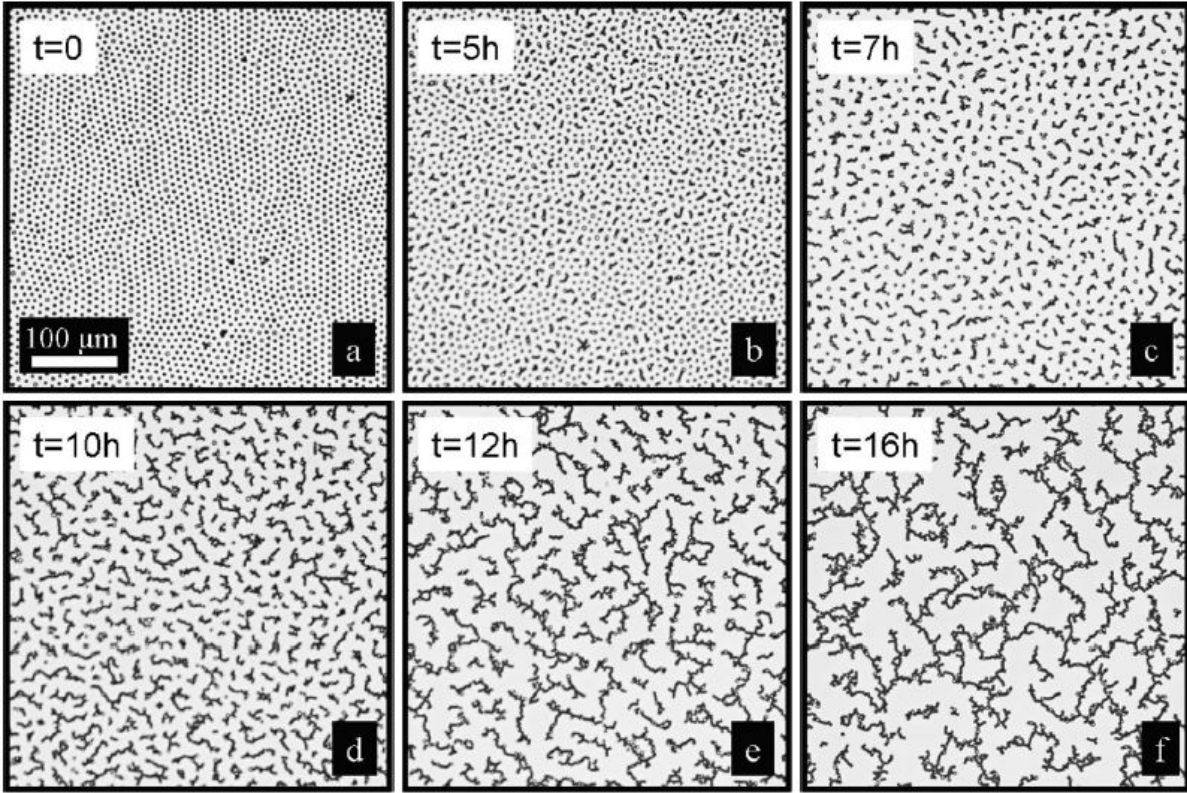


Figure 1.16: Microscopy images showing six steps to complete network percolation of a colloidal network. Snapshot (a) corresponds to the initial crystal structure, just after adding the salt. Images (b)–(e) correspond to the fractal regime, where cluster-cluster aggregation dominates. Snapshot (f) shows the structure when the first percolating backbone was formed. Notice the presence of small aggregates and single particles coexisting with a large structure. The overall surface coverage is approximately 0.1; the time scales refer to the time after the addition of salt and surfactant. Extracted from [Masschaele, 2009]

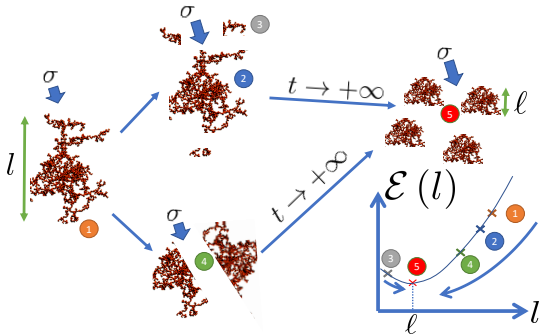


Figure 1.17: Sketch of the disaggregation and reaggregation processes under a uniform external stress σ . The numbers represent different sizes of aggregates with different levels of energy. The aggregates are disaggregating and reaggregating according to the stress solicitation. Transition from state 1 to states 2 and 3 corresponds to a “fragile” rupture, while transition from state 1 to state 4 is an “erosion” process. Extracted from [Bouthier, 2023a].

to find the equilibrium size. The relation is formulated as follows

$$f(t, x) = \frac{1}{s^2(t)} \varphi\left(\frac{x}{s(t)}\right) \quad (1.52)$$

$$\lim_{t \rightarrow +\infty} s(t) = \left(N \frac{A}{B}\right)^{\frac{1}{\chi+2-\lambda}} \quad (1.53)$$

$$A = \iint_{\mathbb{R}_+^2} xy \varphi(x) \varphi(y) K(x, y) dx dy \quad (1.54)$$

$$B = \iint_{\mathbb{R}_+^2} xy \varphi(x+y) F(x, y) dx dy \quad (1.55)$$

with f the probability distribution function depending on time t and on size x , s the average size of the clusters $s(t) = \int_{\mathbb{R}_+} x^2 f(t, x) dx$, φ a function on \mathbb{R}_+ verifying $\int_{\mathbb{R}_+} x \varphi(x) dx = N$ the number of particles, K the aggregation kernel with a homogeneity coefficient λ and F the disaggregation kernel with a homogeneity coefficient χ . As a reminder, a homogeneity coefficient $\theta \in \mathbb{R}$ of a function H verifies for all $(x, y, z) \in \mathbb{R}_+^3$, $H(zx, zy) = z^\theta H(x, y)$. Even if other pa-

Reference	m	D	Type of study
[Hunter, 1980]	0.37-0.47	1.8	E
[Sonntag, 1986; Sonntag, 1987a; Sonntag, 1987b]	0.35	2.2	E
[Brakalov, 1987]	0.58	1.8	E
[Torres, 1991a; Torres, 1991b]	0.50	1.8	E+N
[Harshe, 2011]	0.35	1.7	E+N
[Potanin, 1991; Potanin, 1992]	0.23-0.49	1.8	T
[Wessel, 1992]	0.33	1.8	T
[Potanin, 1996]	0.38-0.56	1.8-2.6	N
[Higashitani, 1998]	-	1.8	N
[Eggersdorfer, 2010]	0.35	1.8	N
[Kimbonguila Manounou, 2014]	0.34	1.8	N
[Zaccone, 2009a]	0.52	2.7	T+E
[Conchúir, 2013]	0.49	2.7	T+E
[Xie, 2010]	2.4	0.31	T+N
	2.47	0.38	N
	2.44	0.40	N
	2.48	0.35	N
[Higashitani, 2001]	2.46	0.38	N
	2.45	0.39	N
	2.43	0.43	N
	1.74	0.42	N
	2.31	0.38	N
	0.25	2.48	N
	0.25	2.49	N
	0.25	2.49	N
	0.25	2.47	N
	0.27	2.47	N
	0.27	2.54	N
	0.26	2.53	N
	0.26	2.54	N
	0.23	2.53	N
	0.25	2.52	N
	0.27	2.54	N
	0.26	2.53	N
	0.23	2.55	N
	0.25	2.57	N
	0.26	2.53	N
	0.23	2.57	N
	0.25	2.58	N
	0.27	2.52	N
	0.25	2.57	N
	0.23	2.58	N
	0.25	2.57	N
	0.27	2.54	N
	0.25	2.55	N
	0.22	2.63	N
	0.30	2.28	N
[Ruan, 2020]	0.29	2.38	N
	0.29	2.43	N
	0.28	2.51	N
	0.27	2.36	N
	0.27	2.38	N
	0.26	2.43	N
	0.28	2.37	N
	0.28	2.41	N
	0.28	2.40	N
	0.26	2.43	N
	0.28	2.54	N
	0.26	2.49	N
	0.27	2.47	N
	0.28	2.58	N
	0.26	2.48	N
	0.27	2.44	N
	0.26	2.46	N
	0.28	2.49	N
	0.25	2.65	N
	0.26	2.57	N
	0.25	2.52	N
	0.36	1.76	N
	0.25	2.60	N
	0.25	2.71	N
	0.24	2.64	N
	0.26	2.66	N
	0.24	2.72	N

Table 1.5: Comparison of scaling laws exponent m with previous studies. "E" means experimental, "N" means numerical and "T" means theoretical. Adapted from [Kimbonguila Manounou, 2014; Bouthier, 2023a]

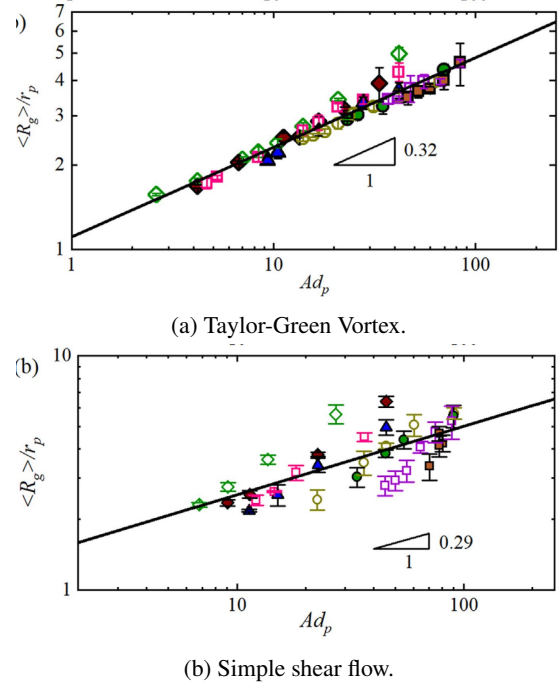


Figure 1.18: Gyration radius of agglomerate at the quasi-steady state as functions of the particle adhesion parameter Ad_p for two different types of flows. Extracted from [Ruan, 2020]

pers tackled the issue of physical impact of this kind equation like [Spicer, 1996] with the steady-state particle size distribution, [Barthelmes, 2003] with the viscosity and the particle size distribution under shear-induced coagulation-fragmentation or [Pratsinis, 1998] in the case of flame aerosol of ceramic powders, the recent studies of this kind of model are rather mathematical in the sense of the existence and/or the uniqueness of the solution according to different conditions (type of aggregation, type of disaggregation, initial conditions, ...). Perfect examples of this kind of study are [Banasiak, 2020a; Banasiak, 2020b] with theoretical considerations with semi-groups framework, [Fornari, 2020] with the nucleation of prion-like neurodegenerative proteins in the brain, [Stadnichuk, 2015] with numerical methods to find the steady-state solution of the equation, [Morbidelli,] in a form of a course of the study of aggregation kinetics and [Wattis, 2006] with general solutions of coagulation-fragmentation equations with simple mathematical form kernels. The construction of this model input functions may come from physical arguments like in [Zaccone, 2009b] in the case of shear-induced reaction limited aggregation in brownian particles suspensions, in [Blandin, 2005] in the case of salicylic acid for their agglomeration, in [Rotstein, 2015] trying to build phenomenological model for aggregation and fragmentation processes, in [Thomas, 1999] reviewing the flocculation modelling or [Jarvis, 2005] reviewing the flocc

strength and breakage, but sometimes lack a bit of physical meaning and satisfy mostly simple forms with easiness of resolution.

1.2.6 About dimensionality

Following the theorem proposed by [Buckingham, 1914; Buckingham, 1915b; Buckingham, 1915a], the use of dimensionless relationships is an objective of simplifications. It brings most of the times, simpler relationships that emphasizes reciprocal dependence between certain variables or parameters. In general, dimensionless numbers are built as a ratio of two quantities which should be weighted against each other in order to decide whether they are comparable or one is negligible/dominant compared to the other. Here is below a list of famous dimensionless numbers used to describe relationships between variables. The description of each dimensionless number is arbitrary in the choice of the quantities compared to each other. The interested reader is invited to apply a particular attention when reporting each number into her/his context.

- The Bingham number Bm is defined as

$$Bm = \frac{\sigma_y L}{\eta u} \quad (1.56)$$

with σ_y the yield stress, L a characteristic length scale, η the dynamic viscosity and u the flow speed. The Bingham number is the ratio of yield stress to the viscous stress. A study of a relative viscosity depending on the Bingham number is presented in figure 1.21.

- The Deborah number De is defined as

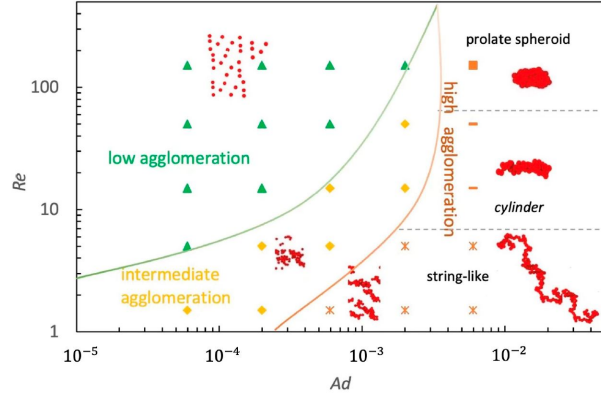
$$De = \frac{t_c}{t_p} \quad (1.57)$$

with t_c the relaxation time and t_p the time of observation or of the process. The Deborah number is defined as the ratio of the time it takes for a material to adjust to applied stresses or deformations, and the characteristic time scale of an experiment or a computer simulation probing the response of the material. A study of channel flows proposed a phase diagram involving the Deborah number and is reported in figure 1.22.

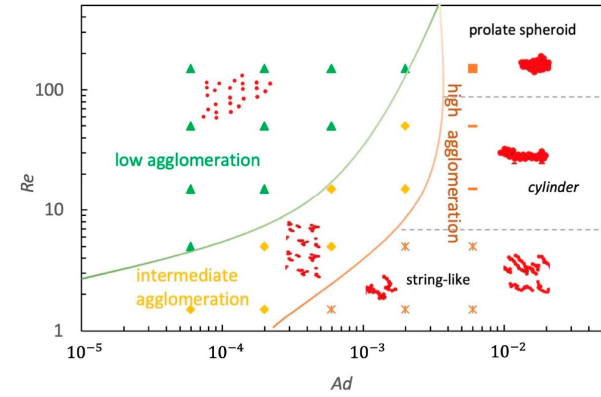
- The Mason number Mn is defined as

$$Mn = \frac{\sigma a \delta^2}{U} = \frac{\eta \dot{\epsilon} a \delta^2}{U} \quad (1.58)$$

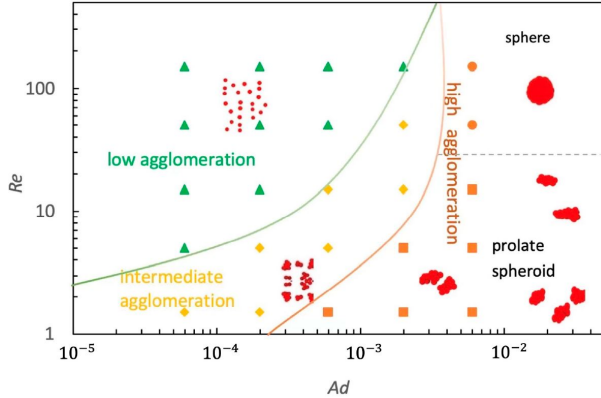
with $\sigma = \eta \dot{\epsilon}$ the shear stress, a the size of the particle, δ the distance of interaction of the interaction potential between the particles, U the depth of the interaction potential well between the particles. It



(a) Particle volume fraction 4.2% with the the JKR model



(b) Particle volume fraction 2.4% with the the JKR model



(c) Particle volume fraction 4.2% with the DMT model

Figure 1.19: Agglomeration regime maps. Phase diagram illustrating the observed cases as a function of the Reynolds number Re and the adhesion number Ad at different solid volume fractions and different models. Extracted from [Qian, 2022].

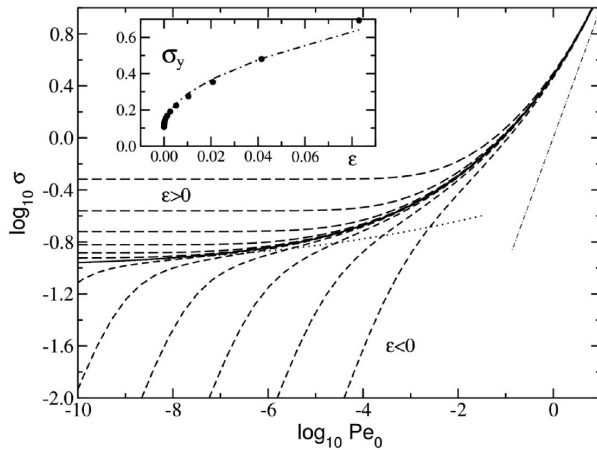


Figure 1.20: Flow curves predicted for a range of temperatures T across the mode-coupling critical temperature T_c ; $\epsilon = T_c - T$ is the distance to the critical temperature, and the shear rate is rescaled by a microscopic time unit τ to form a Péclet number $Pe_0 = \dot{\gamma}\tau$. The inset shows the discontinuous emergence of the yield stress at T_c . Extracted from [Fuchs, 2003]

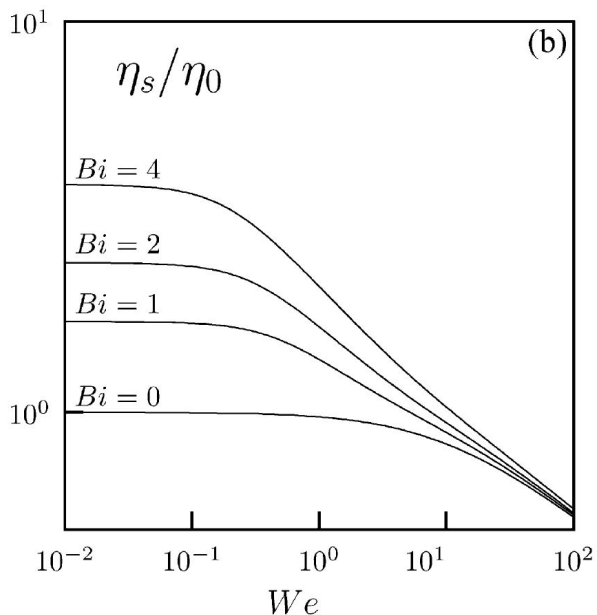
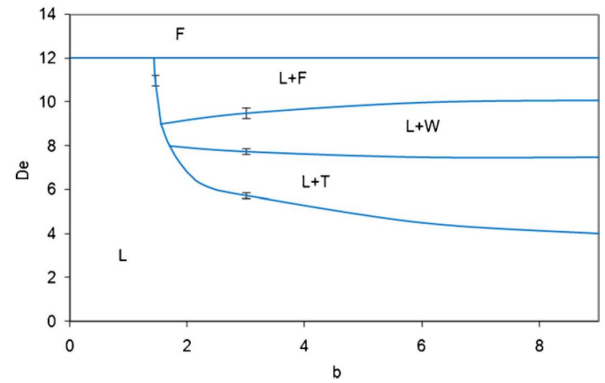
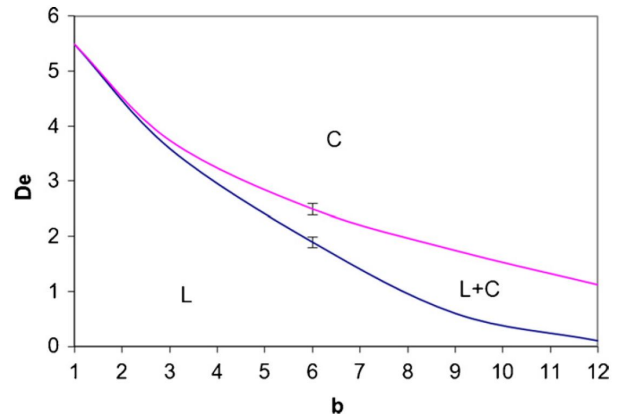


Figure 1.21: Relative steady shear viscosity as a function of the Weissenberg number $We = Wi$ for an upper convective derivative with no additional solvent viscosity for different Bingham numbers $Bi = Bm$. Extracted from [Saramito, 2007]



(a)



(b)

Figure 1.22: Rheological phase diagram in (De, b) -space for rectilinear, (a) wall-driven shear flow with oblate anchoring walls and (b) pressure-driven flow with oblate anchoring walls, $N = 5.35$, and $\beta_s = 0.01$. Regions in (De, b) -space are marked by which states are stable solutions. The possible states are logrolling (L), composite (C), tumbling (T), wagging (W), and flow-aligning (F). In regions where logrolling and inplane solutions are both stable, the initial state determines which state is obtained. The phase diagram is constructed through individual simulations, so error bars estimate the possible range for transition values. Extracted from [Green, 2009].

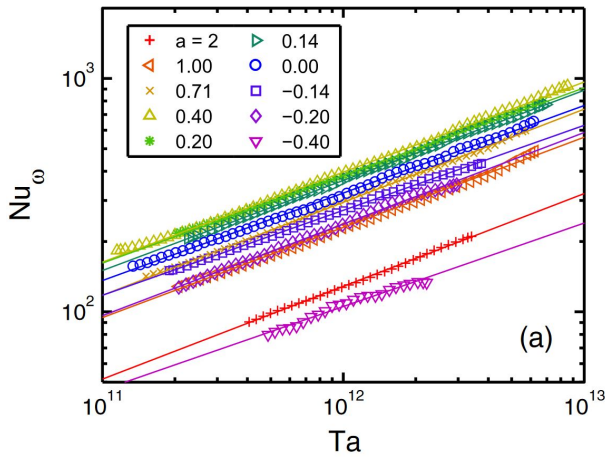


Figure 1.23: Nusselt number Nu_ω as a function of the Taylor number Ta for various a . A universal scaling $Nu_\omega \propto Ta^{0.38}$ is revealed. Extracted from [Gils, 2011].

is also possible to consider the inverse of the Mason number which is called the adhesion number $Ad = Mn^{-1}$. The Mason number is the ratio of the hydrodynamic force over the attractive force of the interaction potential. A study of aggregation and disaggregation of clusters under flow proposed a phase diagram involving the adhesion number and is reported on figure 1.19. Precisely, in [Qian, 2022], a numerical study of aggregation and disaggregation is carried out mapping a phase diagram in terms of the Reynolds number and the Adhesion number. This phase diagram shows a broad variety of cluster aggregations which clearly emphasize the fact that phenomena can be tackled from the angle of dimensionless number which characterises accurately certain conditions and helps to distinguish between various intricate variables.

- The Péclet number Pe is defined as

$$Pe = \frac{uL}{D} \quad (1.59)$$

with u the flow speed, L a characteristic length scale and D a diffusion coefficient (momentum, temperature, species, ...). The Péclet number is defined to be the ratio of the rate of advection of a physical quantity by the flow to the rate of diffusion of the same quantity driven by an appropriate gradient. A study of flow curves for different temperatures proposed an evolution according to the Péclet number and is reported on figure 1.20.

- The Reynolds number Re is defined as

$$Re = \frac{\rho u L}{\eta} = \frac{u L}{\nu} \quad (1.60)$$

with ρ the density of the fluid, u the flow speed, L a characteristic length scale, η the dynamic viscosity and ν the kinematic viscosity. The Reynolds number is the ratio of inertial forces to viscous forces and is fundamental in the description of the drag force on a sphere [Stokes, 1901], the boundary layer profile [Prandtl, 1904; Blasius, 1907] or the pressure loss in pipes [Colebrook, 1937]. A study of aggregation and disaggregation of clusters under flow proposed a phase diagram involving the Reynolds number and is reported on figure 1.19.

- The Taylor number Ta is defined as

$$Ta = \frac{\rho^2 \Omega^2 R_1 (R_2 - R_1)^3}{\eta^2} = \frac{\Omega^2 R_1 (R_2 - R_1)^3}{\nu^2} \quad (1.61)$$

with Ω the angular velocity between two concentric cylinders with an internal radius R_1 and an external radius R_2 , a density ρ , a dynamic viscosity η and a kinematic viscosity ν . The Taylor number is the ratio of the inertial forces over the viscous forces. It is particularly relevant in a Taylor-Couette flow in rheometers to avoid turbulence below $Ta_c = 1700$ [Andereck, 1986]. A study of momentum transport in a Taylor-Couette flow proposed an evolution of the Nusselt number as a function of the Taylor number and is reported on figure 1.23.

- The Weissenberg number Wi is defined as

$$Wi = \lambda \dot{\epsilon} \quad (1.62)$$

with λ a relaxation time and $\dot{\epsilon}$ the shear strain rate. The Weissenberg number compares the elastic forces to the viscous forces. A study of a relative viscosity depending on the Weissenberg number is presented in figure 1.21.

1.2.7 Open remaining questions

From this state of the art, there is a certain number of questions that remain to be answered. A non exhaustive list may be :

- How is it possible to consider a heterogeneous distribution of clusters in a system to overcome the crystalline structure described in figure 1.14? Is it possible with this change of structure to account for dissipative effects in terms of viscosity, loss modulus or plastic events?
- How sizes polydispersity of sizes may be integrated in the different models (scattering, rheology, ...) to take into account the spread of the distributions?

- How a macroscopic-microscopic strong coupling may be closed to properly study the interdependence of rheology and the microstructure?

1.3 Problematic

If we come back to the industrial problem, it is possible to formulate a problematic such as: "what are the main ingredients allowing to understand and predict the fluidification of certain materials under an external solicitation?". However, as it will be described afterwards, there is a broader perspective for this manuscript which tackles the previous issues but also a better understanding of certain phenomena in materials. Hence, the following problematic is proposed:

How microscopic structure, macroscopic behaviour and macroscopic environment are coupled in the case of suspension of particles to be able to influence one with the other?

1.4 Contents

After having presented the state of the art in [chapter 1](#), the macroscopic influence of the macro environment on the microscopic structure will be investigated in [chapter 2](#). Afterwards, in [chapter 3](#), the influence of the microscopic structure on the rheological laws will be presented. Then, the industrial application of the macroscopic-microscopic coupling on the case of sludges under ultrasound is presented in [chapter 4](#). Finally, some conclusions and perspectives will be drawn in [chapter 5](#).

Chapter 2

From the macroenvironment to the microscopic structure

Objectives

The objectives of this chapter are the investigation of the macroscopic influence of external solicitations on the microstructure, the theorization of an aggregation-disaggregation process and the interpenetration of clusters.

2.4 Conclusion 48

Objectifs

Les objectifs de ce chapitre sont l'étude de l'influence macroscopique des sollicitations externes sur la microstructure, la théorisation d'un processus d'agrégation-désagrégation et l'interpénétration des clusters.

Contents

2.1	Introduction	30
2.2	Aggregation-disaggregation phenomena [Bouthier, 2023a]	30
2.2.1	Abstract of the section	30
2.2.2	Content of the section	30
2.2.3	General framework	30
2.2.4	Numerical simulation	32
2.2.5	Proposition of model	35
2.2.6	Discussion	38
2.2.7	Summary of the contribution	40
2.3	Interpenetration of clusters of carbon-black particles [Dagès, 2022]	41
2.3.1	Abstract of the section	41
2.3.2	Introduction	41
2.3.3	Materials and methods	42
2.3.4	Results	43
2.3.5	Discussion	47
2.3.6	Summary of the contribution	48

2.1 Introduction

As discussed in the previous chapter, the macroscopic environment can have an influence on the microscopic structure of certain materials. To give a parallel with fluid mechanics, in [Kolmogorov, 1991] with an incompressible viscous fluid, an external solicitation is produced by a velocity which can be characterized by the macroscopic Reynolds number Re . Due to the viscosity, eddies and turbulent structures are created to divide the energy and dissipate it at the end. The inertial range over which the transmission of energy is conserved before reaching the dissipative level or the most stable size of eddies, namely the Kolmogorov scale, obeys scaling laws that allows to give an estimate of it. Using notations that will be useful in the following part of the chapter, the Kolmogorov scale is given by $\ell/L \propto Re^{-3/4}$ with L the macroscopic size of an object creating the turbulent structures. This characteristic length is a fundamental parameter to consider because it gives order of magnitude of length scales covered by the studied fluid flow. Also, when trying to run numerical simulation, this scale gives the maximum size of a mesh element necessary to reproduce all the turbulent scales in a Direct Numerical Simulation (DNS). Conversely, if the mesh size is bigger than this length scale, either some turbulent phenomena are omitted in the calculation or an additional model for the sub-mesh size turbulent structures is needed like Large Eddy Simulations (LES).

The idea of scaling laws is according to me the quickest ways to have quantitative estimates of certain variables/phenomena. The power-laws are the most usual form of this scaling laws due to the theorem in [Buckingham, 1914; Buckingham, 1915b; Buckingham, 1915a] but can take other types of form. Hence, trying to catch the main ingredients that characterise a phenomenon is the main focus of the present chapter that will try to propose some general ideas about how an external solicitation can be transmitted throughout a structure and have an effect on a microscopic structure such as the size of clusters of particles that compose the colloidal gels. More precisely, if the parallel with turbulence is drawn to the end, in the same way there is a scaling between the characteristic size of the turbulent structure due to the external solicitation of the flow, there is, in the colloidal suspension, a scaling between the microscopic colloidal structures and the external solicitation of stresses or flow. We will describe more accurately this similarity in this chapter as well.

2.2 Aggregation-disaggregation phenomena [Bouthier, 2023a]

The goal of the present section is to propose very general theoretical arguments to predict the steady-state size ℓ of colloidal aggregates submitted to an external solicitation. This section has been published in [Bouthier, 2023a].

2.2.1 Abstract of the section

Aggregation and disaggregation of clusters of attractive particles under flow are studied from numerical and theoretical points of view. Two-dimensional molecular dynamics simulations of both Couette and Poiseuille flows highlight the growth of the average steady-state cluster size as a power law of the adhesion number, a dimensionless number that quantifies the ratio of attractive forces to shear stress. Such a power-law scaling results from the competition between aggregation and disaggregation processes, as already reported in the literature. Here we rationalize this behavior through a model based on an energy function, which minimization yields the power-law exponent in terms of the cluster fractal dimension, in good agreement with the present simulations and with previous works.

2.2.2 Content of the section

Starting from dimensional analysis, we show in [section 2.2.3](#) that the competition between cluster aggregation and disaggregation can be captured through the minimization of an energy function. In [section 2.2.4](#), we then provide evidence for the existence of an energy minimum in simple numerical simulations. We proceed to detail an analytical model in [section 2.2.5](#), which yields a power-law for ℓ as a function of the adhesion number, a dimensionless number that quantifies the ratio of attractive forces to shear stress. Finally, this model is compared to the coagulation-fragmentation approach and to previous experimental and numerical findings in [section 2.2.6](#). Conclusions and open questions are drawn in [section 2.2.7](#).

2.2.3 General framework

Before describing the general approach based on a grand-canonical free energy, we start with simple dimensional arguments to justify that the competition between cluster aggregation led by attractive forces and disaggregation driven by shear forces depends on a single dimensionless group, namely the adhesion number Ad , once the attraction range is fixed. As discussed in Refs. [Kimbonguila Manounou, 2014; Marshall, 2014], attractive forces may be estimated by Ua/δ^2 , with U

the depth of the interaction potential between two particles, a the particle radius, and δ the range of interaction, which can be taken as the center-to-center distance between two particles at equilibrium or as the width of the potential well. Disaggregating forces, on the other hand, may be estimated by σa^2 , with σ the external stress exerted on the clusters. One chooses here, as a distinction from the literature, to consider the stress rather than the shear rate because (i) whenever the shear rate is involved in similar definitions, it appears as multiplied by the solvent viscosity, therefore as a shear stress, and (ii) one is convinced that stress drives the disaggregation, like in plasticity or fracture [Mises, 1913; Griffith, 1921; Irwin, 1957; Creton, 2016], rather than a kinematic quantity. Following Ref. [Marshall, 2014], the adhesion number is defined as the ratio of attractive forces to disaggregating forces:

$$\text{Ad} = \frac{U}{\sigma a \delta^2}. \quad (2.1)$$

The condition $\text{Ad} \ll 1$ implies that hydrodynamic forces dominate, while $\text{Ad} \gg 1$ indicates that attractive forces are predominant. It is important to note that the choice of this adhesion number contains some degree of arbitrariness. Indeed, other similar dimensionless groups may be built more generally by replacing $a\delta^2$ by $a^\alpha \delta^{3-\alpha}$, with $\alpha \in [0, 3]$, in equation (2.1). The precise choice depends on whether one considers energies ($\alpha = 0$), forces ($\alpha = 1$), or stiffnesses ($\alpha = 2$), i.e., energies per unit surface, or energies per unit volume ($\alpha = 3$). Finally, according to the Vaschy-Buckingham theorem [Buckingham, 1914; Buckingham, 1915b; Buckingham, 1915a], any characteristic length that depends on U , σ , a , and δ , such as the maximum cluster size ℓ , may be expressed as $\ell/a = \mathcal{F}(\text{Ad}, \delta/a)$. Therefore, a combination of both Ad and δ/a is expected. Also note that the adhesion number simply corresponds to the inverse of the ‘‘Mason number,’’ $\text{Mn} = \sigma a^2 \delta / U$, a dimensionless group popular in the rheology community that quantifies the ratio of shearing forces to attractive forces [Varga, 2019; Jamali, 2020; Nabizadeh, 2021].

Another dimensionless group exists in [Xie, 2010] and is called the Breakage Number Br . It has approximately the same definition as the Mason number with $\alpha = 3$, that is to say, $\text{Br} = \sigma a^3 / U$.

In order to describe the competition between aggregation and disaggregation, we consider a grand-canonical ensemble with a population of clusters of mass $k \in \mathbb{N}^*$ associated to a number of clusters n_k . Each cluster of mass k has an associated energy $\mathcal{E}(k)$, which we seek to determine. The number of primary particles is not fixed and is related, for each cluster mass k , to a chemical potential α_k/β with $\beta = 1/(k_B T)$, k_B the Boltzmann constant, and T the temperature. Note that the use of a canonical ensemble may seem more appropriate for a problem with a fixed number of particles. However, the calculation of the canonical partition function leads to

the use of the complete Bell polynomials, where each variable is $e^{-\beta \mathcal{E}(k)}$. Inverting the relation is not straightforward, so that computing the distribution of clusters of mass k is very cumbersome within a canonical framework. Here, thanks to the grand-canonical formulation, $\mathcal{E}(k)$, as well as the energy $n_k \mathcal{E}(k)$ associated to all clusters of mass k , may be computed rather easily. The grand canonical partition function reads:

$$\Xi = \sum_{(n_k)_{k \in \mathbb{N}^*} \in \mathbb{N}^{\mathbb{N}^*}} \exp \left(- \sum_{k \in \mathbb{N}^*} (\beta n_k \mathcal{E}(k) - n_k k \alpha_k) \right) \quad (2.2)$$

$$= \prod_{k \in \mathbb{N}^*} (1 - e^{-\beta \mathcal{E}(k) + k \alpha_k})^{-1}. \quad (2.3)$$

The convergence of the series in equation (2.2) is guaranteed if $\alpha_k k < \beta \mathcal{E}(k)$ for all $k \in \mathbb{N}^*$. Moreover, it follows from equation (2.2) that the distribution of each level population n_k is a geometric distribution with a parameter $e^{-\beta \mathcal{E}(k) + k \alpha_k}$. Since the average number of particles $\langle N \rangle$ is related to the average population $(\langle n_k \rangle)_{k \in \mathbb{N}^*}$ of clusters of mass k through $\langle N \rangle = \sum_{k \in \mathbb{N}^*} k \langle n_k \rangle$, one may compute the average number of clusters of mass k and the standard deviation through:

$$\langle n_k \rangle = -\frac{1}{k} \frac{\partial \ln \Xi}{\partial \alpha_k} = (e^{\beta \mathcal{E}(k) - \alpha_k k} - 1)^{-1}, \quad (2.4)$$

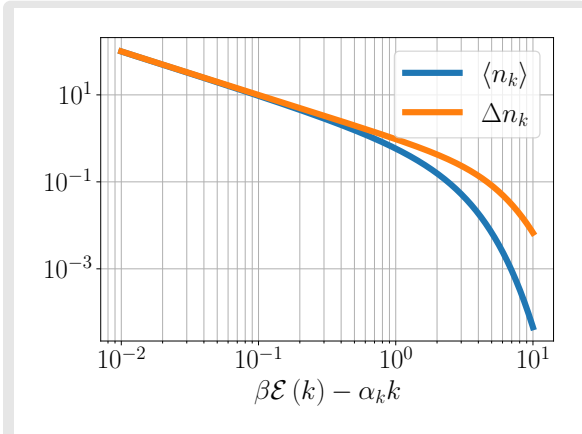
$$\Delta n_k = \frac{1}{k} \sqrt{\frac{\partial^2 \ln \Xi}{\partial \alpha_k^2}} = \sqrt{\langle n_k \rangle (1 + \langle n_k \rangle)} \quad (2.5)$$

$$= \frac{1}{2} \text{csch} \left(\frac{\beta \mathcal{E}(k) - \alpha_k k}{2} \right), \quad (2.6)$$

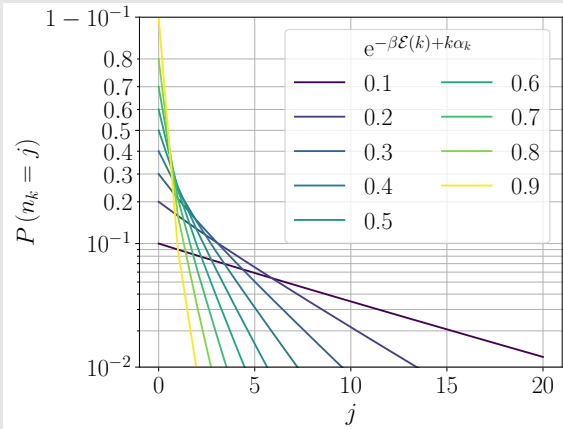
which boils down to the Bose-Einstein statistics.

To give an illustration of the Bose-Einstein Statistics in equations (2.4) to (2.6), in figure 2.1, there is the representations of the average and the standard deviation as a function of the dimensionless energy $\beta \mathcal{E}(k) - \alpha_k k$ and the probability distribution function for different values of $e^{-\beta \mathcal{E}(k) + k \alpha_k}$. It may help the reader to understand the type of probability distribution.

In practice, in an experiment or a simulation, a initial sample of $(n_k)_{k \in \mathbb{N}^*}$ is chosen, which evolves in time according to external conditions. It is clear from the above expressions that the $(n_k)_{k \in \mathbb{N}^*}$ should end up being centered around the averages $(\langle n_k \rangle)_{k \in \mathbb{N}^*}$ with a dispersion $(\Delta n_k)_{k \in \mathbb{N}^*}$. Therefore, a higher number of clusters of mass k also brings a higher dispersion around this value. Since numerical simulations yield a probability distribution function $f(k)$ for the number of cluster of mass k , which is assumed to be equal to the average distribution $\langle n_k \rangle$, i.e., $f(k) = \langle n_k \rangle$, one can find the average potential energy of the clusters and the standard



(a) Evolution of the average and the standard deviation as a function of the dimensionless energy $\beta\mathcal{E}(k) - \alpha_k k$



(b) Probability distribution for any n_k for a given $k \in \mathbb{N}^*$ with different values of $e^{-\beta\mathcal{E}(k) + k\alpha_k}$

Figure 2.1: Illustrations of the Bose-Einstein statistics

deviation respectively through:

$$\beta\mathcal{E}(k) - \alpha_k k = \ln\left(1 + \frac{1}{f(k)}\right) \quad (2.7)$$

$$\Delta(\beta\mathcal{E}(k) - \alpha_k k) = (f(k)(1 + f(k)))^{-\frac{1}{2}} \quad (2.8)$$

$$= 2 \sinh\left(\frac{\beta\mathcal{E}(k) - \alpha_k k}{2}\right) \quad (2.9)$$

$$> \beta\mathcal{E}(k) - \alpha_k k. \quad (2.10)$$

This whole description relies on classical statistical mechanics which is valid for systems at thermodynamic equilibrium. In spite of this, the equilibrium concepts are applied here to systems that are out of thermodynamic equilibrium. It is a point of caution that was necessary to mention.

2.2.4 Numerical simulation

2.2.4.1 Numerical scheme and analysis

To get some insight of the competition between aggregation and disaggregation processes, we turn to simple molecular dynamics simulations of two-dimensional Couette and Poiseuille flows based on the LAMMPS library [Thompson, 2022]. We use reduced units, where the unit size is given by the particle radius. The simulation box is of size $\mathcal{L} \times h$ with periodic boundary conditions along the x direction and solid boundaries along the y direction located at $y = 0$ and $y = h$. The length of the box \mathcal{L} is fixed to $\mathcal{L} = 620$, and the width h is either 103 or 206, much larger than the particle size. Each boundary is constituted of one layer of particles of unit size which positions are fixed and that interact with bulk particles through a repulsive Yukawa potential $w_s(r) = 100e^{-r}/r$, with r the distance between two particles and a cut-off distance $r = 5$ to save computation time. This choice of a purely repulsive potential leads to some depletion of the particles at the walls but allows us to avoid irreversible aggregation on the walls and to focus on bulk aggregation-disaggregation processes. Finally, the interaction potential between two particles in the bulk is a classical 12-6 Lennard-Jones potential $w(r) = 4(r^{-12} - r^{-6})$ with a cut-off distance $r = 40$, again to save computation time.

First, the system is initialised with a particle surface fraction of $\phi = 0.12$. Using a canonical formulation, the temperature is fixed at $T = 0.01$. The time step is taken as $\Delta t = 0.01$, which is small enough to account realistically for temporal variations while keeping the computation time reasonably low. Particles are distributed over a square lattice, and their initial velocities are chosen according to a Maxwell distribution for the given temperature. The system is then let to evolve for a duration 5,000 time units in order to create the initial cluster distribution. More precisely, the equation of motion for

each particle $i \in \llbracket 1, N \rrbracket$, with N the total number of particle, is

$$\frac{d^2 \mathbf{r}_i}{dt^2} = -\frac{\partial \mathcal{W}}{\partial \mathbf{r}_i} \left((\mathbf{r}_j)_{j \in \llbracket 1, N \rrbracket} \right) + \mathbf{B}_i \quad (2.11)$$

$$\mathcal{W} \left((\mathbf{r}_j)_{j \in \llbracket 1, N \rrbracket} \right) = \sum_{k=1}^N \sum_{j=k+1}^N w(|\mathbf{r}_k - \mathbf{r}_j|) \quad (2.12)$$

$$w(r) = 4 \left(r^{-12} - r^{-6} \right), \quad (2.13)$$

with \mathbf{r}_i the position of particle i and \mathbf{B}_i a Brownian white noise for particle i .

In a second step, a drag force $\mathbf{F}_i = C \left(\mathbf{u} - \frac{d\mathbf{r}_i}{dt} \right)$ is applied on each particle $i \in \llbracket 1, N \rrbracket$, with $C = 1$ the drag coefficient¹, $\mathbf{u} = Vy/h\mathbf{e}_x$ for the 2D Couette flow or $\mathbf{u} = 4V(1-y/h)y/h\mathbf{e}_x$ for the 2D Poiseuille flow, where V is the maximum flow velocity. Here, a micro-canonical formulation is used and the time step is set to $\Delta t = 0.001$. The simulation is run for a duration of 1,000 time units. The equation of motion for each particle i thus reads:

$$\frac{d^2 \mathbf{r}_i}{dt^2} = -\frac{\partial \mathcal{W}}{\partial \mathbf{r}_i} \left((\mathbf{r}_j)_{j \in \llbracket 1, N \rrbracket} \right) + F(\mathbf{r}_i) \mathbf{e}_x \quad (2.14)$$

$$F(\mathbf{r}_i) = C \left(-\frac{d\mathbf{r}_i}{dt} \cdot \mathbf{e}_x + \right. \quad (2.15)$$

$$\left. V \frac{\mathbf{r}_i \cdot \mathbf{e}_y}{h} \begin{cases} 1 & \text{2D Couette flow} \\ 4 \left(1 - \frac{\mathbf{r}_i \cdot \mathbf{e}_y}{h} \right) & \text{2D Poiseuille flow} \end{cases} \right). \quad (2.16)$$

The parameters investigated in the present work are $(V, h) \in \{0.1, 0.3, 1, 3, 10, 30, 100\} \times \{103, 206\}$. The values of the adhesion number are then $\text{Ad} \in \{1, 2, 3, 6, 10, 20, 34, 68, 103, 206, 344, 688, 1032, 2065\}$. The numerical scheme used here is a Velocity Verlet algorithm [Swope, 1982]. The computations output are (i) the position of the particles at each time step, and (ii) the clusters to which the particles belong based on a connected-component algorithm [Pearce, 2005] with a distance threshold of 1.4, consistently with the literature [Colombo, 2013; Colombo, 2014b; Colombo, 2014a]. Moreover, we checked that for thresholds ranging from 1.1 to 2.0, the distribution of neighbours does not change, so that the results are not sensitive to the specific choice of threshold. The size of cluster number I is quantified according to the following estimates:

- the radius of gyration R_g^I given by

$$R_g^I = \sqrt{\frac{1}{|P(I)|} \sum_{k \in P(I)} \|\mathbf{r}_k - \bar{\mathbf{r}}\|^2}, \quad (2.17)$$

¹Additional simulations were carried out with various values of C and the main results remained similar in the sense that the time unit has been rescaled according to the value of C .

$$\bar{\mathbf{r}} = \frac{1}{|P(I)|} \sum_{k \in P(I)} \mathbf{r}_k, \quad (2.18)$$

with \mathbf{r}_k the position of the particles in the cluster, $P(I)$ the set of particles in cluster I and $|P(I)|$ the number of particles in cluster I .

- the Feret radii in the x and y directions given by $(\max_{k \in P(I)} \mathbf{r}_k \cdot \mathbf{e}) / 2 - (\min_{k \in P(I)} \mathbf{r}_k \cdot \mathbf{e}) / 2$ with \mathbf{e} the unit vector in the x and y directions respectively.
- the half maximum chord length given by $\max_{(k,l) \in P(I)^2} \|\mathbf{r}_k - \mathbf{r}_l\| / 2$.

In order to infer statistical estimations, each size distribution is further weighted by the number of particles in each cluster. Such weighting is needed because the number of clusters is not constant. Therefore, because the total number of particles is constant, weighting by the mass of each cluster allows one to recover the number of particles when integrating over the whole distribution. Finally, thanks to the reduced units, $U/a\delta^2 = 1$ and the shear stress is $\sigma = CV/h = V/h$ here due to $C = 1$ so that the adhesion number simply reads $\text{Ad} = h/V$. Note that, due to the specific choice of interaction potentials, to the absence of thermal motion and hydrodynamic interactions and to the amount of particles which might be slightly low regarding statistics, the present simulations remain very crude. Thus, their aim is rather to offer a generic view of the evolution of particulate clusters under flow that supports our theoretical approach, than to provide a detailed, realistic picture of the interplay between flow and colloidal interactions at the particle scale.

2.2.4.2 Simulation results

Figure 2.2 shows typical particle distributions computed after the preparation step prior to shearing [figure 2.2(a)], and after application of shear in the Couette geometry [figure 2.2(b)], in spite of some depletion at the walls. It appears clearly that the system starts from a space-spanning ramified structure and evolves toward dense, isolated clusters under shear. Moreover, as shown in figure 2.2(c), the different estimates for the cluster size yield consistent values. In the following, for the sake of simplicity, we shall focus only on the weighted average of the radius of gyration to estimate the cluster size ℓ .

Following the general framework introduced in section 2.2.3, we compute the distribution of the cluster mass and the dimensionless energy $\beta \mathcal{E}(k) - \alpha_k k$ based on equation (2.7). Figure 2.3 shows this energy functional plotted against the mass k of particles within a cluster for adhesion numbers ranging from 1 to about 2,000. More specifically, from our simulations, we extract a probability density function of the steady-

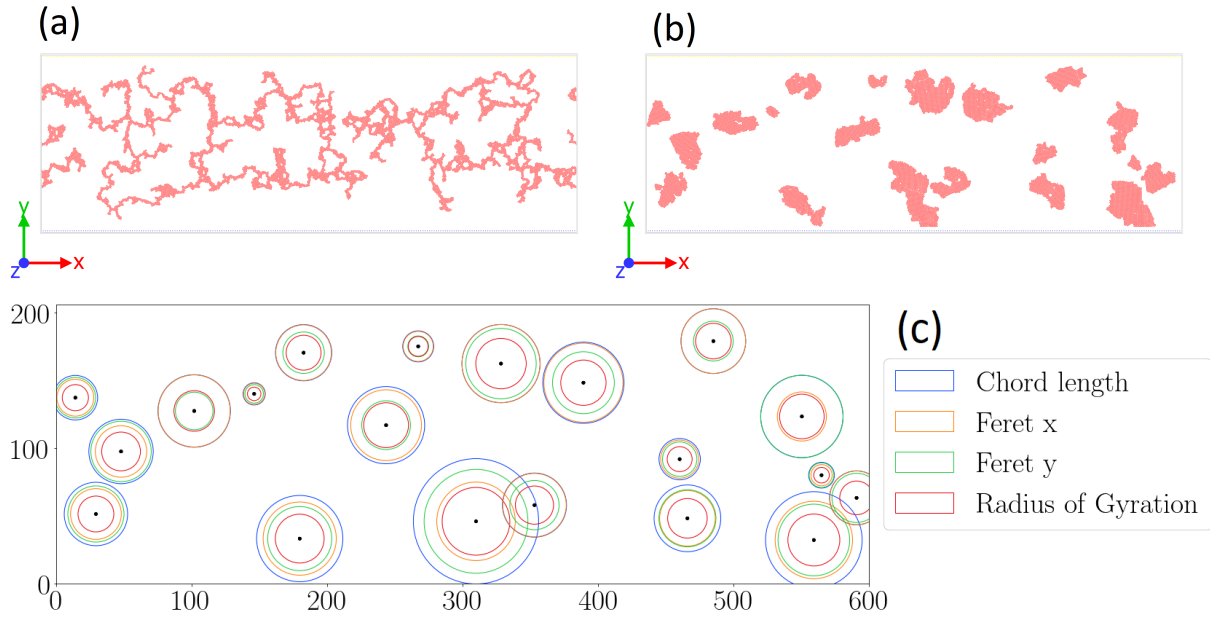


Figure 2.2: Simulated particle distributions for $V = 10$, $h = 206$, and $C = 1$ after the preparation step prior to shearing (a) and at after shearing in the Couette geometry (b). Rendering using *Ovito* [Stukowski, 2010]. (c) Cluster detection and various estimates of the cluster size as defined in the text for the top right particle distribution.

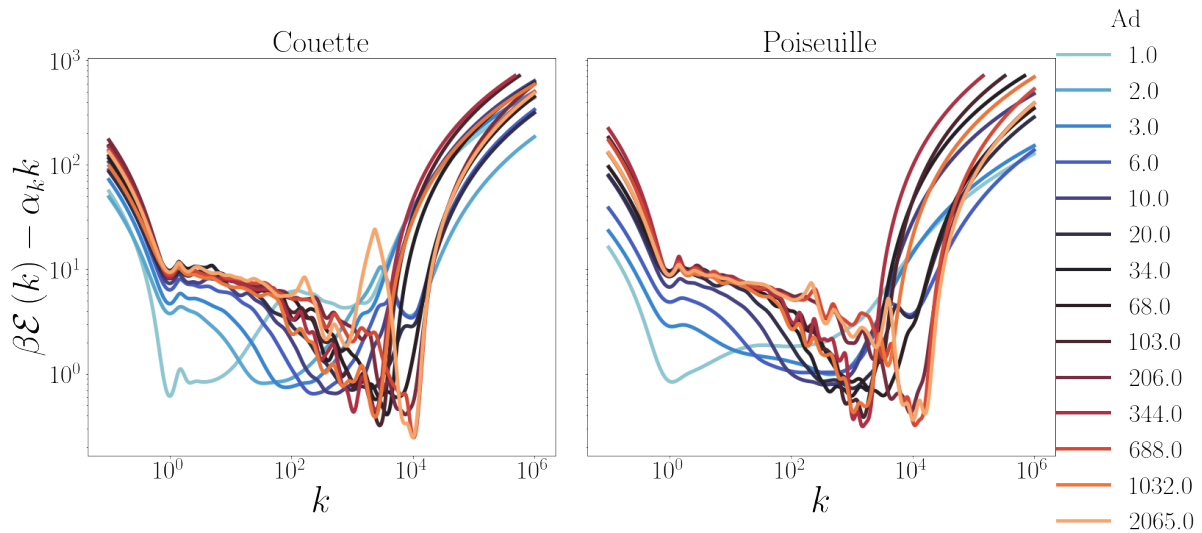


Figure 2.3: Energy functional $\beta\mathcal{E}(k) - \alpha_k k$ computed from equation (2.7) as a function of the number k of particles in a cluster for (left) Couette flow and (right) Poiseuille flow. Colors correspond to the adhesion number Ad as indicated in the legend. Results obtained from simulations performed with $h = 103$ or $h = 206$.

state cluster population in terms of sizes. This probability density function is directly imported into equation (2.7) as $f(k)$, which yields the dimensionless energy $\beta\mathcal{E}(k) - \alpha_k k$. Focusing on one particular curve, when the probability density function goes to 0, the dimensionless energy goes to infinity, which shows that these states are impossible to access. Also, when the probability density function is maximum, the dimensionless energy is minimum because the most probable size minimises the global energy functional. Looking at the small- and large-mass limits, it appears that $\lim_{k \rightarrow 0^+} \beta\mathcal{E}(k) - \alpha_k k = \lim_{k \rightarrow +\infty} \beta\mathcal{E}(k) - \alpha_k k = +\infty$, which indicates that extreme masses are not accessible to the system. Second, in all cases, there exists a global minimum of the energy functional that shifts towards larger values of k as the adhesion number Ad is increased. As expected intuitively, this suggests that the average cluster mass increases with Ad . Moreover, the steeper slope $\partial_{\ln(k)} (\beta\mathcal{E}(k) - \alpha_k k)$ of the energy functional on the right side of the global minimum than on the left side indicates that the system reaches the energy minimum more easily when starting from large masses than from small masses. This confirms the intuition that disaggregation processes are much brutal than aggregation processes. Third, while the value of the global minimum energy does not show any clear trend with Ad , there may exist several local minima in $\beta\mathcal{E}(k) - \alpha_k k$. This means that several metastable states may occur. These states may disappear when increasing the simulation duration or the system size, including also experimentally. Still, this shows that a rather polydisperse population of clusters may be found, at least transiently. This may also be related to the dispersion in the energy minimum illustrated previously.

An interesting feature that can be commented on is the possible bimodality of the distribution of cluster size which can be reproduced in the energy functional graph in figure 2.3, notably at high Adhesion number values. It may be relevant to compare this bimodality with the bimodality observed in [Lattuada, 2016]. Nevertheless, the bimodality may not be of the same nature. More precisely, the bimodality in [Lattuada, 2016] is due to the remaining presence of monomers, or individual particles, in the simulation with a relatively high proportion compared to the clusters. In our case, there is a little bump around individual particles but the biggest bimodality appears around clusters of significant size. Thus, the bimodality is just the co-existence of two types of cluster size but on a larger scale of simulation, it may be expected to have only one mode.

Figure 2.4(a) and figure 2.4(b) respectively show the “equilibrium mass” k_{\min} of the clusters corresponding to the energy minimum, i.e., $k_{\min} = \arg \min_{k \in \mathbb{R}_+} (\beta\mathcal{E}(k) - \alpha_k k)$, and the cluster size ℓ/a taken as the weighted average of their radius of gyration plot-

ted against the adhesion number Ad . For both observables, a power-law regime is identified over almost two decades in adhesion numbers. The exponents inferred from power-law fits for $Ad \in [2, 200]$ are reported in table 2.1. For $Ad \gtrsim 100$, a saturation is observed in k_{\min} together with large variations, for both the Couette and Poiseuille flows. This behavior is most probably linked to finite-size effects as the average cluster size becomes comparable or larger than the system width h . Consistently with figure 2.4(a), the cluster size ℓ increases as a power-law of Ad [figure 2.4(b)]. There, although the data for ℓ do not show such a strong saturation as for k_{\min} , significant deviations from power-law behavior are still observed for $Ad \gtrsim 100$.

Moreover, the exponents for the dependence of ℓ with Ad seem to depend significantly on the geometry, with values 0.35 and 0.57 for the Couette flow and 0.27 and 0.48 for the Poiseuille flow, respectively for $h = 103$ and $h = 206$ (see table 2.1). Similarly, the corresponding exponents for k_{\min} , namely 0.4 and 0.9 for Couette flow, and 0.5 and 1.0 for Poiseuille flow, also differ for the two values of h . At this stage, the reason for such an influence of h in the simple two-dimensional simulations remains unclear, and future work should focus on more realistic interaction potentials and three-dimensional geometries.

Still, it is interesting to note that ℓ/a and k_{\min} are not expected to have the same power-law behavior with the adhesion number because of their intrinsic relationship. More specifically, considering the framework of fractal clusters, the number of particles in a cluster k is related to the geometrical size l through $k = (l/a)^D$ with D the fractal dimension. In the two-dimensional case, D should fall into the range $[1, 2]$. Figure 2.4(c) shows that $\ell/a \propto k_{\min}^{1/2}$, which is compatible with a fractal dimension $D \simeq 2$, i.e., with almost dense aggregates in two dimensions geometries. The fact that very compact aggregates are obtained in the simulations is confirmed visually by looking at figure 2.2(b). Another confirmation comes from the ratio of the exponent for k_{\min} and that for ℓ/a in table 2.1, which is also found to be close to 2 (except for the Couette flow with $h = 103$ but the scatter of the k_{\min} data in this latter case makes it difficult to conclude).

2.2.5 Proposition of model

2.2.5.1 Description of the disaggregation and reaggregation processes

The precise internal structure of the aggregates is really complex, and depends upon many different parameters including the volume fraction, the nature of the interparticle forces and of the solvent, temperature, and chemical environment. Hence, we shall consider the aggregates as a continuum without further internal de-

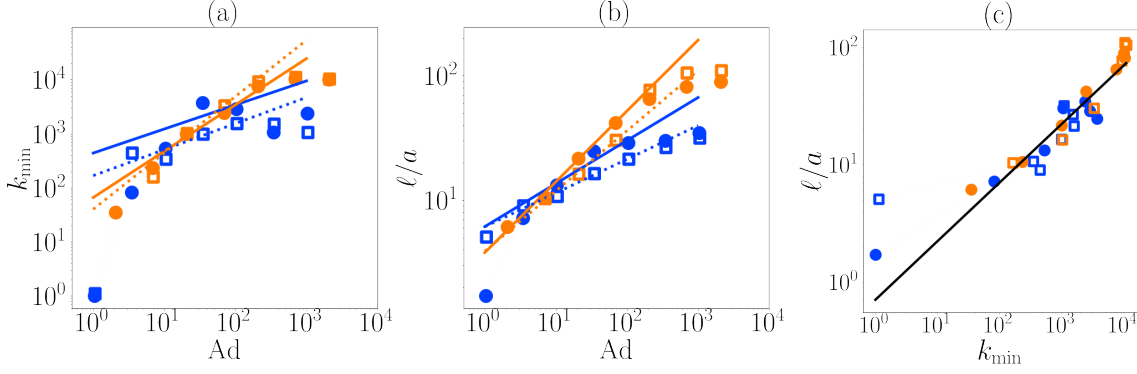


Figure 2.4: (a) Mass k_{\min} of the clusters corresponding to the energy minimum and (b) cluster size ℓ defined as the weighted average of the radius of gyration of the clusters, as a function of the adhesion number Ad for Couette flow (\bullet) and Poiseuille flow (\square) and for two different width $h = 103$ (blue) and $h = 206$ (orange). Solid and dotted lines correspond to the best power-law fits respectively for the Couette and the Poiseuille flow, and computed over $Ad \in [2, 200]$. (c) Cluster size ℓ as a function of the equilibrium mass k_{\min} . The black solid line corresponds to $\ell \propto k_{\min}^{1/2}$. Same symbols and colors as in (a) and (b).

Geometry	h	Variable	Exponent	Prefactor
Couette	103	ℓ/a	0.346 ± 0.009	6.1 ± 0.2
Couette	103	k_{\min}	0.4 ± 0.4	400 ± 700
Couette	206	ℓ/a	0.57 ± 0.03	3.5 ± 0.4
Couette	206	k_{\min}	0.9 ± 0.1	60 ± 30
Poiseuille	103	ℓ/a	0.271 ± 0.007	6.1 ± 0.2
Poiseuille	103	k_{\min}	0.5 ± 0.1	170 ± 70
Poiseuille	206	ℓ/a	0.48 ± 0.03	3.9 ± 0.5
Poiseuille	206	k_{\min}	1.0 ± 0.1	40 ± 20

Table 2.1: Exponents and prefactors of the power-law fits in figure 2.4 for the different geometries, widths, and sizes ℓ and k_{\min} .

tails. We consider a suspension of particles of size a that interact through an attractive potential so that they gather into aggregates as sketched in figure 2.5. Following a statistical approach as in Refs. [Banasiak, 2020a; Banasiak, 2020b; Golse, 2005; Alexeev, 2004; Stadnichuk, 2015], we assume that there exists a distribution $f(t, l, a, U, \delta, \sigma)$ giving the population of aggregates of size l at time t made of particles of size a interacting through a pair potential U over a distance δ under a stress solicitation σ . Such a distribution may be computed through a coagulation-fragmentation equation as in Refs. [Banasiak, 2020a; Banasiak, 2020b; Stadnichuk, 2015]. Yet, this approach requires to identify coagulation kernels and fragmentation coefficients, which involves much effort for theoretical and/or numerical validation. Without ignoring the power of such tools, we aim at a simpler approach through the present statistical approach.

We start by imposing the conservation of the total

number of particles N , which reads:

$$N = \int_0^{+\infty} n\left(\frac{l}{a}\right) f(t, l, a, U, \delta, \sigma) dl = \text{constant}, \quad (2.19)$$

where $n(l/a)$ denotes the number of particles per cluster of relative size l/a . The average size of the aggregates is thus given by:

$$\bar{l}(t, a, U, \delta, \sigma) = \frac{a}{N} \int_0^{+\infty} n\left(\frac{l}{a}\right) \frac{l}{a} f(t, l, a, U, \delta, \sigma) dl. \quad (2.20)$$

From a statistical point of view, and assuming that the aggregates are submitted to a uniform external stress σ far from any boundary, aggregates should evolve from one state to another as sketched in figure 2.5. If the stress is sufficiently large to break some initial aggregate (state 1), a disaggregation occurs either due to “fragile” rupture into two pieces of similar sizes (bottom part of figure 2.5, state 4) or due to “erosion,” where small pieces detach from the initial aggregate (top part of figure 2.5, states 2 and 3). If the larger pieces can still

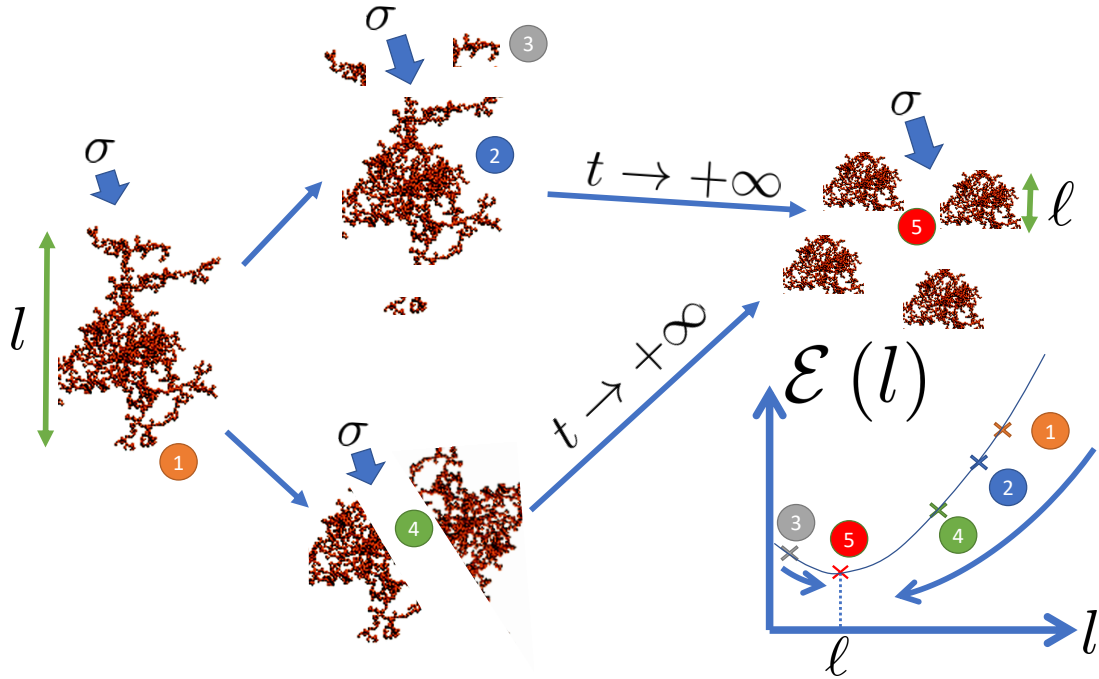


Figure 2.5: Sketch of the disaggregation and reaggregation processes under a uniform external stress σ . The numbers represent different sizes of aggregates with different levels of energy. The aggregates are disaggregating and reaggregating according to the stress sollicitation. Transition from state 1 to states 2 and 3 corresponds to a "fragile" rupture, while transition from state 1 to state 4 is an "erosion" process.

be broken down (states 2 and 4), the process continues. However, if the pieces become too small (state 3), the interparticle attraction dominates and reaggregation occurs. In the process, the aggregates progressively decrease their global energy, until a minimum is reached at long times $t \rightarrow +\infty$. Therefore, the steady state (state 5) eventually corresponds to the optimum of all possible sizes, which results from a dynamical equilibrium between disaggregation and reaggregation processes. More formally, when a steady state is reached, the average aggregate size $\bar{\ell}$ is given by

$$\bar{\ell}(a, U, \delta, \sigma) = \lim_{t \rightarrow +\infty} \bar{\ell}(t, a, U, \delta, \sigma). \quad (2.21)$$

In practice, since t remains finite, we note that the longer the final time, the smaller the spread of the distribution around the steady-state size. An additional comment is that, keeping the previous set of variables for the distribution f , an equivalent form using the Vaschy-Buckingham theorem [Buckingham, 1914; Buckingham, 1915b; Buckingham, 1915a] is found by replacing $f(t, l, a, U, \delta, \sigma) dl$ with $\tilde{f}(l/a, Ad, \delta/a) d(l/a)$, where t can be discarded based on unit independence. Time becomes relevant, however, when the viscosity η of the suspending liquid or any other time-related quantity is considered.

2.2.5.2 Analytical formulation of the model

Let us consider a suspension of particles of diameter a gathered in aggregates. The bond between each particle involves an energy U and an interparticle distance of separation δ . The system is submitted to a uniform stress σ . One aims at estimating the steady-state size of stable aggregates $\bar{\ell}$ as a function of a , U , δ , and σ . Following Eggersdorfer et al. [Eggersdorfer, 2010], for a dense aggregate of size l , the applied mechanical energy per unit area is σl . However, aggregates are not completely dense and one should more generally account for their fractal nature. As already introduced above in section 2.2.4.2, the number of particles in an aggregate of size l is proportional to $(l/a)^D$ with D the fractal dimension of the clusters. Each particle in the aggregates contributes to the overall energy per unit surface. As if they were in parallel, the mechanical energy per unit surface should be weighted by the number of particles in an aggregate because there is fluid flowing inside the aggregates, which interferes with each particle. Hence, on the one hand, the mechanical energy per unit of effective surface of the aggregate $M(l)$ is proportional to $\sigma a (l/a)^{D+1}$. On the other hand, if one isolates an aggregate of size l , the energy per unit surface liberated due to broken bonds E is $E(l) = U\delta^{-2}$, which is independent of the size l [Marshall, 2014]. Indeed, considering an intermolecular potential $w(d)$, with d the intermolecu-

lar distance, one can compute the interparticle potential per unit area through:

$$W(d) = 2\pi\rho^2 \int_d^{+\infty} \int_y^{+\infty} \int_0^{+\infty} rw \left(\sqrt{r^2 + z^2} \right) dr dz dy, \quad (2.22)$$

where ρ is the molecular density inside a particle. Defining δ as the distance that satisfies $W'(\delta) = 0$, or equivalently $\delta = \arg \min_{d \in \mathbb{R}_+^*} W(d)$ — taking some usual examples leads to $\delta \approx \arg \min_{d \in \mathbb{R}_+^*} w(d)$ —, and the energy $U = \delta^2 W(\delta)$, $E(l) = U\delta^{-2}$ indeed corresponds to the energy per unit surface liberated due to broken bonds. This energy is independent of the size of the aggregate because one may assume that, on the boundary of the aggregate, the number of particles per unit surface does not depend on l and is only related to the structure, which is assumed to be fixed in steady state. Finally, the steady-state size ℓ corresponds to the size for which the mechanical energy balances that due to broken bonds, i.e., $M(\ell) = E(\ell)$, which leads to:

$$\frac{\ell}{a} = \left(\frac{U}{\sigma a \delta^2} \right)^{\frac{1}{1+D}} = \text{Ad}^{\frac{1}{1+D}}. \quad (2.23)$$

The same result can be obtained by minimizing the total energy $\mathcal{E}(l) = l^2 (M(l) - E(l))$. Another way to consider this concept is to relate it to Eggersdorfer et al. [Eggersdorfer, 2010]. Indeed, on the one hand, if a stress σ is applied on a cluster of size l with $(l/a)^D$ particles of size a , one may assume that the stress is shared in parallel on all particles, which gives a force $F_{\min} = \sigma a^2$. On the other hand, if the stress is focused on one single particle, there is a force $F_{\max} = \sigma l^2$. Taking the geometrical average of these two extremes leads to $F_{\text{avg}} = \sqrt{F_{\min} F_{\max}} = \sigma l a$. This average force should be summed over the whole chain with $(l/a)^D$ elements, which reads $F_{\text{tot}} = \sigma l a (l/a)^D = \sigma a^2 (l/a)^{1+D}$. Finally, the bearable force between two particles is Ua/δ^2 . Therefore, the link breaks when $\sigma a^2 (l/a)^{1+D} = Ua/\delta^2$, leading to $\ell/a = \text{Ad}^{\frac{1}{1+D}}$ as in equation (2.23). Equation (2.23) also agrees with equation (2.21) through the Vaschy-Buckingham theorem [Buckingham, 1914; Buckingham, 1915b; Buckingham, 1915a]. Indeed,

equation (2.21) may be rewritten as:

$$\frac{\ell}{a} = G \left(\text{Ad}, \frac{\delta}{a} \right). \quad (2.24)$$

Adding that U/δ^2 provides all the information about the interaction potential, one has $\partial_{\delta/a} G = 0$ and thus

$$\frac{\ell}{a} = G(\text{Ad}), \quad (2.25)$$

consistently with equation (2.23). Note that this model may show some limitations especially in the case of very loose aggregates, e.g. fibers or linear chains of adhesive spheres of length l , for which the hydrodynamic stress grows as l^3 due to the transmission of stresses by lubrication forces. This would bring an evolution of the hydrodynamic energy as l^5 , or of the hydrodynamic force as l^4 , which are, to our knowledge, not reported in the literature.

2.2.6 Discussion

In this section, we discuss the theoretical approach and numerical results in light of the literature. We start by comparing the model with the classical coagulation-fragmentation approach. Then, the power-law scaling predicted for the cluster size, $\ell \propto \text{Ad}^{1/(1+D)}$, is confronted to the present simulations and to previous experimental results.

2.2.6.1 Comparison with a coagulation-fragmentation model

The model proposed above in section 2.2.5 may be compared to the coagulation-fragmentation approach introduced in the literature more than thirty years ago [Sorensen, 1987] and subsequently enriched over the years, e.g., through the population balance models [Banasiak, 2020a; Banasiak, 2020b; Latuada, 2016; Puisto, 2012]. In such an approach, the probability density function f of clusters of size x at time t obeys the following dynamical equation:

$$\begin{aligned} \frac{\partial f}{\partial t}(t, x, \bullet) = & \frac{1}{2} \int_0^x K(y, x-y, \bullet) f(t, y, \bullet) f(t, x-y, \bullet) dy - \frac{1}{2} \int_0^x F(y, x-y, \bullet) f(t, x, \bullet) dy \\ & - \int_0^{+\infty} K(x, y, \bullet) f(t, x, \bullet) f(t, y, \bullet) dy + \int_0^{+\infty} F(x, y, \bullet) f(t, x+y, \bullet) dy, \end{aligned} \quad (2.26)$$

with $\bullet = (a, U, \delta, \sigma)$, K the aggregation kernel, and F the fragmentation kernel. Considering the long-term behaviour, it can be shown that f takes the general form

[Banasiak, 2020a; Banasiak, 2020b; Sorensen, 1987]:

$$f(t, x, \bullet) = \frac{1}{s^2(t, \bullet)} \varphi \left(\frac{x}{s(t, \bullet)}, \bullet \right), \quad (2.27)$$

where s and φ are two functions that depend only on time and size respectively, and such that $\int_{\mathbb{R}_+} x\varphi(x, \bullet) dx = N$, the fixed total number of particles. The function s corresponds to the average mass of the clusters according to the distribution f . It can be related to a size through the cluster fractal dimension D by $s \propto l^D$. Then, integrating the previous expression over the size as in equation (2.20), one computes the steady-state average size as:

$$\bar{l}(t, \bullet) = as^{\frac{1}{D}}(t, \bullet), \quad (2.28)$$

with

$$\lim_{t \rightarrow +\infty} s(t, \bullet) = \left(N \frac{A(\bullet)}{B(\bullet)} \right)^{\frac{1}{\alpha+2-\lambda}} \quad (2.29)$$

$$A(\bullet) = \iint_{\mathbb{R}_+^2} xy\varphi(x, \bullet)\varphi(y, \bullet)K(x, y, \bullet) dx dy \quad (2.30)$$

$$B(\bullet) = \iint_{\mathbb{R}_+^2} xy\varphi(x+y, \bullet)F(x, y, \bullet) dx dy, \quad (2.31)$$

where λ and α are the respective homogeneity coefficients of K and F^2 , assuming $\alpha + 2 > \lambda$. It follows from equations (2.21), (2.28) and (2.29) that

$$\frac{\ell}{a} = \left(N \frac{A(\bullet)}{B(\bullet)} \right)^{\frac{1}{D(\alpha+2-\lambda)}}. \quad (2.32)$$

Finally, identifying with equation (2.23), one gets

$$\frac{U}{\sigma a \delta^2} = \left(N \frac{A(\bullet)}{B(\bullet)} \right)^{\frac{1+D}{D(\alpha+2-\lambda)}}. \quad (2.33)$$

Most of the physical quantities appear as multiplicative factors, in the sense that, for example, the coagulation kernel K is usually built with a factor U/η with η the viscosity of the fluid and no other dependence on physical quantities besides the variables x and y . Therefore, the ratio $NA(\bullet)/B(\bullet)$ can be considered as the product of a dimensionless number built in a similar manner as the adhesion number and another factor that depends only on the shape of respective kernels without involving any additional physical parameter. Therefore, in order to keep equation (2.33) true in general, one should impose that the exponent is 1, which leads to

$$1 = D(\alpha + 1 - \lambda). \quad (2.34)$$

This is an important result which, to our knowledge, has not been reported in the literature before. Indeed, equation (2.34) allows one to relate the first mechanical approach to population balance models, where the

²The homogeneity coefficients are defined as $K(\xi x, \xi y) = \xi^\lambda K(x, y)$ and $F(\xi x, \xi y) = \xi^\alpha F(x, y)$ for all $(x, y, \xi) \in \mathbb{R}_+^3$.

homogeneity coefficients may seem disconnected from physical and measurable quantities. This result also emphasizes the fact that the adhesion number is a correct measure of the relative importance of aggregation versus disaggregation.

We note that aggregation kernels are pretty well covered, either in terms of theoretical solutions [Banasiak, 2020a; Banasiak, 2020b; Wattis, 2006; Spicer, 1996] with simple sums or products, or in terms of a physical construction, e.g., based on collisions, thermal fluctuations, and diffusion [Kryven, 2014; Barthelme, 2003]. Fragmentation kernels, however, are more poorly controlled, in the sense that some theoretical solutions impose some strong conditions on these kernels without much physical justification [Banasiak, 2020a; Banasiak, 2020b; Lattuada, 2016; Puisto, 2012], so that the expressions of the fragmentation kernels remain mostly empirical or semi-empirical [Delichatsios, 1976; Kusters, 1991]. Therefore, although the use of coagulation-fragmentation equations is well established, relating some of the main terms to physical phenomena, such as the interaction potential and the flow stresses, is an important step yet to be fully achieved.

2.2.6.2 Comparison with simulations and experiments

Relating the model proposed in section 2.2.5 to the simulations of section 2.2.4, we expect the exponents in table 2.1 to be linked to the fractal dimension respectively by $1/(1+D)$ for the steady-state size ℓ , and $D/(1+D)$ for the equilibrium mass k_{\min} . The broad variability of the exponents does not allow to properly extract a fractal dimension from the simulations. Nevertheless, as discussed above in section 2.2.4.2, the shear-induced clusters are almost dense, so that we may assume a fractal dimension D close to 2. Such a compactness most probably results from the specific interaction potential, i.e. a 12-6 Lennard-Jones potential, which is a central-force potential and is likely to lead to clusters with droplet-like shapes. We note that $D = 2$ would be consistent with the exponent $\beta = (1+D)^{-1} = 1/3$ expected for ℓ as a function of Ad , at least in the smaller geometry, since table 2.1 reports exponents of 0.35 and 0.27 for $h = 103$.

Moreover, the results may be compared to the recent three-dimensional simulations under simple shear flow by [Ruan, 2020], which also report rather dense shear-induced clusters at steady state. Focusing both on the cluster size and on the average number of particles in a cluster as in the present work, the authors extract the cluster fractal dimension D and show that ℓ/a scales as a power-law of the shear stress. The exponents β for ℓ reported in [Ruan, 2020] are replotted as a function of D as blue circles in figure 2.6 and show good agreement with the prediction $\beta = (1+D)^{-1}$. Note that this is

also consistent with the empirical expression proposed in [Ruan, 2020], namely $\beta = S/(S + \langle D \rangle)$, where $\langle D \rangle$ denotes the average cluster fractal dimension, and the fitting parameter S is found to be close to 1.

Additionally, it can be interesting to compare with [Conchúir, 2013; Zaccone, 2009a]. Indeed, in these papers, a theoretical framework is described for the breakup of fractal aggregate to get, for instance, the maximum stable aggregate size. The power-law exponent β is a function of the fractal dimension through

$$\beta = \frac{1}{D - 2.06491D - 0.0180344(3 - D)^{-1} + 4.98585} \quad (2.35)$$

or

$$\beta = \frac{2}{(\dim - D)(2(\zeta + 1) + (\dim - D)^{-1})} \quad (2.36)$$

with $\zeta \approx 3.8$ the exponent relating the mean coordination number to the particle volume fraction in [Alexander, 1998]. These expressions are somewhat similar to the exponent in equation (2.23). The power-law relationship is recovered but with a different analytical approach based on rates of aggregation and disaggregation and on calculations of coordination numbers. Also, there are very close results with [Xie, 2010] where it is easily comparable with figure 2.4.

On the experimental side, a number of works have reported results assessing the size of aggregates under the application of a mechanical stress. However, only a handful of papers explicitly state the values of the various parameters a , U , σ , δ , and D . Table 2.2 and figure 2.6 gather a selection of such previous works. First, table 2.2 shows that equation (2.23) predicts a typical cluster size ℓ_{th} which is of the same order as the experimental size ℓ_{exp} . All the parameters fall into commonly known ranges and justify that the previous approach may be a good proxy to evaluate the most stable cluster size. Second, figure 2.6 probes the sensitivity of ℓ/a with the adhesion number Ad by plotting the power-law exponent β in $\ell/a = Ad^\beta$ as a function of D . Except for a few points that lie far from the average estimation, most exponents are gathered along the prediction of equation (2.23), consistently with the numerical results of [Ruan, 2020], which provides strong support for the approach described in section 2.2.5.

Finally, figure 2.7 provides a sensitivity study of the value of ℓ upon the different parameters of equation (2.23) based on table 2.2. It is clear that the most critical parameters are D and δ as expected from equation (2.23). Therefore, particular attention must be considered to assess accurately these parameters. Yet, when one of these two parameters are unknown, the model can be used to estimate D or δ with good accuracy based on measurements of ℓ .

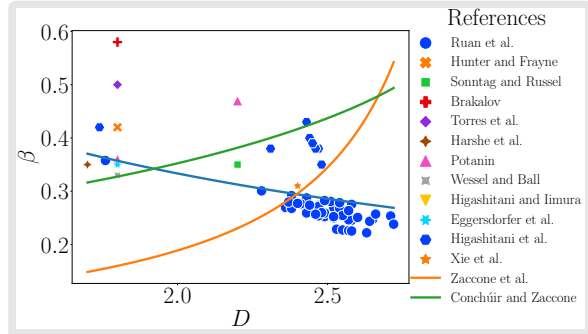


Figure 2.6: Power-law exponent β in $\ell/a = Ad^\beta$ as a function of the fractal dimension D of the aggregates extracted from [Ruan, 2020; Hunter, 1980; Sonntag, 1986; Sonntag, 1987a; Sonntag, 1987b; Brakalov, 1987; Torres, 1991a; Torres, 1991b; Harshe, 2011; Potanin, 1991; Potanin, 1992; Potanin, 1996; Wessel, 1992; Higashitani, 1998; Higashitani, 2001; Eggersdorfer, 2010; Kimbonguila Manounou, 2014; Zaccone, 2009a; Conchúir, 2013; Xie, 2010] (\bullet) and compared to the model prediction $\beta = (1 + D)^{-1}$ (blue solid line).

2.2.7 Summary of the contribution

The contribution of this work comes from the universal approach rationalised by a dimensionless number and an energy functional to describe aggregation and disaggregation processes. More precisely, the adhesion number weighs the balance between aggregating forces originating from the interaction potential and disaggregating forces coming from an external solicitation with a stress. This balance of forces allows to define an equilibrium size or mass which can be calculated through a scaling equation and can be approached through an energy potential with non equilibrium configurations. To our knowledge, this has never been performed in the literature.

Source	[Gibaud, 2020a; Gibaud, 2020b; Dagès, 2021; Varga, 2019]	[Nguyen, 2011; Klimchitskaya, 2000; Visser, 1972; Waite, 2001]
ℓ_{exp} (nm)	500	60
a (nm)	150	6.5
$U/k_B T$	20	60
σ (MPa)	0.1	2
δ (Å)	7	2
D	2.6	1.88
ℓ_{th} (nm)	300	55

Table 2.2: Experimental parameters and measurements of the aggregate size from the literature. ℓ_{exp} is the direct measurement of the aggregate size, while ℓ_{th} is the aggregate size estimated using equation (2.23) based on the parameters defined in the text and reported in the references of the first column.

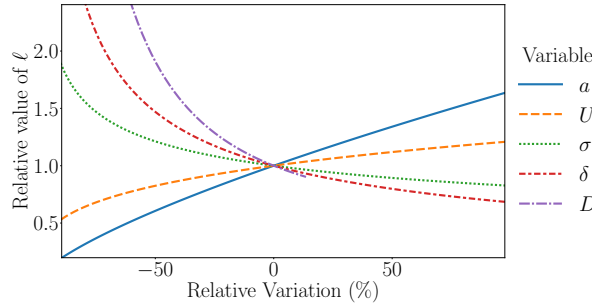


Figure 2.7: Sensitivity study of ℓ predicted by equation (2.23) upon relative variations of the different control parameters around the values listed in the first line of table 2.2 except for the fractal dimension, which is varied from 1 to 3.

2.3 Interpenetration of clusters of carbon-black particles [Dagès, 2022]

After having presented the competition between aggregation and disaggregation processes in a rather universal framework, we propose to focus on a particular case: the carbon-black particle suspension. The following section has been published in [Dagès, 2022]. This section comes from a study done using as entry data measurements by, notably, Noémie Dagès and Thomas Gibaud in *Ecole Normale Supérieure de Lyon*. My contribution lies in the construction of the model and some exploitation of experimental data. Most of the following section presents the experimental protocol and data which will be useful for the models described in chapter 3.

2.3.1 Abstract of the section

Colloidal gels are out-of-equilibrium soft solids composed of attractive Brownian particles that form a space-spanning network at low volume fractions. The elastic properties of these systems result from the network microstructure, which is very sensitive to shear history. Here, we take advantage of such sensitivity to tune the viscoelastic properties of a colloidal gel made of carbon black nanoparticles. Starting from a fluidized state at an applied shear rate $\dot{\gamma}_0$, we use an abrupt flow cessation to trigger a liquid-to-solid transition. We observe that the resulting gel is all the more elastic when the shear rate $\dot{\gamma}_0$ is low and that the viscoelastic spectra can be mapped on a master curve. Moreover, coupling rheometry to small angle X-ray scattering allows us to show that the gel microstructure is different from gels solely formed by thermal agitation where only two length scales are observed: the dimension of the colloidal and the dimension of the fractal aggregates. Competition between shear and thermal energy leads to gels with three characteristic length scales. Such gels structure in a percolated network of fractal clusters that interpenetrate each other. Experiments on gels prepared with various shear histories reveal that cluster interpenetration increases with decreasing values of the shear rate $\dot{\gamma}_0$ applied before flow cessation. These observations strongly suggest that cluster interpenetration drives the gel elasticity.

2.3.2 Introduction

In practice, gels of carbon black nanoparticles were chosen which can be tuned using shear history [Ovarlez, 2013; Helal, 2016; Dagès, 2021]. Here the gelation pathway of these gels is influenced as follows: starting from a fluidized state under an applied shear rate $\dot{\gamma}_0$, an abrupt flow cessation triggers a liquid-to-solid transition. Varying the shear rate intensity $\dot{\gamma}_0$ allows us to generate gels whose viscoelastic properties spans over a decade in stress units. Specifically, lower shear intensities yield more elastic gels upon flow cessation, while the viscoelastic spectrum for different $\dot{\gamma}_0$ shows a robust frequency dependence that can be rescaled onto a master curve. Using rheometry coupled to small angle X-ray scattering (SAXS), we further show that the gel microstructure is composed of clusters of size ξ_c and fractal dimension d_f separated by a cluster center to center distance ξ_s . Those structural parameters depend on $\dot{\gamma}_0$. More importantly, we show that $\xi_s < \xi_c$ meaning that adjacent clusters interpenetrate each others. The degree of interpenetration defined by the ratio ξ_c/ξ_s decreases for increasing values of $\dot{\gamma}_0$. The degree of interpenetration is crucial, as it controls the gel elasticity and captures the impact of $\dot{\gamma}_0$ on the gel viscoelastic properties, as confirmed by a fractal scaling model.

The outline of the section is as follows. The car-

bon black gels as well as our experimental toolbox are introduced in section 2.3.3. Second, in section 2.3.4, the experimental results are presented. How shear history allows tuning the gel viscoelastic properties will be showed, which can be rescaled onto a master curve. The fact that the gel structures itself in fractal clusters that interpenetrate each other is established. Third, in section 2.3.5, after dismissing a superposition principle to account for the scaling of the viscoelastic properties of the gel, a fractal scaling model establishing a direct link between the gel microstructure and the gel network elasticity as a function of the shear rate intensity $\dot{\gamma}_0$ applied before flow cessation is derived.

2.3.3 Materials and methods

2.3.3.1 Carbon black dispersions

Carbon black (CB) particles are fractal carbonated colloids that result from the partial combustion of hydrocarbon oils [Lahaye, 1994; Xi, 2006; Sztucki, 2007]. These particles are widely used in the industry for mechanical reinforcement or to enhance the electrical conductivity of plastic and rubber materials [Wang, 2018]. Among the large variety of carbon black particles [Herd, 1992; Martinez, 2017; Dagès, 2021; Richards, 2017; Hipp, 2021], Vulcan PF particles (Cabot, density $d_{cb} = 2.26 \pm 0.03$) were chosen. The density of Vulcan PF particles is $d_{cb} = 2.26 \pm 0.03$ and their radius of gyration is estimated to $r_g = 35$ nm with a 20% polydispersity, and their fractal dimension to $d_{f0} = 2.9$ (see Appendix appendix A.1 for details).

When dispersed in mineral oil (RTM17 Mineral Oil Rotational Viscometer Standard, Paragon Scientific, viscosity $\eta = 354$ mPa.s at $T = 20^\circ\text{C}$, density $d_{bck} = 0.871$), CB particles are weakly attractive. The depth U of the interparticle potential depends on the type of CB particles, the solvent, and the presence of dispersant, and falls typically in the range $U \sim 10 - 30k_B T$ [Trappe, 2007; Prasad, 2003]. At a working weight concentration in CB particles of $c_w = 4\%$, the particles aggregate to form a gel, i.e., a space-spanning network, which behaves as a viscoelastic soft solid. Indeed, at rest, the elastic modulus G' dominates the viscous modulus G'' in the limit of low frequencies, whereas the sample displays a solid-to-liquid transition beyond a critical strain $\gamma_y \sim 10\%$. Moreover, under steady shear, the flow curve that links the shear stress σ to the shear rate $\dot{\gamma}$ is well fitted by the Herschel-Bulkley model, $\sigma = \sigma_y + K\dot{\gamma}^n$ [Herschel, 1926b], with a dynamical yield stress $\sigma_y = 4.5$ Pa, a consistency index $K = 1.0 \text{ Pa}\cdot\text{s}^{1/0.83}$, and a fluidity index $n = 0.83$ (see figure A.2 in appendix A.2).

2.3.3.2 Rheology

In the present work, a rheometer is used both to measure the mechanical properties of CB gels and to shape up

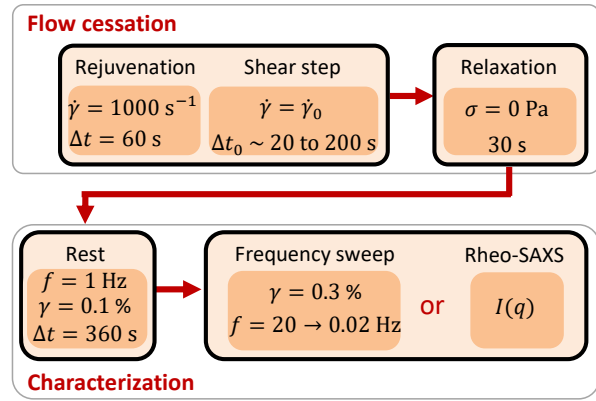


Figure 2.8: Experimental protocol: schematic of the flow cessation and characterization sequences.

their microstructure. Experiments are carried-out with two stress-controlled rheometers: (i) a MCR301 (Anton Paar) equipped with a rough cone (radius 40 mm, angle 1°) and a smooth bottom plate both made of steel, and (ii) a Haake RS6000 (Thermo Scientific) equipped with a Couette geometry composed of concentric polycarbonate cylinders (inner diameter 20 mm, outer diameter 22 mm, and height 40 mm) for rheo-SAXS experiments. Both apparatuses give identical results provided that the shear rate does not exceed 500 s^{-1} in the Couette geometry due to the Taylor-Couette instability [Fardin, 2014].

2.3.3.3 Small angle X-ray scattering

The microstructural properties of the carbon black dispersion were investigated using rheo-SAXS measurements carried out on the ID02 beamline at the European Synchrotron Radiation Facility (ESRF, Grenoble, France) [Narayanan, 2022]. The incident X-ray beam of wavelength 0.1 nm is collimated to a vertical size of $50 \mu\text{m}$ and a horizontal size of $100 \mu\text{m}$. The 2D scattering patterns were measured using an Eiger2 4M pixel array detector and the subsequent data reduction procedure is described elsewhere [Panine, 2003]. The scattering intensity $I(q)$ is obtained by subtracting the two-dimensional scattering patterns of the carbon black gel and the mineral oil. The resulting scattering intensity presented in this article always remained isotropic (see figure A.8 in appendix A.7). Therefore, the normalized intensity pattern is radially averaged to obtain one dimensional $I(q)$. Note that measurements were performed in both radial and tangential configurations, and they turn out to be equivalent due to the isotropy of the gel microstructure.

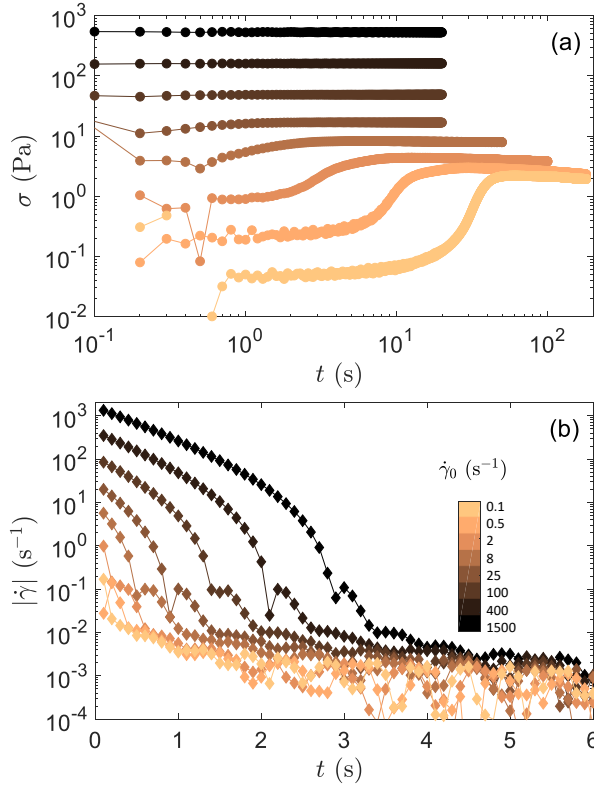


Figure 2.9: Flow cessation sequence performed with different values of the shear rate $\dot{\gamma}_0$ in a $c_w = 4\%$ carbon black dispersions. The sequence is composed of two steps: a quench in shear rate from 1000 s^{-1} to $\dot{\gamma}_0$ yielding a stress response $\sigma(t)$ pictured in (a), followed by a complete flow cessation which results in (b) the relaxation of $|\dot{\gamma}|(t)$ when imposing $\sigma = 0\text{ Pa}$. In (a) and (b) colors encode the value of $\dot{\gamma}_0$ ranging from 1500 (black) to 0.1 s^{-1} (yellow), see legend in (b).

2.3.3.4 Rheological protocol

The protocol is applied and sketched in figure 2.8, which is divided in two sequences: a flow cessation sequence to shape up the gel properties followed by a sequence of characterization of the gel mechanical properties inherited from the flow cessation protocol.

In practice, the flow cessation protocol is divided into three steps. First, a rejuvenation step is carried out during which the sample is sheared at $\dot{\gamma} = 1000\text{ s}^{-1}$ for $\Delta t = 60\text{ s}$ to erase any shear history that would influence the gel mechanical properties later on. Second, the shear intensity is modified by imposing a quench from $\dot{\gamma} = 1000\text{ s}^{-1}$ to a constant shear rate $\dot{\gamma}_0 \in [0.1, 1500]\text{ s}^{-1}$ for a duration $\Delta t_0 \in [20, 200]\text{ s}$. figure 2.9(a) shows the stress response $\sigma(t)$ of the CB gel resulting from quenches to various values of $\dot{\gamma}_0$. For high shear rates $\dot{\gamma}_0$, a duration of $\Delta t_0 = 20\text{ s}$ is sufficient to reach a steady state. However, for $\dot{\gamma}_0 < 10\text{ s}^{-1}$, $\dot{\gamma}_0$ must be imposed for longer durations, as σ increases significantly, before

reaching a maximum and then slowly decreases. The increase of σ at short time scales corresponds to a transient regime necessary for the system to adapt to the new shear rate $\dot{\gamma}_0$ [Dullaert, 2005] (see also appendix A.2). The slow decrease at longer time scales might be due to some slippage of the dispersion at the walls of the shear cell [Meeker, 2004]. Third, a flow cessation is applied by imposing $\sigma = 0\text{ Pa}$ for 30 s , while recording the shear-rate response $\dot{\gamma}(t)$ as displayed in figure 2.9(b). $\dot{\gamma}$ is observed to decrease to values beneath 10^{-3} s^{-1} within a few seconds indicating that the rotor is immobile and that flow cessation is complete. At short time scales, the shear rate decreases exponentially as expected for a simple, viscous fluid. At intermediate timescales, $\dot{\gamma}$ drops faster than exponentially and displays oscillations typical of the viscoelastic ringing observed in soft solids during creep tests [Zölzer, 1993; Baravian, 1998; Ewoldt, 2007; Benmouffok-Benbelkacem, 2010]. This indicates that gels reforms within a few seconds.

Finally, the characterization sequence following flow cessation consists in three steps. First, the system is let to rest for 360 s , while measuring the elastic G' and viscous G'' modulus using oscillations of small amplitude $\gamma = 0.1\%$ at a frequency $f = 1\text{ Hz}$. As shown in the appendix A.4 figure A.3, the viscoelastic moduli of the dispersion rapidly reach a regime where aging is weak. Second a frequency sweep is performed at $\gamma = 0.3\%$ with 10 points per decade for frequencies f ranging from 0.02 to 20 Hz . To gain some insights on the gel microstructure during these two sequences, the entire protocol was carried out in the rheo-SAXS setup for four distinct shear intensity $\dot{\gamma}_0$. The scattered intensity $I(q)$ of the gel obtained after flow cessation is discussed in the next section.

Based on reference [Radhakrishnan, 2017], we estimate that through out the rheological protocol the gel is homogeneously sheared and does not display shear banding. Indeed shear banding may appear in carbon black suspensions. When going from large to low value of the shear rate, shear banding only happens below a critical shear rate of $\dot{\gamma}_{SB}$. $\dot{\gamma}_{SB}$ is easily identifiable on the flow curve by a drop of the shear stress σ at low shear rates. From figure A.2 we determine $\dot{\gamma}_{SB} \sim 0.1\text{ s}^{-1}$. This value justifies carrying out preshear of intensity $\dot{\gamma}_0$ no lower than 0.1 s^{-1} to guarantee the homogeneity of the flow profile in the rheometer.

2.3.4 Results

2.3.4.1 Impact of the shear rate $\dot{\gamma}_0$ on the gel linear viscoelastic spectrum

We first focus on the impact of $\dot{\gamma}_0$ on the linear viscoelastic properties of the gel formed upon flow cessation (see ‘‘Frequency sweep’’ in the characterization sequence sketched in figure 2.8). The gel frequency spec-

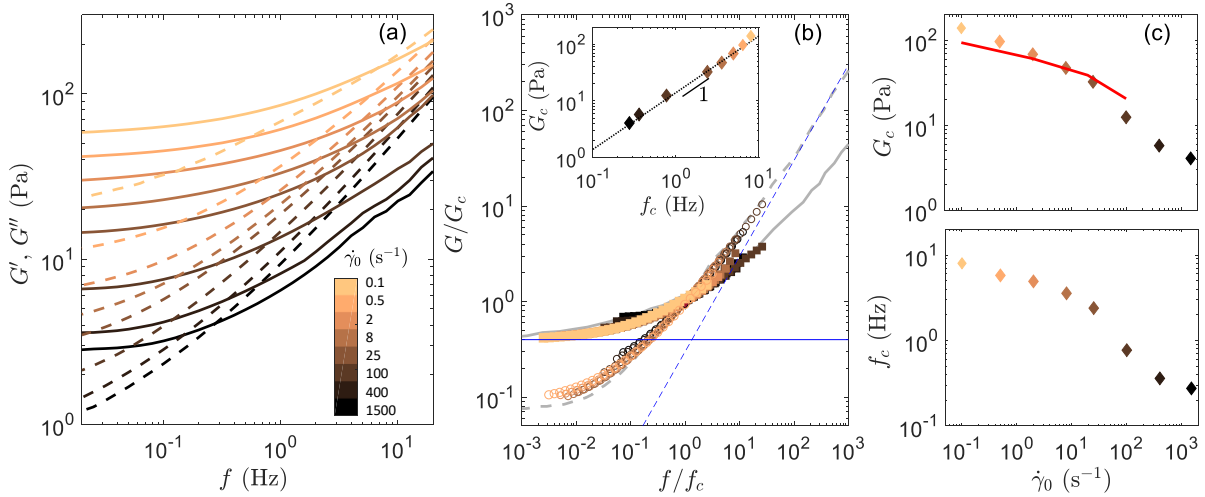


Figure 2.10: (a) Elastic G' and viscous modulus G'' vs. the frequency f in a $c_w = 4\%$ carbon black dispersions. The color codes for the shear rate intensity $\dot{\gamma}_0$ applied before flow cessation. (b) Normalized viscoelastic spectrum: G'/G_c and G''/G_c vs. the normalized frequency f/f_c , where G_c and f_c denote respectively the modulus and the frequency at which $G' = G''$ in (a). The blue curves correspond to a Kelvin-Voigt model (see appendix A.5). The grey curves correspond to the master curves obtained for G' (solid line) and G'' (dashed line) by rescaling viscoelastic spectra of CB dispersions in oil for various volume fractions [data extracted from [Trappe, 2000]]. Inset: G_c vs. f_c . The red dotted line is the best linear fit of the data: $G_c = 14.5 f_c$. (c) Evolution of G_c (top) and f_c (bottom) vs. $\dot{\gamma}_0$. The red line is the best fit of the data using equation (3.1) and the structural information reported in figure 2.12. The best fit is obtained with a single adjustable parameter, namely the prefactor $G_{CB} = 9$ Pa.

trum is reported in figure 2.10(a) for various values of the shear rate intensity $\dot{\gamma}_0$ spanning over four decades. Overall, we observe that low $\dot{\gamma}_0$ produce more elastic gels. More precisely, whatever the shear rate intensity $\dot{\gamma}_0$, the elastic and viscous moduli are increasing functions of the frequency and cross at a frequency f_c that shifts towards larger values for decreasing $\dot{\gamma}_0$. Moreover, in the limit of low frequencies, all spectra show a plateau in elasticity with $G' > G''$, which confirms the solid-like behavior of the sample, regardless of the shear rate intensity applied prior to flow cessation. The shape of the viscoelastic spectrum is robust, and appears merely shifted, which prompts us to construct a master curve from the data in figure 2.10(a). By normalizing each spectra by the coordinate (f_c, G_c) defined by the crossover of G' and G'' , we obtain the master curve reported in figure 2.10(b). This scaling behavior is also clearly visible in the $\tan(\delta) = G''/G'$ representation. Since G' and G'' are scaled by the same factor, building a master curve with $\tan(\delta)$ from different $\dot{\gamma}_0$ only requires to scale the frequency axis as shown in figure A.4. The asymptotic behavior of the master curve corresponds to a Kelvin-Voigt model (see appendix A.5) displayed as blue lines in figure 2.10(b). At low frequencies, i.e., $f \ll f_c$, the elastic modulus G' tends towards a plateau value much larger than G'' , which is the hallmark of a solid-like behavior at rest. At high frequencies, i.e., $f \gg f_c$, the viscous modulus G'' dominates and increases linearly with the frequency and the sol-

vent viscosity η , such that $G'' = 2\pi\eta f$. In this range of frequencies, the variations of G'' correspond to the viscous dissipation due to the thermal fluctuations of the gel network in the background solvent. We note that the master curve can be fully fitted by a fractional Kelvin-Voigt model (see appendix A.5). Such a master curve is strongly reminiscent of that obtained on fractal gels by varying the particle volume fraction, and the interparticle potential [Trappe, 2000; Prasad, 2003; Won, 2005]. In contrast, here, the master curve is generated by varying the shear history on a sample of fixed composition. Yet, rescaled data extracted from [Trappe, 2000] and obtained with different CB particles suspended in another solvent [see gray curves in figure 2.10(b)], fall remarkably well on our master curve. This suggests that various shear histories allows generating gels, whose microstructure shares some similarity with that generated by varying the colloid volume fraction.

The high sensitivity of CB gels to shear history is encoded in the dependence of the locus of G' and G'' crossing point (f_c, G_c) with $\dot{\gamma}_0$. As shown in figure 2.10(c), both f_c and G_c decrease by almost two orders of magnitude when increasing $\dot{\gamma}_0$ from 0.1 s $^{-1}$ to 1500 s $^{-1}$. Such influence of shear history is not obvious, for it shows a trend similar to that observed in boehmite gels [Sudreau, 2022] and silica sphere and rods gels [Das, 2022] but opposite to that reported in depletion gels, where a strong shear yields a more homogeneous and more elastic structure upon flow cessa-

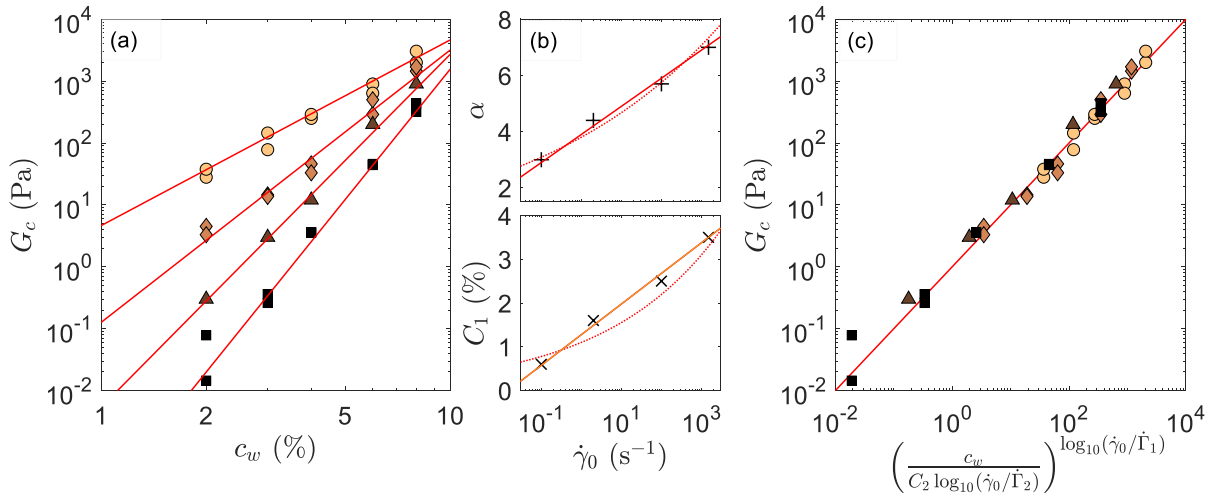


Figure 2.11: (a) Evolution of G_c as a function of the weight concentration in carbon black particles c_w for various shear rates applied prior to flow cessation: $\dot{\gamma}_0 = 0.1$ s $^{-1}$ (circle), 2 s $^{-1}$ (diamond), 100 s $^{-1}$ (triangle) and 1500 s $^{-1}$ (square). Red lines are the best power-law fit of the data $G_c = (c_w/C_1)^\alpha$. Both α and C_1 depend on $\dot{\gamma}_0$. (b) α and C_1 vs. the shear rate $\dot{\gamma}_0$. Red lines are the best logarithmic fit of the data: $\alpha = \log_{10}(\dot{\gamma}_0/\dot{\Gamma}_1)$ with $\dot{\Gamma}_1 = 10^{-3.9}$ s $^{-1}$ and $C_1 = C_2 \log_{10}(\dot{\gamma}_0/\dot{\Gamma}_2)$ with $C_2 = 0.7$ % and $\dot{\Gamma}_2 = 0.015$ s $^{-1}$. Dotted lines are the best power law fits. (c) Evolution of G_c as function of the dimensionless concentration and shear rate.

tion [Koumakis, 2015].

2.3.4.2 Influence of the carbon black weight concentration

The rescaling and the master curve introduced in section 2.3.4.1 are robust to changes in the CB weight concentration, from $c_w = 2$ to 8 %. For instance, the viscoelastic spectrum of a $c_w = 2$ % carbon black dispersion obtained with various shear rate $\dot{\gamma}_0$ applied before flow cessation can be rescaled on the same master curve as that displayed in figure 2.10(b) (see figure A.6 in appendix A.6). Moreover, for a fixed shear intensity $\dot{\gamma}_0$, the modulus G_c increases as a power law of c_w , $c_w = (c_w/C_1)^\alpha$ with a concentration C_1 and an exponent α that depends on $\dot{\gamma}_0$ [figure 2.11(b)]. While a power-law increase of the gel elasticity for increasing particle weight concentration or volume fraction is classically reported in colloidal gels with an exponent α ranging between 2 and 4.5 depending on the range of the interparticle potential and the nature of the particles [Buscall, 1988; Trappe, 2001; Prasad, 2003], the sensitivity of α to shear history is a key result of the present study. Here, in figure 2.11(b), we show that α increases for increasing shear rate intensity applied before flow cessation, varying between $\alpha \approx 3$ for $\dot{\gamma}_0 = 0.1$ s $^{-1}$ to surprisingly high values, i.e. $\alpha \approx 7$ for $\dot{\gamma}_0 = 1500$ s $^{-1}$. Finally, in figure 2.11(c), we show that G_c follows a master curve driven by a dimensionless concentration and shear rate intensity. Although this dependence remains empirical, this master curve highlights the fact that there are many ways to obtain gels with identical G_c . For instance to

get $G_c \approx 3$ Pa one can either prepare a gel at ($c_w = 4$ %, $\dot{\gamma}_0 = 1500$ s $^{-1}$), ($c_w = 3$ %, $\dot{\gamma}_0 = 100$ s $^{-1}$) or ($c_w = 2$ %, $\dot{\gamma}_0 = 2$ s $^{-1}$).

To connect these results to the gel microstructure, one can be tempted to combine the power-law exponent α with the scaling theories developed for fractal gels [Shih, 1990], in order to estimate the cluster fractal dimension d_f . The theory developed in the context of Brownian aggregation distinguishes between two types of network, depending on the relative value of the elastic constant of the inter-cluster links to that of the cluster. In the case of weak links $\alpha = 1/(3 - d_f)$, which yields $2.6 < d_f < 2.9$, whereas in the case of strong links, $\alpha = (3 + x)/(3 - d_f)$ with $x < d_f$ the fractal dimension of the gel backbone, and $1.5 < d_f < 2.5$ (see figure A.7 in appendix A.6). These values motivate an experimental characterization of the gel microstructure, and especially of the cluster fractal dimension to test the relevance of such scaling theories.

2.3.4.3 Microstructure of the gel as function of the shear $\dot{\gamma}_0$ applied before flow cessation

To better understand the interplay between shear history and the gel microstructural properties, we perform rheo-SAXS experiments using the protocol sketched in figure 2.8. The scattering intensity $I(q)$ measured 360 s after flow cessation protocol for four different shear rate intensities $\dot{\gamma}_0$ prior to flow cessation is reported in figure 2.12(a), as a function of the wave number q . In all four cases, the scattered intensity $I(q)$ presents similar features. First, $I(q)$ is isotropic, i.e., tangential and ra-

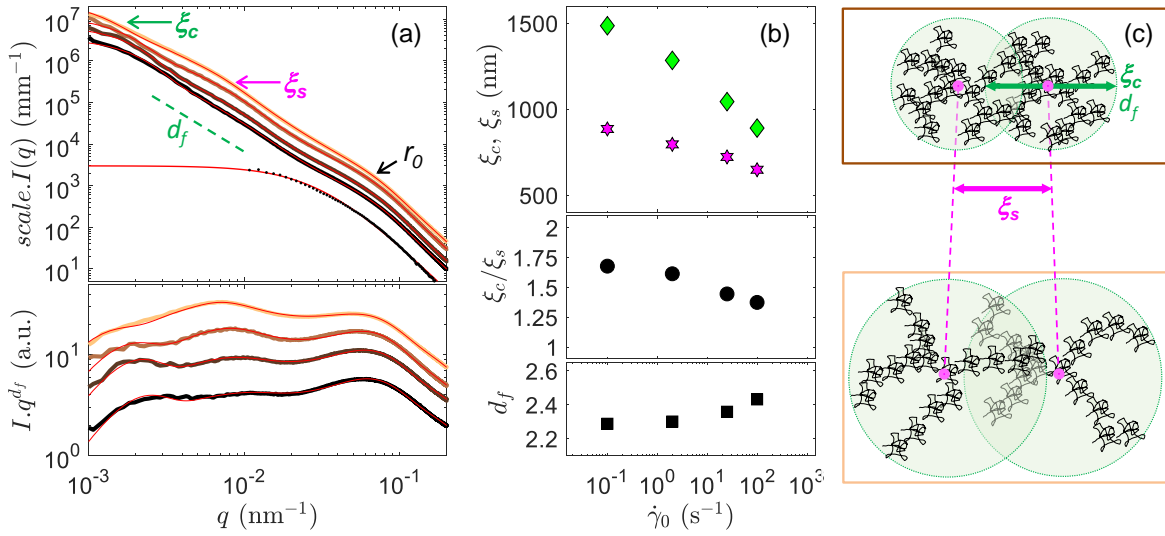


Figure 2.12: Structure of the gel obtained after flow cessation. The scattering intensity $I(q)$ is measured 360 s after the end of the flow cessation test for different preshear $\dot{\gamma}_0$ in carbon black dispersions at $c_w = 4\%$. (a) The thick lines represent the evolution of $I(q)$ (top) and $I \cdot q^{d_f}$ (bottom) as a function of the wave vector q . Color codes from pink to black for $\dot{\gamma}_0 = 0.1, 2, 20$ and $100 s^{-1}$. The dotted line is the form factor obtained at $c_w = 0.1\%$. Red lines are fit to the experimental data by a two-level Beaucage model composed of the CB particles of radius r_0 and clusters of size ξ_c with fractal dimension d_f , modified by an intercluster structure factor that accounts for the center-to-center distance ξ_s between the clusters. The scattering intensity $I(q)$ and $I \cdot q^{d_f}$ are translated along the y-axis for better readability. (b) Evolution of the fit parameters ξ_c (green diamond), ξ_s (pink star), ξ_c/ξ_s (circle) and d_f (square) as a function of $\dot{\gamma}_0$. For the four fits, we obtained radius of gyration $r_0 = 28.5$ nm. (c) Schematic of the clusters evolution as the preshear $\dot{\gamma}_0$ decreases between the top and bottom panels.

dial measurements are equivalent (see figure A.8 in appendix A.7). Therefore, the gel displays an isotropic structure at all length scales probed by SAXS, which is why we only report the azimuthally averaged $I(q)$. Second, $I(q)$ presents three characteristic bumps around $0.04, 0.01$ and $0.002 nm^{-1}$ characteristic of three length scales. This structure is atypical. Indeed, in gels driven solely by thermal agitation, $I(q)$ classically displays only two characteristic length scales: the particle size r_0 and the cluster size ξ_c separated by a power-law regime, and the exponent of which is related to the cluster fractal dimension [Courtens, 1987].

Here, we attribute the high- q bump to the CB particles of size r_0 , the low- q bump to clusters of size ξ_c and fractal dimension d_f , and the bump at intermediate q to the structural distance ξ_s between the centers of two adjacent clusters. Those bumps appear more clearly in the Kratky-like representation $I \cdot q^{d_f}$ reported in figure 2.12(a). In the Kratky-like representation we used the d_f displayed in figure 2.12(b).

A description of the gel microstructure based on three characteristic length scales is implemented in a modified two-level Beaucage model. In short, the two-level Beaucage model [Beaucage, 1995; Beaucage, 1996] accounts for the scattering of clusters of size ξ_c and fractal dimension d_f composed of particles of size r_0 . To

account for the increase of scattering at ξ_s , we have multiplied the cluster scattering intensity term in the Beaucage model by an ad-hoc inter-cluster structure factor (see appendix A.7 for more details). This modified Beaucage model provides an excellent fit to the experimental data obtained for different shear histories [figure 2.12(a)]. Moreover, since the gel weight concentration is identical in the four measurements, the fit parameters r_0 , ξ_c , d_f and ξ_s should obey mass conservation. In practice, such a constraint can be expressed at the scale of the unit cell of the gel network, i.e., the minimum structural repeating unit necessary to construct the gel structure defined by the correlation length ξ_s . The number of particles $N = (\xi_c/r_0)^{d_f}$ in a unit cell corresponds to the number of particles in the cluster of size ξ_c and fractal dimension d_f . Based on the values of the fit parameters obtained from adjusting the modified two-level Beaucage model to the SAXS data, we check that, indeed, $\rho = (\xi_c/r_0)^{d_f}/\xi_s^3$ remains constant across the four measurements with $\rho = 7250 \pm 230$ particles/ μm^3 . This value is also in agreement with the carbon black weight concentration $c_w = 4\%$ (see figure A.10 in appendix A.7), which confirms that our analysis of the scattering data is self-consistent.

Figure 2.12(b) shows the dependence of the fit parameters ξ_c , ξ_s , and d_f with the shear rate intensity $\dot{\gamma}_0$ ap-

plied before flow cessation. A gel prepared with a lower shear intensity shows a larger and looser microstructure since ξ_c increases and d_f decreases for decreasing $\dot{\gamma}_0$. Considering the evolution of only those two parameters suggests a decrease of the gel elasticity for decreasing values of $\dot{\gamma}_0$, in stark contrast with our observations. However, ξ_c and d_f are not the only parameters, and the correlation length ξ_s , which corresponds to the cluster to cluster center distance, plays an important role. In particular, ξ_s is smaller than the cluster size ξ_c , indicating that the clusters interpenetrate each other. Such cluster interpenetration has recently been suggested in carbon black gels to interpret step down shear rate rheology experiments [Wang, 2022]. In our case, for lower shear rate intensity $\dot{\gamma}_0$ prior to flow cessation, the ratio ξ_c/ξ_s increases, i.e., the clusters become more interpenetrated, accounting for the reinforcement of the gel elasticity. We therefore hypothesize that the gel elasticity is related to the cluster interpenetration, increasing the elasticity of the gel network as compared to the case where clusters would be packed in a random close-packing configuration [figure 2.12(c)].

2.3.5 Discussion

We have used mechanical shear to explore various configurations of carbon black gels. Starting from a fluidized state under an applied shear rate $\dot{\gamma}_0$, we use an abrupt flow cessation to trigger a liquid-to-solid transition. Varying $\dot{\gamma}_0$ allows us to tune the gel viscoelastic properties, whose spectrum can be mapped on a single master curve asymptotically defined at low frequencies by the elasticity of the gel network G_∞ and at high frequencies by the viscosity η of the background solvent. Coupling rheometry and SAXS, we have shown that the gel microstructure is composed of fractal clusters that interpenetrate each other, and the degree of interpenetration appears to be a key parameter contributing to the gel elasticity. We have validated this hypothesis developing an interpenetration ϕ -power law model that account for the decrease of elasticity as $\dot{\gamma}_0$ increases.

2.3.5.1 Is the scaling behavior of the viscoelastic spectrum a consequence of an underlying superposition principle?

In light of the scaling behavior of the viscoelastic spectrum, it is tempting to interpret the master curve obtained by varying $\dot{\gamma}_0$ as the result of some shear-frequency superposition principle. Superposition principles in soft matter mechanics rely on the idea that dynamical processes in soft materials can be accessed equivalently using time or frequency and another well-chosen variable. For example, time-temperature superposition in polymer melts [Van Gurp, 1998] relies on the acceleration of all activated processes at high tempera-

tures, enabling probing of longer effective time scales at high temperatures. In other words, the average relaxation time of the material changes with temperature without affecting the shape of its viscoelastic spectrum.

This is not what we observe here, for the rescaling of the viscoelastic spectrum requires a shift along the frequency axis and a shift along the viscoelastic moduli. Such behavior has, however, been observed in different systems and still attributed to a superposition principle such as in colloidal low-methoxyl pectin [Huang, 2021] in the context of gelling time/relaxation time superposition, protein condensates [Jawerth, 2020] in the context of aging Maxwell fluids, in triblock copolymer solutions [Krishnan, 2010] in the context of time-composition superposition, and in soft colloidal glasses [Wen, 2015; Wen, 2014] in the context of time-concentration superposition. In the case of carbon black gels subject to various shear rate intensities before flow cessation, the viscoelastic spectrum scaling is attributed to deep structural changes, such as the cluster fractal dimension d_f (the gel does not have self-similar structures) rather than changes in the dynamics. Such results rule out a superposition principle. In other words, it is possible to form carbon black gels with the same value of the elastic plateau G_∞ using different gels structures through shear history and concentration as shown in figure 2.11(c).

2.3.5.2 Physical origin of the gel structure

The multiple metastable gels formed following various shear preparations belong to the category of fractal gels. This is probably why our results do not match the trends observed in [Koumakis, 2015] which belong to gels formed through arrested phase separation. We find clusters of fractal dimension $d_f \in [2.3, 2.5]$ larger than the prediction from diffusion-limited cluster aggregation DLCA where $d_f \sim 1.8$ [Weitz, 1984] or reaction-limited cluster aggregation RLCA where $d_f \sim 2.1$ [Schaefer, 1984] but smaller than the value obtained for sheared fractal aggregates where $d_f \sim 2.6$ [Wessel, 1992].

In our system, the Brownian time $\tau_B = R^3 6\pi\eta/k_B T \in [0.07; 1600]$ s is set by the diffusion of particles of size R ranging from the CB dimension $r_0 = 35$ nm to the cluster size $\xi_c \sim 1$ μ m. τ_B compares to the time necessary for flow cessation to take place $\tau_{fc} < 4$ s (figure 2.9) supporting again the fact that aggregation and flow cessation are coupled.

The interplay between flow and structure in gels has been tackled mainly in the flow regime [Hipp, 2021; Nabizadeh, 2021] but has not been formalized to model multiple metastable gel states induced by a shear protocol. This is an important challenge in the pursue of memory materials [Keim, 2019] which aim to encode, access, and erase signatures of past history in the state of a system.

The flow cessation protocol inducing the sol-gel transition could be addressed qualitatively through the use of the Mason number Mn [Varga, 2018; Jamali, 2020], which is here in the range $[3.5 \times 10^{-4}, 5.2]$, and agrees rather well with the values in [Jamali, 2019a; Jamali, 2020], or the adhesion number Ad [Eggersdorfer, 2010; Marshall, 2014; Kimbonguila Manounou, 2014], which is here in the range $[3.6, 5.5 \times 10^4]$ weighting the relative importance of adhesion forces compared to shear forces and quantitatively using coagulation-fragmentation equation [Banasiak, 2020a; Stadnichuk, 2015; Sorensen, 1987] which embrace the competition between different aggregation mechanism and fragmentation through shear or collisions.

Finally, we suggest another way to apprehend the multiple metastable gels formed through flow cessation. Indeed, carbon black gels as many other systems display delayed yielding [Gibaud, 2010; Sprakel, 2011; Grenard, 2014], i.e., when pushed at a constant shear stress σ , the gel initially at rest will start flowing on time scales that decrease exponentially with increasing value of σ . Our results prompt us to revisit delayed yielding phenomena and answer the following questions: How does gel prepared through flow cessation impact the delayed yielding mechanism? Is delayed yielding still characterized by an Arrhenius law? If so, is the energy barrier necessary to flow in the delayed yielding experiment related to the energy barrier to form the gel state induced by flow cessation?

2.3.6 Summary of the contribution

We have demonstrated that carbon-black particles suspensions may be modified from the microscopic structure point of view and from a rheological point of view. How the microscopic structure evolves according to the preshear protocol is a direct consequence of the previous more general framework. The data correctly fit microstructure model to follow the evolution of it under external solicitation. We will see in the next chapter how there is a feedback from the microscopic structure to the rheology of the system.

2.4 Conclusion

In this whole chapter, we have investigated how the macroscopic environment may influence the microscopic structure of a gel. Starting from the competition between aggregation and disaggregation processes, we have rationalized the balance with an overall energy functional which should be minimize to reach the equilibrium size coming from the macroscopic solicitation and the microscopic adhesion forces. A similar framework has been considered in the case of carbon-black particles where the micro-

scopic structure was caught through SAXS measurements under specific rheological conditions. In the case of pre-sheared gel studied at rest or studied during flow, the competition of forces highlights an equilibrium which tends to grow when the macroscopic solicitation decreases. We have thus emphasized that this is a universal phenomenon which needs further research to properly be quantified according to macroscopic and microscopic conditions.

Chapter 3

From the microscopic structure to the rheology

Objectives

This chapter is dedicated to the construction of rheological laws, that come directly from materials microstructures. Regarding suspensions, we will precisely talk about how multiple fractal structures and clusters interpenetration leads to specific rheological behaviours.

Objectifs

Ce chapitre est consacré à la construction de lois rhéologiques, qui proviennent directement des microstructures des matériaux. En ce qui concerne les suspensions, nous parlerons précisément de la façon dont les multiples structures fractales et l'interpénétration des clusters conduisent à des comportements rhéologiques spécifiques.

3.3.5	Summary of the contribution .	57
3.4	The clusters of clusters vs the interpenetrating clusters approach [Bouthier, 2023b]	58
3.4.1	Abstract of this section	58
3.4.2	Content of this section	58
3.4.3	Three length scales carbon black gels resulting from flow cessations	58
3.4.4	Structure of the gels	60
3.4.5	Modelling gels elasticity	62
3.4.6	Summary of the contribution .	68
3.5	Conclusion	69

Contents

3.1	Introduction	50
3.2	Interpenetration of clusters [Dagès, 2022]	50
3.2.1	Abstract of this section	50
3.2.2	A structure based model to account for gel elasticity	50
3.2.3	The interpenetration model	51
3.2.4	Summary of the contribution	52
3.3	Multiple fractal [Bouthier, 2022]	53
3.3.1	Abstract of this section	53
3.3.2	Content of this section	53
3.3.3	Theoretical approach	53
3.3.4	Comparing with the literature	57

3.1 Introduction

After having studied how an external solicitation of the macroscopic environment can modify the microscopic structure of a material in the previous chapter, I will present here how a given microscopic structure can bring certain rheological behaviours. As before, scaling laws are crucial in this kind of reasoning and are based on arrangements of simple rheological elements such as springs in parallel or in series. The difficulty relies on the need to find the proper relevant length scale and form factor used to extrapolate microscopic interactions towards the macroscopic scale.

Hence, two different microstructure models created from known structure in the literature are presented: namely the interpenetration of clusters and the multiple fractal model. These models will be derived theoretically before trying to apply them on experimental data and to compare their performances.

3.2 Interpenetration of clusters [Dagès, 2022]

My contribution in this section relies on the complete construction of the model, the demonstration of the formulas and discussions comparing what exists in the literature. Hence, this model has to be put in perspective with the experimental results of [section 2.3](#).

3.2.1 Abstract of this section

Our results, which are in stark contrast to previous literature, where gel elasticity was either linked to cluster connectivity or to bending modes, highlight a novel local parameter controlling the macroscopic viscoelastic properties of colloidal gels

3.2.2 A structure based model to account for gel elasticity

There are numerous models accounting for the elastic properties of fractal gels derived from microscopic considerations, namely the ϕ -power law models, especially in the context of diffusion-limited cluster aggregation (DLCA) and reaction-limited cluster aggregation (RLCA) [Wessel, 1992; Shih, 1990; Kantor, 1984a; Kantor, 1984b; Mewis, 2012; Marangoni, 2000; Gravelle, 2021; Roldughin, 2003; Mellema, 2002; Wu, 2001]. However, these models do not take into consideration the case where shear history interferes with the gelation pathway activated by thermal energy. Therefore, unsurprisingly, such models cannot capture our observations (see [figure A.7](#) in [appendix A.7](#))¹. These

¹In short, [figure A.7](#) recalls that the fractal dimension d_f estimated from SAXS measurements are not compatible with both the weak-link

models notably predict that the cluster size ξ_c is set by its fractal dimension d_f , the particle volume fraction ϕ and the particle size r_0 in stark contrast with our observations where the shear applied prior to flow cessation appears as an additional key parameter that act on the gel structure. Moreover, in these models, the elastic properties of colloidal gels are either connected to the local bending cost of the particle network, or to the cluster connectivity. However, to the best of our knowledge, none of these approaches accounts for an overlap, or equivalently for an interpenetration, of two neighboring clusters.

Here, we introduce the interpenetration ϕ -power law model. This model is an implementation of the ϕ -power law models proposed in [Shih, 1990; Mellema, 2002; Wu, 2001]. In practice, we assume that the gel is composed of particles of size r_0 that form clusters of size ξ_c and fractal dimension d_f separated by a center-to-center distance ξ_s . If $\xi_s > \xi_c$, the clusters are independent and the dispersion is a fluid. However, if $\xi_s < \xi_c$, clusters interpenetrate each other and form a gel. We have mostly replaced the factor from the ϕ -power law models that accounts for the elasticity of two adjacent clusters by an elongation elasticity due to the interpenetration. We assumed a decomposition of the microscopic stiffnesses in three contributions as springs in series, namely the intra-cluster, the intermicroscopic and the interpenetration, respectively. We additionally assumed that the interpenetration stiffness is negligible at the microscopic scale, thus dominates the macroscopic rheological behaviour. The gel elastic modulus G'_∞ at low frequencies is calculated in [section 3.2.3](#) and yields the following expression:

$$G' = \underbrace{\frac{U}{r_0 \delta^2}}_{G_{CB}} \underbrace{\frac{1}{2} \left(\frac{\xi_c}{r_0}\right)^{d_f} \left(1 + \frac{\xi_s}{2\xi_c}\right)^{\frac{d_f}{3}} \left(1 - \frac{\xi_s}{\xi_c}\right)^{\frac{2d_f}{3}}}_{g_{\text{Interp}}} \times \underbrace{\phi \left(\frac{\xi_s}{r_0}\right)^2 \left(\frac{\xi_c}{r_0}\right)^{-d_f}}_{g_{\text{Net}}} \quad (3.1)$$

This expression displays an elasticity that follow the hierarchical structural properties of the gel. G_{CB} is the elasticity arising from colloid-colloid interactions where U and δ are respectively the depth and the range of the carbon black attraction. g_{Interp} corresponds to the scaling that accounts for the cluster-cluster interpenetration and g_{Net} is the scaling attributed to the network formed by the clusters at the macroscopic scale.

To test the relevance of interpenetration ϕ -power law model, we report in [figure 2.10\(c\)](#) the best fit of G_c as a function of $\dot{\gamma}_0$ using [equation \(3.1\)](#) with the values of the structural parameters inferred from [figure 2.12\(b\)](#), the regime and the strong-link regime as presented in [Shih, 1990].

fact that $G'_\infty = 0.3G_c$ (see section 3.2.3), and the sole adjustable parameter $G_{CB} = 9\text{Pa}$. The model correctly captures the decrease of the elasticity of the gel network as $\dot{\gamma}_0$ increases. However, taking $U = 10 k_B T$ and $\delta = 0.2r_0$ we obtain $G_{CB} \sim 2000 \text{ Pa}$ a value much larger than the fit value: the model fails to capture the absolute value of the gel elasticity.

The interpenetration ϕ -power law model thus shows that cluster interpenetration accounts for the scaling of the mechanical properties of the gels and allows to rationalize the counter-intuitive observation that lower shear rate intensities before flow cessation yield stronger gels. Such results raise open questions, which are listed below.

3.2.3 The interpenetration ϕ -power law model, a model of the gel elasticity based on scaling arguments

We assume that the gel is composed of particles of size r_0 that form clusters of size ξ_c and fractal dimension d_f separated by a center to center distance ξ_s . If $\xi_s > \xi_c$, the clusters are independent and the dispersion is a fluid. However, if $\xi_s < \xi_c$, clusters interpenetrate each other and form a gel. To model the elastic constant of the gel network, we follow the demonstrations of the ϕ -power law models proposed in [Shih, 1990; Mellema, 2002; Wu, 2001] which allows to write

$$G'_\infty = \frac{K}{L} \quad (3.2)$$

$$K = \left(\frac{L}{\xi_s}\right)^{\text{dim}-2} K_{\text{eff}} \quad (3.3)$$

$$\phi = \frac{N_p r_0^3}{L^3} = \left(\frac{r_0}{\xi_s}\right)^3 \left(\frac{\xi_c}{r_0}\right)^{d_f} \left(\frac{\xi_s}{L}\right)^{3-\text{dim}} \quad (3.4)$$

with G'_∞ the linear storage modulus, ϕ the particle volume fraction, K the macroscopic stiffness of the gel, L the macroscopic size, K_{eff} the elementary effective stiffness of clusters and dim the dimension of the network which can be equal to the dimension of the euclidean space. These ϕ -power law models are based on building the relationship between a microscopic stiffness due to the interaction potential between the colloids and a macroscopic scale through different extrapolation by mean of scaling laws. Then, to demonstrate our interpenetration ϕ -power law model, we assume that K_{eff} may be written

$$\frac{1}{K_{\text{eff}}} = \frac{1}{K_c} + \frac{1}{K_{\text{ext}}} + \frac{1}{K_i} \quad (3.5)$$

with K_c , K_{ext} and K_i the elastic stiffness related to the inside of the cluster, the intermicroscopic links (see Ref[Wu, 2001]) and the interpenetration of the cluster, respectively. These different stiffnesses are considered

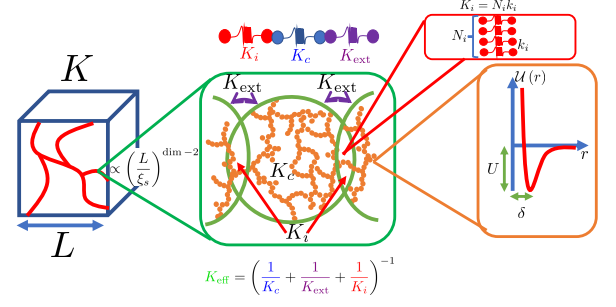


Figure 3.1: Sketch of the contributions to the gel elasticity associated with the gel hierarchical structure.

as spring in series as sketched on figure 3.1 and as commonly assumed in the literature [Wu, 2001].

Let us now quantify K_i . K_i is assumed to be proportional to the number of contact N_i between interpenetrating clusters: $K_i = N_i k_i$, where k_i is a reference interpenetration stiffness. The last expression comes from the fact that we assumed that the contacts in the interpenetration zone are parallel springs: this justifies the additivity of the stiffnesses. This point has never been highlighted in the literature and is part of our proposition for the interpenetration ϕ -power law model. Also, the reference interpenetration stiffness k_i is a hard point in the model. Indeed, referring ourselves to [Kantor, 1984a; Kantor, 1984b], there may be a competition between elongation stiffness and bending stiffness. Without any true experimental insights about the interpenetration zone, it is hard to disentangle the contribution of each and we will assume that it is directly related to the depth of the interaction potential U and the distance of interaction δ through $k_i = U/\delta^2$. Due to the fractal nature of the clusters, there are $N_i = (6V_i/\pi r_0^3)^{d_f/3}$ particles inside the intersection volume V_i between two clusters. Geometrically assimilating clusters to spheres leads to an intersection volume [Polyanin, 2007; Kern, 1967, p. 97]

$$V_i = \frac{\pi}{12} \xi_c^3 \left(2 + \frac{\xi_s}{\xi_c}\right) \left(1 - \frac{\xi_s}{\xi_c}\right)^2 \mathbf{1}_{\{\xi_s < \xi_c\}}. \quad (3.6)$$

We assume that each particle brought by each cluster in V_i forms a contact adding rigidity to the whole system. Therefore, the numbers of contact is roughly N_i . Putting together the last expressions, we get

$$K_i = \frac{U}{2\delta^2} \left(\frac{\xi_c}{r_0}\right)^{d_f} \left(1 + \frac{\xi_s}{2\xi_c}\right)^{d_f/3} \left(1 - \frac{\xi_s}{\xi_c}\right)^{2d_f/3} \mathbf{1}_{\{\xi_s < \xi_c\}}. \quad (3.7)$$

Let us now compare K_i with K_c and K_{ext} . There are different ways to consider that $K_i \ll \min(K_c, K_{\text{ext}})$. To

simplify the comparison, following [Wu, 2001], we will write

$$\frac{1}{K_c} + \frac{1}{K_{\text{ext}}} = \frac{1}{K_c} \left(\frac{K_c}{K_{\text{ext}}} \right)^\alpha \quad (3.8)$$

with $\alpha \in [0, 1]$ allowing to make a transition between the weak-link and the strong-link regime. A first way to compare K_i with $K_c (K_{\text{ext}}/K_c)^\alpha$ is to say that the system is in the regime $\xi_c/\xi_s \gtrsim 1$. Thus, one can re-write equation (3.7) as

$$K_i \underset{\xi_c/\xi_s \gtrsim 1}{\propto} \frac{U}{2\delta^2} \left(1 - \frac{\xi_s}{\xi_c} \right)^{\frac{2d_f}{3}} \quad (3.9)$$

telling us that K_i depends strongly on the distance of ξ_c/ξ_s from unity. Therefore, K_i is negligible when $\xi_c/\xi_s \gtrsim 1$ compared to $K_c (K_{\text{ext}}/K_c)^\alpha$ and equation (3.5), we get $K_{\text{eff}} \approx K_i$.

The other way to consider the system is, following previous approaches in [Kantor, 1984a; Kantor, 1984b; Shih, 1990; Wu, 2001; Mellema, 2002; Wessel, 1992], estimating $K_c (K_{\text{ext}}/K_c)^\alpha \propto \xi_s^{-\mu}$ with $\mu \in [1, 5]$ function of the fractal dimension d_f , the dimension of the elastic backbone and the regime of strong-link or weak-link because ξ_s is similar to a cluster size with contact. Recalling that $(\xi_c/r_0)^{d_f} \propto \xi_s^3$, one gets in this case

$$\frac{K_i}{K_c} \left(\frac{K_c}{K_{\text{ext}}} \right)^\alpha \propto \xi_s^{3+\mu} \left(1 + \frac{\xi_s}{2\xi_c} \right)^{\frac{d_f}{3}} \left(1 - \frac{\xi_s}{\xi_c} \right)^{\frac{2d_f}{3}}. \quad (3.10)$$

Assuming that ξ_s does not vary much, $K_i/K_c (K_c/K_{\text{ext}})^\alpha$ is governed by the values of $\xi_c/\xi_s \mapsto (1 + \xi_s/(2\xi_c))^{\frac{d_f}{3}} (1 - \xi_s/\xi_c)^{\frac{2d_f}{3}}$ on [1.2, 1.8]. Referring to figure 3.2, $K_i/K_c (K_c/K_{\text{ext}})^\alpha$ is between 0.1 and 0.3. Therefore, one can assume that $K_i \ll K_c (K_{\text{ext}}/K_c)^\alpha$, at least for the first values, and following equation (3.5), we get $K \approx K_i$.

Generally, the closer K_i is getting to $K_c (K_{\text{ext}}/K_c)^\alpha$, the more difficult it is to consider that only one phenomenon prevails. If one wants to completely understand the balance between the different contributions, one needs to model both phenomena and their coupling. This is not the goal of this model which tries to give some orders of magnitude without exhaustively modeling the system.

This final expression of the interpenetration ϕ -power law model is then, assuming that $1/K_i$ dominate,

$$G' = \underbrace{\frac{U}{r_0\delta^2}}_{G_{\text{CB}}} \underbrace{\frac{1}{2} \left(\frac{\xi_c}{r_0} \right)^{d_f} \left(1 + \frac{\xi_s}{2\xi_c} \right)^{\frac{d_f}{3}} \left(1 - \frac{\xi_s}{\xi_c} \right)^{\frac{2d_f}{3}}}_{g_{\text{Interp}}} \times \underbrace{\phi \left(\frac{\xi_s}{r_0} \right)^2 \left(\frac{\xi_c}{r_0} \right)^{-d_f}}_{g_{\text{Net}}} \quad (3.11)$$

expliciting that G_{CB} corresponds to the elasticity arising from colloid-colloid interaction with U and δ respectively the depth and the range of the attraction, g_{Interp} is the elementary scaling for elasticity to account for interpenetration and may be changed according to [Shih, 1990] and g_{Net} is the network contribution from the element of elasticity to the macroscopic scale. The dimension of the network dim is not required in the final expression due to the contribution of the effective volume fraction through the particle volume fraction and the fractal dimension related to ξ_s .

The difference with the usual ϕ -power law model [Shih, 1990] relies on the fact that $K_i = N_i k_i$ for our interpenetration ϕ -power law model and $K_i = (\xi_s/r_0)^{-2-x} k_i$ with x the chemical dimension or the dimension of the elastic backbone for the usual ϕ -power law model [Shih, 1990]. If we assume $\text{dim} = 3$, it is possible to find a weak-link like regime [Shih, 1990] with $G'_\infty \propto \phi^{\frac{1}{3-d_f}}$.

To summarize the approach and the assumptions:

- Mosts of the ingredients come from the previous ϕ -power law models building elasticity from microscopic quantities [Shih, 1990; Wu, 2001; Mellema, 2002]. The scaling between the macroscopic stiffness and the effective microscopic stiffness is conserved, the colloid-colloid interaction is conserved without expliciting the relations with bending or elongation, and the construction of the effective microscopic stiffness as spring in series is conserved as well.
- We assumed the predominance in the behaviour of K_i instead of the other stiffnesses, at least at the beginning of the interpenetration. As discussed above, the more pronounced the interpenetration, the more questionable this hypothesis is. In a fully interpenetrated case, the contribution of each phenomenon may be of the same order of magnitude and the previous demonstration does not hold anymore. The derivation of an exhaustive model allowing the transition from one case to the other will be out of the scope of this paper. However, we encourage future research to dig into this model to make it complete and exhaustive against the literature and the present results.

3.2.4 Summary of the contribution

We have created a model of elasticity based on scaling arguments and considering the interpenetration of clusters as the microscopic structure. It is directly an extension of previous models in the literature.

I acknowledge the novelty and the originality of such approaches compared to the literature. How-

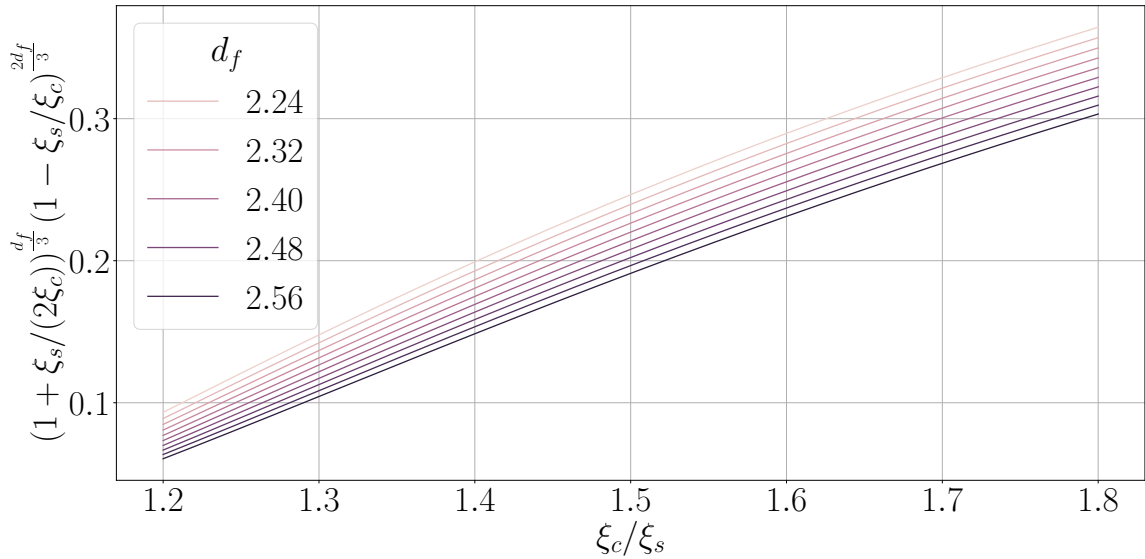


Figure 3.2: Evolution of $\xi_c/\xi_s \mapsto (1 + \xi_s/(2\xi_c))^{\frac{d_f}{3}} (1 - \xi_s/\xi_c)^{\frac{2d_f}{3}}$ for different values of d_f on $[1.2, 1.8]$

ever, I am not totally convinced about this type of microstructure in a global 3D material. I do not see properly how the interpenetration can span all the directions with such complex arrangements. As what will be discussed in [section 3.4](#), the cluster of cluster model developed in [section 3.3](#) seems much more convincing to me.

3.3 Multiple fractal [Bouthier, 2022]

3.3.1 Abstract of this section

Colloidal suspensions and the relation between their rheology and their microstructure are investigated. The literature showed great evidence of the relation between rheological quantities, cluster geometry and particle volume fraction, ignoring the influence of cluster size. We propose to extend previous models using a new double fractal structure which allows, first, to recover the well-known models in the case of percolated system and, second, to capture the influence of cluster size. This new model emphasizes the necessity of such a structure to account for recent experimental results. Then, the model is compared with data coming from the literature and shows close agreement.

3.3.2 Content of this section

The goal of this section is an attempt to describe a new model of suspension to get rheological quantities as well as recovering well-known models. This section tries to

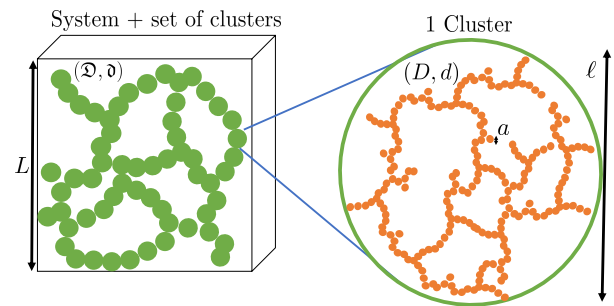


Figure 3.3: Sketch of the double fractal structure transmitting stresses in the system, inside the clusters and between the particles

propose extensions of the previous models, assuming a double fractal structure and to invite other research to investigate, maybe, this opportunity. Therefore, first, the description of the model is presented in [section 3.3.3](#). Afterwards, the results are showed, discussed according to the literature in [section 3.3.4](#), and some conclusions are drawn in [section 3.3.5](#).

3.3.3 Theoretical approach

To build the storage modulus of a colloidal suspension, let us consider a percolated system of macroscopic size L (see [figure 3.3](#)) in an Euclidean space of dimension dim . The gel is composed of particles of size a with a volume fraction ϕ aggregated in clusters of size ℓ with an interaction potential U and a distance of interaction

δ (see Refs. [Marshall, 2014; Kimbonguila Manounou, 2014; Eggersdorfer, 2010]). The size of the cluster ℓ can be determined by multiple factors (volume fraction, interaction potential, external solicitation, ...). Some models demonstrate this kind of relationship [Sorensen, 1987; Ruan, 2020; Kimbonguila Manounou, 2014] but one will consider this size here as a variable. Then, compared to previous models [Shih, 1990; Mellema, 2002; Marangoni, 2000; Wu, 2001], this size is not assumed to follow $\phi(\ell/a)^{\dim-D} = 1$ (D being the fractal dimension). Indeed, in this paper, one assumes the existence of a double fractal structure in the system, each one having two parameters, as depicted on figure 3.3. This assumption, discussed in the rest of the paper, is crucial and arises from both the existence of size of clusters ℓ and of the percolated elasticity: the coexistence of both latter ones implies the former assumption. The first structure relates the particles and the clusters, having a fractal dimension D and a chemical dimension or shortest path dimension d . d is also the dimension of the elastic backbone and is between 1.1 and 1.4 [Herrmann, 1984; Grassberger, 1992b]. The second structure is between the clusters and the macroscopic system, having a fractal dimension \mathfrak{D} and a chemical dimension \mathfrak{d} . For now, there are no more assumptions about the value of $(\mathfrak{D}, \mathfrak{d})$ respectively to (D, d) . The assumption of double structure is related to the fact that, in a percolated system, the clusters are gathered in a somewhat structure which covers the whole system: to be able to handle elastic deformation, the volume is spanned with a network of clusters which are themselves composed of particles that span space. Indeed, this assumption is typically supported by small angle scattering measurements [Gibaud, 2020a; Dagès, 2021; Weitz, 1984; Weitz, 1985]. If this double structure would not exist, the identification of a cluster size would not show any difference between the sup-cluster and the sub-cluster structure, then would not allow to identify properly a size ℓ . In other words, the double fractal structure is required to identify a cluster size. If this structure was regular such as a generalized cubic network, then we would have $(\mathfrak{D}, \mathfrak{d}) = (\dim, 1)$. However one leaves the possibility to have a more complex structure above the clusters. This will impact the capacity of the gel to change its storage modulus according to the microscopic structure.

Our expression of the storage modulus G' follows the reasoning proposed in Refs. [Shih, 1990; Mellema, 2002; Marangoni, 2000; Wu, 2001] in which assumptions of springs in series in a fractal structure are made. Therefore, it is necessary to know the macroscopic stiffness K of the system, which reads, as a first approach $G' = K/L^{\dim-2+2\epsilon\alpha}$, where $\epsilon \in [0, 1]$ (considering the range between pure stretching $\epsilon = 0$ and pure bending $\epsilon = 1$) and $\alpha \in [0, 1]$ (considering the range between strong-link regime $\alpha = 1$ and weak-link regime $\alpha = 0$ [Shih, 1990; Mellema, 2002; Marangoni, 2000; Wu,

2001])². The power $\dim - 2 + 2\epsilon\alpha$ for the macroscopic size L is an attempt to take into account the different regimes proposed in the previous models in the literature and modify the dimensions of K from a linear spring to a torsion spring. Then K is linked to the stiffness of each cluster k_c as if the clusters were in series, which brings $K = k_c (\ell/L)^{\mathfrak{d}\alpha}$. The distinction between strong-link and weak-link regime is blatant because, in the former case, all clusters of size ℓ are contributing to the global stiffness, whereas, for the latter, only the extreme clusters are playing a role, thus only one cluster appears. Furthermore, the stiffness k_c is related to the stiffness between the particles k_p having a similar behaviour of springs in series, which leads to $k_c = k_p a^{2\epsilon\alpha} (a/\ell)^{\mathfrak{d}\alpha}$. The power $\mathfrak{d}\alpha$ is directly related to the difference between strong-link and weak-link regimes, where either all the particles contribute in the series or only the particles at the boundary. Also, the factor $a^{2\epsilon\alpha}$ relates the particle interaction stiffness to more general movement from stretching to bending through curved paths. Finally, the stiffness of each particle bond k_p is linked to the interaction potential with $k_p = U\delta^{-2}$. It is then possible to assemble the previous assumptions to get

$$G = \frac{a^{2\epsilon\alpha}}{L^{\dim-2+2\epsilon\alpha}} \left(\frac{\ell}{L}\right)^{\mathfrak{d}\alpha} \left(\frac{a}{\ell}\right)^{\mathfrak{d}\alpha} \frac{U}{\delta^2} \quad (3.12)$$

Moreover, because of the system fractal structure, one has $\phi_{\text{eff}} = \phi(\ell/a)^{\dim-D} = (\ell/L)^{\dim-\mathfrak{D}}$. This finally brings, replacing the macroscopic size L with the particle volume fraction ϕ ,

$$G' = \frac{U}{a\delta^2} \phi^{\frac{\dim-1+f(\mathfrak{d})}{\dim-\mathfrak{D}}} \left(\frac{\ell}{a}\right)^{\frac{\dim-D}{\dim-\mathfrak{D}}(\dim-1+f(\mathfrak{d}))-\dim+1-f(d)} \quad (3.13)$$

with $f(x) = \alpha(2\epsilon + x) - 1$.

A first comment for this equation is that assuming a percolated system with $\phi_{\text{eff}} \approx 1$, one recovers the known behaviour $G' \propto \phi^{\frac{\dim-1+f(d)}{\dim-D}}$ [Mellema, 2002; Marangoni, 2000; Shih, 1990; Wu, 2001]. Another comment is that if $\mathfrak{D} = \dim$ there is no opportunity for the system to let the clusters influence the rheology: thus this assumption of $\mathfrak{D} \neq \dim$ is absolutely necessary. This becomes relevant when one considers a generalized cubic network system where there is no particular reason for the network to break under a change of structure. Also, if \mathfrak{D} would be equal to \dim , L would not have any influence on the rheology which is definitely not true, considering that the assembly of clusters is bringing the overall stiffness of the system: a higher or lower number of clusters may bring differences in the macroscopic stiffness. About the function f , depending on the values of

²In the case of weak-link regime, the values of ϵ , d and \mathfrak{d} are useless due to the irrelevance of information of these values on internal elastic backbone.

$\alpha \in [0, 1]$, $\epsilon \in [0, 1]$, $d \in [1.1, 1.4]$ and $\mathfrak{d} \in [1.1, 1.4]$, it is varying between -1 and 2.4 approximately.

This approach can also be extended to express the linearity limit of strain γ_{NL} . For instance, using the same approach shown in [Shih, 1990; Mellema, 2002; Marangoni, 2000; Wu, 2001], one assumes that $\sigma_y = G' \gamma_{NL}$ should not depend on d , \mathfrak{d} , ϵ and α because it is intrinsic and depends mainly on the pair interaction potential. Also, following previous approaches with their set of hypothesis, $\sigma_y \propto \ell^{1-\dim}$ and $\sigma_y \propto \phi^{\frac{\dim-1}{\dim-\mathfrak{D}}}$. Finally, this reads

$$\gamma_{NL} = \frac{\delta}{a} \phi^{\frac{-f(\mathfrak{d})}{\dim-\mathfrak{D}}} \left(\frac{\ell}{a} \right)^{-\frac{\dim-\mathfrak{D}}{\dim-\mathfrak{D}} f(\mathfrak{d})+f(d)} \quad (3.14)$$

Assuming again a percolated system with $\phi_{\text{eff}} \approx 1$, one recovers $\gamma_{NL} \propto \phi^{\frac{-f(d)}{\dim-\mathfrak{D}}}$ [Mellema, 2002; Marangoni, 2000; Shih, 1990; Wu, 2001]. Hence, the yield stress σ_y may be obtain thanks to equations (3.13) and (3.14) to get

$$\sigma_y = \frac{U}{a^2 \delta} \phi^{\frac{\dim-1}{\dim-\mathfrak{D}}} \left(\frac{\ell}{a} \right)^{\frac{(\dim-1)(\mathfrak{D}-D)}{\dim-\mathfrak{D}}} \quad (3.15)$$

which brings the well-known behaviour $\sigma_y \propto \phi^{\frac{\dim-1}{\dim-\mathfrak{D}}}$ in a percolated system with $\phi_{\text{eff}} \approx 1$ [Mellema, 2002; Marangoni, 2000; Shih, 1990; Wu, 2001]. It is clear from equation (3.15) that if $\mathfrak{D} = D$, there is no more influence of the size of clusters ℓ on the yield stress. More generally, from equations (3.13) to (3.15), if $(\mathfrak{D}, \mathfrak{d}) = (D, d)$ as a classical percolated system, the size of the clusters ℓ will not have any influence on rheology.

This consequence can be interpreted as a critical phenomenon because it is necessary to have a difference between $(\mathfrak{D}, \mathfrak{d})$ and (D, d) . Heterogeneity in the double fractal structure leads to fragility and to the possibility of breakage. Also, depending on the values of $(D, d, \alpha, \epsilon, \mathfrak{D}, \mathfrak{d})$, it is clear that the evolution of G' and σ_y according to ϕ is always increasing, the evolution of γ_{NL} according to ϕ may be either increasing or decreasing, and the evolution of G' , γ_{NL} and σ_y according to ℓ/a may be either increasing or decreasing. Thus, this model allows a variety of systems with different phenomenologies, depending on the real behaviour of the material.

A comparison of the different models present in the literature is given in table 3.1. It is then blatant that each previous model is an application of the here above model specifying certain values for α and ϵ .

Convincingly, a sensitivity study can be carried leading to figure 3.4. The most critical parameters in this study are then ϕ , \mathfrak{D} , ϵ , D and δ as suggested by equations (3.13) to (3.15). Experimental measurements of these parameters are then of particular interest and needs to bring accurate values.

One can also try to identify the intensity spectrum of such a system which can be directly inferred through

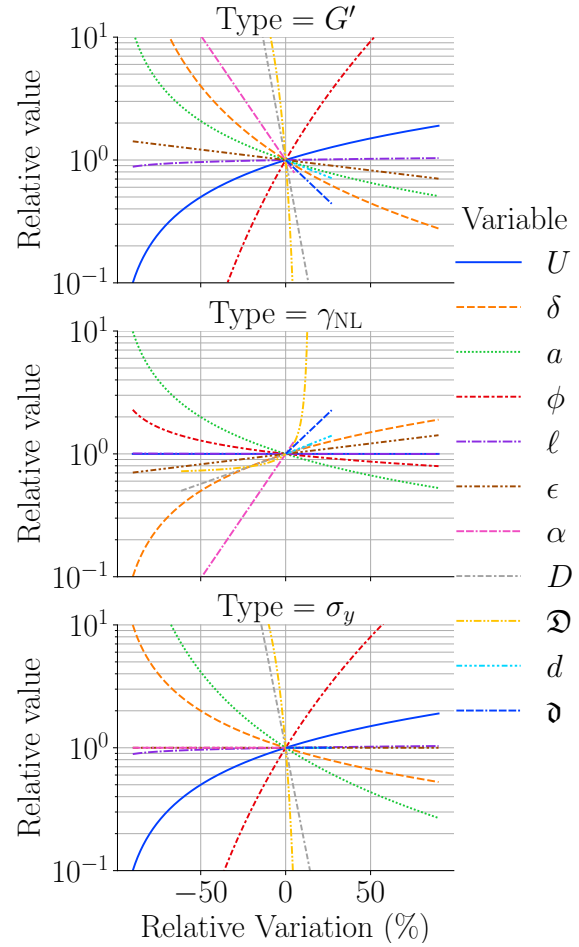


Figure 3.4: Sensitivity study of G' , γ_{NL} and σ_y from top to bottom respectively, according to equations (3.13) to (3.15) following the relative variation of the parameters around the value given in table 3.2. The conditions $(d, \mathfrak{d}) \in [1.1, 1.4]^2$, $(D, \mathfrak{D}) \in]2, 3[^2$, $\epsilon \in [0, 1]$, $\alpha \in [0, 1]$ and $\dim = 3$ have been implemented.

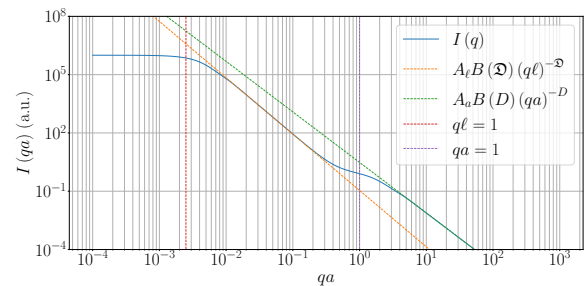


Figure 3.5: Example of intensity spectrum extracted from equation (3.16) with $A_\ell = 10^6 \text{a.u.}$, $A_a = 1 \text{a.u.}$, $\ell/a = 400$, $D = 2.6$ and $\mathfrak{D} = 2.9$

Source	Condition	$\frac{\ln\left(\frac{a\delta^2 G'}{U}\right)}{\ln\left(\phi^{\frac{1}{\dim-D}}\right)}$	$\frac{\ln\left(\frac{a\gamma_{\text{NL}}}{\delta}\right)}{\ln\left(\phi^{\frac{1}{\dim-D}}\right)}$	$\frac{\ln\left(\frac{a^2\delta\sigma_y}{U}\right)}{\ln\left(\phi^{\frac{1}{\dim-D}}\right)}$
[Shih, 1990]	Weak-link regime $\alpha = 0$	$\dim - 2$	1	$\dim - 1$
[Shih, 1990]	Strong-link regime $\alpha = 1, \epsilon = 1$	$\dim + d$	$-1 - d$	$\dim - 1$
[Mellema, 2002]	Transition between bending and stretching $\alpha = 1$	$\dim - 2 + 2\epsilon + d$	$-2\epsilon - d + 1$	$\dim - 1$
[Wu, 2001]	Transition between strong-link and weak-link regime $\epsilon = 1$	$\dim - 2 + \alpha(2 + d)$	$-\alpha(2 + d) + 1$	$\dim - 1$

Table 3.1: Comparison of the different models of the literature relating rheological quantities to microstructure. One can note that $\phi = \left(\frac{\ell}{a}\right)^{D-\dim}$ in all these models.

[Gibaud, 2020a; Dagès, 2021; Sorensen, 2001; Ham-mouda, 2010]

$$I(q) = A_\ell \left[\exp\left(-\frac{q^2\ell^2}{3}\right) + \frac{B(\mathfrak{D})}{(q\ell)^{\mathfrak{D}}} \exp\left(-\frac{q^2a^2}{3}\right) \text{erf}\left(\frac{q\ell}{\sqrt{6}}\right) \right] + A_a \left[\exp\left(-\frac{q^2a^2}{3}\right) + \frac{B(D)}{(qa)^D} \text{erf}\left(\frac{qa}{\sqrt{6}}\right) \right] \quad (3.16)$$

with

$$B(\Delta) = \Delta \left(\frac{3\Delta^2}{(2+\Delta)(1+\Delta)} \right)^{\frac{\Delta}{2}} \Gamma\left(\frac{\Delta}{2}\right), \quad (3.17)$$

A_a and A_ℓ being empirical constants to fit, q the wave vector norm, erf the error function and Γ the Gamma function. The Guinier regime at low values of q [Sorensen, 2001] is recovered with the exponential terms in equation (3.16) and the other terms with $\text{erf}\left(x/\sqrt{6}\right)^3/x \underset{x \rightarrow 0}{\sim} x^2(2/3\pi)^{3/2}$. The fractal slope is recovered with the fast decaying exponential, the limit value of the error function towards infinity and the power law decrease involving the fractal dimension. One thing to note to properly identify the intensity spectra is that the range investigated $[q_{\min}, q_{\max}]$ and the system should verify $aq_{\max} > 2\pi$, $\ell \gtrsim 50a$, $50q_{\min}\ell \lesssim 2\pi$ which leads to $q_{\max}/q_{\min} > 2,500$ which is rather large in terms of orders of magnitude. Few methods, particularly scattering techniques, and physical systems allow to reach such a broad range for the wave vector. One example of spectrum is given on figure 3.5 where it is easy to identify a with the rupture of slope on the right, ℓ with the rupture of slope on the left, D with the power law slope on the right and \mathfrak{D} with the power law slope on the left.

A development of the model for multiple levels may be proposed. Indeed, the previous model can be extended to $n \in \mathbb{N} \setminus \{0, 1\}$ number of steps depending on the type of the considered system. The more steps, the larger the quantity of parameter to identify. Therefore,

the construction may be interesting but should either remain seldom due to the broad variability of parameters or, be supported by microstructural measurements like scattering experiments.

As a snapshot, giving a set $(\ell_i, D_i, d_i)_{i \in \llbracket 1, n \rrbracket}$ of sizes, fractal dimension and chemical dimension, $n \in \mathbb{N} \setminus \{0, 1\}$, $\ell_0 = a$, $\ell_n = L$, equations (3.13) to (3.15) read respectively

$$G' = \frac{U}{a\delta^2} \phi^{\frac{\dim-1}{\dim}} \prod_{i=1}^n \left(\frac{\ell_{i-1}}{\ell_i}\right)^{f(d_i)+D_i\frac{\dim-1}{\dim}} \quad (3.18)$$

$$\gamma_{\text{NL}} = \frac{\delta}{a} \prod_{i=1}^n \left(\frac{\ell_{i-1}}{\ell_i}\right)^{-f(d_i)} \quad (3.19)$$

$$\sigma_y = \frac{U}{a^2\delta} \phi^{\frac{\dim-1}{\dim}} \prod_{i=1}^n \left(\frac{\ell_{i-1}}{\ell_i}\right)^{D_i\frac{\dim-1}{\dim}} \quad (3.20)$$

$$\phi = \left(\frac{a}{L}\right)^{\dim} \prod_{i=1}^n \left(\frac{\ell_{i-1}}{\ell_i}\right)^{-D_i}. \quad (3.21)$$

In order to recover an expression similar to the previous ones in terms of the volume fraction, one needs to integrate *partial* volume fractions taking into account the volume fraction into a cluster of a certain size. Considering these previous expressions, one can extend to a continuum of length scales with two functions $\ell \mapsto d(\ell)$ and $\ell \mapsto D(\ell)$ for the chemical dimension and the fractal dimension respectively to get

$$G' = \frac{U}{a\delta^2} \phi^{\frac{\dim-1}{\dim}} \times \quad (3.22)$$

$$\exp\left(-\int_a^L \frac{1}{\ell} \left(f(d(\ell)) + \frac{\dim-1}{\dim} D(\ell)\right) d\ell\right) \quad (3.23)$$

$$\gamma_{\text{NL}} = \frac{\delta}{a} \exp\left(\int_a^L \frac{f(d(\ell))}{\ell} d\ell\right) \quad (3.24)$$

$$\sigma_y = \frac{U}{a^2\delta} \phi^{\frac{\dim-1}{\dim}} \exp\left(-\frac{\dim-1}{\dim} \int_a^L \frac{D(\ell)}{\ell} d\ell\right) \quad (3.25)$$

$$\phi = \exp\left(\int_a^L \frac{D(\ell)}{\ell} d\ell\right) \left(\frac{a}{L}\right)^{\dim}. \quad (3.26)$$

With these expressions, it is straightforward to recover the model with one fractal structure or two fractal structures taking constant functions or two-step constant functions respectively over $[a, L]$.

This kind of continuum multifractal structure can be found, for example, in [Foderà, 2013]. In this paper, the aggregation of protein in Amyloid superstructures creates a continuous evolution of the fractal dimension from $D = 3$ below $l = 10\text{nm}$ to $D = 1.5$ for $l \geq 1\mu\text{m}$. Hence, with this kind of data, it is possible to fit the evolution of the fractal dimension, use the fit in the expressions above to get the rheological parameters and compare with experimental data.

Source	[Gibaud, 2020a; Dagès, 2021]
G'_{exp} (kPa)	1.2
$\gamma_{\text{NL}}^{\text{exp}}$ (%)	1
σ_y^{exp} (Pa)	12
G'_{th} (kPa)	0.96
$\gamma_{\text{NL}}^{\text{th}}$ (%)	0.34
σ_y^{th} (Pa)	3.4
ϕ (%)	20
a (nm)	150
U (kT)	20
ℓ (nm)	500
δ (Å)	3
D	2.6
d	1.1
\mathfrak{D}	2.61
\mathfrak{d}	1.1
ϵ	0.05
α	0.95
dim	3

Table 3.2: Results and parameters to assess the rheological properties in [Gibaud, 2020a; Dagès, 2021]. G'_{exp} , $\gamma_{\text{NL}}^{\text{exp}}$ are the direct measurements of the storage modulus at strain $\gamma \rightarrow 0$ and the limit strain of linearity of the carbon black particle suspension, respectively. Also, $\sigma_y^{\text{exp}} = G'_{\text{exp}} \gamma_{\text{NL}}^{\text{exp}}$. Then, G'_{th} , $\gamma_{\text{NL}}^{\text{th}}$ and σ_y^{th} are the estimated storage modulus according to equation (3.13), the limit strain of linearity according to equation (3.14) and the yield stress according to equation (3.15), respectively, with the other parameters.

3.3.4 Comparing with the literature

One can look at the assessment of the storage modulus, the linear limit of strain and the yield stress according to literature results. Using equations (3.13) to (3.15) and table 3.2, the values of d and \mathfrak{d} have been assumed close to the lower boundaries of their range (i.e. $[1.1, 1.4]$), \mathfrak{D} has been chosen close to D , but remaining higher to have an increase of the storage modulus G' according to ℓ/a , and ϕ is chosen according to the structure of the carbon black fractal particles. The theoretical value of storage modulus is $G'_{\text{th}} = 0.96\text{kPa}$ which is close to the experimental value $G'_{\text{exp}} = 1.2\text{kPa}$. Also, the theoretical value of the limit of linearity strain $\gamma_{\text{NL}}^{\text{th}} = 0.34\%$ is also close to the experimental value $\gamma_{\text{NL}}^{\text{exp}} = 1\%$. Finally, the theoretical value of the yield stress $\sigma_y^{\text{th}} = 3.4\text{Pa}$ is close to the experimental value $\sigma_y^{\text{exp}} = 12\text{Pa}$ too.

3.3.5 Summary of the contribution

We have proposed a new model following previous demonstrations in the literature assuming a double fractal structure. This is an interesting contribution to relate complex microstructure to rheological quantities.

As discussed already in section 3.2.4, I am more convinced by a multiple fractal approach or a cluster of cluster approach than an interpenetrating cluster approach. This uses the same ingredients and does not display any trivial difficulty to build the microscopic structure besides the fact there are more than two levels now. This demonstration is also a good stepping stone for anyone who wants to dig further in this topic due to the universal summary of the literature as cases of applications of the previous model, which will be also shown in section 3.4. Improvements in experimental measurements with certain types of material will complement greatly these

theoretical perspectives.

3.4 Three length scales colloidal gels: the clusters of clusters *versus* the interpenetrating clusters approach [Bouthier, 2023b]

In this section, we will compare the two previous models: interpenetration of clusters and clusters of clusters models. This section has been published in [Bouthier, 2023b].

3.4.1 Abstract of this section

Typically, in quiescent conditions, attractive colloids at low volume fractions form fractal gels structured into two length scales: the colloidal and the fractal cluster scales. However, when flow interferes with the gelation of colloidal fractal gels, it may display three distinct length scales [Dagès, 2022]. Following those recent experimental investigations, we derive two models that account for the structure and the rheological properties of such atypical colloidal gels. The gel elasticity is inferred from scaling arguments, and the structure is translated into scattering intensities following the global scattering functions approach proposed by Beaucage and, typically, measured in small-angle x-ray scattering (SAXS). In both models, we consider that the colloids condensate into fractal clusters. In the clusters of clusters model, the clusters form superaggregates that then build the gel network. In the interpenetrating clusters model, the clusters interpenetrate one another to form the gel network. Those two models are then used to analyze rheo-SAXS experiments carried out on carbon black gels formed through flow cessation.

3.4.2 Content of this section

In section 3.4.3, we first present the measured mechanical and structural properties of a three length scales carbon black gels obtained from flow cessations [Dagès, 2022]. We then discuss the implications of such results at a fundamental level and in terms of applications to motivate the models developed in the next section. In section 3.4.4, we present the structure of two models that display three distinct length scales: the clusters of clusters model which describes gels structured in a network of superaggregates formed by clusters of particles [Bouthier, 2022] and the interpenetration of clusters model which describes gels formed by a network of interpenetrating clusters of particles [Dagès, 2022]. We then fit the small angle X-ray scattering data

(SAXS) presented in section 3.4.3 with both models using a global scattering functions approach proposed by Beaucage. In section 3.4.5, we derive the mechanical properties of the clusters of clusters model and the interpenetration of clusters model previously introduced. The derivation of such mechanical models is greatly inspired by the ϕ -power law models initially built to describe classical colloidal gels with two distinct length scales, typically obtained in the DLCA or the RLCA context. The derivation yields an analytical expression of the gel elastic modulus. This is the main result of this paper. This analytical expression combined with the assessment of the gel structure obtained by SAXS allows us to fit the gel elasticity G' as function of the gel length scales, cluster fractal dimension, volume fraction, colloidal interactions, etc... The results of the fits indicate that the three length scale carbon black gels obtained through flow cessations [Dagès, 2022] can be fitted by both models. We however identify two general trends: the gel elasticity originates from stretching bonds at all length scales and the gel structure becomes denser as the gel characteristic length scales increase.

3.4.3 Three length scales carbon black gels resulting from flow cessations

Carbon black particles are fractal carbonated colloids that result from the partial combustion of hydrocarbon oils [Lahaye, 1994; Xi, 2006; Sztucki, 2007]. These particles are widely used in the industry for mechanical reinforcement or to enhance the electrical conductivity of plastic and rubber materials [Wang, 2018]. Dispersed in oil, the carbon black particles are attractive and form gels at low volume fractions [Trappe, 2000]. Such gels present peculiar rheological properties [Gibaud, 2020b] including rheopexy [Ovarlez, 2013; Helal, 2016; Hipp, 2019], delayed yielding [Gibaud, 2010; Grenard, 2014], fatigue [Gibaud, 2016; Perge, 2014] and rheo-acoustic properties [Gibaud, 2020a; Dagès, 2021]. Here, we are interested in revisiting carbon black gels resulting from flow cessations [Dagès, 2022]. The flow cessation protocol were carried out in carbon black dispersion (Vulcan PF) at $c = 4 \text{ \%}_w$ ($\phi = 1.58 \text{ \%}$) in mineral oil and is described in [Dagès, 2022]. In brief, the protocol consists in (i) a rejuvenation step at a strain rate $\dot{\gamma} = 1000 \text{ s}^{-1}$ during 60 s, (ii) a preshear step at $\dot{\gamma} = \dot{\gamma}_0$ during 20 to 200 s, (iii) a flow cessation induced by $\sigma = 0 \text{ Pa}$ for 30 s, (iv) a rest period of 360 s during which the viscoelastic moduli are monitored and finally (v) a frequency sweep or a SAXS measurement. The gel mechanical and structural properties (figure 3.6) as measured in step (v) of the protocol depend on the value of $\dot{\gamma}_0$, the shear rate carried out before flow cessation.

Figure 3.6(a) displays the evolution of the elastic modulus G'_∞ of the gel measured during a frequency sweep experiment in the low frequencies domain as a

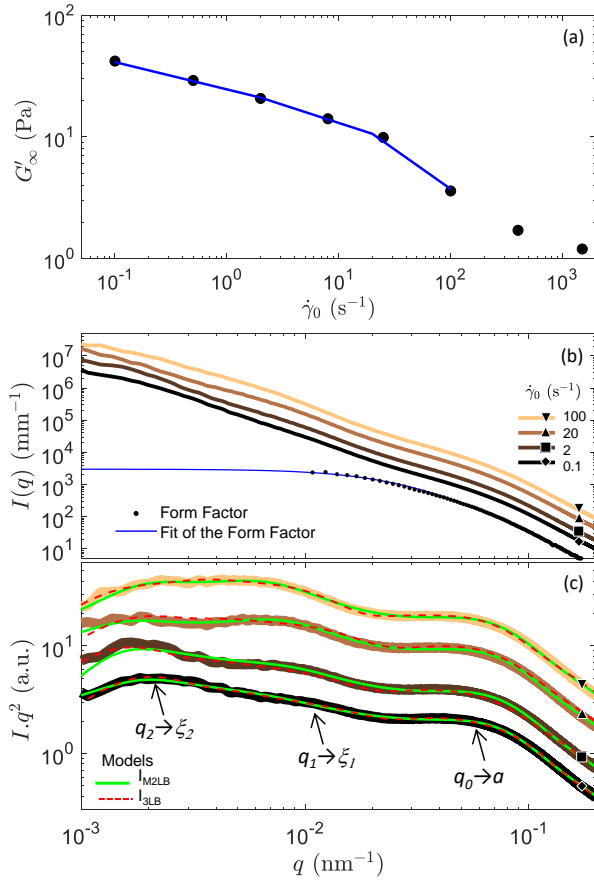


Figure 3.6: Carbon black gels properties resulting from flow cessation. (a) Evolution of the gel elasticity G'_∞ (●) as a function of $\dot{\gamma}_0$ the shear rate intensity before flow cessation. The blue line represents the fits (a) through (d) listed in table 3.3. The fits are indistinguishable. (b) Gel scattered intensity $I(q)$ as a function of the wave vector q . The colors from light orange to black correspond to a decreasing $\dot{\gamma}_0$. The black dots correspond to the experimental form factor of the carbon black particles and the blue solid line is the fit of this form factor. $I(q)$ resulting from $\dot{\gamma}_0 = 0.1$ s $^{-1}$ is on absolute scale. The rest of the data is translated along the y-axis for better readability. (c) Kratky representation, $I(q)q^2$ versus q , of the data shown in (b). The arrows point to the three bumps at q_0 , q_1 and q_2 , associated respectively to the length scales a , ξ_1 and ξ_2 . The green lines correspond to the two level modified Beaucage model (equation (3.35)) and the red dash lines correspond to three level beaucage model (equation (3.30)). Experimental data are extracted from [Dagès, 2022].

function of $\dot{\gamma}_0$ the shear intensity before flow cessation. The gel becomes stronger as $\dot{\gamma}_0$ decreases: its elasticity can be tuned by a factor 50, from ~ 1 Pa at high $\dot{\gamma}_0$ to ~ 50 Pa at low $\dot{\gamma}_0$.

The structural properties of the gel as a function of $\dot{\gamma}_0$ are determined based on SAXS experiments. The scattered intensities $I(q)$ as a function of the wave number q are displayed in figure 3.6(b). The $I(q)$ are isotropic in the q -range tested. $I(q)$ show the usual decreasing trend due to the proportional relationship of the intensity with the number of scatterers in volume defined by the length-scale $1/q$. More precisely, the intensity roughly decay as $1/q^2$ which is expected for fractal gels. We therefore turn to the Kratky representation in figure 3.6(c) and displays Iq^2 versus q . In this representation, a structure of fractal dimension 2 at all length scales is an horizontal line. Any deviation from this flat line are highlighted by the Kratky representation. We observe three bumps at low, intermediate and high q related to three length scale. Those bumps are particularly visible in the Kratky representation in figure 3.6(c). The high- q bump at q_0 is related to the radius a of the carbon black particles and the two other peaks at intermediate- q (q_1) and low- q (q_2) correspond to two additional length scales ξ_1 and ξ_2 respectively. This structure is atypical. Indeed, in gels driven solely by thermal agitation, $I(q)$ classically displays only two characteristic length scales: the particle size a and the cluster size ξ separated by a power-law regime, the exponent of which is related to the cluster fractal dimension [Courten, 1987].

Those rheology and SAXS results have strong implications. On the application level, such an interplay between shear and gelation is involved in numerous industrial processes, and especially in additive manufacturing where shear coupled with 3D printing allows tuning the microstructure and the properties of the printed materials [Raney, 2018]. On a fundamental level, as already well discussed in the literature, shear may interfere with the gelation pathway of particulate colloidal gels and lead to multiple metastable gels with properties, microstructure [Koumakis, 2015; Das, 2022], connectivity [Helal, 2016] or yield stress [Ovarlez, 2013] that depend on the flow cessation protocol. Experiments displayed in figure 3.6 are ideal for exploring the interplay between microstructure and mechanics: as the gel originates from the same dispersion, the colloid volume fraction and interactions remain unchanged, while variations in the gel mechanical properties only result from microstructural changes.

In [Dagès, 2022], the three length scales were interpreted using the interpenetration cluster model in the weak-link regime assuming an homogeneous network. This analysis, as mentioned in [Dagès, 2022], has however some serious drawbacks that we intend to address in this paper. First, there is a discrepancy between the local particle density ρ obtained from the SAXS analy-

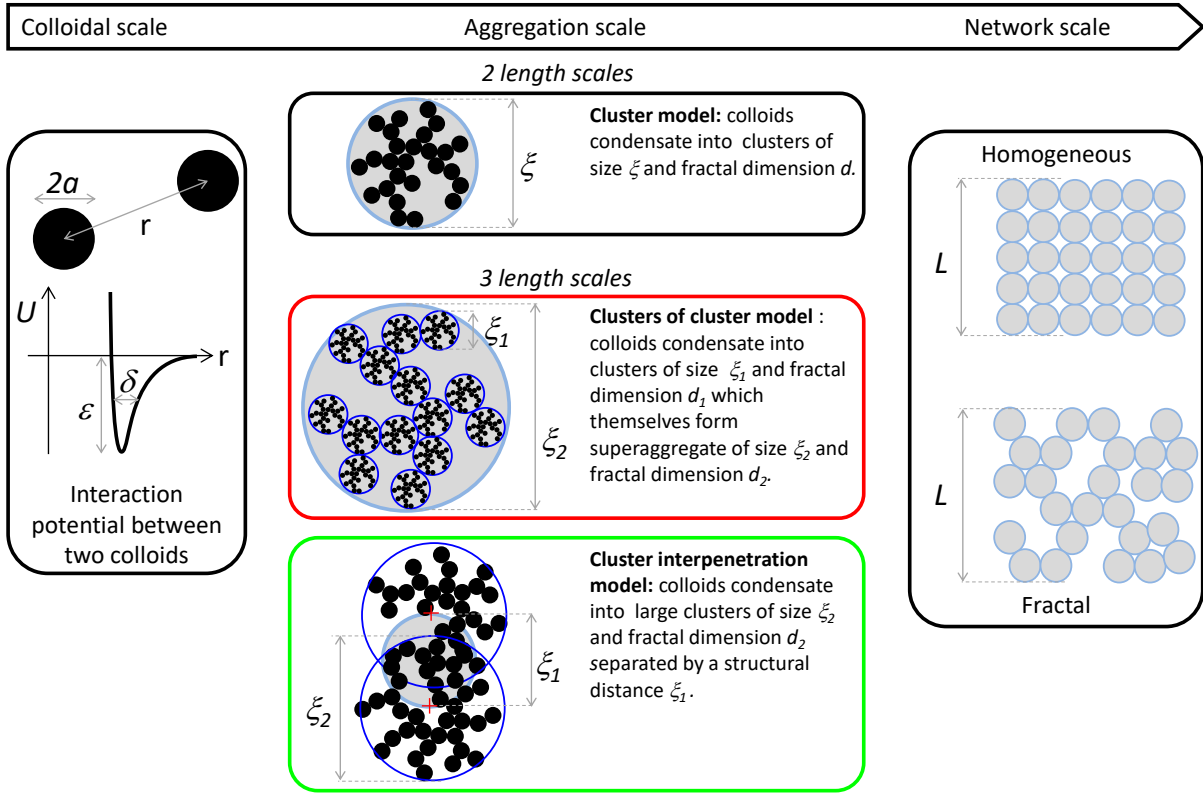


Figure 3.7: Sketch of the gel hierarchical structures. ϕ -power law models which model the gel elasticity G' are based at the particle scale on the colloid-colloidal interactions, at the meso scale on the aggregated structures and at the macroscopic scale on the network topology. The structural length ξ_s defined at the aggregation scale sets the coarse grain scale for the network scale. In the cluster ϕ -power law model $\xi_s = \xi$, in the clusters of clusters ϕ -power law model $\xi_s = \xi_2$ and in the interpenetration of clusters ϕ -power law model $\xi_s = \xi_1$.

sis and the average density $\bar{\rho}$ obtained from the carbon black concentration: $\rho > \bar{\rho}$. Second, using the interpenetration model in the weak-link regime for an homogeneous network, the elasticity resulting from the carbon black inter particle interaction G_{cc} is underestimated by orders of magnitudes. This suggests that the network is heterogeneous. Finally, the SAXS data can also be interpreted differently, in clusters of clusters [Kim, 2004; Sztucki, 2007] rather than in interpenetrated clusters. In the next section, as it is currently lacking in the literature, we develop three-length-scales gel rheological models to address the above problems and to establish a quantitative relation between the structure and the elasticity of carbon black gels resulting from flow cessation.

3.4.4 Structure of the gels

We construct two three-length-scales gel models to fit the data presented in the previous section. The clusters of clusters ϕ -power law model describes gels structured in a network of superaggregates formed by clusters of particles. The interpenetration of clusters ϕ -power law

model describes gels formed by a network of interpenetrating clusters of particles. The models structure are sketched in figure 3.7. In this section, we first present the model from a structural perspective then we fit and discuss the SAXS data.

3.4.4.1 Structural models

In the clusters of clusters ϕ -power law model [Bouthier, 2022], we consider that colloidal particles of radius a assemble into clusters of dimension ξ_1 and fractal dimension d_1 which themselves aggregates into superaggregates of dimension ξ_2 and fractal dimension d_2 to form the gel network as sketched in the figure 3.7. In figure 3.6(c), the high- q peak at q_0 corresponds to the carbon black particles of radius a , the intermediate- q peak corresponds to the cluster size ξ_1 and the low- q peak corresponds to the super-aggregates of size ξ_2 . The fractal dimensions d_1 and d_2 are related to the slope of the scattering intensity $I(q)$ measured between the peaks (q_0, q_1) and (q_1, q_2) respectively.

The intensity spectrum $I(q)$ may then be fitted by a three-level Beaucage model [Beaucage, 1995; Beaucage, 1996; Hammouda, 2010] through

$$I_{3LB}(q) = I_2(q) + I_1(q) + I_a(q), \quad (3.27)$$

with

$$I_2(q) = G_2 \exp\left(-\frac{q^2 \xi_2^2}{3}\right) + \frac{B_2}{q^{d_2}} \exp\left(-\frac{q^2 \xi_1^2}{3}\right) \operatorname{erf}\left(\frac{q \xi_2}{\sqrt{6}}\right)^{3d_2}, \quad (3.28)$$

$$I_1(q) = G_1 \exp\left(-\frac{q^2 \xi_1^2}{3}\right) + \frac{B_1}{q^{d_1}} \exp\left(-\frac{q^2 a^2}{3}\right) \operatorname{erf}\left(\frac{q \xi_1}{\sqrt{6}}\right)^{3d_1}, \quad (3.29)$$

$$I_a(q) = G_0 \exp\left(-\frac{q^2 a^2}{3}\right) + \frac{B_0}{q^{d_0}} \operatorname{erf}\left(\frac{qa}{\sqrt{6}}\right)^{3d_0}. \quad (3.30)$$

The three-level Beaucage model sums the scattering contribution $I_2(q)$ of the superaggregates of size ξ_2 and fractal dimension d_2 , the contribution $I_1(q)$ of the clusters of size ξ_1 and fractal dimension d_1 and the contribution $I_a(q)$ of the constituent colloidal particles of size a and fractal dimension d_0 . The terms multiplied by $(G_i)_{i=0,1,2}$ correspond to the approximation of the Guinier regime when the wave vector number tends towards 0 which vanishes when the wave vector number goes above the inverse length scale designated by each level a , ξ_1 or ξ_2 . The terms multiplied by $(B_i)_{i=0,1,2}$ correspond to the approximation of fractal behaviour with a power-law scaling in q when its values are above the designated length scale and vanishing values relatively to the Guinier regime when q tends to 0 with the combination of the error function and the power-law in q . The exponential terms associated with the terms multiplied by B_1 and B_2 are here to make the contribution vanish when the smaller length scale level is reached.

In the interpenetration of clusters ϕ -power, we consider that colloidal particles of radius a assemble into clusters of size ξ_2 and fractal dimension d_2 . The clusters of size ξ_2 interpenetrate one another, such that their center to center distance ξ_1 is smaller than ξ_2 , to form a network as sketched in the figure 3.7. In figure 3.6(c), the high- q peak at q_0 corresponds to the carbon black particles of radius a . The intermediate- q peak is a structural peak and corresponds to ξ_1 the center to center distance between two adjacent clusters. The low- q peak corresponds to the cluster of size ξ_2 and fractal dimension d_2 . The fractal dimensions d_2 is related to the slope of the scattering intensity $I(q)$ measured between the peaks (q_0, q_2) .

The intensity spectrum $I(q)$ may then be fitted by a modified two level Beaucage model [Beaucage, 1995; Beaucage, 1996; Keshavarz, 2021] through

$$I_{M2LB}(q) = I_2(q) S_1(q) + I_a(q) \quad (3.31)$$

with

$$I_2(q) = G_2 \exp\left(-\frac{q^2 \xi_2^2}{3}\right) + \quad (3.32)$$

$$\frac{B_2}{q^{d_2}} \exp\left(-\frac{q^2 a^2}{3}\right) \operatorname{erf}\left(\frac{q \xi_2}{\sqrt{6}}\right)^{3d_2}, \quad (3.33)$$

$$S_1(q) = 1 + C_1 \left(\left(\frac{q \xi_1}{2\pi}\right)^2 + \left(\frac{2\pi}{q \xi_1}\right)^2 \right)^{-1}, \quad (3.34)$$

$$I_a(q) = G_0 \exp\left(-\frac{q^2 a^2}{3}\right) + \frac{B_0}{q^{d_0}} \operatorname{erf}\left(\frac{qa}{\sqrt{6}}\right)^{3d_0}. \quad (3.35)$$

The two-level Beaucage model sums the scattering contribution $I_2(q)$ of the clusters of size ξ_2 and fractal dimension d_2 and the contribution $I_a(q)$ of the constituent colloidal particles of size a . To account for the clusters interpenetration, the cluster intensity $I_2(q)$ is multiplied by an ad-hoc inter-cluster structure factor $S_1(q)$ leading to an increase of scattering at intermediate q . $S_1(q)$ is function that peaks at $q_1 = 2\pi/\xi_1$ to a maximum value $1 + C_1/2$ and that converges to 1 away from $q_1 = 2\pi/\xi_1$. Such a choice of $S_1(q)$ is simple but not completely satisfactory as it fails in the thermodynamic limit. Indeed, $S_1(q \rightarrow 0) = 1$ whereas it should be proportional to the isothermal compressibility.

In the beaucage models, the length scales a , ξ_1 and ξ_2 reflect a high order moment of the aggregate log-normal size distribution in the Beaucage functions and are indicative of the higher limit of the size distribution of the aggregates [Kammler, 2005; Beaucage, 2012].

3.4.4.2 Discussion about the gel structure

We now fit the SAXS data shown in figure 3.6(b-c) using the structural models for the clusters of cluster model (equation (3.30)) and the interpenetration cluster model (equation (3.35)). As shown in figure 3.6(c), the scattering intensities are nicely fitted using both models. The fits are carried out in log-scale on data re-sampled with 20 points per decade.

Let us first discuss the fit results obtained using the cluster interpenetration model. In figure 3.8a, as $\dot{\gamma}_0$ increases, we observe that the gel is composed of clusters which size ξ_2 decreases while becoming denser ($d_2 \nearrow$) and less interpenetrated ($\xi_2/\xi_1 \searrow$). As the flow cessation gels are obtained from the same carbon black dispersion, the density of carbon black particles should be conserved. There are two ways to calculate this density. Based on the carbon black volume fraction, the average density is $\bar{\rho} = \phi/a^3 \simeq 900 \mu\text{m}^{-3}$. Based on the SAXS data, assuming an homogeneous network, we can measure the local particle density ρ . The unit cell of the network is defined by the structural length ξ_1 . This unit cell of volume ξ_1^3 contains one cluster with $(\xi_2/a)^{d_2}$ particles so that $\rho = (\xi_2/a)^{d_2} / \xi_1^3$. In figure 3.8a, we measure $\rho \simeq 7200 \mu\text{m}^{-3}$ a value larger than $\bar{\rho}$.

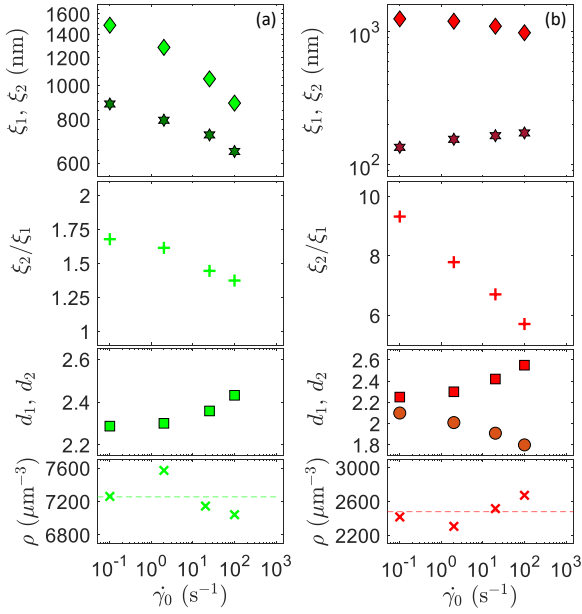


Figure 3.8: Parameters of the scattering models resulting from fitting the scattering intensity $I(q)$ in figure 3.6, (a) using the cluster interpenetration approach (equation (3.35), green symbols) and (b) using the clusters of the clusters approach (equation (3.30), red symbols). From top to bottom: ξ_1 (\blacklozenge), ξ_2 (\blackstar), ξ_1/ξ_2 ($+$), d_1 (\bullet), d_2 (\blacksquare) and ρ (\times) as a function of the applied shear rate $\dot{\gamma}_0$ before flow cessation. The carbon black radius a is constant in all the fits and equal to $a = 27$ nm.

In figure 3.8b, we display the fit results based on the clusters of clusters model. As $\dot{\gamma}_0$ increases, we observe that the gel is composed of superaggregates which become smaller ($\xi_2 \searrow$) and denser ($d_2 \nearrow$) while the clusters that compose them become larger ($\xi_1 \nearrow$) and looser ($d_1 \searrow$). Again we can compare ρ and $\bar{\rho}$. The unit cell of the network is defined by the structural length ξ_2 . In the volume ξ_2^3 , there is exactly one superaggregate composed of $(\xi_2/\xi_1)^{d_2}$ clusters themselves composed of $(\xi_1/a)^{d_1}$ particles. Hence, we get $\rho = (\xi_2/\xi_1)^{d_2} (\xi_1/a)^{d_1} / \xi_2^3$. We measure $\rho \approx 2500 \mu\text{m}^{-3}$ a value again larger than $\bar{\rho}$.

Both approach verify that ρ remains constant throughout the $\dot{\gamma}_0$ series (figure 3.8). This infers that our approach is self-consistent. However, the value of ρ calculated with the structure parameters is way larger compared to the one calculated based on the volume fraction of the carbon black particles, $\bar{\rho} \approx 900 \mu\text{m}^{-3}$. This discrepancy between the two ways of calculating the density suggests that the gel network is heterogeneous. We dismiss shear banding as discussed in [Dagès, 2022] and fractures which would lead to a strong enhanced scattering and a Porod regime at low q [Dagès, 2021]. We vouch for a fractal network. This remains hypothetical as the hallmark of this fractal network is not measurable

in the SAXS experiments. Indeed, this network fractal dimension should appear in $I(q)$ in the very low q -regime for $q_2 < 2\pi/\xi_2 \sim 0.002 \text{ nm}^{-1}$. As the lowest q in the SAXS experiment is 0.001 nm^{-1} , we cannot probe the existence of D nor measure its value.

When the network is not homogeneous, $\rho > \bar{\rho}$. Assuming the gel network is fractal, is there a way to determine D from $\bar{\rho}$ and ρ ? This would greatly help as the measure of D is not accessible in the SAXS experiment. To tackle the issue of the local density of particles, Ref.[Tang, 2008; Gravelle, 2021] used an heterogeneous mass distribution which has an impact on the rheological properties as derived by [Shih, 1990; Wu, 2001; Mellema, 2002]. More precisely, the authors used the probability of an inter-cluster bond at any location in a cluster chain to become stress-carrying given the condition that all other bonds are not stress-carrying as a constant. This assumption gives rise to an exponential probability distribution in terms of the number of inter-cluster bonds in a small unit of volume. This approach reads a final expression of the storage modulus as a power law of the particle volume fraction multiplied by $(1 - \exp(-k\phi^b))^\beta$ with (k, b, β) some constants of the material. In the limit of low volume fraction, the usual power law in ϕ is recovered but the multiplicative factor allows a deviation from the power law at higher volume fraction. Even if we do not consider this approach for the rheological data, the perspective of a heterogeneous distribution of particles as in a fractal structure is a promising way to account for structural and rheological discrepancies. It is expected then that the local density ρ can be related to the average density $\bar{\rho}$ through the influence of the fractal dimension but it remains a challenge out of the scope of this paper.

3.4.5 Modelling gels elasticity

In this section, we first describe the common basis to derive the elastic modulus from the clusters of clusters ϕ -power law model and the interpenetration of clusters ϕ -power law model. We then derive an analytical expression of the elastic modulus for each model. Finally, using this analytical expressions together with the structure parameters displayed in figure 3.8, we fit the rheology data presented in figure 3.6(a) and discuss the rheology fit parameters.

3.4.5.1 Common basis for both models

Both the clusters of clusters ϕ -power law model and the interpenetration of clusters ϕ -power law model belong to the class of ϕ -power law models which aim to provide an analytical expression to fit the gel storage modulus G'_∞ as shown in figure 3.6(a). The derivation of such models follows a top down approach. The macroscopic storage modulus G' is *a priori* related to the macro-

scopic stiffness K of the system of size L [Mellema, 2002] by:

$$G' = \frac{K}{L^{1+2\epsilon\alpha}}. \quad (3.36)$$

The nature of K is solely defined by dimension analysis. Depending on the value of the exponent of L , K is a stretching stiffness (L^1) or a bending stiffness (L^3). The exponent ϵ [Mellema, 2002] allows one to have a mix of both stiffness as it varies from $\epsilon = 0$ (pure stretching) to $\epsilon = 1$ (pure bending). The exponent α indicates the proportion of the weak-link to strong-link regime [Wu, 2001]. In the weak-link limit where the inside of the clusters is stiffer than the connection between the clusters, $\alpha = 0$. In the strong-link limit where the inside of the cluster is less stiff than the connection between the clusters, $\alpha = 1$. The origin of the previous expression is purely dimensional trying to relate the macroscopic stiffness to the macroscopic storage modulus with precisely defined dimensions. The previous exponents are coming from mixed approaches taking into account multiple types of phenomena. The extreme values of the exponents isolate the different cases depending on the type of interaction between the clusters (bending, stretching, dominated by the links, dominated by the internal stiffness of the clusters).

The expression of K is model dependent and is conditioned at the macroscopic scale by the network topology, at intermediate scale by the nature of the aggregates and their interactions and at the particle scale by the colloid-colloidal interactions as shown by figure 3.7. Indeed, the gel elasticity can be decomposed *a posteriori* in [Shih, 1990; Wu, 2001; Mellema, 2002; Bouthier, 2022]

$$G' = G_{cc} S_{agg} S_{net} S_{MBS} \quad (3.37)$$

where G_{cc} is the elasticity resulting from the colloid-colloid interaction potential \mathcal{U} , S_{agg} is the scaling coming from the aggregation scale, S_{net} is the scaling contribution from the network scale and S_{MBS} is the scaling coming from the macroscopic influence of bending or stretching. This model is hierarchical. The different factors come from the iterative demonstration procedure and the identification of the different contribution in the final formulas. The construction of the storage modulus directly expressing the different factors is impossible and needs the following demonstrations. However, we will emphasize these contributions in the final formulas of each model. The radius of the colloid a sets the colloidal scale, the structural dimension ξ_s set the scale at the aggregation level and serves as the coarse grain unit to construct the network. In our case, compared to the clusters ϕ -power law models [Shih, 1990; Wu, 2001; Mellema, 2002], we have kept the colloidal scale unchanged and modified the aggregation and the network scale.

At the colloidal scale, the elasticity G_{cc} is set by the

characteristics of the attractive interaction potential \mathcal{U} , namely its depth U and its range δ . This leads, in the case of monodisperse colloidal spheres, to a storage modulus [Shih, 1990; Wu, 2001; Bouthier, 2022]

$$G_{cc} = \frac{U}{\delta^2 a}. \quad (3.38)$$

Typically, U is few tens of $k_B T$, with k_B the Boltzman constant and T the temperature, and δ a few percent of the colloid radius a . G_{cc} is the only term in equation (3.37) that has the dimensionality of a shear modulus and therefore it sets the amplitude scale of the gel elasticity G' .

At the macroscopic scale, the network topology is determinant and two options are possible. Either the aggregates of structural length ξ_s fill the space in a close packing configuration or they form a fractal structure of upper limit the size of the sample L and a fractal dimension D . In the case of the fractal network, it is possible to distinguish the weak-link regime and the strong-link regime [Shih, 1990; Wu, 2001]. On one hand, in the weak-link regime, the connections between the clusters are weaker than the clusters themselves thus they dominate at the larger scale due to the assumption of springs in series. Therefore, the contribution of the network is

$$S_{net} = 1. \quad (3.39)$$

On the other hand, in the strong-link regime, the inside clusters cohesion is weaker than the links between clusters, hence it dominates at the larger scale. It is then relevant to introduce the dimension \mathfrak{D} (also commonly named chemical dimension) of the elastic backbone of the network which is typically in the range [1, 1.5] [Grassberger, 1985; Grassberger, 1992b; Grassberger, 1992a] and accounts for the network path that sustain the network stress. The contribution of the network is then

$$S_{net} = \left(\frac{\xi_s}{L}\right)^{\mathfrak{D}}. \quad (3.40)$$

Both previous equations (3.39) and (3.40) may be unified,

$$S_{net} = \left(\frac{\xi_s}{L}\right)^{\mathfrak{D}\alpha}. \quad (3.41)$$

The exponent α then indicates the weak-link and strong-link proportion, $\alpha \in [0, 1]$ [Wu, 2001].

In the close packing case, rather than adopting a random close packing structure, one assumes a cubic crystal structure to simplify calculations [Shih, 1990; Mellema, 2002; Wu, 2001]. The local elastic entities of the network are organised in a crystal structure with springs in parallel and in series. Assuming that all distances are equal to ξ_s , there are $(L/\xi_s)^{\dim-1}$ springs in parallel, with \dim the dimension of the euclidean space, themselves composed by L/ξ_s springs in series. Summing the stiffnesses or the inverse of the stiffnesses for

the springs in parallel or in series respectively, this reads to the factor

$$S_{\text{net}} = \left(\frac{L}{\xi_s} \right)^{\text{dim}-2}. \quad (3.42)$$

Finally, the macroscopic influence of bending or stretching S_{MBS} is characterised by a dimensionless factor to the exponent $1 + 2\epsilon\alpha$ as expressed in equation (3.36). This factor will be expressed thoroughly in the following sections of the paper.

For reference, in the clusters ϕ -power law model [Shih, 1990], hypothesising an homogeneous network, the gel elasticity is

$$\frac{G'}{G_{\text{cc}}} = \begin{cases} \left(\frac{\xi_s}{a} \right)^{2-\text{dim}} = \phi^{\frac{\text{dim}-2}{\text{dim}-d}} & \text{weak-link regime} \\ \left(\frac{\xi_s}{a} \right)^{-\text{dim}} = \phi^{\frac{\text{dim}+b}{\text{dim}-d}} & \text{strong-link regime} \end{cases} \quad (3.43)$$

In this model the structural length is the cluster size $\xi_s = \xi$ and ϕ is the particle volume fraction. d and b represent respectively the fractal dimension of the cluster and the dimension of the cluster back-bone.

3.4.5.2 Clusters of clusters ϕ -power law model

In the clusters of clusters ϕ -power law model [Bouthier, 2022], we consider that colloidal particles of radius a assemble into clusters of dimension ξ_1 and fractal dimension d_1 which themselves aggregate into super-aggregates of dimension ξ_2 and fractal dimension d_2 to form the gel network as sketched in the figure 3.7. We note respectively δ_1 and δ_2 the dimension of elastic back-bone of cluster and super-aggregates³. At the aggregation scale, the structural length scale used to built the network is $\xi_s = \xi_2$. The macroscopic stiffness K is related to the superaggregate local elasticity K_{sa} through the close packing assumption bringing

$$K = \left(\frac{L}{\xi_2} \right)^{\text{dim}-2} K_{\text{sa}} = S_{\text{net}} K_{\text{sa}}. \quad (3.44)$$

Moreover, the superaggregates local elasticity K_{sa} is related to the cluster local elasticity K_c through the elastic back-bone scaling of the flocs which reads

$$K_{\text{sa}} = \left(\frac{\xi_1}{\xi_2} \right)^{\delta_2\alpha} K_c, \quad (3.45)$$

with $\alpha \in [0, 1]$ the proportion of weak-link regime ($\alpha = 0$) and strong-link regime ($\alpha = 1$) according to [Wu, 2001]. Furthermore, the cluster local elasticity is related to the local particle elasticity K_p with the elastic back-

bone scaling of the cluster which brings

$$K_c = \left(\frac{a}{\xi_1} \right)^{\delta_1\alpha} a^{2\epsilon\alpha} K_p. \quad (3.46)$$

Hence, the aggregation level contribution is

$$S_{\text{agg}} = \left(\frac{\xi_1}{\xi_2} \right)^{\delta_2\alpha} \left(\frac{a}{\xi_1} \right)^{\delta_1\alpha}. \quad (3.47)$$

Finally, the local particle elasticity K_p is expressed by

$$K_p = \frac{U}{\delta^2}. \quad (3.48)$$

All the geometrical quantities may be related to the particle volume fraction through

$$\phi = \left(\frac{\xi_2}{L} \right)^{3-\text{dim}} \left(\frac{\xi_1}{\xi_2} \right)^{3-d_2} \left(\frac{a}{\xi_1} \right)^{3-d_1}. \quad (3.49)$$

Putting equation (3.36)-equation (3.49) together reads

$$G' = \frac{U}{a\delta^2} \phi^{1+\frac{2\epsilon\alpha}{3-\text{dim}}} \left(\frac{\xi_1}{\xi_2} \right)^{\delta_2\alpha-2+d_2+\frac{d_2-\text{dim}}{3-\text{dim}}2\epsilon\alpha} \times \left(\frac{a}{\xi_1} \right)^{\delta_1\alpha-2+d_1+\frac{d_1-\text{dim}}{3-\text{dim}}2\epsilon\alpha} \quad (3.50)$$

and can be rewritten $G'/G_{\text{cc}} = S_{\text{agg}}S_{\text{net}}S_{\text{MBS}}$ with

$$S_{\text{net}} = \left(\phi^{-\frac{1}{3-\text{dim}}} \left(\frac{\xi_1}{\xi_2} \right)^{\frac{3-d_2}{3-\text{dim}}} \left(\frac{a}{\xi_1} \right)^{\frac{3-d_1}{3-\text{dim}}} \right)^{\text{dim}-2}, \quad (3.51)$$

$$S_{\text{MBS}} = \left(\phi^{-\frac{1}{3-\text{dim}}} \left(\frac{\xi_1}{\xi_2} \right)^{\frac{6-d_2-\text{dim}}{3-\text{dim}}} \left(\frac{a}{\xi_1} \right)^{\frac{6-d_1-\text{dim}}{3-\text{dim}}} \right)^{-1-2\epsilon\alpha}, \quad (3.52)$$

$$S_{\text{agg}} = \left(\frac{\xi_1}{\xi_2} \right)^{\delta_2\alpha} \left(\frac{a}{\xi_1} \right)^{\delta_1\alpha}. \quad (3.53)$$

When looking at equations (3.50) and (3.53), there are some variables where the exponent has a denominator equals to $3 - \text{dim}$. This difficulty is actually present in most of the demonstrations in the literature [Shih, 1990; Wu, 2001; Mellema, 2002] but is omitted considering proportional relationship between the relevant variables, the particle volume fraction and the microstructure variables. For example, in Eq. (10) in [Shih, 1990], there is the influence of the macroscopic size L in the macroscopic stiffness and the particle volume fraction, the cluster size and the macroscopic size are related between each other. Hence, we know the existence of this difficulty which is consistent with the approach described usually in the literature.

To avoid this difficulty, one can decide to impose $\epsilon =$

³For details about chemical dimension or dimension of elastic back-bone, [Grassberger, 1985; Grassberger, 1992b; Grassberger, 1992a] give some useful insights.

0 to be in the stretching regime and to get

$$G' = \frac{U}{a\delta^2} \phi \left(\frac{\xi_1}{\xi_2} \right)^{d_2\alpha-2+d_2} \left(\frac{a}{\xi_1} \right)^{d_1\alpha-2+d_1}, \quad (3.54)$$

which can be simplified in the weak-link regime ($\alpha = 0$) to

$$G' = \frac{U}{a\delta^2} \phi \left(\frac{\xi_1}{\xi_2} \right)^{d_2-2} \left(\frac{a}{\xi_1} \right)^{d_1-2}. \quad (3.55)$$

Another possibility of the model is to change the homogeneous network into heterogeneous fractal network. In this case, equations (3.44) and (3.49) are replaced respectively by

$$S_{\text{net}} = \left(\frac{\xi_2}{L} \right)^{\mathfrak{D}\alpha} \quad (3.56)$$

$$\phi = \left(\frac{\xi_2}{L} \right)^{3-D} \left(\frac{\xi_1}{\xi_2} \right)^{3-d_2} \left(\frac{a}{\xi_1} \right)^{3-d_1} \quad (3.57)$$

with D the network fractal dimension and \mathfrak{D} the dimension of the elastic back-bone. Equation (3.50) is then replaced by

$$G' = \frac{U}{a\delta^2} \phi \frac{\frac{\mathfrak{D}\alpha+1+2\epsilon\alpha}{3-D} \left(\frac{\xi_2}{\xi_1} \right)^{(3-d_2)\frac{\mathfrak{D}\alpha+1+2\epsilon\alpha}{3-D}-d_2\alpha-1-2\epsilon\alpha}}{\left(\frac{\xi_1}{a} \right)^{(3-d_1)\frac{\mathfrak{D}\alpha+1+2\epsilon\alpha}{3-D}-d_1\alpha-1-2\epsilon\alpha}} \times \quad (3.58)$$

which can be rewritten $G'/G_{\text{cc}} = S_{\text{agg}}S_{\text{net}}S_{\text{MBS}}$ with

$$S_{\text{net}} = \left(\phi \left(\frac{\xi_2}{\xi_1} \right)^{3-d_2} \left(\frac{\xi_1}{a} \right)^{3-d_1} \right)^{\frac{\mathfrak{D}\alpha}{3-D}}, \quad (3.59)$$

$$S_{\text{MBS}} = \left(\left(\phi \left(\frac{\xi_2}{\xi_1} \right)^{3-d_2} \left(\frac{\xi_1}{a} \right)^{3-d_1} \right)^{\frac{1}{3-D}} \left(\frac{\xi_2}{\xi_1} \right)^{-1} \left(\frac{\xi_1}{a} \right)^{-1} \right)^{1+2\epsilon\alpha}, \quad (3.60)$$

$$S_{\text{agg}} = \left(\frac{\xi_2}{\xi_1} \right)^{-d_2\alpha} \left(\frac{\xi_1}{a} \right)^{-d_1\alpha}. \quad (3.61)$$

3.4.5.3 Interpenetration of clusters ϕ -power law model

In the Interpenetration of clusters ϕ -power law model, the size a still corresponds to the particle size but the size ξ_1 corresponds to the center-to-center distance between the clusters composed of particles of size a and the size ξ_2 corresponds to the cluster size and fractal dimension d_2 , as sketched on figure 3.7. The structure length scale ξ_s for the network is now $\xi_s = \xi_1$. The macroscopic gel linear storage modulus G' is again given by equation (3.36). To simplify the calculations, we dismissed the bending contributions so that K is a purely stretching linear elastic stiffness ($\epsilon = 0$). Adopt-

ing a close packing configuration for the network leads to

$$S_{\text{net}} = \left(\frac{L}{\xi_1} \right)^{\text{dim}-2}. \quad (3.62)$$

The mass conservation can then be written

$$\phi = \left(\frac{a}{\xi_1} \right)^3 \left(\frac{\xi_2}{a} \right)^{d_2} \left(\frac{\xi_1}{L} \right)^{3-\text{dim}}. \quad (3.63)$$

For the aggregation level, we decompose the elementary effective stiffness of the clusters as in [Wu, 2001] with

$$\frac{1}{K_{\text{eff}}} = \frac{1}{K_c} + \frac{1}{K_{\text{ext}}} + \frac{1}{K_i} \quad (3.64)$$

with K_c , K_{ext} and K_i the elastic stiffness related to the inside of the cluster, the intermicroscopic links (see [Wu, 2001]) and the interpenetration of the cluster, respectively.

Let us now quantify K_i . K_i is assumed to be proportional to the number of contact N_i between interpenetrating clusters: $K_i = N_i k_i$, where k_i is a reference interpenetration stiffness. The last expression comes from the fact we assumed that the contacts in the interpenetration zone are parallel springs: this justifies the additivity of the stiffnesses. We assume that the reference interpenetration stiffness k_i is directly related to the depth of the interaction potential U and the distance of interaction δ through $k_i = U/\delta^2$. Due to the fractal nature of the clusters, there are $N_i = \left(6V_i/\pi a^3 \right)^{\frac{d_2}{3}}$ particles inside the intersection volume V_i between two clusters. Geometrically assimilating clusters to spheres leads to an intersection volume [Polyanin, 2007; Kern, 1967, p. 97]

$$V_i = \frac{\pi}{12} \xi_2^3 \left(2 + \frac{\xi_1}{\xi_2} \right) \left(1 - \frac{\xi_1}{\xi_2} \right)^2 \mathbf{1}_{\{\xi_1 < \xi_2\}}. \quad (3.65)$$

We assume that each particle brought by each cluster in V_i form a contact adding rigidity to the whole system. Putting together the last expressions, we get

$$K_i = \frac{U}{2\delta^2} \left(\frac{\xi_2}{a} \right)^{d_2} \left(1 + \frac{\xi_1}{2\xi_2} \right)^{\frac{d_2}{3}} \left(1 - \frac{\xi_1}{\xi_2} \right)^{\frac{2d_2}{3}} \mathbf{1}_{\{\xi_1 < \xi_2\}}. \quad (3.66)$$

Let us now compare K_i with K_c and K_{ext} . There are different ways to consider that $K_i \ll \min(K_c, K_{\text{ext}})$. To simplify the comparison, following [Wu, 2001], we write

$$\frac{1}{K_c} + \frac{1}{K_{\text{ext}}} = \frac{1}{K_c} \left(\frac{K_c}{K_{\text{ext}}} \right)^\alpha \quad (3.67)$$

with $\alpha \in [0, 1]$ allowing to make a continuous transition between the weak-link and the strong-link regime. A first way to compare K_i with K_c (K_{ext}/K_c) $^\alpha$ is to say that the system is in the regime $\xi_2/\xi_1 \gtrsim 1$. Thus, one can

re-write equation (3.66) as

$$K_i \underset{\xi_2/\xi_1 \geq 1}{\propto} \frac{U}{2\delta^2} \left(1 - \frac{\xi_1}{\xi_2}\right)^{\frac{2d_2}{3}}. \quad (3.68)$$

K_i depends strongly on the distance of ξ_2/ξ_1 from unity. Therefore, K_i is negligible when $\xi_2/\xi_1 \geq 1$ compared to $K_c (K_{\text{ext}}/K_c)^\alpha$ and, in equation (3.64), we get $K_{\text{eff}} \approx K_i$.

The other way to consider the system is, following previous approaches in [Kantor, 1984a; Kantor, 1984b; Shih, 1990; Wu, 2001; Mellema, 2002; Wessel, 1992], estimating $K_c (K_{\text{ext}}/K_c)^\alpha \propto \xi_1^{-\mu}$ with $\mu \in [1, 5]$ function of the fractal dimension D , the dimension of the elastic back-bone and the regime of strong-link or weak-link because ξ_1 is similar to a cluster size with contact. Recalling that $(\xi_2/a)^{d_2} \propto \xi_1^3$, one gets in this case

$$\frac{K_i}{K_c} \left(\frac{K_c}{K_{\text{ext}}}\right)^\alpha \propto \xi_1^{3+\mu} \left(1 + \frac{\xi_1}{2\xi_2}\right)^{\frac{d_2}{3}} \left(1 - \frac{\xi_1}{\xi_2}\right)^{\frac{2d_2}{3}}. \quad (3.69)$$

Assuming that ξ_1 does not vary much, $K_i/K_c (K_c/K_{\text{ext}})^\alpha$ is governed by the values of $\xi_2/\xi_1 \mapsto (1 + \xi_1/(2\xi_2))^{\frac{d_2}{3}} (1 - \xi_1/\xi_2)^{\frac{2d_2}{3}}$ on $[1.2, 1.8]$. $K_i/K_c (K_c/K_{\text{ext}})^\alpha$ is, according to Dagès et al. [Dagès, 2022], between 0.1 and 0.3. Therefore, one can assume that $K_i \ll K_c (K_{\text{ext}}/K_c)^\alpha$, at least for the first values, and following equation (3.64), we get $K_{\text{eff}} \approx K_i$.

Generally, as K_i is getting closer to $K_c (K_{\text{ext}}/K_c)^\alpha$, it becomes difficult to consider that only one phenomenon prevails. If one wants to completely understand the balance between the different contributions, one needs to model both phenomena and their coupling. This is not the goal of this model which tries to give some orders of magnitude without exhaustively modeling the system.

This final expression of the interpenetration ϕ -power law model is then

$$G' = \frac{U}{2a\delta^2} \left(1 + \frac{\xi_1}{2\xi_2}\right)^{\frac{d_2}{3}} \left(1 - \frac{\xi_1}{\xi_2}\right)^{\frac{2d_2}{3}} \phi \left(\frac{\xi_1}{a}\right)^2 \quad (3.70)$$

which can be rewritten $G'/G_{\text{cc}} = S_{\text{agg}} S_{\text{net}} S_{\text{MBS}}$ with

$$S_{\text{net}} = \left(\phi \left(\frac{\xi_1}{a}\right)^3 \left(\frac{\xi_2}{a}\right)^{-d_2}\right)^{\frac{2-\text{dim}}{3-\text{dim}}}, \quad (3.71)$$

$$S_{\text{MBS}} = \frac{a}{\xi_1} \left(\phi \left(\frac{\xi_1}{a}\right)^3 \left(\frac{\xi_2}{a}\right)^{-d_2}\right)^{\frac{1}{3-\text{dim}}}, \quad (3.72)$$

$$S_{\text{agg}} = \frac{1}{2} \left(\frac{\xi_2}{a}\right)^{d_2} \left(1 + \frac{\xi_1}{2\xi_2}\right)^{\frac{d_2}{3}} \left(1 - \frac{\xi_1}{\xi_2}\right)^{\frac{2d_2}{3}}. \quad (3.73)$$

The dimension of the network dim is not required in the final expression due to the contribution of the effective volume fraction through the particle volume fraction and the fractal dimension related to ξ_1 .

If we now replace the homogeneous network by a het-

erogeneous network of fractal dimension D and back-bone dimension \mathfrak{D} , equations (3.62) and (3.63) become respectively

$$S_{\text{net}} = \left(\frac{\xi_1}{L}\right)^{\mathfrak{D}\alpha} \quad (3.74)$$

$$\phi = \left(\frac{a}{\xi_1}\right)^3 \left(\frac{\xi_2}{a}\right)^{d_2} \left(\frac{\xi_1}{L}\right)^{3-D}. \quad (3.75)$$

The storage modulus is then

$$G' = \phi^{\frac{1+\mathfrak{D}\alpha}{3-D}} \frac{U}{2a\delta^2} \left(\frac{\xi_1}{a}\right)^{\frac{3\mathfrak{D}\alpha+D}{3-D}} \left(\frac{\xi_2}{a}\right)^{d_2 \frac{2-D-\mathfrak{D}\alpha}{3-D}} \times \left(1 + \frac{\xi_1}{2\xi_2}\right)^{\frac{d_2}{3}} \left(1 - \frac{\xi_1}{\xi_2}\right)^{\frac{2d_2}{3}} \quad (3.76)$$

which can be rewritten $G'/G_{\text{cc}} = S_{\text{agg}} S_{\text{net}} S_{\text{MBS}}$ with

$$S_{\text{net}} = \left(\phi \left(\frac{\xi_1}{a}\right)^3 \left(\frac{\xi_2}{a}\right)^{-d_2}\right)^{\frac{\mathfrak{D}\alpha}{3-D}}, \quad (3.77)$$

$$S_{\text{MBS}} = \left(\frac{\xi_1}{a}\right)^{-1} \left(\phi \left(\frac{\xi_1}{a}\right)^3 \left(\frac{\xi_2}{a}\right)^{-d_2}\right)^{\frac{1}{3-D}}, \quad (3.78)$$

$$S_{\text{agg}} = \frac{1}{2} \left(\frac{\xi_2}{a}\right)^{d_2} \left(1 + \frac{\xi_1}{2\xi_2}\right)^{\frac{d_2}{3}} \left(1 - \frac{\xi_1}{\xi_2}\right)^{\frac{2d_2}{3}}. \quad (3.79)$$

In conclusion of this section 3.4.4, contrary to the classical ϕ -power law model in equation (3.43), we observe that the scaling of the gel elasticity not only depends on ϕ but also the ratios between the length scales of the gel.

3.4.5.4 Discussion of the gel elasticity

Next, we turn to the elastic properties of the carbon black gels obtained through the flow cessation protocol. Figure 3.6 displays the evolution of the elastic modulus G'_∞ of the gel measured during a frequency sweep experiment in the low frequencies domain as a function of $\dot{\gamma}_0$. The gel becomes weaker as $\dot{\gamma}_0$ increases.

Fitting G'_∞ with the ϕ -power law models is complex given the number of parameters in the equations. The fit is underdetermined: there are more parameters than available data to fit. To remain relevant, we constrain the fit parameters. First, we set ξ_1 , d_1 , ξ_2 and d_2 to the values of the SAXS models as shown in figure 3.8. Second, we set the elasticity scale G_{cc} and take the value from the simulations by Varga et al. [Varga, 2019]: $G_{\text{cc}} = 6 \times 10^7$ Pa with $U = 30 k_B T$ and $\delta = 0.01a$. Third, based on the SAXS analysis, we only consider the models with a fractal gel network. This hypothesis is indeed verified as all models in the homogeneous network limit fail to fit G'_∞ with the constrain $G_{\text{cc}} = 6 \times 10^7$ Pa. Fourth, we choose to constrain the fit to explore the parameter space and decide to study limiting cases: the weak-link

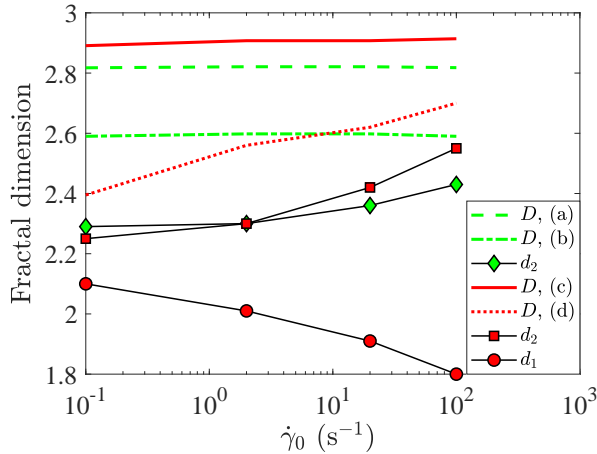


Figure 3.9: Evolution of the gel network fractal dimension D as a function of $\dot{\gamma}_0$ for the models (a) through (d) which parameters are listed in table 3.3. The fractal dimension d_1 and d_2 from figure 3.8 are also plotted for comparison. The green data is related to the interpenetrating cluster models whereas the red data is related to the cluster of clusters model.

limit $\alpha = 0$ (model (a) and (c)) and the strong-link limit $\alpha = 1$ in the stretching limit $\epsilon = 0$ (model (b) and (d)) or the bending limit $\epsilon = 1$ (model (e)). Again to simplify the model, when $\alpha \neq 0$, we constrained the dimensions of the elastic back-bones to $\mathfrak{D} = \mathfrak{d}_1 = \mathfrak{d}_2 = 1.25$, an intermediate value between its extremes 1 and 1.5 [Grassberger, 1985; Grassberger, 1992b; Grassberger, 1992a]. Finally, we note, that, if $D \simeq d_2$, there is no contrast in the scattering intensity $I(q)$ between the aggregate of fractal dimension d_2 and the gel network of fractal dimension D . Therefore, one must have $d_2 \neq D$. With those constrains, the only fitting parameter is D . Model (e) fails to fit the data whereas models (a) to (d) successfully fit G_∞ as shown in figure 3.6. The fit parameters are listed in table 3.3 and D as a function of $\dot{\gamma}_0$ is plotted in figure 3.9.

The models (a) through (d) are not discriminatory. In the weak link limit, models (a) and (c) yield a very high value of D , and the gel network is almost homogeneous. In the strong link limit, models (b) and (d) yield a weaker value of D , around 2.6. In all cases, the models show a hierarchical organisation of the fractal dimensions, $D > d_2 > d_1$ or $D > d_2$ if d_1 does not exist as in the cluster interpenetration model. It is known [Zacccone, 2009c; Conchuir, 2014; Ruan, 2020; Varga, 2019; Jamali, 2019a; Jacquin, 2018; Jamali, 2020; Jamali, 2019b] that clusters under shear tend to become denser. A usual understanding of the phenomenon is that the competition between attractive forces due to the interaction potential and disaggregating forces due to shear impose the clusters size and fractal dimension. It is usually assumed that the cluster grows with decreasing shear

rate and it is assumed but rarely measured that the cluster fractal dimension is constant [Wessel, 1992; Kimbonguila Manounou, 2014; Eggersdorfer, 2010]. In turbulent flows of non-Brownian particles it is consistently measured that the clusters become larger and looser as the shear rate decreases [Spicer, 1998; Bubakova, 2013]. However there is no clear understanding of this trend. Measurements presented in figure 3.6 shows that, in the case of carbon black dispersions, the picture is much more complex and involves hierarchical structures with varying fractal dimensions. Moreover, the clusters are not isolated but form a space spanning network. Assuming that the structure during flow is very similar to one after flow cessation, the question is then, how does the flow before flow cessation propagate from large to small length scales?

In turbulence [Kolmogorov, 1991], the energy cascades from the large to the small scales. Loss in energy only occurs at the small scales due to viscous dissipation. Hence, the largest structure in the system, here the network of dimension L sees directly the imposed shear flow which sets its fractal dimension D . For the aggregation level, the shear flows perceived by the intermediate clusters is diminished by the surrounding higher levels organisation. The intermediate structures have then less constraints to build up their structure which allows lower fractal dimension or less dense structures. To give some quantitative arguments, in the turbulent energy cascade [Kolmogorov, 1991], the rate of dissipation of energy e , which is also the rate of energy brought by the larger scales to the smaller scales, is independent of the length scale and considered constant after being set up by the macroscopic flow. Assessing the values of the rate of dissipation in our system, there is no inertia and only purely viscous dissipation. Hence, the rate of energy dissipation per unit volume is

$$e = \frac{\eta}{2} \|\nabla \mathbf{u}\|^2 \approx \frac{\eta u^2}{h^2} \quad (3.80)$$

with η the dynamic viscosity, u the velocity and h a certain length scale over which the velocity varies. It is necessary to estimate the velocity u and the length scale h . Using the Darcy law framework, the porosity of the gel is given by $1 - \phi_{\text{eff}}(l)$ with ϕ_{eff} the effective volume fraction of particles-cluster-superaggregates for a certain window size l . The effective volume fraction ϕ_{eff} increases with l , tends to ϕ when $l = 0$, 1 when $l = L$, the network size. ϕ_{eff} also depends on the particle volume fraction ϕ , the different typical length scales ξ_i and the fractal dimensions d_i and D . However, the global trend of the function ϕ_{eff} is sufficient. Assuming that a fixed flow rate per unit area Q is fixed and in order to recover the fluid volume, the velocity and the length scale are given by $Q/u = (h/l)^3 = 1 - \phi_{\text{eff}}(l)$. Therefore, the rate

Model	α	ϵ	G_{cc} (Pa)	$d_1 = d_2 = \mathfrak{D}$	D	Fit?
Interpenetration of clusters ϕ-power law model, equation (3.76)						
Parameters ξ_1, ξ_2 and d_2 are set by the experiments, figure 3.8(a)						
(a)	0	-	6×10^7	-	2.84	yes
(b)	1	-	6×10^7	1.25	2.64	yes
Clusters of clusters ϕ-power law model, equation (3.58)						
Parameters ξ_1, d_1, ξ_2 and d_2 are set by the experiments, figure 3.8(b)						
(c)	0	-	6×10^7	-	2.91	yes
(d)	1	0	6×10^7	1.25	figure 3.9	yes
(e)	1	1	6×10^7	1.25	-	no

Table 3.3: Parameters of the models that fit G'_{∞} in figure 3.6. α and ϵ define the models. We set $G_{cc} = 6 \times 10^7$ Pa as in [Varga, 2019]. ξ_1, d_1, ξ_2 and d_2 are determined by the experiments (figure 3.8). \mathfrak{D}, d_1, d_2 are kept constant to 1.25. D is the free fit parameter. Its values as a function of γ_0 are displayed in figure 3.9. Model (e) could not fit the data for any D value.

of energy dissipation per unit volume is given by

$$e \approx \frac{\eta Q}{l^2} (1 - \phi_{\text{eff}}(l))^{-\frac{8}{3}}. \quad (3.81)$$

To conclude the demonstration, in our case e decreases when l decreases from L to a as opposed to the turbulent case where e is constant. Thus, the energy is not continuously distributed among all the length scales from L to a but there is a decrease of the amount of energy brought to the smaller scales which ends up to decrease the constraints on the intermediate structures and allows for looser structures. If we pursue such reasoning it is possible to find then a decreasing density of the material, in terms of fractal dimension for example, from the largest scale to the lowest scale. This continuum briefly presented in [Bouthier, 2022] can find an experimental demonstration here.

This demonstration support two hypothesis, (i) the effective flow rate decreases as it propagates from large to small scale structures and (ii) the fractal dimension adopted by the structure decreases as the flow rate decreases. We therefore expect that the fractal dimension diminish as we go to lower length scales: $D > d_2 > d_1$ as inferred by the data and the fits.

Following the fit results, the models (a-e) show that the carbon black gel elasticity comes from stretching the bonds at all length scales and that bending can be dismissed ($\epsilon = 0$). Bending is prevalent in gels forming strands such as arrested phase separation gels [Gibaud, 2013] but also in fractal colloidal gels with a fractal dimension $d \sim 2$ where long thin chains of colloid come into play [Pantina, 2006; Dinsmore, 2006]. In the carbon black gels formed through flow cessation, its fractal structure is very dense, especially at large length scales, and seems to prevent bending from contributing significantly to the gel elasticity.

The derivation of the three length scales rheological

models opens future work directions. First, revisiting the classical ϕ -power law model [Shih, 1990] which is widely used in the literature, we have pointed out an issue which has been eluded up to now: the elasticity goes as $\phi^{\frac{1}{3-\text{dim}}}$ and therefore diverges when the euclidean space dimension is equal to $\text{dim} = 3$ (equations (3.53) and (3.73)). We have shown that this problem can be avoided when taking into account a fractal gel network (equations (3.61) and (3.79)) or having $\epsilon = 0$ (equation (3.54)). Nevertheless this issue remains to be solved in future work. Second, we have developed an approach allowing to go continuously from the weak link to the strong link regime and from the stretching to the bending limit. Those hypotheses based solely on scaling arguments (equation (3.36)) would benefit from in-depth numerical simulation or theoretical investigation. Finally, we hope that the case of three length scales colloidal gels is not specific to carbon black gels and that our model can be confronted in the future to other experimental systems.

3.4.6 Summary of the contribution

We have compared the two models with experimental data coming from carbon-black particles suspensions. We have highlighted the common points and the divergences between the two models while expliciting some difficulties originally present in this kind of scaling arguments. We have opened the door for some future reflections about complex models supported by complex microstructural data.

3.5 Conclusion

We have demonstrated how the microscopic structure may influence the rheology through different scaling models namely the interpenetration of clusters model and the clusters of clusters model. As already discussed, I may have a preference for the latter one which is closer to the historical models and does use additional arguments to be built. It allows also to extend to multiple levels with more than three length scales which is not possible with the former model.

Chapter 4

Application of ultrasound on materials

Objectives

This chapter aims for the application of the macroscopic-microscopic coupling on an industrial case : the mixing of radioactive sludges under ultrasound.

Objectifs

Ce chapitre vise à appliquer le couplage macroscopique-microscopique à un cas industriel : le mélange de boues radioactives sous ultrasons.

Contents

4.1	Introduction	71
4.2	Analytical description	71
	4.2.1 Derivation of the solution . . .	71
	4.2.2 Discussion about the solution . .	72
4.3	Numerical case	73
4.4	Describing the phenomenology on radioactive sludges	75
4.5	Conclusion	76

4.1 Introduction

After having investigated the coupling between the macroscopic environment and the microscopic structure, it is interesting to come back to the initial problem related to the CEA "sludges". In this chapter, some insights will be presented about easy estimates of predictable effects when ultrasound are applied.

4.2 Analytical description

4.2.1 Derivation of the solution

As a general thought, the problem of a medium where ultrasound are applied can be tackled through a half space medium $\mathbb{R}^2 \times \mathbb{R}_+$ with a point force in a specific direction which can be assumed to be the z -axis at the origin [Selvadurai, 2001; Itou, 2020; Kim, 1991]. Considering the equation of motion, we get in an incompressible medium

$$\operatorname{div}(\mathbf{u}) = 0 \quad (4.1)$$

$$\rho \frac{d\mathbf{u}}{dt} = \mathbf{div}(\boldsymbol{\sigma}) \quad (4.2)$$

with \mathbf{u} the velocity, ρ the density and $\boldsymbol{\sigma}$ the Cauchy stress tensor. The assumption of incompressibility is due to the fact that the media considered are mainly soft aqueous suspensions. Therefore, the shear modulus is negligible compared to the bulk modulus. Hence, because we are interested in the evolution of the deformation induced by the ultrasound in the viscoelastic skeleton, the compressive waves in the solvent will be ignored. The expression of the stress tensor is composed of a viscoelastic component which may have a complex nature and the pressure component. Assuming small perturbations, the equations become linear and read, using the \cdot notation,

$$\operatorname{div}(\mathbf{u}') = 0 \quad (4.3)$$

$$\rho \frac{\partial \mathbf{u}'}{\partial t} = \mathbf{div}(\boldsymbol{\sigma}'). \quad (4.4)$$

Assuming a periodic solution with pulsation ω , it is possible to express linearly the stress tensor in terms of the strain tensor with a complex modulus G which spans the range between completely elastic and completely viscous behaviours depending on the local conditions writing, with the $\bar{\cdot}$ notation,

$$\mathbf{div}(\bar{\mathbf{v}}) = 0 \quad (4.5)$$

$$\mathbf{div}\left(G\left(\nabla\bar{\mathbf{v}} + \nabla\bar{\mathbf{v}}^T\right)\right) + \rho\omega^2\bar{\mathbf{v}} = \mathbf{grad}(\bar{p}) \quad (4.6)$$

with \mathbf{v} the displacement and \bar{p} the amplitude of the pressure. A strong coupling will need a coupled problem resolution between the displacement and the rheological law. It can be possible to remove the pressure in the stress tensor applying the curl operator to the previous equations and get, with the vorticity $\mathbf{v} = \mathbf{curl}(\bar{\mathbf{v}})$,

$$\mathbf{div}(\bar{\mathbf{v}}) = 0 \quad (4.7)$$

$$\rho\omega^2\mathbf{v} - \mathbf{grad}(G) \times \mathbf{curl}(\mathbf{v}) + \mathbf{div}(G\nabla\mathbf{v}) = 0. \quad (4.8)$$

Because it is impossible to solve analytically, we will consider G as a constant and will make the value vary in the complex plane. In the case of the point force problem, the displacement field can be reduced to a 2D field in spherical coordinates with a symmetry of revolution. It is then straightforward to invoke the Stokes stream function ψ in the case of an incompressible medium defined as

$$\bar{\mathbf{v}} = \frac{1}{r^2 \sin(\theta)} \frac{\partial\psi}{\partial\theta} \mathbf{e}_r - \frac{1}{r \sin(\theta)} \frac{\partial\psi}{\partial r} \mathbf{e}_\theta \quad (4.9)$$

with the zenith direction in the point force direction. The conservation of mass is then automatically satisfied. The vorticity has then only one component. It can be demonstrated afterwards that

$$\begin{aligned} \mathcal{D}\psi &= -\frac{1}{r \sin(\theta)} \left(\frac{\partial^2\psi}{\partial r^2} + \frac{\sin(\theta)}{r^2} \frac{\partial}{\partial\theta} \left(\frac{1}{\sin(\theta)} \frac{\partial\psi}{\partial\theta} \right) \right) \\ &= \nu \end{aligned} \quad (4.10)$$

Finally, replacing equation (4.10) in equation (4.8) with a constant G leads to a simplified equation

$$0 = \mathcal{A}\mathcal{D}\psi \quad (4.11)$$

$$\mathcal{D}\psi = -\frac{1}{r \sin(\theta)} \left(\frac{\partial^2\psi}{\partial r^2} + \frac{\sin(\theta)}{r^2} \frac{\partial}{\partial\theta} \left(\frac{1}{\sin(\theta)} \frac{\partial\psi}{\partial\theta} \right) \right) \quad (4.12)$$

$$\mathcal{A}g = \frac{1}{r^2} \frac{\partial}{\partial\theta} \left(\frac{1}{\sin(\theta)} \frac{\partial}{\partial\theta} (\sin(\theta)g) \right) + \quad (4.13)$$

$$\frac{1}{r} \frac{\partial^2}{\partial r^2} (rg) + k^2 g \quad (4.14)$$

with r the distance from the origin and the angle θ from the direction of the point force and $k^2 = \rho\omega^2/G$ the square of the wavevector number. Calling the intensity of the point force F , the problem can be solved to get

$$\psi = \frac{F}{8\pi\rho\omega} \frac{2 \sin^2(\theta)}{r} \left((1 + ikr) e^{-ikr} - 1 \right). \quad (4.15)$$

4.2.2 Discussion about the solution

Some discussions are needed on this solution. First, assuming that the pulsation ω tends to 0, the solution reaches the static form presented in [Selvadurai, 2001; Itou, 2020] which is

$$\psi = \frac{F\omega}{8\pi G} \sin^2(\theta) r. \quad (4.16)$$

The static solution gives that the stresses are proportional to r^{-2} with a typical length scale $\sqrt{F/G}$. However, the dynamical solution gives a typical length scale

$$L_c = \sqrt{\frac{G}{\rho\omega^2}} \quad (4.17)$$

which is independent of the intensity of ultrasound applied. Assuming that G spans from E the pure elastic modulus to $i\eta\omega$ the pure viscous modulus using the table 4.1 values which were obtained with rheological measurements at 1Hz, we find dynamical length scales between 1 μm and 10 μm which are well below what can be expected in an industrial application. Some critics can be drawn from the values in table 4.1 because these values are taken from rheological experiments at 1Hz. It is well known [Sollich, 1997; Sollich, 1998; Dagès, 2022] that rheological properties depend on the frequency domain. A usual example of this is a linear Maxwell fluid [Maxwell, 1867] which is viscous at low frequencies and elastic at high frequencies.

Nevertheless, the general conclusion of such model is that assuming a strong coupling between the microstructure and the macroscopic environment may lead to a coupled rheological law which affects the values of the complex modulus. Assuming that the complex modulus depends on the norm of the stress tensor with a purely elastic behaviour at low stress values and a pure viscous behaviour at high stress values with a certain threshold to indicate the transition, there will be around the point force a zone of influence whose size depends on the rheological parameter and the intensity of ultrasound: more powerful

Variable	Value
U	1.5 μm
E	1kPa
η	25mPa.s
$\omega/2\pi$	50kHz
ρ	1kg/L
b	3cm
σ_c	30Pa
c_p	4185 J/K/kg

Table 4.1: Orders of magnitude for the rheological parameters to evaluate typical length scales. U is the amplitude of displacement imposed by the ultrasound and b is the width of the transducer used to produce the ultrasound.

ultrasound will lead to a larger zone of influence and higher values of rheological properties will lead to a larger zone due to a better transmission of the sound wave. Then, inside the zone of influence, the material is globally viscous, whereas, outside the zone, the material is globally elastic. This is due to the fact that the ultrasound source creates a zone of high values of stress (diverging in the case of a point force, finite in the case of a spread surface of action [Itou, 2020]) which tends to fluidify locally the material without affecting the material far from the source.

To give more details about the movement in the material, the streamlines of equation (4.15) are represented on figure 4.1. Only the dimensionless real part is represented because this will be the actual movement in permanent regime. It is interesting to recall that the streamlines are the lines where the velocity is aligned at each point of this line. The intensity or the norm of the velocity is coloured along these lines. Starting from the left, the material is purely elastic without any dissipation. Therefore, the transverse wave is transmitted in the medium without any problem. The particles are moving along the streamlines in a periodic motion depending on the portion of cycle in the time period. On the right, the material is purely viscous, there is no transmission of the waves which are only dissipated. There is a concentration of the velocity near the application point of the force. Also, because there is no elasticity, thus no speed of sound, the whole system is moving in block with, by conservation of mass, a decrease of the velocity far from the source. In the middle, there is a mix of both behaviours where there is a kind of wave transmission with two or three oscillations but the amplitude of the displacement is quickly dissipated far from the source. If we want to consider the strongly coupled case, this will be a mix of all these solutions. Indeed, near the

application point of the ultrasound, the stresses will be really high, inducing a viscous behaviour, hence, close to the source, the solution will start as a purely viscous material moving as a block. When the amplitude of the stresses will go down as the distance increases from the source, there will be a transition from the viscous material to an elastic material. Therefore, far from the source, the oscillation of displacement will start again but with a much lower amplitude due to the initial dissipation in the viscous core near the source. The continuous transition from purely viscous to purely elastic will draw a zone of influence with a given radius depending on the stress threshold σ_c , the elastic modulus E , the viscosity η , the intensity of the ultrasound F , the density ρ and the pulsation ω .

4.3 Numerical case

Starting from the previous analytical study, it is possible to emphasize that the width of the application of the ultrasound $b \approx 3$ cm is much larger than the wavelength or the size of the zone of influence which is between 1 μm and 10 μm . Hence from the point of view of the simulations, monitoring the evolution of the displacement in the material can be reduced to a one dimension problem where the displacement is imposed at $x = 0$. Therefore, it is possible to write a differential equation for the displacement $\mathbf{u} = (u_x, u_y, u_z)$. Knowing that everything depends only on the direction x of the application of ultrasound and the displacement is divergence free, $u_x = 0$. Also, as discussed in the previous chapters and the present one, it can be interesting to consider that the rheology is tuned by the intensity of the stress. Hence, keeping our resolution in the linear regime, it is possible to propose a viscoelastic modulus G which depends directly on the norm of the stress tensor σ . Due to the fact that we want to mimic the fluidisation of radioactive sludges which are initially elastic, it is straightforward to assume an elastic behaviour at very low stress intensity and a viscous behaviour at very high stress intensity. More precisely, the viscoelastic modulus G will evolve from a linear elastic modulus E at low values of stress to a linear viscous modulus $i\eta\omega$ at high values of stress. The transition between the two regime may be designated by a yield stress σ_c which depends on the material. To be more explicit and illustrate this description, considering the complex plane, going from low stress values to high stress values, the viscoelastic modulus will evolve from the x -axis at a value E to the y -axis at a value $i\eta\omega$ with a phase angle of $\pi/4$ when $\sigma = \sigma_c$. This whole description is shown on figure 4.2. It can also be summarised by the

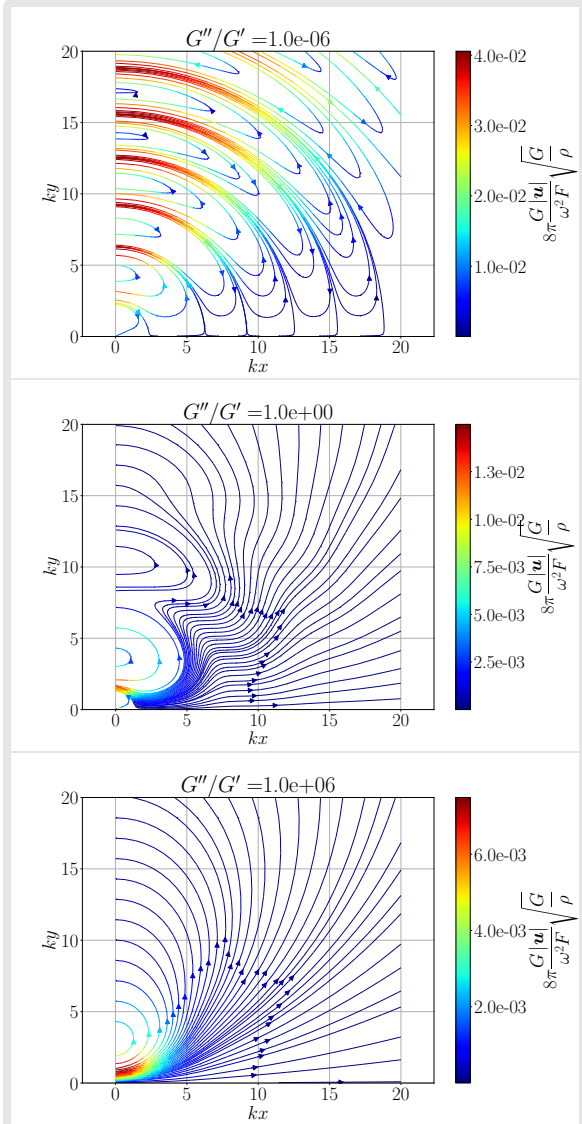


Figure 4.1: Streamlines oriented by the direction of the displacement and colored according to the dimensionless norm of the displacement $8\pi\sqrt{G}/\rho G|u|/\omega^2 F$ in the xy plane assuming that the point force is in the x direction and applied at the origin $(0,0)$. The xy plane is actually a radial plane containing the force vector due to symmetry of revolution. The space units are taken as the wavelength. To compare with equation (4.15), $r^2 = x^2 + y^2$ and $\tan(\theta) = y/x$. From top to bottom, ratio of the loss modulus G'' over the storage modulus G' increases from 10^{-6} to 10^6 .

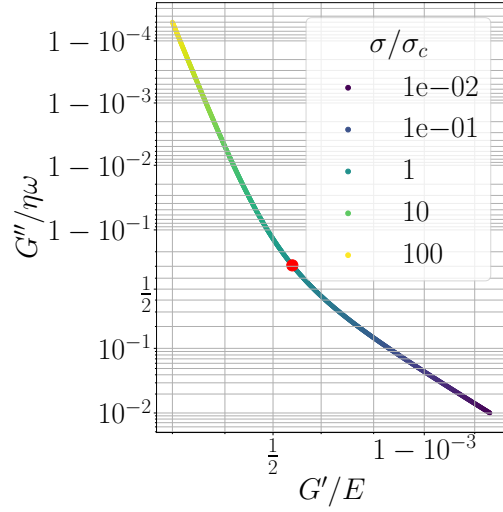


Figure 4.2: Evolution of the viscoelastic modulus G in the complex plane as a function of the stress intensity σ . The big red dot (\bullet) is a reference point with $\sigma = \sigma_c$.

following equation

$$G = \left(E + i\eta\omega \frac{\sigma}{\sigma_c} \right) \left(1 + \left(\frac{\sigma}{\sigma_c} \right)^2 \right)^{-1/2} \quad (4.18)$$

which respects exactly the evolution of figure 4.2.

If one wants now to express σ , it is actually depending directly on $d_x u_y$ and $d_x u_z$ through

$$\sigma = |G| \sqrt{\left| \frac{du_y}{dx} \right|^2 + \left| \frac{du_z}{dx} \right|^2}. \quad (4.19)$$

This is then the proof of the strong coupling happening in this kind of material because both sides of equation (4.18) depends on G through equation (4.19). Putting everything together, the equations of motion in one dimension are then reading

$$\frac{d\mathbf{X}}{dx} = \frac{1}{G} \begin{pmatrix} 0 & 0 & 1 & 0 \\ 0 & 0 & 0 & 1 \\ -\rho\omega^2 G & 0 & 0 & 0 \\ 0 & -\rho\omega^2 G & 0 & 0 \end{pmatrix} \mathbf{X} \quad (4.20)$$

$$G = \left(E + i\eta\omega \frac{\sqrt{|X_3|^2 + |X_4|^2}}{\sigma_c} \right) \left(1 + \frac{|X_3|^2 + |X_4|^2}{\sigma_c^2} \right)^{-1/2} \quad (4.21)$$

$$\mathbf{X} = \left(u_y, u_z, G \frac{du_y}{dx}, G \frac{du_z}{dx} \right) = (X_i)_{i \in \llbracket 1,4 \rrbracket}. \quad (4.22)$$

Imposing $u_y(0) = 1\mu\text{m}$, $u_z(0) = \lim_{x \rightarrow +\infty} u_y(x) =$

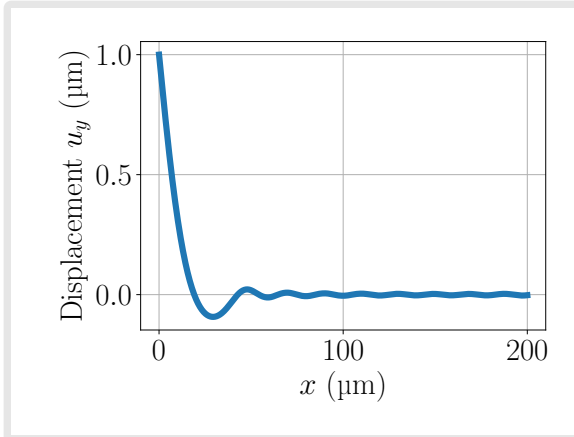


Figure 4.3: Evolution of the real part of displacement u_y as a function of the distance x from the application point of ultrasound.

$\lim_{x \rightarrow +\infty} u_z(x) = 0$ and the values of table 4.1 brings figure 4.3 for u_y and $u_z = 0$. It is blatant that the displacement at $x = 0$ is approximately totally dissipated before $x = 50 \mu\text{m}$ which corresponds approximately to the size of the zone of influence because it corresponds to five times the wavelength as illustrated on figure 4.1. After $x = 50 \mu\text{m}$, the material is globally elastic and propagates without dissipating the wave. The previous zone of influence is then recovered here.

The length of $50 \mu\text{m}$ may seem ridiculously low when considering the industrial scale of radioactive waste which can be estimated around 1 m corresponding to the size of a barrel. Also, there is the fact that temperature may increase in the sludges under the ultrasound solicitation, which is not taken into account in the previous approach. Maybe it helps to increase the length of influence but, in reality, the temperature tends to increase the loss of energy locally which implies a more abrupt decrease of the ultrasound in the material and will decrease the length of influence or, in the spirit of equation (4.17), the viscosity tends to decrease with the temperature and thus makes the length of influence decrease.

Nevertheless, there may be an interesting perspective because the current approach is completely instantaneous, taking that the material is instantaneously adapting itself to the external solicitation: there is no delay involved. It may be interesting to think about a kinetic of adaptation, recalling the previous analysis on aggregation and disaggregation. Precisely, it is obvious that breaking microscopic structure is much faster than rebuilding it due to flow or thermal motion. In this case, even if only a layer of $50 \mu\text{m}$ thick is fluidized, this gives the opportunity for the ultrasound device to dig into the material and

progress layer by layer. If the reaggregation process is slow compared to the motion of the device, a much bigger zone may be covered and allow the fluidification of an *industrial* scale portion of the material. It may be interesting to give an order of magnitude of the thermally dissipated energy in terms of evolution of temperature per unit time. Using the heat equation, the rate of temperature per unit time $\Delta T/\Delta t$ is given by

$$\frac{\Delta T}{\Delta t} = \frac{\eta \omega^2}{\rho c_p} \varepsilon^2 \quad (4.23)$$

with ε the strain due to the ultrasound. To estimate this strain, we can consider that it is equal to the amplitude of the deformation U divided by the length of influence $5L_c = 5\sqrt{\eta/\rho\omega}$. Hence, we obtain

$$\frac{\Delta T}{\Delta t} = \frac{U^2 \omega^3}{25c_p} = 0.67 \text{K/s} \quad (4.24)$$

with the values of table 4.1. It is interesting to note in equation (4.24) that there is no dependence of the rate of temperature increase on the rheological characteristics: only the characteristics of the wave and the heat capacity are needed. Furthermore, there may be two time scales to consider in this problem: the first one related to the disaggregation process and the other one for the aggregation process. As a first assumption, we can consider the former as equal to zero to stick to the instantaneous model above and use only one time scale τ for aggregation. A first approach may be to rewrite equation (4.21) as

$$\tau \frac{\partial G}{\partial t} \Theta \left(-\frac{\partial |X_3|^2 + |X_4|^2}{\partial t} \right) + G = \left(E + i\eta\omega \frac{\sqrt{|X_3|^2 + |X_4|^2}}{\sigma_c} \right) \left(1 + \frac{|X_3|^2 + |X_4|^2}{\sigma_c^2} \right)^{-1/2} \quad (4.25)$$

with Θ the Heaviside function. This equation considers that at each macroscopic time step, the material has a complex viscoelastic modulus due to the short time scale of the ultrasound: there is immediate adaptation of the material in the permanent oscillating regime. The only time dependence is due to the aggregation process of the microscopic structure.

4.4 Describing the phenomenology on radioactive sludges

Following the brief prediction developed in the previous paragraphs, it can be interesting to describe the phenomenology that may happen in the real context of radioactive sludges. Using figure 4.4, one can

apply some external solicitation like powerful ultrasound on a certain orange area on the left of figure 4.4. In the same trend as the point force resolution, in a first approximation, it can be considered that this surface of solicitation is a sum over the same surface of similar point forces which add their effects on the system. As before, these effects create a volume of influence sketched with a blue disk on figure 4.4. This volume of influence has a radius R_c which is roughly given by equation (4.17). The volume of influence size depends then, in a first approximation, only on the material characteristics and not the intensity of the solicitation. This volume of influence cuts the system in different zones each having its own rheological behaviour. For instance, inside this volume close to the source and as illustrated in figures 4.1 to 4.3, there will be a local fluidization of the material. Using also chapters 2 and 3, this fluidization comes from the strong coupling between the microstructure, the rheology and the external stress, in the sense that the high external stress will tend to disaggregate locally the clusters, which then induce an overall lower transmission of stresses, creating a softer and more fluid rheology. If we continue to get further from the source, due to the more fluid like material behind, there will be a strong dissipation of the source input energy. Hence, the overall stress intensity will decrease as illustrated on figures 4.1 and 4.3 and, referring again to chapters 2 and 3, the equilibrium size of the clusters will grow compared to those closer to the source ; the system rheology will then become more solid like than fluid like. Finally, on the other end of the system in figure 4.4, far from the source on the right, continuing the decrease of the stress intensity by the dissipation, the system reaches a quasi purely elastic behaviour due to the fact that the stress intensity is so low that it does not change the initial configuration of the microstructure and the rheology of the material coupled to it. Therefore, far from the source, the material remains approximately unaffected by the solicitation, as the localization of the fluidization may predict.

The whole previous reasoning has been given in a semi-infinite medium as described in the beginning of the chapter. If the dimensions of the macroscopic system compared to the volume of influence or solicitation zone are much larger, then this approximation holds. In the case of a more confined configuration, some adaptations need to be done but the overall principle remains in the sense that there will be a localisation of the fluidization when boundaries are far from the source or in the whole system with some detrimental effects on the experimental material (echoing, vibration, rupture, ...) if an exceeding amount of energy is not evacuated.

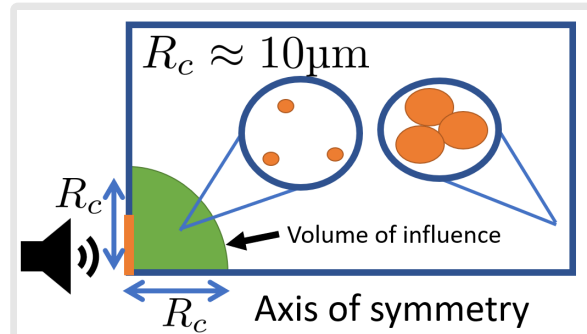


Figure 4.4: Description of the potential fluidisation process happening in the radioactive sludges

4.5 Conclusion

We have studied the application of ultrasound on materials through an analytical solution with a point force and a one dimension simulation taking into account the macroscopic-microscopic coupling. We have highlighted the existence of two regimes with a transition zone in between : a fluid-like behaviour, close to the source where the dissipation of energy is dominant, and an elastic-like behaviour, far from the source, which allows to transmit the ultrasound wave. For the purpose of the study, in order to fluidize a system through ultrasound, we identified a zone of influence which is the zone where the solicitation has a direct impact relatively to the goal searched. The characteristics of this zone depends strongly on the characteristics of the wave but not necessarily its amplitude. Hence, to understand properly the behaviour of the material is a key to predict its behaviour under an ultrasound solicitation.

Chapter 5

General conclusion and perspectives

5.1 Conclusion of the study

Several insights regarding the general case of macroscopic-microscopic couplings in suspensions of particles and, in particular, the case of sludges of radioactive waste have been presented in this manuscript.

Indeed, in [chapter 1](#), a review of the existing literature started the manuscript relating models and phenomena, bridging the gap between macroscopic solicitations and rheological laws, and changes of microscopic structure. The overall framework of continuum mechanics has been detailed to precisely focus on the perspective of rheology bringing step by step more complexity. It was an opportunity to assess the wide range of possibilities but also to point out some discussions about the selection of rheological models and their relevance in different conditions (large deformations, three dimensions, ...). Looking at the microstructure of certain materials and clusters more specifically, their influence on the rheology has been highlighted. Addressing their construction, it has helped to build up the scaling laws from the microscopic interactions to the macroscopic rheology. The reverse path was considered too to analyse clusters under external solicitation. A variety of phenomena has been unveiled to describe the interaction and some analytical descriptions of the quantitative relationship between them were listed and discussed. A final discussion related to dimensional analysis was reported to help researcher to tackle complex problems reducing the amount of variability. This relevant tool allowed to open the remaining questions in the field of colloidal suspensions and the understanding of the interplay between the microscopic structure, the rheology and the environment. Lots of models and approaches are available which rely on different kinds of arguments: mechanical, physical, geometrical or probabilistic. Assuming a certain amount of

hypothesis, these models allow the prediction of several phenomena both qualitatively and quantitatively. The specific case of colloidal suspensions is actually a very rich and broad topic of physics.

Then, in [chapter 2](#), the influence of the macroscopic environment on the microscopic structure was addressed. Specifically, a description of the competition between aggregation and disaggregation phenomena was proposed. The equilibrium between aggregating forces and disaggregating forces was pictured through an energy functional whose minimum depends on the relative importance of these two forces in a form of a power-law relationship consistent with the literature. This concept was illustrated afterwards with the interpenetration of clusters and the clusters of clusters structures in carbon black particle suspensions. Through the coupling of structural measurement with scattering experiments and rheological measurements, the evolution of the microscopic structure displaying more than the two standard sizes was in contradiction with historical frameworks but allowed to investigate the effect of external shear on clusters structure. The overall conclusion of this is the selection by the macroscopic variables of a certain microscopic size of clusters in order to better represent real systems. There is an equilibrium between aggregation forces, due to the interaction potential between the particles, and disaggregation forces, due to an external solicitation like flow, ultrasound, ...

Besides, in [chapter 3](#), the influence of the microscopic structure on a rheological response was tackled. Continuing with the interpenetrating clusters or the clusters of clusters concepts, rheological laws have been derived starting from models available in the literature. The former models were based on scaling arguments from the microscopic interactions between the particles and the macroscopic scale. Reconsidering their set of hypothesis and adding some new ingredients like a distance of interpenetration, an

additional cluster size or a fractal filling of the space for the gel network, they have been extended to account for the new available experimental data which presented some discrepancies compared to classical approaches. These extensions have a common basis that unifies them and allows to recover all the previous models developed in historical papers. These newly written models have been compared to the literature to demonstrate their relevance in recent studies and applied on carbon black particle suspensions at rest and under flow. Due to their tunable structure through external shear solicitation showed in [chapter 2](#), the rheology of carbon black particle suspensions evolves accordingly and arises from different microscopic contributions as detailed in [chapter 3](#). This coupling allowed additionally to open paths for the study of hierarchy of structures in the sense of a variation of density from larger scales to smaller scales due to an eventual shielding effect of larger scales towards the lower scales.

Finally, in [chapter 4](#), after having investigated the reciprocal relationship between the macroscopic environment, the rheology and the microscopic structure, an industrial application is tackled. An analytical description of a solution mimicking the actual industrial setup brings some insights about relevant orders of magnitudes. Then, implementing a coupled numerical case in one dimension allows to have more insights about the evolution of such problem with a strong coupling. The idea of zone of influence is relevant in both cases saying that only a local portion of the material will be fluidized and some movements are needed by the material or the external solicitation to propagate the fluidification on a larger portion of the material. The overall description of this chapter is in a linear regime hypothesis to capture the triggering of fluidification. If someone wants to completely predict the behaviour of the material, some more complex frameworks will be needed to catch large deformations, maybe turbulence, time evolution or other more complex effects. Moreover, the simplified geometry of a semi-infinite medium is an interesting but rather poor description of an actual industrial system which needs heavier tools to decently solve the actual problem.

A remarkable feature of this study is the broad range of concepts from fundamental physics to applied physics. Indeed, the starting point of the research was the need for the CEA to manage their radioactive sludges which are complex fluids coming from the treatment process of radioactive waste. The conditioning of radioactive waste is a key aspect in the nuclear industry to ensure safety and a durable use of radioactive materials to produce electricity for instance. Hence, we pulled back the framework to a

smaller amount of ingredients to understand what is the source of the problem that needs to be overcome. This is the general attitude taken by scientists, engineers or researchers to capture the roots of a problem and create solutions or tools which are suitable to the precise case. From this perspective, it was a good opportunity to tackle some theoretical models and their assumptions. Papers published decades ago were crucial sources of information to understand the current mindsets of state of the art scientists and, simultaneously, critical points displaying weaknesses or, at least, discrepancies. Working on these old framework and trying to supplement them with the latest ingredients developed or discussed currently helped to bring an interesting contribution to the colloidal suspension community. This path in fundamental physics brought us then to some ideal applications with carbon-black particle suspensions submitted to several conditions and circumstances. There was the use of several experimental techniques as rheometry and small angle X-Ray scattering. Even if this manuscript is generally related to theory and modelling, these cases of applications were an essential aspect of the construction of this work in the sense that the theoretical arguments were built and strengthened *via* the interaction with experiments and experimentalists' critics. Finally, after some work on model materials, the industrial application with applied physics was considered in order to predict some phenomena happening from the few ingredients we started with. Indeed, the complete resolution of the industrial problem was not achieved. However, the remarkable gathering of knowledge from numerous people has created an interesting contribution which may be useful for future investigations on the same topic or in a somewhat different context. Therefore, a whole spectrum has been covered in one project from fundamental science to applied science.

5.2 Perspectives

The outcomes of this study lead to broader investigations in the future. For instance, from a fundamental point of view, there is an opening for future works regarding usual models that have not been reconsidered for years. Due to new experimental techniques like Large Amplitude Oscillating Strain (LAOS), it is now interesting to build some theoretical approaches to account for the new descriptions encountered during this research. Investigations similar to the one described in [appendix B.1](#) can be very interesting to pursue in order to take into account large deformations. Furthermore, as a general comment about rheology but in particular in the case of colloidal suspension, considering non isotropic systems where three dimen-

sional effects may play a role and a proper tensor extension should be considered. For example, seminal papers like [Halphen, 1975; Saramito, 2007] where the generalised standard materials approach was developed were an excellent extension of non linear rheological laws from one dimension to tensor form through the use of energy and dissipation potentials. In the same spirit, it may be clever to summarise the scaling laws from the microscopic structure to the rheology to one ingredient which can be used to extend easily to three dimensions tensor forms. Besides, an issue which has never been addressed yet due to its subsequent complexity is the scaling laws for the viscous contribution. More precisely, in [Shih, 1990; Mellema, 2002; Wu, 2001], all the construction has been done to extrapolate the microscopic particle pair interaction to the macroscopic elasticity. From a theoretical point of view, the only source of dissipation in this framework is the viscous solvent. Hence, how is it possible to extrapolate the local viscous dissipation of a particle to the macroscopic scale of the gel to get, for example, an expression for the loss moduli G'' can be a huge achievement to complete the modelling. In general, there may be two ways of sophistication of all the current work: either a more precise and robust description of the microscopic interactions and structure is developed to scale more precisely the rheological laws, or, a generalised 3D form of all the previous laws with thermodynamic roots is produced to bridge completely the gap between theory and experiments. This affirmation can be complemented by the fact that assumptions should be addressed in order to understand the limits of the current models and propose new frameworks of understanding.

To give an inspiring perspective, remaining in the field of suspensions but in biological gels, [Storm, 2005] succeeded to demonstrate a universal behaviour through the use of very simple ingredients of bending rods. This type of master curve is very admirable due to its simplicity in the conception and in the communication. This should be perhaps one of the goals for future investigations in order to gather all knowledge on colloidal suspensions. In our case for instance, in figure 2.11(c), there was the opportunity to compare on the same level the particle volume fraction and the shear rate in the sense that the storage modulus is a direct competition between the amount of particle, with their relative strength of interaction, and the strength of the external shear applied. As already mentioned, the work presented in [Halphen, 1975] is substantially inspiring due to its purity and the generalisation of lots of existing behaviours, materials and systems. Another paper that has helped a lot and is still very relevant in the approach is [Kolmogorov, 1991]. The description of turbulence was detailed for

the first time in this paper and launched a huge part of fluid mechanics. The simplicity of the arguments and the demonstration, as enhanced hopefully in this manuscript, is a key feature to understand a really complex problem. The line of descent which arose after the publication continued on the same perspective making it progressively very robust and a source of creation of new tools like numerical modelling of turbulence such as Reynolds Average Navier-Stokes (RANS), Large Eddy Simulation (LES) or other numerous simulation tools. Precisely, turbulence still remains, like complex fluids, a difficult problems to solve. Nevertheless, some crucial landmarks were set like [Kolmogorov, 1991] and opened a wide paths helping many scientists to dig further those issues.

On a more practical point of view, this PhD is an ignition of a larger project involving an experimental approach, hoping that the present work will help to interpret the future results of both experimental study and the industrial process, and an industrial application for CEA radioactive waste management. It is one of the most important aspects of the nuclear industry, and the source of the most frequent critics. How to ensure the safety of the population and of nature while warehousing or storing geologically the radioactive waste is a big challenge. It is not certain if nuclear power should remain a main source of energy in France, however, the already produced waste should be managed properly.

Appendices

Appendix **A**

Interpenetration of clusters for **chapter 2** and according to [Dagès, 2022]

Objectives

This chapter is a compilation of useful details and data presented in **chapter 2**.

Objectifs

Ce chapitre est une compilation de détails et de données utiles présentés dans **chapter 2**.

Contents

A.1	Carbon black particles	83
A.2	Flow properties of Carbon black gels	84
A.3	Evolution of the viscoelastic moduli during rest	84
A.4	$\tan(\delta)$ representation of the viscoelastic spectrum	85
A.5	Model for the normalized viscoelastic spectrum of carbon black gels	85
A.6	Influence of the concentration c_w	86
A.7	Analysis of the rheo-SAXS data	87

A.1 Carbon black particles

Figure A.1 shows the scattering intensity vs. wave vector q for a dilute dispersion of CB particles (Vulcan PF, Cabot). Individual CB particles are fractal-like particles composed of fused nanoparticles of carbon [Martinez, 2017; Sztucki, 2007], which motivates the use of a mass fractal model [Teixeira, 1988] to fit $I(q)$. The fit yields a radius of gyration $r_g = 35$ nm with 20% polydispersity and a fractal dimension $d_{f0} = 2.9$. Density measurements of CB powder were performed by helium pycnometer (AccuPyc II 1340, Micromeritics). Before the measurements, the powder was dried in an oven at 80°C during 72 hours (2 % in weight was lost). Two sets of measurements were done with 5 measurements in a row for the first sample ($m = 0.8619$ g) and 10 measurements in a row for the second sample ($m = 0.779$ g). The samples were poured in a 10 cm³ aluminum vessel. We obtained a density of the carbon black particles $d_{cb} = 2.26 \pm 0.03$.



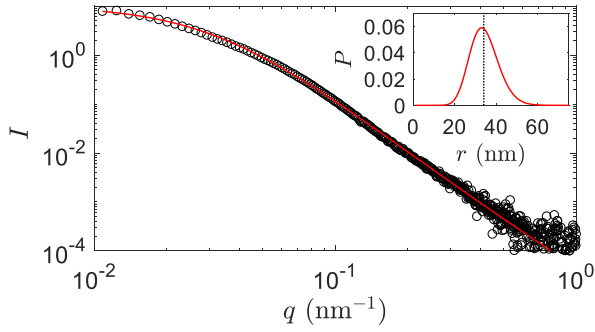


Figure A.1: Scattering intensity I vs. scattering wave number q of dilute dispersion of carbon black Vulcan PF nanoparticles in the RTM17 mineral oil ($c_w = 0.01\%$). The red line is a mass fractal fit of such a form factor using a fractal dimension $d_{f0} = 2.9$ and a Schulz particle radius distribution $P(r)$ centered on a radius of gyration $r_g = 35$ nm (dashed line) with a polydispersity of 20 % as shown in the inset.

A.2 Flow properties of Carbon black gels

Figure A.2 reports the flow curve $\sigma(\dot{\gamma})$ of a $c_w = 4\%$ CB dispersion obtained by a decreasing ramp of shear rate. The flow curve is fitted with a Herschel-Bulkley model, $\sigma = \sigma_y + K\dot{\gamma}^n$, and yields a dynamical yield stress $\sigma_y = 4.5$ Pa, a fluidity index $n = 0.83$, and a consistency index $K = 1.0$ Pa.s^{1/0.83}.

In figure A.2, we also show flow curve extracted from the preshear at $\dot{\gamma}_0$. We observe that those flow curve are not stationary. This is mostly due to the fact that the dispersion needs time to adapt from the jump in shear from 1000 s⁻¹ to $\dot{\gamma}_0$.

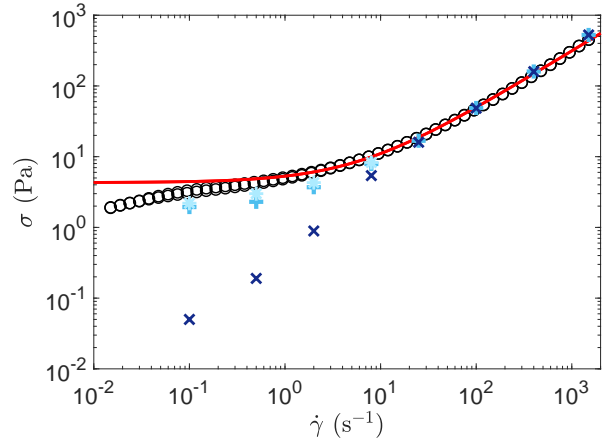


Figure A.2: Flow curve of the carbon black dispersion at $c_w = 4\%$ showing the evolution of the measured stress σ as a function of the imposed shear rate $\dot{\gamma}$. $\dot{\gamma}$ is ramped down then up between 1500 s⁻¹ to 0.015 s⁻¹ with 10 points per decades at a rate of one point every 1 s. The red line is an Herschel-Bulkley fit. Unstationary flow curve extracted from the preshear at $\dot{\gamma}_0$ in figure 2.9b at $t = 1$ s (\times), at the maximum of σ ($+$) and at the end of the protocol ($*$).

A.3 Evolution of the viscoelastic moduli during rest

During the rest period that follows the flow cessation protocol, we measured the viscoelastic moduli of the dispersion in its linear regime, figure A.3. For high $\dot{\gamma}_0$ the gel reach within ~ 100 s a regime where aging becomes very slow. For low $\dot{\gamma}_0$ this slow aging regime is reached within a few seconds.

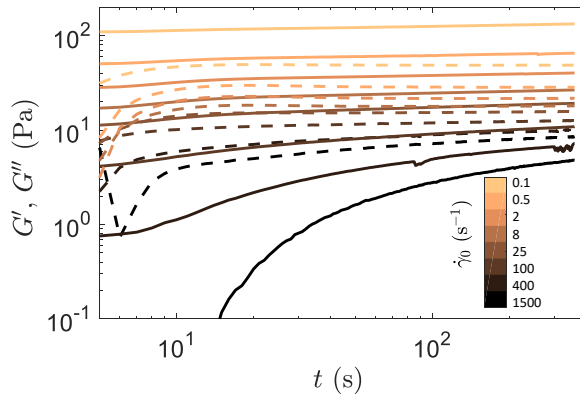


Figure A.3: Evolution of the viscoelastic moduli during the rest just after the flow cessation protocol. The viscoelastic moduli G' (line) and G'' (dash) are measured during 360 s at an oscillation amplitude of $\gamma = 0.1\%$ and a frequency of $f = 1$ Hz.

A.4 $\tan(\delta)$ representation of the viscoelastic spectrum

Alternatively, the viscoelastic spectrums plotted in [figure 2.10a](#) may be represented by $\tan(\delta) = G''/G'$ as a function of the frequency f , [figure A.4a](#). In this representation, $\tan(\delta) > 1$ indicates that dissipation dominates the rheological behavior whereas $\tan(\delta) < 1$ indicates a solid-like behavior at the corresponding frequency. In [figure 2.10b](#), the viscoelastic spectrum is rescaled according to the coordinate (f_c, G_c) . In the $\tan(\delta)$ representation as G' and G'' are rescaled by the same factor G_c only the frequency axis needs to be rescaled. Doing so the $\tan(\delta)$ measured for different $\dot{\gamma}_0$ scale on a master curve as displayed in [figure A.4b](#).

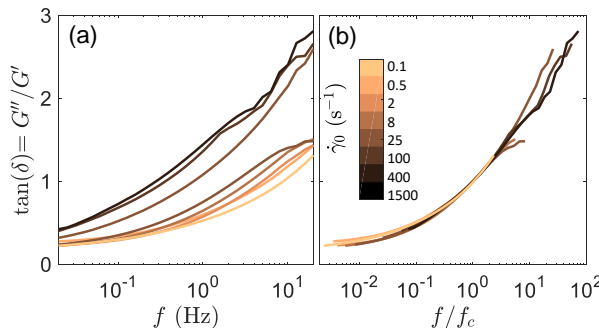


Figure A.4: $\tan(\delta)$ representation of the viscoelastic spectrum measured in [figure 2.10a-b](#). (a) $\tan(\delta)$ as a function of the frequency f . (b) $\tan(\delta)$ as a function of the normalized frequency f/f_c .

A.5 Model for the normalized viscoelastic spectrum of carbon black gels

The master curve reported in [figure 2.12](#) is fitted using a Kelvin-Voigt model and a fractional Kelvin-Voigt model [Schiessel, 1995b], as illustrated in [figure A.5](#). The fractional Kelvin-Voigt model consists of two springpots in parallel, defined by their quasi-properties (\mathbb{V}, \mathbb{E}) and their dimensionless exponents (α, β) . Each springpot can be understood as a mechanical element having intermediate properties between that of a spring when its exponent is 0 and a dashpot when its exponent is 1. The resolution of the fractional Kelvin-Voigt model leads to

$$\begin{cases} G' = \mathbb{E}f^\beta \cos(\beta\pi/2) + \mathbb{V}f^\alpha \cos(\alpha\pi/2) \\ G'' = \mathbb{E}f^\beta \sin(\beta\pi/2) + \mathbb{V}f^\alpha \sin(\alpha\pi/2) \end{cases} \quad (\text{A.1})$$

In the limit where $\alpha = 1$ and $\beta = 0$ we recover the classical Kelvin-Voigt model, which is defined by a dashpot of viscosity η in parallel with a spring of elasticity G_∞ .

$$\begin{cases} G' = \mathbb{E} = G_\infty \\ G'' = \mathbb{V}f = 2\pi\eta f \end{cases} \quad (\text{A.2})$$

As shown in [figure A.5](#) the fractional model fits relatively well the normalized viscoelastic spectrum of carbon black gels in mineral oil using $(\mathbb{V}/G_c = 0.56, \alpha = 0.91)$ and $(\mathbb{E}/G_c = 1.09, \beta = 0.11)$. Its classical counterpart can only capture the asymptotic behavior of the viscoelastic spectrum, i.e., the network elasticity $G_\infty = G'(f \ll f_c)$ and the background viscosity $\eta = G''(f \gg f_c)/(2\pi f)$. We note that $G_\infty = 0.3G_c$.

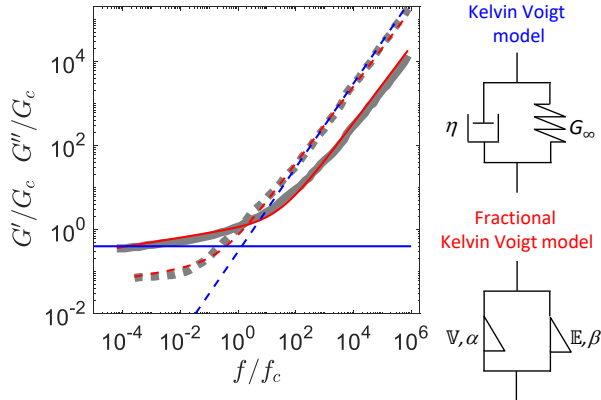


Figure A.5: Model of the normalized viscoelastic spectrum. Evolution of the normalized elastic G'/G_c (grey line) and viscous G''/G_c (dashed grey line) moduli as a function of the frequency f/f_c , extracted from [Trappe, 2000]. (f_c, G_c) are the coordinates of the crossover between G' and G'' . The Kelvin-Voigt model is pictured in blue and the fractional Kelvin-Voigt model in red.

A.6 Influence of the concentration c_w

Following the protocol displayed in figure 2.8 we test the influence of the concentration for $c_w = 2, 3, 6$ and 8% in addition to $c_w = 4\%$. Such concentration series are presented in figure A.6 for $\dot{\gamma}_0 = 1500 \text{ s}^{-1}$. We observe that high concentrations shift the viscoelastic spectrum to higher elasticities. The cross over point is not always reachable within the frequency window. We scale the viscoelastic spectrum G', G'' on the master curve displayed in Fig. figure 2.10b to determine (f_c, G_c) and plot the results in figure 2.11.

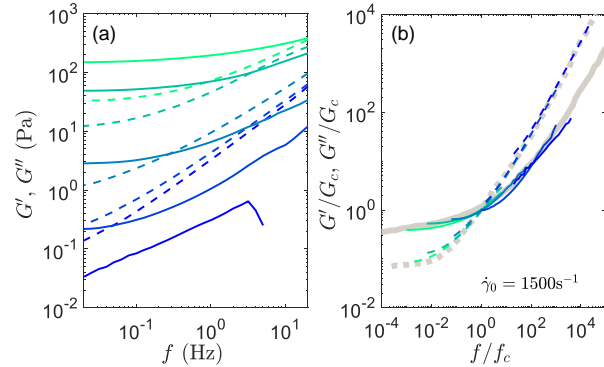


Figure A.6: Evolution of the viscoelastic spectrum for different gel concentration c_w at $\dot{\gamma}_0 = 1500 \text{ s}^{-1}$. (a) G' (line) and G'' (dash) as a function of f . The concentration is varied from $c_w = 2$ (blue) to 8% (green). (b) Rescaled viscoelastic spectrum. The grey curves are taken from [Trappe, 2000] and corresponds to the master curve obtained by scaling a concentration series of carbon black dispersion in oil.

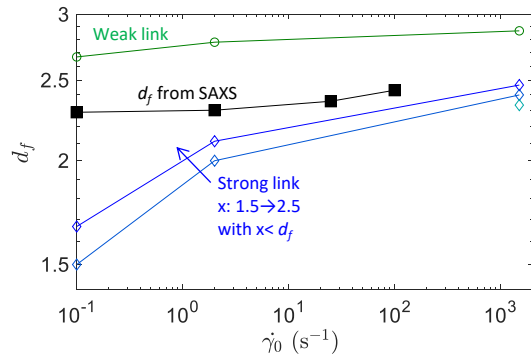


Figure A.7: Fractal dimension d_f as a function of the shear step $\dot{\gamma}_0$. Measurements of d_f extracted from the SAXS fits in figure 2.12 (square) and evaluated from figure 2.11 using the weak link model (circle) and the strong link model (diamond) from [Shih, 1990]. The fractal dimension x of the gel backbone has been varied from $x=1.5$ (light blue) to $x=2.5$ (dark blue) in the strong link model.

A.7 Analysis of the rheo-SAXS data

The CB gel scattered intensities $I_{rad}(q)$ and $I_{tan}(q)$ are respectively measured in the radial and the tangential configuration. In the radial configuration, the X-ray beam probes the microstructure in the flow-vorticity plane, while in the tangential configuration, the X-ray beam probes the sample along velocity gradient-vorticity plane as sketched in figure A.8. After the rest step in the protocol from figure 2.8, the radial and tangential scattered intensities are compared. More precisely the radial scattering I_{rad} is decomposed in its perpendicular $I_{rad\perp}$ and parallel $I_{rad\parallel}$ components. In figure A.8, we observe that $I_{tan} = I_{rad\perp} = I_{rad\parallel}$. The scattering intensity is isotropic and equal in all configurations. For better statistics, we focus on the tangential signal and radially average its 2D spectrum. In the paper, we note $I(q) = I_{tan}(q)$.

The intensity scattered by the carbon black is fitted in log scale using a modified Beaucage model [Beaucage, 1995; Beaucage, 1996; Keshavarz, 2021], figure A.9:

$$I(q) = \underbrace{\left[G_1 \exp\left(-\frac{q^2 r_1^2}{3}\right) + B_1 \exp\left(-\frac{q^2 r_2^2}{3}\right) q_1^{*p_1} \right]}_{\text{Beaucage, Cluster level, } I_1} \underbrace{\left[1 + C_0 \left(\left(\frac{q}{q_s}\right)^2 + \left(\frac{q_s}{q}\right)^2 \right)^{-1} \right]}_{\text{Inter-Cluster structure, } S_1} \underbrace{\left[G_2 \exp\left(-\frac{q^2 r_2^2}{3}\right) + B_2 q_2^{*p_2} \right]}_{\text{Beaucage, CB particle level, } I_2},$$

with $q_{i=1,2}^* = \text{qerf}\left(\frac{qr_i}{\sqrt{6}}\right)^{-3}$. (A.3)

In equation (A.3), $I_2(q)$ refers to scattering due to the CB particle of size $r_0 = r_2$ and fractal dimension $d_f = -p_2$. The scattering due to the clusters of size

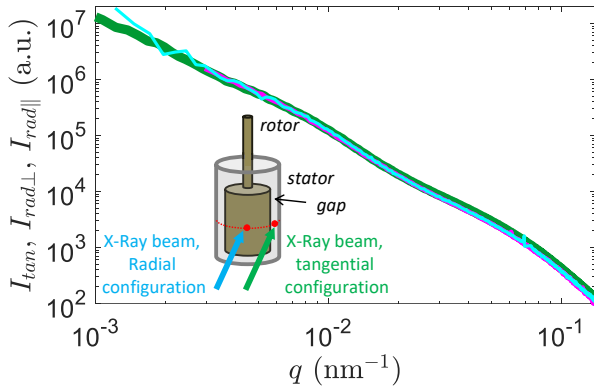


Figure A.8: Comparison of the scattering intensity between the tangential I_{tan} (green) and radial $I_{rad\perp}$ (cyan) $I_{rad\parallel}$ (magenta) configuration.

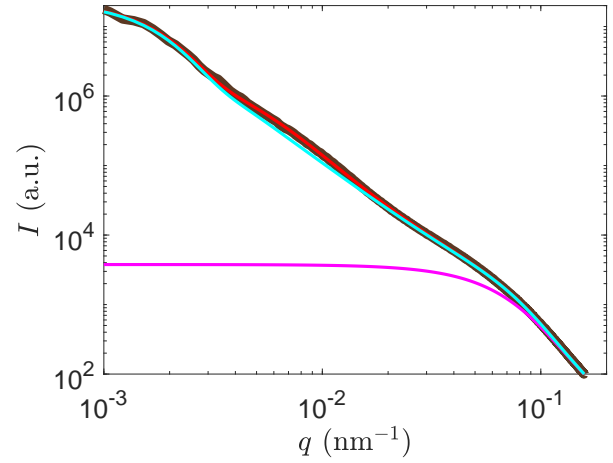


Figure A.9: Decomposition of the modified Beaucage model as written in equation (A.3). Scattering intensity $I(q)$ as a function of q : experimental data (black), I_2 (pink), $I_1 + I_2$ (cyan), $I_1.S_1 + I_2$ (red).

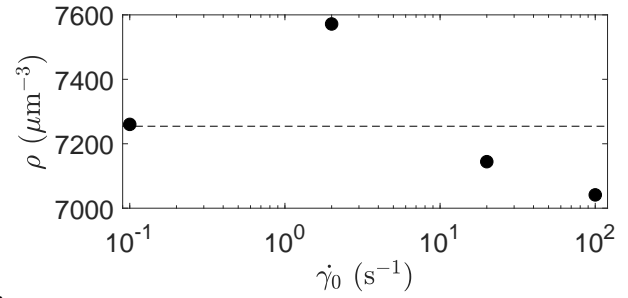


Figure A.10: Density of particles per unit cell ρ as the function of the step shear $\dot{\gamma}_0$. ρ is calculated from the values r_0 , ξ_c , d_f and ξ_s obtained fitting the scattering intensity $I(q)$ plotted in figure 2.12a with equation (A.3). The dash line is the average.

$\xi_c = r_1$ and fractal dimension $d_f = -p_1$ is contained in the term $I_1(q)$. The modification of the two level Beaucage model consists in introducing an inter cluster structure factor $S_1(q)$ that accounts for the center-to-center distance between adjacent clusters, $\xi_s = 2\pi/q_s$. $S_1(q)$ is a function that peaks at q_s to a maximum value $S_1(q_s) = 1 + C_0/2$ and that converges to 1 away from q_s .

This fit is constrained by mass conservation. Indeed, as the multi-stable gels result from the same carbon black dispersion, all the gels have the exact same average number of particles at the macroscopic scale and in their unit cell. The unit cell is the minimum structural repeating unit necessary to construct the gel. In our case, the gel network unit cell is defined by the structural length ξ_s . The number of particles $N = (\xi_c/r_0)^{d_f}$ in a unit cell corresponds to the number of particles in the cluster of size ξ_c and fractal dimension d_f . This gives a particle density $\rho = \frac{(\xi_c/r_0)^{d_f}}{\xi_s^3} = cste$. This

constrain is well verified based on parameters obtained by fitting the SAXS data. As shown in figure A.10, $\rho = 7250 \pm 230$ particles/ μm^3 is constant within a margin of error of 3%. Moreover, ρ can be related to the particle concentration c_w provided a good knowledge of the background oil density $d_{\text{bck}} = 0.871$ ($T = 20^\circ\text{C}$), the individual carbon black particle density $d_{\text{cb}} = 2.26 \pm 0.03$ ($T = 20^\circ\text{C}$) and the volume of a carbon black particle v_{cb} . The carbon black density ρ in the gel is then

$$\rho = \frac{\phi}{v_{\text{cb}}}, \quad (\text{A.4})$$

$$\phi = c_w \left(c_w + \frac{d_{\text{cb}}}{d_{\text{bck}}} (1 - c_w) \right)^{-1}. \quad (\text{A.5})$$

As it is hard to measure v_{cb} given the particle fractal nature, v_{cb} was evaluated from ρ . Using $v_{\text{cb}} = 4/3\pi r_\rho^3$ we obtain $r_\rho = 8.1$ nm a value lower than the radius of gyration of 35 nm extracted from the form factor measured in SAXS (figure A.1). This value is a bit smaller because the CB particles are fractal and polydisperse. Moreover, SAXS measurements tend to overestimate the particle size distribution as SAXS is more sensitive to larger particles. Finally, we might overestimate ρ as we assumed that the clusters pack the space homogeneously. Despite the fact that r_ρ is a bit small, we find $\rho = c_{ste}$ which tells us that the model is self-consistent.

Appendix **B**

Other tools to develop and perspectives for future work

Objectives

This chapter is a compilation of previous works that are not completed yet but can be interesting to convey the broad perspective I worked on during my PhD and useful tool for this topic.

Objectifs

Ce chapitre est une compilation de travaux antérieurs qui ne sont pas encore achevés mais qui peuvent être intéressants pour transmettre la large perspective sur laquelle j'ai travaillé au cours de mon doctorat et constituer un outil utile pour ce sujet.

Contents

B.1	Extension of Sequence of Physical Processes relating the second Piola-Kirchhoff stress tensor to the Green-Lagrange strain tensor	89
B.1.1	Derivation of the extension	89
B.1.2	Application	91
B.2	Multi-phase problem : Level-Set methods	95
B.2.1	Abstract	95
B.2.2	Introduction	95
B.2.3	Level-Set methods	95
B.2.4	Other relevant tools for the Level-Set method	96
B.2.5	Application cases	97
B.3	Use of the canonical framework for the aggregation-disaggregation formulation	97

B.1 Extension of Sequence of Physical Processes relating the second Piola-Kirchhoff stress tensor to the Green-Lagrange strain tensor

B.1.1 Derivation of the extension

To recall the usual sequence of Physical Processes presented in [Rogers, 2017; Donley, 2019; Rogers, 2011; Rogers, 2012b; Rogers, 2012a], via the Frénet-Serret apparatus, it is possible to find a transient viscoelastic modulus G_t relating the shear stress σ to the shear strain ε and the shear strain rate $\dot{\varepsilon}$. The whole demonstration relies on the fact that there is a linear relationship in the frequency domain between the stress tensor σ and the strain tensor ε of the form $\sigma = \mathbb{C}\varepsilon$ with \mathbb{C} a fourth order tensor gathering the material properties. Acknowledging the power of such tools, it is relevant to question the validity of these last assumptions. For instance, when increasing the amplitude of the oscillation of the shear strain, rheological non-linearities may appear as well as geometrical non-linearities. Then, it may be interesting to decorrelate both previous effects to study only the rheological non-linearities. Such a framework exists in continuum mechanics and is related to hyperelastic materials. Precisely, the Cauchy stress tensor σ and the linear strain tensor ε are properly defined in the deformed configuration of a material. When the latter undergoes large deformation, the deformed configuration becomes pretty different from the reference configuration. Therefore, it is possible to create two quantities that are defined in the reference configuration and allow to connect stresses and deformations: namely, the second Piola-Kirchhoff stress tensor S and the Green-Lagrange strain tensor e . To recall the construction of such quantities,

the transformation from the reference configuration to the deformed configuration is determined by the deformation gradient of the displacement \mathbf{F} . Using some differential transformation of distances, areas and volumes, the deformations from the reference configuration are properly measured by the Green-Lagrange strain tensor defined by

$$\mathbf{e} = \frac{1}{2} (\mathbf{F}^T \mathbf{F} - \mathbf{I}) \quad (\text{B.1})$$

with \cdot^T the transpose of a tensor and \mathbf{I} the identity tensor. Simultaneously, the forces in the deformed configuration acting on areas in the deformed configuration are given by the Cauchy stress tensor $\boldsymbol{\sigma}$ and can be pulled back to forces in the reference configuration acting on areas in the reference configuration through the second Piola-Kirchhoff stress tensor \mathbf{S} defined by

$$\mathbf{S} = J \mathbf{F}^{-1} \boldsymbol{\sigma} \mathbf{F}^{-T} \quad (\text{B.2})$$

with $J = \det(\mathbf{F})$. In the case of small deformation, $J \approx 1$, $\mathbf{F} \approx \mathbf{I} + \nabla \mathbf{u}$ with \mathbf{u} the displacement thus the Green-Lagrange strain tensor \mathbf{e} is equal to the usual linear strain tensor $\boldsymbol{\varepsilon}$ and the second Piola-Kirchhoff stress tensor \mathbf{S} is equal to the usual Cauchy stress tensor $\boldsymbol{\sigma}$. However, in the case of large transformations, the Green-Lagrange strain tensor and the second Piola-Kirchhoff stress tensor account for rotations and large deformations. Relating ourselves to the hyperelastic materials framework, it can be demonstrated that the second Piola-Kirchhoff stress tensor and the Green-Lagrange strain tensor are energy conjugates meaning that a rheological law involving an expression of \mathbf{S} as a function of \mathbf{e} or its derivatives is objective and properly defined. In addition, it can be demonstrated [Le Tallec, 2019] that the mechanical energy per unit volume in the reference configuration due to the material is equal to $\mathbf{S} : \dot{\mathbf{e}}$ with $:$ the double contracted product and $(\dot{\cdot})$ for the time derivative. Therefore, in the Fourier domain, it is straightforward to consider, as a first approach, that it exists a complex fourth order tensor \mathbb{H} reading $\mathbf{S} = \mathbb{H} \mathbf{e}$.

Now with these previous remarks, it is possible to extend the usual Sequence of Physical Processes method. In this framework, an imposed oscillatory shear strain $\varepsilon = \varepsilon_0 \sin(\omega t)$ with ε_0 the shear strain amplitude and ω the pulsation drives the deformation of the material. Assuming that the shear strain is imposed in the xy plane in cartesian coordinates and using the definition of the deformation gradient \mathbf{F} and equations (B.1) and (B.2), one gets

$$\mathbf{F} = \mathbf{I} + \varepsilon \mathbf{e}_x \otimes \mathbf{e}_y \quad (\text{B.3})$$

$$\mathbf{S} = \boldsymbol{\sigma} - \varepsilon \begin{pmatrix} 2\sigma_{xy} - \varepsilon\sigma_{yy} & \sigma_{yy} & \sigma_{yz} \\ \sigma_{yy} & 0 & 0 \\ \sigma_{yz} & 0 & 0 \end{pmatrix} \quad (\text{B.4})$$

$$2\mathbf{e} = \varepsilon (\mathbf{e}_x \otimes \mathbf{e}_y + \mathbf{e}_y \otimes \mathbf{e}_x) + \varepsilon^2 \mathbf{e}_y \otimes \mathbf{e}_y. \quad (\text{B.5})$$

Hence, while in the usual Sequence of Physical Processes, one can write $\boldsymbol{\sigma} = G' \boldsymbol{\varepsilon} + G'' \dot{\boldsymbol{\varepsilon}}/\omega$ with $\dot{\boldsymbol{\varepsilon}}$ the shear strain rate, here one gets

$$S = G' \varepsilon + G'' \frac{\dot{\varepsilon}}{\omega} + H' \varepsilon^2 + H'' \frac{2\varepsilon \dot{\varepsilon}}{\omega} \quad (\text{B.6})$$

with S any components of \mathbf{S} and G', G'', H', H'' the various moduli of the rheological law which are going to be extended in instantaneous values. To build these instantaneous values, instead of considering a three dimensions space with a position vector $\mathbf{x} = (\varepsilon, \dot{\varepsilon}/\omega, \sigma)$, lets consider a position vector $\mathbf{x} = (\varepsilon, \dot{\varepsilon}/\omega, \varepsilon^2, 2\varepsilon\dot{\varepsilon}/\omega, S)$ and lets try to build a Frénet-Serret apparatus on this five dimensions space. Following the Gram-Schmidt procedure for the vector family $(\mathbf{d}_t^j \mathbf{x})_{j \in \llbracket 1,5 \rrbracket}$, we define a family $(\mathbf{e}_i)_{i \in \llbracket 1,5 \rrbracket}$ of orthonormal vectors constructing the local instantaneous coordinate system following, for all $j \in \llbracket 2, 4 \rrbracket$,

$$\mathbf{e}_1 = \frac{d\mathbf{x}}{dt} \left\| \frac{d\mathbf{x}}{dt} \right\|^{-1} \quad (\text{B.7})$$

$$\bar{\mathbf{e}}_j = \frac{d^j \mathbf{x}}{dt^j} - \sum_{i=1}^{j-1} \left(\frac{d^j \mathbf{x}}{dt^j} \cdot \mathbf{e}_i \right) \mathbf{e}_i \quad (\text{B.8})$$

$$\mathbf{e}_j = \frac{\bar{\mathbf{e}}_j}{\|\bar{\mathbf{e}}_j\|} \quad (\text{B.9})$$

$$\mathbf{e}_5 = \mathbf{e}_1 \times \mathbf{e}_2 \times \mathbf{e}_3 \times \mathbf{e}_4. \quad (\text{B.10})$$

Following the demonstration in [Rogers, 2017; Donley, 2019], one can find at the end

$$\begin{pmatrix} G'_t \\ G''_t \\ H'_t \\ H''_t \end{pmatrix} = -\frac{1}{e_5^S} \begin{pmatrix} e_5^\varepsilon \\ e_5^{\dot{\varepsilon}/\omega} \\ e_5^{\varepsilon^2} \\ e_5^{2\varepsilon\dot{\varepsilon}/\omega} \end{pmatrix} \quad (\text{B.11})$$

with e_5^i where $i \in \{\varepsilon, \dot{\varepsilon}/\omega, \varepsilon^2, 2\varepsilon\dot{\varepsilon}/\omega, S\}$ is the component on the axis i in the 5 dimensions space of the vector \mathbf{e}_5 . If someone wants to completely write the expressions of G', G'', H', H'' as a function of $(\varepsilon, \dot{\varepsilon}/\omega, \varepsilon^2, 2\varepsilon\dot{\varepsilon}/\omega)$, one gets by conservation of the generated vector spaces in the Gram-Schmidt process,

$$\bar{\mathbf{e}}_5 = \frac{d\mathbf{x}}{dt} \times \frac{d^2 \mathbf{x}}{dt^2} \times \frac{d^3 \mathbf{x}}{dt^3} \times \frac{d^4 \mathbf{x}}{dt^4} \quad (\text{B.12})$$

Using the dot notation for the time derivatives, one gets

$$DG'_t = - \begin{vmatrix} \dot{x}_2 & \dot{x}_3 & \dot{x}_4 & \dot{x}_5 \\ \ddot{x}_2 & \ddot{x}_3 & \ddot{x}_4 & \ddot{x}_5 \\ \dddot{x}_2 & \dddot{x}_3 & \dddot{x}_4 & \dddot{x}_5 \\ \ddddot{x}_2 & \ddddot{x}_3 & \ddddot{x}_4 & \ddddot{x}_5 \end{vmatrix} \quad (\text{B.13})$$

$$DG_t'' = \begin{vmatrix} \dot{x}_1 & \dot{x}_3 & \dot{x}_4 & \dot{x}_5 \\ \ddot{x}_1 & \ddot{x}_3 & \ddot{x}_4 & \ddot{x}_5 \\ \dddot{x}_1 & \dddot{x}_3 & \dddot{x}_4 & \dddot{x}_5 \\ \ddddot{x}_1 & \ddddot{x}_3 & \ddddot{x}_4 & \ddddot{x}_5 \end{vmatrix} \quad (\text{B.14})$$

$$DH_t' = - \begin{vmatrix} \dot{x}_1 & \dot{x}_2 & \dot{x}_4 & \dot{x}_5 \\ \ddot{x}_1 & \ddot{x}_2 & \ddot{x}_4 & \ddot{x}_5 \\ \dddot{x}_1 & \dddot{x}_2 & \dddot{x}_4 & \dddot{x}_5 \\ \ddddot{x}_1 & \ddddot{x}_2 & \ddddot{x}_4 & \ddddot{x}_5 \end{vmatrix} \quad (\text{B.15})$$

$$DH_t'' = \begin{vmatrix} \dot{x}_1 & \dot{x}_2 & \dot{x}_3 & \dot{x}_5 \\ \ddot{x}_1 & \ddot{x}_2 & \ddot{x}_3 & \ddot{x}_5 \\ \dddot{x}_1 & \dddot{x}_2 & \dddot{x}_3 & \dddot{x}_5 \\ \ddddot{x}_1 & \ddddot{x}_2 & \ddddot{x}_3 & \ddddot{x}_5 \end{vmatrix} \quad (\text{B.16})$$

$$D = \begin{vmatrix} \dot{x}_1 & \dot{x}_2 & \dot{x}_3 & \dot{x}_4 \\ \ddot{x}_1 & \ddot{x}_2 & \ddot{x}_3 & \ddot{x}_4 \\ \dddot{x}_1 & \dddot{x}_2 & \dddot{x}_3 & \dddot{x}_4 \\ \ddddot{x}_1 & \ddddot{x}_2 & \ddddot{x}_3 & \ddddot{x}_4 \end{vmatrix}. \quad (\text{B.17})$$

It is interesting to note that the whole derivation above is also valid in a stress controlled framework where we replace the position vector $\mathbf{x} = (\varepsilon, \dot{\varepsilon}/\omega, \varepsilon^2, 2\dot{\varepsilon}\varepsilon/\omega, S)$ by $\mathbf{x} = (S_{xy}, \dot{S}_{xy}/\omega, S_{xx}, \dot{S}_{xx}/\omega, \vartheta)$ with $\vartheta \in \{\varepsilon, \varepsilon^2\}$ to get the equivalent of compliances J_t', J_t'' in large transformations that we can call J_t', J_t'', K_t' and K_t'' .

B.1.2 Application

B.1.2.1 Maxwell model

Let us consider a Maxwell model

$$\mathbf{S} + \lambda \dot{\mathbf{S}} = 2\eta \dot{\boldsymbol{\varepsilon}}. \quad (\text{B.18})$$

The equations are then

$$S_{xx} + \lambda \dot{S}_{xx} = 0, \quad (\text{B.19})$$

$$S_{xy} + \lambda \dot{S}_{xy} = \eta \dot{\varepsilon}, \quad (\text{B.20})$$

$$S_{xz} + \lambda \dot{S}_{xz} = 0, \quad (\text{B.21})$$

$$S_{yy} + \lambda \dot{S}_{yy} = 2\eta \dot{\varepsilon} \varepsilon, \quad (\text{B.22})$$

$$S_{yz} + \lambda \dot{S}_{yz} = 0, \quad (\text{B.23})$$

$$S_{zz} + \lambda \dot{S}_{zz} = 0. \quad (\text{B.24})$$

Assuming that $\mathbf{S}(0) = \mathbf{0}$, one solves to get $S_{zz} = S_{xz} = S_{yz} = S_{xx} = 0$ and

$$S_{yy}(t) = 2\frac{\eta}{\lambda} e^{-t/\lambda} \int_0^t e^{s/\lambda} \dot{\varepsilon}(s) \varepsilon(s) ds, \quad (\text{B.25})$$

$$S_{xy}(t) = \frac{\eta}{\lambda} e^{-t/\lambda} \int_0^t e^{s/\lambda} \dot{\varepsilon}(s) ds. \quad (\text{B.26})$$

If one assumes additionally that for all $t \in \mathbb{R}_+$, $\varepsilon(t) = \varepsilon_0 \sin(\omega t)$ with ω a certain pulsation, one gets

$$S_{yy}(t) = \eta\omega\varepsilon_0^2 \frac{\sin(2\omega t) - 2\lambda\omega \cos(2\omega t) + 2\lambda\omega e^{-t/\lambda}}{1 + (2\lambda\omega)^2}, \quad (\text{B.27})$$

$$S_{xy}(t) = \eta\omega\varepsilon_0 \frac{\lambda\omega \sin(\omega t) + \cos(\omega t) - e^{-t/\lambda}}{1 + (\lambda\omega)^2}. \quad (\text{B.28})$$

What can be interesting is to look at the permanent oscillatory regime when $t \rightarrow +\infty$, which reads

$$S_{yy}(t) = \eta\omega\varepsilon_0^2 \frac{\sin(2\omega t) - 2\lambda\omega \cos(2\omega t)}{1 + (2\lambda\omega)^2}, \quad (\text{B.29})$$

$$S_{xy}(t) = \eta\omega\varepsilon_0 \frac{\lambda\omega \sin(\omega t) + \cos(\omega t)}{1 + (\lambda\omega)^2}. \quad (\text{B.30})$$

It is blatant that $S_{yy} \propto \varepsilon_0^2$ and $S_{xy} \propto \varepsilon_0$, thus, when $\varepsilon_0 \rightarrow 0$, S_{yy} will become negligible compared to S_{xy} , which is the usual case with small oscillatory shear knowing also that, in this limit, $\sigma_{xy} \approx S_{xy}$. Analysing equations (B.29) and (B.30), we recover the usual solution for the shear component S_{xy} replacing \mathbf{S} by $\boldsymbol{\sigma}$ in equation (B.18), however, there is an axial component S_{yy} which oscillates with a double frequency 2ω compared to the original strain oscillation.

Now if we come back to the Cauchy stress tensor, one gets

$$\boldsymbol{\sigma} = \mathbf{S} + \varepsilon \begin{pmatrix} 2S_{xy} + \varepsilon S_{yy} & S_{yy} & S_{yz} \\ S_{yy} & 0 & 0 \\ S_{yz} & 0 & 0 \end{pmatrix} \quad (\text{B.31})$$

which gives, components by components,

$$\sigma_{xx} = 2\varepsilon S_{xy} + \varepsilon^2 S_{yy}, \quad (\text{B.32})$$

$$\sigma_{xy} = S_{xy} + \varepsilon S_{yy}, \quad (\text{B.33})$$

$$\sigma_{yy} = S_{yy}, \quad (\text{B.34})$$

$$\sigma_{xz} = \sigma_{yz} = \sigma_{zz} = 0. \quad (\text{B.35})$$

Replacing now with equations (B.29) and (B.30) and doing some trigonometric calculations, one obtains

$$\sigma_{xx}(t) = \eta\omega\varepsilon_0^2 (c_0^{xx} + c_2^{xx} \cos(2\omega t) + s_2^{xx} \sin(2\omega t) +$$

$$+ c_4^{xx} \cos(4\omega t) + s_4^{xx} \sin(4\omega t)), \quad (\text{B.36})$$

$$c_0^{xx} = \frac{\lambda\omega}{2} \left(\frac{2}{1 + (\lambda\omega)^2} + \frac{\varepsilon_0^2}{1 + (2\lambda\omega)^2} \right), \quad (\text{B.38})$$

$$c_2^{xx} = -\lambda\omega \left(\frac{1}{1 + (\lambda\omega)^2} + \frac{\varepsilon_0^2}{1 + (2\lambda\omega)^2} \right), \quad (\text{B.39})$$

$$s_2^{xx} = \frac{1}{2} \left(\frac{2}{1 + (\lambda\omega)^2} + \frac{\varepsilon_0^2}{1 + (2\lambda\omega)^2} \right), \quad (\text{B.40})$$

$$c_4^{xx} = \frac{\lambda\omega\varepsilon_0^2}{2} \frac{1}{1 + (2\lambda\omega)^2}, \quad (\text{B.41})$$

$$s_4^{xx} = -\frac{\varepsilon_0^2}{4} \frac{1}{1 + (2\lambda\omega)^2}, \quad (\text{B.42})$$

$$\sigma_{xy}(t) = \eta\omega\varepsilon_0 (c_1^{xy} \cos(\omega t) + s_1^{xy} \sin(\omega t) +$$

B.1. Extension of Sequence of Physical Processes relating the second Piola-Kirchhoff stress tensor to the Green-Lagrange strain tensor

$$+c_3^{xy} \cos(3\omega t) + s_3^{xy} \sin(3\omega t), \quad (\text{B.44}) \quad \text{then doing the calculations for } S_{xy} \text{ brings}$$

$$c_1^{xy} = \frac{1}{1 + (\lambda\omega)^2} + \frac{\varepsilon_0}{2} \frac{1}{1 + (2\lambda\omega)^2}, \quad (\text{B.45})$$

$$s_1^{xy} = \lambda\omega \left(\frac{1}{1 + (\lambda\omega)^2} + \frac{\varepsilon_0}{1 + (2\lambda\omega)^2} \right), \quad (\text{B.46})$$

$$c_3^{xy} = -\frac{\varepsilon_0}{2} \frac{1}{1 + (2\lambda\omega)^2}, \quad (\text{B.47})$$

$$s_3^{xy} = -\frac{\lambda\omega\varepsilon_0}{1 + (2\lambda\omega)^2}, \quad (\text{B.48})$$

$$\sigma_{yy}(t) = \eta\omega\varepsilon_0^2 \frac{\sin(2\omega t) - 2\lambda\omega \cos(2\omega t)}{1 + (2\lambda\omega)^2}. \quad (\text{B.49})$$

What is really interesting from the equations above is that, in the Cauchy stress tensor, there are non zero σ_{xy} and σ_{yy} components but also the σ_{xx} component. Also, the σ_{yy} component remains identical to S_{yy} , with the double frequency oscillation, but σ_{xy} has two harmonics, the first and the third, and σ_{xx} has three harmonics, the zeroth, the second and the fourth. The non-zero average of σ_{xx} is equal to

$$\lim_{T \rightarrow +\infty} \frac{1}{T} \int_0^T \sigma_{xx}(t) dt = \frac{\eta\lambda\omega^2\varepsilon_0^2}{2} \left(\frac{2}{1 + (\lambda\omega)^2} + \frac{\varepsilon_0^2}{1 + (2\lambda\omega)^2} \right). \quad (\text{B.50})$$

It is now possible to compare the usual Sequence of Physical Process with the extended version presented here. In the usual Sequence of Physical Process, the transient moduli are calculated through

$$\mathcal{G}'_t(\sigma_{xy}) = -\frac{\ddot{\varepsilon}\dot{\sigma}_{xy} - \ddot{\sigma}_{xy}\dot{\varepsilon}}{\dot{\varepsilon}\ddot{\varepsilon} - \ddot{\varepsilon}^2}, \quad (\text{B.51})$$

$$\mathcal{G}''_t(\sigma_{xy}) = -\omega \frac{\dot{\sigma}_{xy}\ddot{\varepsilon} - \ddot{\sigma}_{xy}\dot{\varepsilon}}{\dot{\varepsilon}\ddot{\varepsilon} - \ddot{\varepsilon}^2}. \quad (\text{B.52})$$

Using the expressions above in the limit $\varepsilon_0 \rightarrow 0$, one obtains

$$\mathcal{G}'_t(\sigma_{xy}) = \eta\omega \frac{\lambda\omega}{1 + (\lambda\omega)^2}, \quad (\text{B.53})$$

$$\mathcal{G}''_t(\sigma_{xy}) = \frac{\eta\omega}{1 + (\lambda\omega)^2} \quad (\text{B.54})$$

as a usual linear Maxwell model with the variables σ and $\dot{\varepsilon}$. Using the new extended version with the second Piola-Kirchhoff tensor, it is possible to obtain with the previous notations

$$D = \begin{pmatrix} \dot{x}_1 & \dot{x}_2 & \dot{x}_3 & \dot{x}_4 \\ \ddot{x}_1 & \ddot{x}_2 & \ddot{x}_3 & \ddot{x}_4 \\ \dddot{x}_1 & \dddot{x}_2 & \dddot{x}_3 & \dddot{x}_4 \end{pmatrix} = 18\varepsilon_0^6\omega^{10} \quad (\text{B.55})$$

$$G'_t(S_{xy}) = \eta\omega \frac{\lambda\omega}{1 + (\lambda\omega)^2}, \quad (\text{B.56})$$

$$G''_t(S_{xy}) = \frac{\eta\omega}{1 + (\lambda\omega)^2}, \quad (\text{B.57})$$

$$H'_t(S_{xy}) = 0, \quad (\text{B.58})$$

$$H''_t(S_{xy}) = 0, \quad (\text{B.59})$$

and for S_{yy} brings

$$G'_t(S_{yy}) = 0, \quad (\text{B.60})$$

$$G''_t(S_{yy}) = 0, \quad (\text{B.61})$$

$$H'_t(S_{yy}) = \eta\omega \frac{4\lambda\omega}{1 + (2\lambda\omega)^2}, \quad (\text{B.62})$$

$$H''_t(S_{yy}) = \frac{2\eta\omega}{1 + (2\lambda\omega)^2}. \quad (\text{B.63})$$

Hence, we find transient moduli both in the shear direction xy and in the axial direction xx with very interesting relationships like

$$\frac{H'_t(S_{yy})}{H''_t(S_{yy})} = 2 \frac{G'_t(S_{xy})}{G''_t(S_{xy})} = 2\lambda\omega. \quad (\text{B.64})$$

Another interesting feature which may be highlighted is the fact that, due to construction with equation (B.6) and looking at equations (B.29), (B.30), (B.56), (B.57), (B.62) and (B.63), each component of S is a linear combination of ε , $\dot{\varepsilon}/\omega$, ε^2 and $2\dot{\varepsilon}\varepsilon/\omega$ with the transient moduli G'_t , G''_t , H'_t and H''_t as factors.

It is now possible to find the last moduli for σ_{xx} , σ_{xy} and σ_{yy} . The easiest one is σ_{yy} thanks to equation (B.34) thus

$$G'_t(\sigma_{yy}) = 0, \quad (\text{B.65})$$

$$G''_t(\sigma_{yy}) = 0, \quad (\text{B.66})$$

$$H'_t(\sigma_{yy}) = \eta\omega \frac{4\lambda\omega}{1 + (2\lambda\omega)^2}, \quad (\text{B.67})$$

$$H''_t(\sigma_{yy}) = \frac{2\eta\omega}{1 + (2\lambda\omega)^2}. \quad (\text{B.68})$$

For σ_{xx} and σ_{xy} , the fourth and the third harmonics, respectively, are disturbing a quick calculations so the overall framework should be applied. In the case of σ_{xx} , one gets

$$G'_t(\sigma_{xx}) = 8\eta\omega \left(c_4^{xx} (3 \sin(5\omega t) - 5 \sin(3\omega t)) + \right. \quad (\text{B.69})$$

$$\left. + s_4^{xx} (5 \cos(3\omega t) - 3 \cos(5\omega t)) \right) \quad (\text{B.70})$$

$$G''_t(\sigma_{xx}) = 8\eta\omega \left(c_4^{xx} (3 \cos(5\omega t) + 5 \cos(3\omega t)) + \right. \quad (\text{B.71})$$

$$+s_4^{xx} (5 \sin(3\omega t) + 3 \sin(5\omega t)) \quad (\text{B.72})$$

$$H'_i(\sigma_{xx}) = 2\eta\omega (c_2^{xx} + \quad (\text{B.73})$$

$$+5c_4^{xx} (\cos(6\omega t) + 3 \cos(2\omega t)) + \quad (\text{B.74})$$

$$+5s_4^{xx} (\sin(6\omega t) + 3 \sin(2\omega t)) \quad (\text{B.75})$$

$$H''_i(\sigma_{xx}) = 2\eta\omega (s_2^{xx} + \quad (\text{B.76})$$

$$+5c_4^{xx} (\sin(6\omega t) - 3 \sin(2\omega t)) + \quad (\text{B.77})$$

$$+5s_4^{xx} (-\cos(6\omega t) + 3 \cos(2\omega t)) \quad (\text{B.78})$$

and for σ_{xy} , one obtains

$$G'_i(\sigma_{xy}) = \eta\omega (s_1^{xy} + \quad (\text{B.79})$$

$$+5c_3^{xy} (2 \sin(2\omega t) - \sin(4\omega t)) \quad (\text{B.80})$$

$$+5s_3^{xy} (\cos(4\omega t) - 2 \cos(2\omega t)) \quad (\text{B.81})$$

$$G''_i(\sigma_{xy}) = \eta\omega (c_1^{xy} + \quad (\text{B.82})$$

$$-5c_3^{xy} (2 \cos(2\omega t) + \cos(4\omega t)) \quad (\text{B.83})$$

$$-5s_3^{xy} (\sin(4\omega t) + 2 \sin(2\omega t)) \quad (\text{B.84})$$

$$H'_i(\sigma_{xy}) = 2\eta\omega (c_3^{xy} (5 \cos(\omega t) + \cos(5\omega t)) + \quad (\text{B.85})$$

$$+s_3^{xy} (5 \sin(\omega t) + \sin(5\omega t)) \quad (\text{B.86})$$

$$H''_i(\sigma_{xy}) = 2\eta\omega (c_3^{xy} (-5 \sin(\omega t) + \sin(5\omega t)) + \quad (\text{B.87})$$

$$+s_3^{xy} (5 \cos(\omega t) - \cos(5\omega t)) \quad (\text{B.88})$$

With the previous equations, it can be interesting to compare the usual Sequence of Physical Processes with the present extended version. Thus, using equations (B.53) and (B.54) and the average values according to time of equations (B.79) to (B.84), one obtains

$$\langle G'_i(\sigma_{xy}) \rangle - \mathcal{G}'_i(\sigma_{xy}) = \eta\omega\varepsilon_0 \frac{\lambda\omega}{1 + (2\lambda\omega)^2} \quad (\text{B.89})$$

$$\langle G''_i(\sigma_{xy}) \rangle - \mathcal{G}''_i(\sigma_{xy}) = \frac{\eta\omega\varepsilon_0}{2} \frac{1}{1 + (2\lambda\omega)^2}. \quad (\text{B.90})$$

To give more clarity of understanding, it is possible to plot the variations of these moduli according to different parameters. Noting that the moduli of S_{xy} , S_{yy} and σ_{yy} are constant according to time, the figure B.1 illustrates the frequency plot of those moduli. We recognise easily the usual behaviour of the linear Maxwell model for S_{xy} but the contribution on S_{yy} or σ_{yy} is of the same order of magnitude when ε_0 is of the order of unity or higher. Also, the time scales are a bit different and shows an earlier shift in the trends.

Now if we look at the expressions for σ_{xx} and σ_{xy} , we see that there are non zero contribution of each component. Normally, one would expect only the σ_{xy} component to play a role but here, due to the increase of the strain amplitude ε_0 , additional contributions appear. It is possible to recover the usual linear Maxwell model

expressed in terms of the Cauchy stress tensor σ when $\varepsilon_0 \rightarrow 0$. However, at high strain amplitude, there are variations in time of the various transient moduli. So here is the actual novelty of this approach because, with the steady-state approach, one would only find the average values over time. Now, one can find some more intricate evolutions to properly understand the behaviour of the materials. To give some illustrations to those equations, there are displayed on figure B.2 the time evolution of the various transient moduli of σ_{xx} and σ_{xy} with the parameters $\varepsilon_0 = \lambda\omega = 1$. To give another perspective, the figure B.3 gives the Cole-Cole plot, i.e. the viscous transient moduli as a function of the elastic transient moduli, with the same set of parameters. An interesting thing when looking at figure B.3 is that, focusing on the black line for $G'_i(\sigma_{xy})$, which is usually observed in experiments with the 3 peaks, there exist some portion of the cycle where either or both $G'_i(\sigma_{xy})$ and $G''_i(\sigma_{xy})$ are negative. This is interpreted sometimes as sign of elastic recoil or negative dissipation. However, this example demonstrates that even for a model where the rheological parameters are properly defined without any doubts on the thermodynamic, there is some strange behaviour happening which may lead to consider some odd interpretations. In this case, a simple geometrical transformation of the Cauchy stress tensor σ into the second Piola-Kirchhoff stress tensor \mathcal{S} leads to a rheological analysis which is much simpler due to the fact that the newly obtained moduli will be constant and corresponding exactly to a linear Maxwell fluid. All these remarks are just a warning for people who are looking for a characterisation and an identification of their materials: some processing may be needed on experimental data to analyse properly the rheological behaviour getting rid of useless complications.

We can carry out the overall analysis as in [Rogers, 2017; Donley, 2019; Rogers, 2011; Rogers, 2012b; Rogers, 2012a] but we leave the rest of the comparison to the reader.

In general, what is interesting is that when $\varepsilon_0 \gg 1$, the main stress components are σ_{xx} first due to the proportionality to ε_0^4 , then S_{yy} , σ_{xy} and σ_{yy} with the proportionality to ε_0^2 and finally, the shear components S_{xy} which is linear in ε_0 .

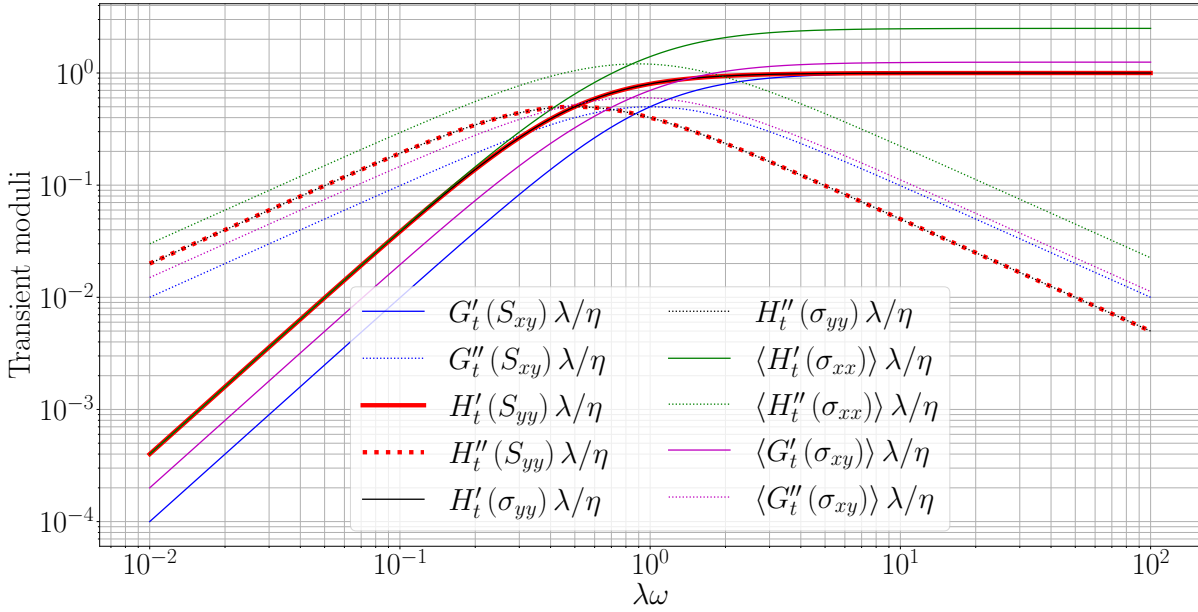


Figure B.1: Evolution of the transient moduli of S_{xy} , S_{yy} and σ_{yy} and the average according to time of transient moduli of σ_{xx} and σ_{xy} , all divided by η/λ as a function $\lambda\omega$ with $\varepsilon_0 = 1$.

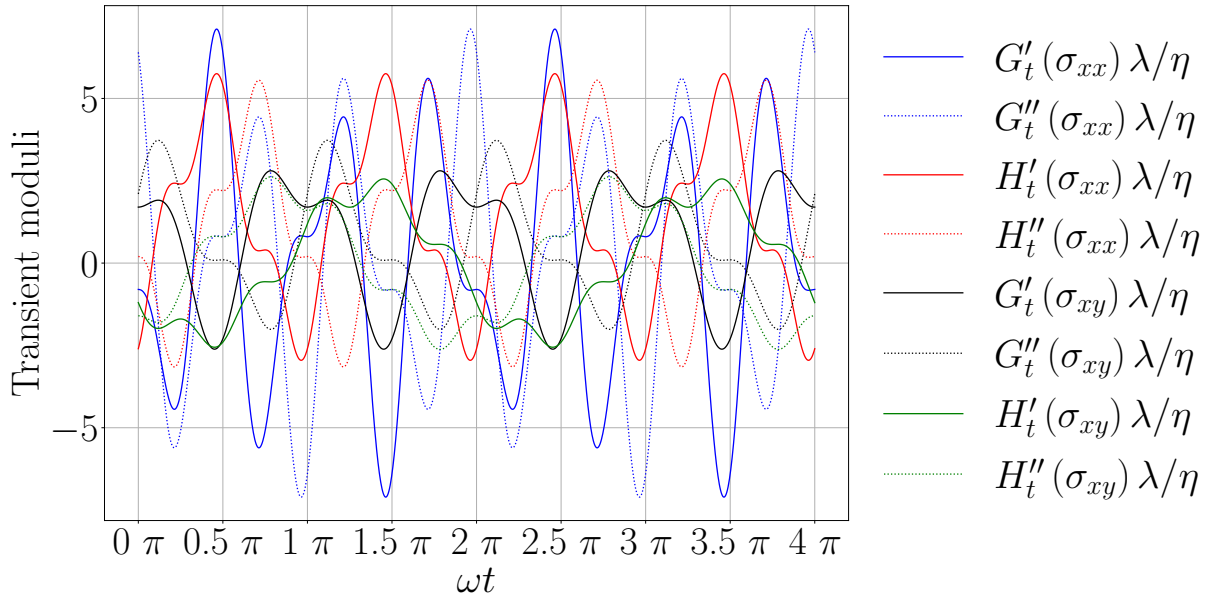


Figure B.2: Evolution of the various moduli of σ_{xy} and σ_{xx} divided by η/λ as a function ωt imposing $\lambda\omega = \varepsilon_0 = 1$.

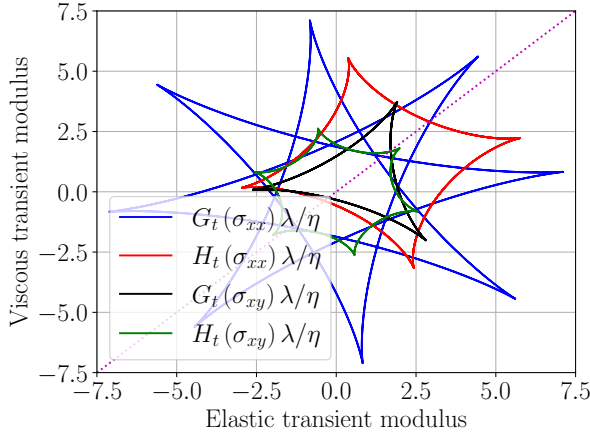


Figure B.3: Evolution of the viscous moduli of σ_{xy} and σ_{xx} divided by η/λ as a function of the elastic moduli divided by η/λ imposing $\lambda\omega = \varepsilon_0 = 1$. The purple dotted line corresponds to the first bisector $y = x$.

B.2 Multi-phase problem : Level-Set methods

B.2.1 Abstract

Level-set methods have been used widely in the community to run multiphase simulations in continuum mechanics. It allows a smooth transition between different media which qualifies as a relevant tool in numerical simulation. The initial transport equation used for the level-set function is simple but needs, to abide by its definition, some regularization techniques. The corrections used in the literature are various with the Hamilton-Jacobi equation, the use of filtered level-set function with linear, sinusoidal, logistic or convolution filters, or the re-initialization of the transport equation according to these filters. In this section, we have reviewed the different recent techniques used in the literature to run performing numerical simulations using level-set methods, assessed for each of them the advantages and the drawbacks, and compared some of the methods on standard numerical cases. In addition of this overview, we propose to share with the community some complementary tools like anisotropic mesh adaptation and other robust methods that increase substantially the quality of numerical simulations. These tools may help anyone who tries to model multiphase systems using level-set methods.

B.2.2 Introduction

Multiphase flows are ubiquitous in continuum mechanics, from natural fields like climate [Stranne, 2016; Stumpf, 2000] or biology [Abolhasani, 2016] or industrial applications like oil [Kolev, 2012], nuclear hydraulics [Kolev, 2015], melting [He, 2020; Buliński,

2018] or coating [Yin, 2016]. Due to the very high complexity of such calculations, analytical tools are rapidly overwhelmed and numerical simulations are needed to account for phenomena observed in experiments. Several numerical methods exist to handle multiple phases in numerical flow simulation. The use Lagrangian techniques for very low volume fraction phases may be interesting [Yin, 2016]. For equivalent volume fraction phases, Eulerian methods are used such as the Volume of Fluid [van Sint Annaland, 2005; Xie, 2016], the Front Tracking Method [Sint Annaland, 2006; Hua, 2007; Hua, 2008], the Lattice Boltzmann Method [Cheng, 2010; Yu, 2009; Amaya-Bower, 2010; Yu, 2011], the Smoothed Particle Hydrodynamics [Szewc, 2013; Grenier, 2013; Zhang, 2015], the Phase Field method [Khanwale, 2020] and the Level-Set method [Croce, 2010; Bahbah, 2019; Quezada de Luna, 2020].

B.2.3 Level-Set methods

B.2.3.1 Classical Level-set method

We will focus in this section on the Level-Set method which has had lots of improvement in the recent years. Let consider, for sake of simplicity, a system in a space $\Omega \subset \mathbb{R}^d$ where $d \in \{2, 3\}$ with two phases 1 and 2 occupying respectively the spaces Ω_1 and Ω_2 . The extension to more than two phases is possible but the details are left to the reader. The boundary between Ω_1 and Ω_2 is called Γ and we note that $\Omega = \Omega_1 \sqcup \Omega_2$. The starting point of the Level-Set method, according to [Marioni, 2017; Bahbah, 2020], is the use of a scalar function α , called the *Level-Set function*, defined by

$$\alpha : \Omega \mapsto \begin{cases} \mathbb{R} \\ \alpha(x) > 0 & \text{if } x \in \Omega_1 \\ 0 & \text{if } x \in \Gamma \\ \alpha(x) < 0 & \text{if } x \in \Omega_2 \end{cases} \quad (\text{B.91})$$

The interest of such a function is that it is possible to use a scaling function $H : \mathbb{R} \mapsto [0, 1]$ to define

$$\beta = \beta_2 + H(\alpha)(\beta_1 - \beta_2) \quad (\text{B.92})$$

for any property β of the fluid like density ρ , viscosity, elasticity, specific heat capacity or the inverse of the thermal conductivity. Because of this definition, the Level-Set function verifies $\|\mathbf{grad}(\alpha)\| = 1$ which is true for any signed distance function. Also, due to its definition stating the boundaries between Ω_1 and Ω_2 , the Level-Set function should be transported by the fluid which brings

$$\frac{d\alpha}{dt} = \frac{\partial\alpha}{\partial t} + \mathbf{u} \cdot \mathbf{grad}(\alpha) = 0 \quad (\text{B.93})$$

with \mathbf{u} the velocity of the fluid. This is the classical Level-Set method which brings an additional transport equation to solve. Nevertheless, there is a direct implementation of such transport equations in the codes. For instance, looking at the mass conservation equation

$$\frac{d\rho}{dt} + \rho \operatorname{div}(\mathbf{u}) = 0. \quad (\text{B.94})$$

Using equation (B.92) with constant densities ρ_1 and ρ_2 with two incompressible media, we find

$$\frac{d\rho}{dt} = \frac{dH}{d\alpha} (\rho_1 - \rho_2) \frac{d\alpha}{dt} = 0 \quad (\text{B.95})$$

thanks to equation (B.93). Therefore, reconsidering the mass conservation equation (B.94), it leads to

$$\operatorname{div}(\mathbf{u}) = 0 \quad (\text{B.96})$$

which is exactly the same equation as in one phase incompressible flow. Therefore, the classical Level-Set method is directly achievable once a single phase continuum mechanics code is implemented.

B.2.3.2 Re-initialized Level-Set method

The equations $\|\mathbf{grad}(\alpha)\| = 1$ and $d_t\alpha = 0$ are incompatible in the sense that the transport equation does not keep the former equation valid. In order, to correct this problem, it is possible to re-initialize the transport equation equation (B.93) using a Hamilton-Jacobi equation (see [Sussman, 1994]) as follows

$$\frac{d\alpha}{dt} + \operatorname{sgn}(\|\mathbf{grad}(\alpha)\| - 1) = 0 \quad (\text{B.97})$$

with $\operatorname{sgn} = 2\Theta - 1$ the sign function. This equation will allow to help to preserve the signed distance function property of the Level-Set function.

B.2.3.3 Re-initialized filtered Level-Set method

Due to sharp gradients of the Level-Set function, trying to design a smoother level-set function can be a relevant improvement. The filter consists in finding an odd function $\gamma : \mathbb{R} \mapsto \mathbb{R}$ such as the variation between positive values and negative values is smooth and the limit values at $\pm\infty$ are bounded. Several examples exist in the literature (see [Marioni, 2017; Bahbah, 2019]) like

$$\gamma(\alpha) = A \begin{cases} \operatorname{sgn}(\alpha) & |\alpha| \geq \varepsilon \\ \frac{1}{2} \left(\frac{\pi\alpha}{\varepsilon} + \sin\left(\frac{\pi\alpha}{\varepsilon}\right) \right) & |\alpha| < \varepsilon \end{cases} \quad (\text{B.98})$$

with A and ε positive numbers assigning the limits at $\pm\infty$ and the sharpness of the variation around 0 respectively, or

$$\gamma(\alpha) = \tanh\left(\frac{\alpha}{\varepsilon}\right) \quad (\text{B.99})$$

with ε the sharpness of the variation around 0. The goal of the filter function γ is to be as close as possible to an infinitely derivable function C^∞ . If we want to replace α by $\gamma \circ \alpha$ in the calculation, it is necessary to change the transport equation equation (B.97) according to the new filtered Level-Set function. An advantage of equation (B.99) over equation (B.98) is that, in equation (B.99), it is possible to express analytically α as a function of γ or, more formally, to find γ^{-1} . However, in equation (B.98), the expression of γ^{-1} is not trivial due to the lack of injectivity. Therefore, when someone wants to implement the filter in equation (B.98), there is a need to solve additional equations in order to express properly α and $\gamma \circ \alpha$. To be specific, the filtered re-initialized transport equation for the filtered Level-Set function equation (B.99) is

$$\frac{\partial\gamma}{\partial t} + (\mathbf{u} + \lambda\mathbf{U}) \cdot \mathbf{grad}(\gamma) = \frac{\operatorname{sgn}(\gamma)\lambda}{\varepsilon} (1 - \gamma^2) \quad (\text{B.100})$$

with λ a constant helping the re-initialisation and $\mathbf{U} = \mathbf{grad}(\gamma) / \|\mathbf{grad}(\gamma)\|$ the re-initialisation velocity. In general, the filtered re-initialised transport equation for the filtered Level-Set function can be written

$$\frac{\partial\gamma}{\partial t} + (\mathbf{u} + \lambda\mathbf{U}) \cdot \mathbf{grad}(\gamma) = \operatorname{sgn}(\gamma)\lambda \frac{d\gamma}{d\alpha} \quad (\text{B.101})$$

which can then be integrated in the mass conservation equation equation (B.94) using equation (B.92) to bring

$$\operatorname{div}(\mathbf{u}) = \lambda \frac{d \ln(\rho)}{d\gamma}(\gamma) \left(\mathbf{U} \cdot \mathbf{grad}(\gamma) - \operatorname{sgn}(\gamma) \frac{d\gamma}{d\alpha} \right). \quad (\text{B.102})$$

B.2.4 Other relevant tools for the Level-Set method

After having presented the different existing Level-Set methods with their characteristics, it is interesting to complement the discussion with additional tools which help the calculation to be improved. More specifically, one of the first tools is the use of anisotropic adaptive mesh. Based on [Coupez, 2011; Coupez, 2013], the method uses an edge-based error estimation coupled with a gradient recovery procedure which allows to adapt the mesh where needed, for example, where the gradients are very important like the gradient of the (filtered) Level-Set function at the boundary between Ω_1 and Ω_2 .

Another additional tool is parallel computing which helps to handle complexities brought jointly by the Navier-Stokes equation (RANS model [Singhal, 2018; Alhulaifi, 2012], Reynolds Stress Model [Yin, 2016], Direct Numerical Simulation [Raelison, 2020] or Variational Multi-Scale [Hachem, 2010]), the anisotropic mesh adaptation and the re-initialised filtered Level-Set method (or more generally the multiphase flow). The

parallel computing consists in (i) partitioning the initial mesh, (ii) reading the mesh and solving the equations, (iii) adapting the mesh after the calculations, (iv) updating the solution on the new mesh created over multiple cores, (v) repartitionning the mesh to start the cycle over.

Then, an additional tool can be the density scaled continuum surface force model following [Yokoi, 2014; Yokoi, 2016; Yamamoto, 2017]. Indeed, this method allows to introduce a surface force similar to a surface tension due to capillarity which is using a density-scaled function to create the transition between the two phases. This additional tool improves the quality of the simulation and particularly the accuracy of the boundary between the two phases.

B.2.5 Application cases

B.2.5.1 Case 1 : Kelvin-Helmholtz instability

Following [Drazin, 1970], the case of Kelvin-Helmholtz instability can be described as follows. The computational domain can be either a 2D box or a 3D box. Let assume that the direction of the flow is x , the normal direction of the interface between the two fluid is z and that it may exist a third component y if a 3D box is considered. On the boundary $x = 0$, one assumes that, for $z > 0$, there is a velocity U_2 in the x direction with a density ρ_2 and, for $z < 0$, there is a velocity U_1 in the x direction with a density ρ_1 . We assume the existence of the gravity g in the opposite direction of z and the interfacial tension between the two fluids is σ . The interface ζ between the two fluids is initially at $\zeta(x, y, t = 0) = 0$. Assuming a perfect incompressible fluid with a potential flow ϕ and keeping only the linear terms in the equations, we get the following solution according to [Drazin, 1970]

$$\phi = -\text{sgn}(z) A \frac{s + i\alpha(U_1 + \Theta(z)(U_2 - U_1))}{\sqrt{\alpha^2 + \beta^2}} \quad (\text{B.103})$$

$$\exp\left(st + i(\alpha x + \beta y) - |z| \sqrt{\alpha^2 + \beta^2}\right) \quad (\text{B.104})$$

$$\zeta = A \exp(st + i(\alpha x + \beta y)) \quad (\text{B.105})$$

$$s = -\frac{i\alpha(\rho_1 U_1 + \rho_2 U_2)}{\rho_1 + \rho_2} \quad (\text{B.106})$$

$$\pm \left(\frac{\alpha^2 \rho_1 \rho_2 (U_1 - U_2)^2}{(\rho_1 + \rho_2)^2} - \frac{g(\rho_1 - \rho_2) \sqrt{\alpha^2 + \beta^2}}{\rho_1 + \rho_2} + \right. \quad (\text{B.107})$$

$$\left. - \frac{(\alpha^2 + \beta^2)^{\frac{3}{2}} \sigma}{\rho_1 + \rho_2} \right) \quad (\text{B.108})$$

with α and β the wave numbers in the x and y direction respectively, sgn the sign function, Θ the Heaviside

function and A a constant. The most pronounced amplitude are in the plane $y = 0$, which justifies the possibility to limit ourselves to 2D geometries. The solution is then reduced to

$$\phi = -\text{sgn}(z) A \frac{s + i\alpha(U_1 + \Theta(z)(U_2 - U_1))}{\alpha} \quad (\text{B.109})$$

$$\exp(st + i\alpha x - |z|\alpha) \quad (\text{B.110})$$

$$\zeta = A \exp(st + i\alpha x) \quad (\text{B.111})$$

$$s = -\frac{i\alpha(\rho_1 U_1 + \rho_2 U_2)}{\rho_1 + \rho_2} \quad (\text{B.112})$$

$$\pm \sqrt{\frac{\alpha^2 \rho_1 \rho_2 (U_1 - U_2)^2}{(\rho_1 + \rho_2)^2} - \frac{g(\rho_1 - \rho_2)\alpha}{\rho_1 + \rho_2} - \frac{\alpha^3 \sigma}{\rho_1 + \rho_2}} \quad (\text{B.113})$$

The interesting fact with the case is that depending on the combination of $(\rho_1, U_1, \rho_2, U_2, g, \sigma, \alpha)$, there may be either an unstable behaviour or a stable one. Precisely, the stability of the solution depends on the sign of

$$\frac{\alpha \rho_1 \rho_2 (U_1 - U_2)^2}{(\rho_1 + \rho_2)^2} - \frac{g(\rho_1 - \rho_2)}{\rho_1 + \rho_2} - \frac{\alpha^2 \sigma}{\rho_1 + \rho_2} \quad (\text{B.114})$$

for all $\alpha > 0$. Therefore, it depends on the sign of

$$\Delta = \rho_1^2 \rho_2^2 (U_1 - U_2)^4 - 4g(\rho_1 + \rho_2)^2 (\rho_1 - \rho_2) \sigma \quad (\text{B.115})$$

if $\sigma \neq 0$ or is conditionally unstable otherwise or if $g = \sigma = 0$, the system is unconditionally unstable. If $\Delta < 0$, the square root of s is pure imaginary and it is stable. If $\Delta \geq 0$, there may exist some values of α for which the system is unstable.

We will investigate and describe the instability according to these parameters.

B.2.5.2 Case 2 : Rayleigh-Taylor instability

The Rayleigh-Taylor instability happens in a 2D box or 3D box as for the Kelvin-Helmholtz instability. The same initial setup is proposed but there is no imposed velocity, we assume $\rho_2 > \rho_1$ and $\sigma = 0$. There is an instability of the interface under gravity which can be expressed by

$$\zeta = A \exp\left(i\alpha x + t \sqrt{\frac{\rho_2 - \rho_1}{\rho_1 + \rho_2} g \alpha}\right) \quad (\text{B.116})$$

B.3 Use of the canonical framework for the aggregation-disaggregation formulation

An idea that may be interesting to pursue, in the spirit of chapter 2 and [Bouthier, 2023a], is to use the canonical framework to get results like equation (2.7) instead of

using the grand canonical framework. For instance a first step is, with the same assumptions of additivity of energy and $N \in \mathbb{N}^*$ the number of particles, we obtain as partition function

$$Z = \frac{1}{N!} B_N \left(\left(e^{-\beta \mathcal{E}(k)} \right)_{k \in \llbracket 1, N \rrbracket} \right) \quad (\text{B.117})$$

$$B_N \left((x_k)_{k \in \llbracket 1, N \rrbracket} \right) = N! \sum_{\substack{(i_k)_{k \in \llbracket 1, N \rrbracket} \in \mathbb{N}^N \\ \sum_{k=1}^N k i_k = N}} \prod_{k=1}^N \frac{x_k^{i_k}}{i_k! (k!)^{i_k}} \quad (\text{B.118})$$

with B_N the complete Bell polynomial used to calculate the number of ways to partition a set of N elements. If we note for all $k \in \mathbb{N}^*$, n_k the random variable accounting the number of cluster of size k , one can find the joint probability for all $(i_k)_{k \in \llbracket 1, N \rrbracket} \in \mathbb{N}^N$ such that $\sum_{k=1}^N k i_k = N$,

$$P \left(\bigcap_{k=1}^N (n_k = i_k) \right) = \frac{1}{Z} \prod_{k=1}^N \frac{e^{-\beta i_k \mathcal{E}(k)}}{i_k! (k!)^{i_k}} \quad (\text{B.119})$$

or equals 0 if $\sum_{k=1}^N k i_k \neq N$. Hence, it is possible to find an average distribution of each random variable writing for all $k \in \mathbb{N}^*$

$$\langle n_k \rangle = \sum_{i_k=1}^N i_k P(n_k = i_k) \quad (\text{B.120})$$

$$P(n_k = i_k) = \sum_{\substack{(i_j)_{j \in \llbracket 1, N \rrbracket} \setminus \{k\} \in \mathbb{N}^{N-1} \\ \sum_{j=1}^N j i_j = N}} P \left(\bigcap_{j=1}^N (n_j = i_j) \right) \quad (\text{B.121})$$

There are then N equations relating two sets of N variables : $(\langle n_k \rangle)_{k \in \llbracket 1, N \rrbracket}$ and $(\beta \mathcal{E}(k))_{k \in \llbracket 1, N \rrbracket}$. Therefore, it is possible to extract the expression of the latter in terms of the former theoretically thanks to equations (B.117) to (B.121). Nevertheless, it is practically impossible to express the solution analytically. It is thus necessary to use numerical resolution tools such as inverse-problem resolution. For example, it may be interesting to write $\mathbf{n} = (\langle n_k \rangle)_{k \in \llbracket 1, N \rrbracket}$ and $\mathbf{E} = (\beta \mathcal{E}(k))_{k \in \llbracket 1, N \rrbracket}$ for the unknown variable and $\mathbf{f} = (f(k))_{k \in \llbracket 1, N \rrbracket}$ for the experimental sample ; it is then possible to minimize the following function

$$\mathfrak{J}(\mathbf{X}) = \|\mathbf{n}(\mathbf{X}) - \mathbf{f}\|^2 \quad (\text{B.122})$$

$$\|\mathbf{Y}\|^2 = \sum_{k=1}^N y_k^2 \quad (\text{B.123})$$

to find

$$\mathbf{E} = \arg \min_{\mathbf{X} \in \mathbb{R}^N} \mathfrak{J}(\mathbf{X}). \quad (\text{B.124})$$

In addition, we consider large systems with $N \geq 10^4$. It may then be interesting to know the asymptotic behaviour of the previous relations when N tends towards

$+\infty$. The difficult part of the problem is to know the asymptotic behaviour of the complete Bell polynomial B_N at large N due to the multiple variables involved. To give an order of magnitude, for a given $k \in \mathbb{N}^*$, we select only the family of N such as $N = pk$ with $p \in \mathbb{N}^*$ tending to $+\infty$ and assume a configuration where only the clusters of size k may exist. In this case, one obtains using the Stirling approximation

$$B_N = \frac{(pk)! x^p}{p! (k!)^p} \underset{p \rightarrow +\infty}{\sim} \sqrt{k} \left(\left(\frac{p}{e} \right)^{k-1} \frac{k^k}{k!} x \right)^p = O(N^N) \quad (\text{B.125})$$

which gives with $N = 10^4$ a coefficient in the order of $10^{40,000}$ with 40,000 zeros.

To pursue the reasoning, it may be interesting to consider a modified partition function

$$\mathcal{Z} = \frac{1}{N!} B_N \left(\left(e^{-\beta_k \mathcal{E}(k)} \right)_{k \in \llbracket 1, N \rrbracket} \right) \quad (\text{B.126})$$

which is equal to the actual partition function Z when all the variables $(\beta_k)_{k \in \llbracket 1, N \rrbracket}$ are all equal to β . Thanks to this function, we can write for all $k \in \llbracket 1, N \rrbracket$, $\partial_{\beta_k} \mathcal{Z}$ in two different ways. On the one hand, thanks to the properties of the Bell polynomials, for all $k \in \llbracket 1, N \rrbracket$

$$\frac{\partial \mathcal{Z}}{\partial \beta_k} = -\frac{\mathcal{E}(k) e^{-\beta_k \mathcal{E}(k)}}{N!} \binom{N}{k} B_{N-k} \left(\left(e^{-\beta_j \mathcal{E}(j)} \right)_{j \in \llbracket 1, N-k \rrbracket} \right) \quad (\text{B.127})$$

On the other hand, for all $k \in \llbracket 1, N \rrbracket$

$$\frac{\partial \mathcal{Z}}{\partial \beta_k} = \sum_{\substack{(i_j)_{j \in \llbracket 1, N \rrbracket} \in \mathbb{N}^N \\ \sum_{j=1}^N j i_j = N}} -\mathcal{E}(k) i_k \prod_{j=1}^N \frac{e^{-\beta_j i_j \mathcal{E}(j)}}{i_j! (j!)^{i_j}} \quad (\text{B.128})$$

$$= \sum_{\substack{(i_j)_{j \in \llbracket 1, N \rrbracket} \in \mathbb{N}^N \\ \sum_{j=1}^N j i_j = N}} -\mathcal{E}(k) i_k \mathcal{Z} P \left(\bigcap_{j=1}^N (n_j = i_j) \right) \quad (\text{B.129})$$

$$= -\mathcal{E}(k) \mathcal{Z} \langle n_k \rangle \quad (\text{B.130})$$

thanks to equations (B.119) to (B.121) assuming that for all $j \in \llbracket 1, N \rrbracket$, $\beta_j = \beta$. Therefore, using equations (B.127) and (B.130), it is possible to demonstrate that for all $k \in \llbracket 1, N \rrbracket$

$$\langle n_k \rangle = e^{-\beta \mathcal{E}(k)} \frac{B_{N-k} \left(\left(e^{-\beta \mathcal{E}(j)} \right)_{j \in \llbracket 1, N-k \rrbracket} \right)}{B_N \left(\left(e^{-\beta \mathcal{E}(j)} \right)_{j \in \llbracket 1, N \rrbracket} \right)} \binom{N}{k} \quad (\text{B.131})$$

and then, using the previous equation for $k = N$, for all $k \in \llbracket 1, N \rrbracket$

$$\langle n_k \rangle = \langle n_N \rangle e^{\beta(\mathcal{E}(N) - \mathcal{E}(k))} B_{N-k} \left(\left(e^{-\beta \mathcal{E}(j)} \right)_{j \in \llbracket 1, N-k \rrbracket} \right) \binom{N}{k} \quad (\text{B.132})$$

To simplify the calculation, it may be interesting to assume that $\mathcal{E}(N) = 0$ due to the fact it is an energy po-

tential defined with an arbitrary constant, and to define for all $k \in \llbracket 1, N \rrbracket$,

$$z_k = \frac{\langle n_{N-k} \rangle}{\langle n_N \rangle} \binom{N}{k}^{-1} \quad (\text{B.133})$$

to read in the end, for all $k \in \llbracket 0, N - 1 \rrbracket$,

$$z_k = e^{-\beta \mathcal{E}(N-k)} \mathcal{B}_k \left(\left(e^{-\beta \mathcal{E}(j)} \right)_{j \in \llbracket 1, k \rrbracket} \right) \quad (\text{B.134})$$

which is a concise way to write the problem. Nevertheless, trying to solve by hand the previous problem for $N = 3$ or $N = 4$, it is blatant that the resolution needs to find roots of polynomials with a maximum degree N , which is analytically impossible for large values of N like 10,000. There is hence an absolute need of numerical approximation to solve the previous problem.

Appendix C

Testing latest artificial intelligence tools

Objectives

The goal of the chapter is to experiment an artificial intelligence tool on the content of this manuscript to assess the quality of the former.

Objectifs

Le but de ce chapitre est d'expérimenter un outil d'intelligence artificielle sur le contenu de ce manuscrit afin d'en évaluer la qualité.

Contents

C.1	Introduction	101
C.2	Questions about chapter 1	101
C.3	Questions about chapter 2	105
C.4	Questions about chapter 3	107
C.5	Conclusion	110

C.1 Introduction

From a pure curiosity point of view and to assess the quality of trendy tools, I propose to ask an artificial intelligence tool specific questions about the topic of this manuscript and to criticise the quality of the answer using the content presented here. For instance, I use *ChatGPT* (Chat Generative Pre-trained Transformer)^a, the artificial intelligence tool created by the company *OpenAI*, which is used by more than 100 million users (figures from February 2023). As a reminder, it is an algorithmic tool to generate texts based on language and links found in the training dataset. Being in the news because of its massive use, its usefulness but also its detraction notably in academic and professional circles, it seemed interesting to us to criticize what an algorithm could think, through its learning, of the tools that we proposed.

To help the reader to follow the reasoning, we have splitted the text in three different groups :

^a<https://chat.openai.com/>

The questions will be showed in a red box

The answers will be showed in a green box

The analysis will be showed in a blue box

C.2 Questions about chapter 1

The content of the discussion is available at this link : <https://chat.openai.com/share/4b00db e7-f5fe-4417-a131-b4a981ca91a3>

Question 1. (Asked on 5 May 2023 at 9am) Give me a state of the art of knowledge about microscopic and macroscopic coupling in mechanics in colloidal suspension.

Answer 1. Colloidal suspensions are mixtures of particles ranging in size from nanometers to micrometers, dispersed in a solvent. The behavior of colloidal suspensions is influenced by both microscopic and macroscopic factors, and understanding the coupling between these factors is crucial for predicting and controlling their mechanical properties.

At the microscopic level, the behavior of individual particles in colloidal suspensions is influenced by Brownian motion, electrostatic interactions, van der Waals forces, and steric effects. These interactions determine the particle's motion and orientation, as well as its interactions with neighboring particles. The resulting microstructure of the suspension strongly affects its mechanical properties.

At the macroscopic level, the mechanical behavior of colloidal suspensions is characterized by its rheology, or flow properties. The rheology of colloidal suspensions is influenced by the microstructure of the suspension, as well as external factors such as temperature, pressure, and shear rate. Understanding the coupling between microstructure and rheology is crucial for predicting the behavior of colloidal suspensions under various conditions.

Recent advances in experimental and theoretical techniques have greatly enhanced our understanding of the coupling between microscopic and macroscopic factors in colloidal suspensions. For example, high-resolution imaging techniques such as confocal microscopy and electron microscopy can provide detailed information about the microstructure of suspensions. Computational methods such as molecular dynamics simulations and coarse-grained models can be used to simulate the behavior of suspensions at the microscopic level and predict their rheological properties.

Overall, the state of the art in the study of microscopic and macroscopic coupling in mechanics in colloidal suspensions involves a multidisciplinary approach, combining experimental, theoretical, and computational techniques to gain a comprehensive understanding of the complex behavior of these systems.

Analysis 1. The introduction is rather hollow but does not use false declaration. The second paragraph is perfectly true about forces and interactions but lack a bit of details. For the third paragraph, there is clearly a lack of details except the fact that some factors have an influence. The fourth paragraph is pretty accurate about experimental and numerical methods even if I miss some examples or other methods to compare. The last paragraph is a poor conclusion without an added value.

Question 2. Give me references for this state of the art

Answer 2. ^a Here are some references that provide an overview of the state of the art in the study of microscopic and macroscopic coupling in mechanics in colloidal suspensions:

- K. S. Schweizer and J. G. Curro, "Rheological and structural properties of concentrated colloidal suspensions," *Annual Review of Physical Chemistry*, vol. 59, pp. 219-243, 2008.
- M. Laurati, "Mechanics of colloidal suspensions: From microstructure to rheology," *Journal of Physics: Condensed Matter*, vol. 27, no. 10, p. 103102, 2015.
- S. U. Egelhaaf, "Mechanical properties of colloidal suspensions," *Current Opinion in Colloid & Interface Science*, vol. 8, no. 1, pp. 34-40, 2003.
- P. R. Chaikin and T. C. Lubensky, *Principles of Condensed Matter Physics*, Cambridge University Press, 2000. [Chaikin, 1995]
- R. G. Larson, *The Structure and Rheology of Complex Fluids*, Oxford University Press, 1999. [Larson, 1999]
- J. Mewis and N. J. Wagner, *Colloidal Suspension Rheology*, Cambridge University Press, 2012. [Mewis, 2012]
- W. B. Russel, D. A. Saville, and W. R. Schowalter, *Colloidal Dispersions*, Cambridge University Press, 1989. [Russel, 1989]

These references cover a range of topics related to the study of colloidal suspensions, including microstructure, rheology, mechanics, and computational modeling.

Answer 2 (continued)

^aThe hyperlink Bib_TE_X bibliographic references were added by me to have a proper reference in the bibliography.

Analysis 2. The list seems authentic and relevant but some interesting things can be analysed :

- The first and the third references do not exist at all.
- The second reference does not exist as it is but the reference without the title and the author exists under [Huber, 2015] which is a completely different article in terms of authors and topic.
- The fourth reference exists but is slightly wrong.
- The sixth, the seventh and the eight are correct.
- The fifth exists but does not really treat colloidal suspensions.

Hence, except books, it is not possible to rely on this artificial intelligence tool to get a proper list of reference.

Question 3. (Asked on 5 May 2023 at 12pm)
Write a state of the art of rheological models giving equations and references for each

Answer 3. ^a Rheological models are used to describe the relationship between the deformation and stress in materials, including liquids, polymers, and complex fluids. Here's a state of the art of some rheological models, along with their equations and references:

Newtonian fluid model: The simplest and most common rheological model is the Newtonian fluid model, which assumes that the viscosity of a fluid is constant and does not depend on the shear rate or stress. The relationship between shear stress and shear rate is given by:

$$\sigma = \eta \dot{\gamma} \quad (\text{C.1})$$

where σ is the shear stress, $\dot{\gamma}$ is the shear rate, and η is the viscosity. This model is often used to describe low-viscosity fluids such as water or air.

Reference: R. B. Bird, R. C. Armstrong, and O. Hassager, Dynamics of Polymeric Liquids, Volume 1: Fluid Mechanics, John Wiley & Sons, 1987. [Bird, 1987]

Power-law fluid model: Many fluids, par-

Answer 3 (continued)

ticularly non-Newtonian fluids, exhibit shear-thinning or shear-thickening behavior, where the viscosity changes with the shear rate. The power-law fluid model describes this behavior using the following relationship:

$$\sigma = K \dot{\gamma}^n \quad (\text{C.2})$$

where K is a constant, n is the flow behavior index, and $\dot{\gamma}$ is the shear rate. This model is often used to describe materials such as paints, slurries, and food products.

Reference: H. A. Barnes, J. F. Hutton, and K. Walters, An Introduction to Rheology, Elsevier, 1989.[Barnes, 1993]

Herschel-Bulkley fluid model: The Herschel-Bulkley model extends the power-law model by including a yield stress, below which the material does not flow. The relationship between shear stress and shear rate is given by:

$$\sigma = \tau_0 + K \dot{\gamma}^n \quad (\text{C.3})$$

where τ_0 is the yield stress. This model is often used to describe materials such as drilling fluids, muds, and concrete.

Reference: R. L. Tanner and F. N. Catchmark, "Herschel-Bulkley flow in drilling fluids," Society of Petroleum Engineers Journal, vol. 7, no. 3, pp. 253-264, 1967.

Maxwell fluid model: The Maxwell fluid model describes viscoelastic materials, which exhibit both viscous and elastic behavior. The model consists of a dashpot and spring in series, and the relationship between stress and strain is given by:

$$\sigma = \mu \varepsilon + \eta \frac{d\varepsilon}{dt} \quad (\text{C.4})$$

where μ is the viscosity, η is the elastic modulus, ε is the strain, and $d\varepsilon/dt$ is the strain rate. This model is often used to describe materials such as polymers and biological fluids.

Reference: R. B. Bird, R. C. Armstrong, and O. Hassager, Dynamics of Polymeric Liquids, Volume 2: Kinetic Theory, John Wiley & Sons, 1987.[Bird, 1987]

Generalized Maxwell fluid model: The generalized Maxwell model extends the Maxwell model by including multiple dashpots and springs in series. The relationship between stress and strain is given by:

$$\sigma = \mu \varepsilon + \sum_i \left(\eta_i \frac{d\varepsilon}{dt} \right) \quad (\text{C.5})$$

Answer 3 (continued)

Where μ is the viscosity, η_i is the elastic modulus of the i -th spring, and $d_t \varepsilon_i$ is the strain rate of the i -th dashpot. This model is often used to describe complex fluids such as emulsions and suspensions.

Reference: E. W. Merrill and R. G. Larson, "Constitutive equations for polymer melts and concentrated solutions," *Journal of Rheology*, vol. 41, no.

^aThe hyperlink BibTeX bibliographic references were added by me to have a proper reference in the bibliography.

Analysis 3. Starting with the Newtonian fluid model in equation (C.1), it is indeed one of the simplest model to list so it deserves to be the first in the state of the art. The relationship is displayed and described correctly while giving relevant examples. The reference exists properly.

For the power-law fluid in equation (C.2), it is also a relevant sequel following the Newtonian fluid model. The relationship is displayed, described and illustrated with examples properly. I regret that the various behaviours like shear-thinning and shear-thickening were not related to the flow index n . The reference exists also and is relevant.

For the Herschel-Bulkley fluid model in equation (C.3), the description, the relationship and the examples are reported correctly. Nevertheless, as before, the reference, because it is an article, does not exist.

The Maxwell fluid model given in equation (C.4) shows a big confusion. Indeed, the actual Maxwell fluid model exists and exhibits a spring and a dashpot in series but does not express the relationship as in equation (C.4). Equation (C.4) is the relationship for the Kelvin-Voigt model [Kelvin, 1890; Voigt, 1890] with a spring and a dashpot in parallel. The actual relationship for the Maxwell model is

$$\frac{\sigma}{\eta} + \frac{1}{\mu} \frac{d\sigma}{dt} = \frac{d\varepsilon}{dt}. \quad (\text{C.6})$$

Even if the source is correct, the restitution is wrong.

The Generalized Maxwell model in equation (C.5) is consequently wrong due to the previous comments and the source is substantially non existing.

Question 4. (Asked on 5 May 2023 at 12pm) Do the same for rheological models more related to colloidal suspensions

Answer 4. Sure, here's a state of the art of some rheological models that are more related to colloidal suspensions, along with their equations and references:

1. Dynamic Yield Stress Fluid Model:

The dynamic yield stress fluid model is used to describe the rheological properties of complex fluids, including colloidal suspensions, which exhibit a yield stress. The model describes the stress response of the suspension using a Herschel-Bulkley-like equation with the addition of a time-dependent term:

$$\sigma = \tau_y + K \dot{\gamma}^n + \eta_0 \frac{d}{dt} \left(\frac{\dot{\gamma}}{\dot{\gamma}_0} \right)^m \quad (\text{C.7})$$

where σ is the shear stress, τ_y is the yield stress, K is a consistency index, $\dot{\gamma}$ is the shear rate, n is the flow behavior index, η_0 is a time constant, and $\dot{\gamma}_0$ is a reference shear rate. The parameter m is related to the magnitude of the time-dependent term.

Reference: A. Fall, Y. Zou, and J. M. Chaikin, "Direct measurement of the yield stress in a colloidal glass," *Physical Review Letters*, vol. 98, no. 11, p. 118301, 2007.

2. Soft Glassy Rheology Model:

The soft glassy rheology model is used to describe the nonlinear viscoelastic behavior of complex fluids, including colloidal suspensions. The model assumes that the suspension is composed of soft particles that interact through a repulsive potential. The relationship between the stress and strain rate is given by:

$$\sigma = G_\infty \gamma + \frac{G_0}{(1 + \tau_0 \dot{\gamma})^n} \quad (\text{C.8})$$

where σ is the shear stress, γ is the strain rate, G_∞ is the high-frequency modulus, G_0 is the low-frequency modulus, τ_0 is a time constant, and n is a nonlinear exponent.

Reference: S. H. Lee and S. R. Nagel, "Rheology of soft materials," *Annual Review of Condensed Matter Physics*, vol. 1, no. 1, pp. 347-369, 2010.

3. Colloid Gel Model:

The colloid gel model is used to describe the gelation behavior of colloidal suspensions. The model assumes that the suspen-

Answer 4 (continued)

sion consists of colloidal particles that interact through a repulsive potential, leading to the formation of a gel network. The relationship between the stress and strain is given by:

$$G(t) = G_0 \left(1 - \frac{\phi(t)}{\phi_c}\right)^2 \quad (\text{C.9})$$

where $G(t)$ is the time-dependent elastic modulus, G_0 is the initial elastic modulus, $\phi(t)$ is the volume fraction of the gel, and ϕ_c is the critical volume fraction at which the gel forms.

Reference: P. Sollich, "Rheological constitutive equation for a model of soft glassy materials," *Physical Review E*, vol. 58, no. 6, pp. 738-759, 1998.

Analysis 4. This question is more technical but is interesting to assess.

1. I was not able to properly find the Dynamic Yield Stress Fluid Model. I cannot tell if this is an actual model and if the mathematical expression in [equation \(C.7\)](#). The interesting thing is that the description of the [equation \(C.7\)](#) is clear and complete with the Herschel-Bulkley model [Herschel, 1926a; Herschel, 1926b] and the complement. As usual, the source does not exist.
2. The Soft Glassy Rheology model exists and is well described in [Sollich, 1997; Sollich, 1998] but is not associated to the description and the [equation \(C.8\)](#). The model in [equation \(C.8\)](#) may actually exist but is totally unrelated with the Soft Glassy Rheology Model. The citation is, as usual for articles, not existing in the literature.
3. The Colloid Gel Model may exist but the formulation of [equation \(C.9\)](#) is not linked to this model as well as the reference of [Sollich, 1998] which is actually linked to the previous Soft Glassy Rheology Model. Hence each information independently may be interesting but their relationship is not relevant.

In conclusion of this analysis, the artificial intelligence tool *ChatGPT* may be very interesting for having a first approach, but does not allow a comprehensive perspective of this field and, maybe, other fields in general.

C.3 Questions about chapter 2

The content of the discussion is available at this link : <https://chat.openai.com/share/f02eae5e-75cd-4744-b72e-32739bac2b78>

Question 5. (Asked 12 April 2023 at 4pm) In the context of colloidal suspension, can you give the relationship between the adhesion number and the Mason number ?

Answer 5. The adhesion number and the Mason number are both dimensionless quantities used to characterize colloidal suspensions. The adhesion number (Ad) is a measure of the tendency of particles in a suspension to adhere to a surface, while the Mason number (Ma) is a measure of the degree of agitation or turbulence in the suspension.

The relationship between Ad and Ma depends on the specific characteristics of the suspension, but in general, a higher Ad corresponds to a higher likelihood of particle adhesion to surfaces, while a higher Ma corresponds to a greater degree of mixing and dispersion of the particles in the suspension.

In some cases, a higher Ad may lead to particle accumulation near surfaces, which can reduce the effective Mason number and increase the likelihood of particle agglomeration or settling. In other cases, a higher Ma may help to prevent particle adhesion by keeping the particles in suspension and preventing them from settling or accumulating near surfaces.

In summary, while there is no simple formula to relate Ad and Ma , they are both important factors that can affect the behavior of colloidal suspensions and should be carefully considered when designing and analyzing colloidal systems.

It is true that the adhesion number and the Mason number are two dimensionless quantities. The fact that the adhesion number is the measure of the tendency of the particle to adhere to a surface is partly true because, here, it is more about the adhesion between the particles. However, the Mason number is not a measure of the degree of agitation or turbulence in a suspension because, normally, (i) there is no turbulence in such rheological applications and (ii) the agitation is directly related to the potential of interaction in the sense that the depth of the potential well is usually expressed in terms of thermal agitation.

It is true that the adhesion number and the Mason number are two dimensionless quantities. The fact that the adhesion number is the measure

Answer 5 (continued)

of the tendency of the particle to adhere to a surface is partly true because, here, it is more about the adhesion between the particles. However, the Mason number is not a measure of the degree of agitation or turbulence in a suspension because, normally, (i) there is no turbulence in such rheological applications and (ii) the agitation is directly related to the potential of interaction in the sense that the depth of the potential well is usually expressed in terms of thermal agitation.

Analysis 5. It is true that the adhesion number and the Mason number are two dimensionless quantities. The fact that the adhesion number is the measure of the particle tendency to adhere to a surface is partly true because, here, it is more about the adhesion between the particles. However, the Mason number is not a measure of the degree of agitation or turbulence in a suspension because, normally, (i) there is no turbulence in such rheological applications and (ii) the agitation is directly related to the potential of interaction in the sense that the depth of the potential well is usually expressed in terms of thermal agitation.

The second paragraph is partly true but there is no clear relationship expressed.

The third paragraph described roughly the good phenomenology even if we are not interested in surfaces in general.

We were expecting to write $Ad Ma = 1$ which is not the explicit answer received.

Question 6. (Asked on 12 April 2023 at 5pm) Can you write a mathematical relationship between Ad and Ma ?

Answer 6. There is no single, universal mathematical relationship between Ad and Ma that applies to all colloidal suspensions, as the specific relationship depends on the physical and chemical properties of the particles and the fluid in which they are suspended.

However, for some specific systems, empirical relationships have been proposed to relate Ad and Ma . One example is the following equation proposed by Mason and Malinauskas for spherical particles:

$$Ad = \frac{4\pi\eta a\sigma_g}{3(1-\phi)k_B T} \quad (C.10)$$

$$Ma = \frac{\rho a^3 \omega^2}{\eta D} \quad (C.11)$$

Answer 6 (continued)

where η is the viscosity of the fluid, a is the particle radius, σ_g is the surface energy of the particles, ϕ is the volume fraction of the particles, k_B is the Boltzmann constant, T is the temperature, ρ is the density of the fluid, ω is the angular velocity of the agitation, and D is the diffusion coefficient of the particles.

This equation can be used to explore the relationship between Ad and Ma for specific colloidal systems, but it should be noted that it is only applicable to spherical particles and does not take into account other factors that can affect the behavior of colloidal suspensions, such as particle shape, charge, and interactions with the surrounding fluid.

Analysis 6. If we analyse equations (C.10) and (C.11), we see that Ad has the unit of $\text{kg}\cdot\text{m}^{-2}\cdot\text{s}^{-1}$ and Ma has the unit of m^{-1} which are not dimensionless and contradicts the previous answer defining these two numbers.

Question 7. (Asked on 12 April 2023 at 6pm) Can you prove mathematically that $Ad = 4\pi\eta a\sigma_g/3(1-\phi)k_B T$?

Answer 7. The derivation of the equation $Ad = 4\pi\eta a\sigma_g/3(1-\phi)k_B T$ for the adhesion number involves several steps and assumptions based on the DLVO theory. Here, I will provide a brief outline of the derivation, but please note that this is a simplified summary and some of the details have been omitted for brevity.

Consider two spherical particles of radius a , separated by a distance h , in a fluid of viscosity η and at a temperature T . The van der Waals interaction energy between the particles can be expressed as:

$$E_{\text{vdw}} = -\frac{A}{12\pi h^2} \quad (C.12)$$

where A is the Hamaker constant, which depends on the material properties of the particles and the surrounding medium.

The total interaction energy between the particles can be expressed as the sum of the van der Waals energy and the repulsive electrostatic energy:

$$E_{\text{total}} = E_{\text{vdw}} + E_{\text{electrostatic}} \quad (C.13)$$

The electrostatic energy can be approximated by the DLVO potential:

Answer 7 (continued)

$$E_{\text{electrostatic}} = \frac{k_e Z^2 e^2}{h \exp(\kappa a)} \quad (\text{C.14})$$

where k_e is the Coulomb constant, Z is the zeta potential of the particles, e is the elementary charge, κ is the Debye-Hückel screening parameter, and a is the particle radius.

The adhesion number Ad is defined as the ratio of the van der Waals interaction energy to the thermal energy ($k_B T$):

$$\text{Ad} = -\frac{E_{\text{vdw}}}{k_B T} \quad (\text{C.15})$$

Substituting the expression for E_{vdw} and simplifying, we obtain:

$$\text{Ad} = \frac{4\pi\eta a \sigma_g}{3(1-\phi)k_B T} \quad (\text{C.16})$$

where σ_g is the surface energy of the particles, defined as:

$$\sigma_g = \frac{9Aa}{16\pi} \quad (\text{C.17})$$

The derivation of this equation involves several assumptions and simplifications, and the resulting equation is only applicable under certain conditions and for certain types of particles. However, it provides a useful approximation for the adhesion number and can be used to estimate the tendency of particles to adhere to surfaces in colloidal suspensions.

Analysis 7. Looking at the expression of the adhesion number in equation (C.10) may ring comparing to previous studies we have shown. Nevertheless, the factor $1 - \phi$ at the denominator does not seem right regardless of the context. When we ask the artificial intelligence to demonstrate this expression, we find that the transition between equations (C.15) and (C.16) is completely wrong because ϕ and η did not play any role in the previous assumptions, π disappeared in the Van der Waals energy expression, $h^2 = a^2$ moved to the numerator and 12 became 4/3. Nevertheless, we can acknowledge that the DLVO theory is properly described with the Van der Waals and the electrostatic contribution taking into account the Debye length.

I think that this is an interesting argument to consider carefully some properties declared by artificial intelligence tools.

C.4 Questions about chapter 3

The content of the discussion is available at this link : <https://chat.openai.com/share/7d7a1767-d5b5-4b24-8de4-43192f178c84>

Question 8. (Asked on 1 May 2023 at 6pm) In the context of colloidal suspensions, can you give me mathematical scaling laws relating the storage elastic modulus to the particle volume fraction ?

Answer 8. Yes, there are several mathematical scaling laws that relate the storage elastic modulus (G') of colloidal suspensions to the particle volume fraction (ϕ). Here are some of the most commonly used:

1. Einstein's equation: This is a classical result that relates the viscosity of a dilute suspension to the size and number density of the suspended particles. By assuming that the particles are small compared to the suspension volume, and that they move randomly and independently of one another, Einstein derived the following equation:

$$G' = \frac{k_B T \phi}{6\pi\eta a} \quad (\text{C.18})$$

where k_B is the Boltzmann constant, T is the absolute temperature, η is the viscosity of the suspending medium, a is the radius of the suspended particles, and ϕ is the volume fraction of particles. This equation assumes that the suspension is dilute and that the particles are non-interacting, so it is only valid for very low ϕ .

2. Scaling law for attractive suspensions: When particles are attracted to one another, they can form clusters or aggregates that affect the rheological properties of the suspension. In this case, the storage modulus can be related to the particle volume fraction by the following scaling law:

$$G' \sim \phi^n \quad (\text{C.19})$$

where n is a power law exponent that depends on the strength and range of the interparticle attraction. For weakly attractive or short-range interactions, n is typically around 2. For strongly attractive or long-range interactions, n can be as high as 4.

3. Jamming transition: At high particle volume fractions, colloidal suspensions can undergo

Answer 8 (continued)

a jamming transition, where the particles become tightly packed and the system transitions from a liquid-like to a solid-like state. Near the jamming point, the storage modulus can be related to the distance from the critical volume fraction (ϕ_c) by the following scaling law:

$$G' \sim |\phi - \phi_c|^a \quad (\text{C.20})$$

where a is a critical exponent that characterizes the behavior of the system near the jamming point. The value of a depends on the details of the interparticle interactions, but it is typically between 0.5 and 1.5.

These scaling laws are useful for understanding the behavior of colloidal suspensions as a function of particle volume fraction, and can help predict their rheological properties in different regimes. However, it's important to keep in mind that these laws are based on simplifying assumptions and may not be exact for all systems.

Analysis 8. If I start step by step to analyse the answer there are some valid statements and some wrong declarations :

1. About [equation \(C.18\)](#), this looks very similar to the Stokes-Einstein relationship at low Reynolds number with Brownian particles. However, it is only resemblance due to the fact that the right side of [equation \(C.18\)](#) has the unit $\text{kg}\cdot\text{m}^{-1}\cdot\text{s}^{-2}$ where as the left side has the unit $\text{m}^2\cdot\text{s}^{-1}$. The correct Stokes-Einstein relationship is

$$D = \frac{k_B T}{6\pi\eta a} \quad (\text{C.21})$$

with D the diffusion coefficient of the particles.

2. About [equation \(C.19\)](#), this one is really close to what is studied in this manuscript and actually rather valid so I will dig further about this notion in the next question.
3. About [equation \(C.20\)](#), this relationship is also relatively true in the sense that close to the jamming point most of the interesting quantities depends on a power-law relationship between the quantity and the distance of the variable of control from the value of this variable at the critical point, in this case the particle volume fraction. I cannot comment

Analysis 8 (continued)

on the value of the exponent because it is not the focus of this manuscript but it seems reasonable to me.

I agree also with the concluding remarks on the fact that it helps for predictions but rely on simplifying assumptions that should be well understood before applying blindly.

Question 9. (Asked 1 May 2023 at 7pm) On which parameters n depends ? Give an analytical expression of this dependence

Answer 9. The power law exponent n in the scaling law for attractive suspensions, $G' \sim \phi^n$, depends on the strength and range of the interparticle attraction. There is no general analytical expression for n that holds for all types of interparticle interactions, but for some specific cases, it is possible to derive an expression for n .

For example, in the case of hard-sphere-like repulsions and short-range attractions, the exponent n can be expressed analytically as:

$$n = 2 + \frac{9\pi}{16} \left(\frac{\sigma}{a}\right)^2 (1 - \epsilon)^{-2} \quad (\text{C.22})$$

where σ is the diameter of the particles, a is the range of the attraction, ϵ is the depth of the attraction potential in units of $k_B T$, and $k_B T$ is the thermal energy. This expression is derived from a perturbative expansion of the pair distribution function of the particles, and it assumes that the attractions are weak compared to the repulsions.

For other types of interactions, such as electrostatic repulsions or van der Waals attractions, the exponent n may have a different functional form, and an analytical expression may not be available. In general, the value of n can be determined empirically from rheological measurements of the suspension as a function of particle volume fraction.

Analysis 9. In comparison with the content exposed in [chapter 3](#), there is no dependence on the exponent n on the fractal dimension of aggregates. I was not able to find the analytical expression of [equation \(C.22\)](#) thus I cannot assess the quality of the expression nor the relevance in the case of a hard-sphere suspension.

Question 10. (Asked on 1 May 2023 at 7pm) Is there a dependence of n on the fractal dimension?

Question 10 (continued)

If yes, give the mathematical expression

Answer 10. Yes, in the case of attractive suspensions where the particles form fractal aggregates, the power law exponent n can depend on the fractal dimension of the aggregates. The fractal dimension (D_f) is a measure of how much space the aggregates fill up, and it can be related to the particle volume fraction by the following scaling law:

$$\phi \sim R^{-D_f} \quad (\text{C.23})$$

where R is the characteristic radius of the aggregates.

The relationship between the fractal dimension and the power law exponent n depends on the details of the interparticle interactions, and there is no general expression that holds for all cases. However, for some specific types of interactions, it is possible to derive an expression for n in terms of D_f .

For example, in the case of diffusion-limited cluster aggregation (DLCA) where the aggregates form by random sticking of particles, the exponent n can be related to the fractal dimension by the following expression:

$$n = \frac{D_f + 1}{3} \quad (\text{C.24})$$

This expression assumes that the interparticle attraction is short-ranged and that the aggregates are large compared to the particle size. For other types of interactions or aggregate formation mechanisms, the relationship between n and D_f may be different.

Analysis 10. The relationship of equation (C.23) is wrong because the usual assumption of models relating rheological quantities to microscopic structure [Shih, 1990; Wu, 2001; Mellema, 2002] is, with the same notations,

$$\phi \propto R^{D_f - \text{dim}}. \quad (\text{C.25})$$

Hence, it is totally misleading even if the spirit is the same. Also, I have tried to overcome the previous assumption in chapter 3. About equation (C.24), from all the usual models, there is no dependence of the numerator of the exponent n on the fractal dimension D_f but on the chemical dimension d instead. The denominator should also show a difference between dim and D_f as reported in [Bouthier, 2022]. Finally, the Diffusion Limited Cluster Aggregation does not have any

Analysis 10 (continued)

impact on the mechanics: it has an impact on the value of the fractal dimension D_f but not on the relationship between the storage modulus G' and the particle volume fraction.

Question 11. (Asked on 6 June 2023 at 11am)
Can you demonstrate $n = (D_f + 1)/3$?

Answer 11. Certainly! I can demonstrate the relationship between the power law exponent n and the fractal dimension D_f for diffusion-limited cluster aggregation (DLCA).

In DLCA, particles randomly move in space, and when they come into contact, they stick together to form aggregates. The aggregates grow through the random sticking of particles, resulting in a fractal structure. The fractal dimension D_f characterizes the space-filling properties of these aggregates.

To relate the fractal dimension to the power law exponent, we start with the assumption that the storage modulus G' scales with the particle volume fraction ϕ according to the power law:

$$G' \sim \phi^n \quad (\text{C.26})$$

Next, we use the scaling relation between the particle volume fraction and the aggregate size R :

$$\phi \sim R^{-D_f} \quad (\text{C.27})$$

Taking the logarithm of both sides, we have:

$$\ln(\phi) \sim -D_f \ln(R) \quad (\text{C.28})$$

Now, let's differentiate both sides of the equation with respect to $\ln(R)$ (keeping in mind that $\ln(R)$ is related to the fractal dimension):

$$\frac{d \ln(\phi)}{d \ln(R)} = -D_f \quad (\text{C.29})$$

Next, we differentiate the power law relation $G' \sim \phi^n$ with respect to $\ln(R)$:

$$\frac{d \ln(G')}{d \ln(R)} = n \quad (\text{C.30})$$

Now, we can substitute the expression for $\frac{d \ln(\phi)}{d \ln(R)}$ into the equation above:

$$\frac{d \ln(G')}{d \ln(R)} = -D_f \quad (\text{C.31})$$

Answer 11 (continued)

This gives us:

$$n = -D_f \quad (\text{C.32})$$

Finally, we rearrange the equation to get n in terms of D_f :

$$n = \frac{D_f + 1}{3} \quad (\text{C.33})$$

This demonstrates the relationship between the power law exponent n and the fractal dimension D_f for diffusion-limited cluster aggregation (DLCA).

It's important to note that this relationship holds specifically for DLCA, and for other types of interactions or aggregate formation mechanisms, the relationship between n and D_f may be different.

Analysis 11. I think that no further comments are needed for both assumptions and demonstration.

C.5 Conclusion

To summarise this chapter, we have shown that on our specific topic some general information may have been caught by the artificial intelligence but some basic contradictions undermined the answers which gives in the end a very poor quality results. The critical mind is then absolutely necessary to filter the information. We are not criticising all the efforts made to build such an artificial intelligence tools but we clearly warn the reader that, even if it might be useful to introduce a topic, a sound expertise is still needed to properly catch the right information.

List of Figures

1.1	Map of the nuclear power plants in France in 2019. Extracted from [RTE, 2023]	2
1.2	Maps of the radioactive materials locations and of the radioactive waste warehousing and storage sites on 31 December 2021. Extracted from [ANDRA, 2023]	3
1.3	Usual rheological elements used to build rheological laws. From left to right, there are a spring of constant E , a dashpot of viscosity η and a friction element of yield stress σ_y	5
1.4	Elastoviscoplastic model proposed by [Saramito, 2007] to account for multiple physical processes in some materials taking a thermodynamic framework approach	7
1.5	Ladder arrangements used to model scaling behaviours. According to the physical regime, the box B represents (a) a Maxwell element (pregel), (b) an infinite ladder (critical gel), and (c) a spring (postgel). Extracted from [Schiessel, 1995a]	8
1.6	General curves of shear stress vs shear rate: (1) Newtonian; (2) shear thinning; (3) shear thickening; (4), (5) materials with yield stress. Extracted from [Mewis, 2012].	9
1.7	Predictions from Truesdell, Green-Naghdi and Jaumann objective stress rates under simple shear test of a hypoelastic material with constant elastic moduli. The ratio of the shear stress to the displacement is plotted as a function of time. The same moduli are used with the three objective stress rates. Extracted from [Wikipedia contributors, 2022b] and inspired from [Dienes, 1979]	10
1.8	Temperature versus volume fraction phase diagram. The glass lines separate the 'liquid' regions, where particles are able to diffuse, from the 'glass' regions. The vertical black dashed line represents the hard-sphere glass line. In the case of short-range attractive colloids, the re-entrant (non-monotonic) shape of the glass line (solid red and blue lines) creates a pocket of liquid states that are stabilized by the short-range attraction. The location of the theoretical glass-glass transition line (thick blue line) and the proposed connection between the gel-line (at low volume fractions) and the attractive glass line (solid blue line) are also indicated. Equilibrium (and metastable) lines between gas, liquid and solid phases — which in the case of attractive colloids are significantly different from the case of long-range attractions — are not shown. Extracted from [Sciortino, 2002].	12
1.9	Construction of clusters	14
1.10	Generic depiction of scattering from a mass fractal aggregate of radius R with a fractal dimension D_m made up of spherical, smooth surfaced monomers of radius a . Upper curve is for point particles, second curve is for spherical particles, lowest curve is the product of these. Extracted from [Sorensen, 2001]	15
1.11	Dynamics of aggregation and breakage for discretised population balance, adapted from [Biggs, 2002; Jeldres, 2018]	16
1.12	The ratio of the number flux of droplets of kind j to its value at $x = 0$ as a function of the dimensionless distance z_j for various values of $(t_j + 1)/s_j$. Extracted from [Williams, 1985]	16
1.13	Schematic structure of a colloidal gel. The circles indicate fractal clusters of size ξ . The regions between the flocs are regarded as links. Extracted from [Shih, 1990]	16
1.14	Sketch to explain the scaling relationship between the macroscopic stiffness K and the microscopic stiffness k for a network of size L with an element size l and a dimension dim . The arrows represent the stretching/compressing direction.	18
1.15	Storage modulus and limit of linearity strain as a function of the particle volume fraction for Catal and Dispal particles. Extracted from [Shih, 1990]	19

1.16	Microscopy images showing six steps to complete network percolation of a colloidal network. Snapshot (a) corresponds to the initial crystal structure, just after adding the salt. Images (b)–(e) correspond to the fractal regime, where cluster-cluster aggregation dominates. Snapshot (f) shows the structure when the first percolating backbone was formed. Notice the presence of small aggregates and single particles coexisting with a large structure. The overall surface coverage is approximately 0.1; the time scales refer to the time after the addition of salt and surfactant. Extracted from [Masschaele, 2009]	22
1.17	Sketch of the disaggregation and reaggregation processes under a uniform external stress σ . The numbers represent different sizes of aggregates with different levels of energy. The aggregates are disaggregating and reaggregating according to the stress solicitation. Transition from state 1 to states 2 and 3 corresponds to a “fragile” rupture, while transition from state 1 to state 4 is an “erosion” process. Extracted from [Bouthier, 2023a].	22
1.18	Gyration radius of agglomerate at the quasi-steady state as functions of the particle adhesion parameter Ad_p for two different types of flows. Extracted from [Ruan, 2020]	23
1.19	Agglomeration regime maps. Phase diagram illustrating the observed cases as a function of the Reynolds number Re and the adhesion number Ad at different solid volume fractions and different models. Extracted from [Qian, 2022].	24
1.20	Flow curves predicted for a range of temperatures T across the mode-coupling critical temperature T_c ; $\epsilon = T_c - T$ is the distance to the critical temperature, and the shear rate is rescaled by a microscopic time unit τ to form a Péclet number $Pe_0 = \dot{\gamma}\tau$. The inset shows the discontinuous emergence of the yield stress at T_c . Extracted from [Fuchs, 2003]	25
1.21	Relative steady shear viscosity as a function of the Weissenberg number $We = Wi$ for an upper convective derivative with no additional solvent viscosity for different Bingham numbers $Bi = Bm$. Extracted from [Saramito, 2007]	25
1.22	Rheological phase diagram in (De, b) -space for rectilinear, (a) wall-driven shear flow with oblate anchoring walls and (b) pressure-driven flow with oblate anchoring walls, $N = 5.35$, and $\beta_s = 0.01$. Regions in (De, b) -space are marked by which states are stable solutions. The possible states are logrolling (L), composite (C), tumbling (T), wagging (W), and flow-aligning (F). In regions where logrolling and inplane solutions are both stable, the initial state determines which state is obtained. The phase diagram is constructed through individual simulations, so error bars estimate the possible range for transition values. Extracted from [Green, 2009].	25
1.23	Nusselt number Nu_ω as a function of the Taylor number Ta for various a . A universal scaling $Nu_\omega \propto Ta^{0.38}$ is revealed. Extracted from [Gils, 2011].	26
2.1	Illustrations of the Bose-Einstein statistics	32
2.2	Simulated particle distributions for $V = 10$, $h = 206$, and $C = 1$ after the preparation step prior to shearing (a) and at after shearing in the Couette geometry (b). Rendering using <i>Ovito</i> [Stukowski, 2010]. (c) Cluster detection and various estimates of the cluster size as defined in the text for the top right particle distribution.	34
2.3	Energy functional $\beta\mathcal{E}(k) - \alpha_k k$ computed from equation (2.7) as a function of the number k of particles in a cluster for (left) Couette flow and (right) Poiseuille flow. Colors correspond to the adhesion number Ad as indicated in the legend. Results obtained from simulations performed with $h = 103$ or $h = 206$	34
2.4	(a) Mass k_{\min} of the clusters corresponding to the energy minimum and (b) cluster size ℓ defined as the weighted average of the radius of gyration of the clusters, as a function of the adhesion number Ad for Couette flow (\bullet) and Poiseuille flow (\square) and for two different width $h = 103$ (blue) and $h = 206$ (orange). Solid and dotted lines correspond to the best power-law fits respectively for the Couette and the Poiseuille flow, and computed over $Ad \in [2, 200]$. (c) Cluster size ℓ as a function of the equilibrium mass k_{\min} . The black solid line corresponds to $\ell \propto k_{\min}^{1/2}$. Same symbols and colors as in (a) and (b).	36
2.5	Sketch of the disaggregation and reaggregation processes under a uniform external stress σ . The numbers represent different sizes of aggregates with different levels of energy. The aggregates are disaggregating and reaggregating according to the stress solicitation. Transition from state 1 to states 2 and 3 corresponds to a "fragile" rupture, while transition from state 1 to state 4 is an "erosion" process.	37

2.6	Power-law exponent β in $\ell/a = Ad^\beta$ as a function of the fractal dimension D of the aggregates extracted from [Ruan, 2020; Hunter, 1980; Sonntag, 1986; Sonntag, 1987a; Sonntag, 1987b; Brakalov, 1987; Torres, 1991a; Torres, 1991b; Harshe, 2011; Potanin, 1991; Potanin, 1992; Potanin, 1996; Wessel, 1992; Higashitani, 1998; Higashitani, 2001; Eggersdorfer, 2010; Kimbonguila Manounou, 2014; Zaccone, 2009a; Conchúir, 2013; Xie, 2010] (●) and compared to the model prediction $\beta = (1 + D)^{-1}$ (blue solid line).	40
2.7	Sensitivity study of ℓ predicted by equation (2.23) upon relative variations of the different control parameters around the values listed in the first line of table 2.2 except for the fractal dimension, which is varied from 1 to 3.	41
2.8	Experimental protocol: schematic of the flow cessation and characterization sequences.	42
2.9	Flow cessation sequence performed with different values of the shear rate $\dot{\gamma}_0$ in a $c_w = 4\%$ carbon black dispersions. The sequence is composed of two steps: a quench in shear rate from 1000 s^{-1} to $\dot{\gamma}_0$ yielding a stress response $\sigma(t)$ pictured in (a), followed by a complete flow cessation which results in (b) the relaxation of $ \dot{\gamma} (t)$ when imposing $\sigma = 0\text{ Pa}$. In (a) and (b) colors encode the value of $\dot{\gamma}_0$ ranging from 1500 (black) to 0.1 s^{-1} (yellow), see legend in (b).	43
2.10	(a) Elastic G' and viscous modulus G'' vs. the frequency f in a $c_w = 4\%$ carbon black dispersions. The color codes for the shear rate intensity $\dot{\gamma}_0$ applied before flow cessation. (b) Normalized viscoelastic spectrum: G'/G_c and G''/G_c vs. the normalized frequency f/f_c , where G_c and f_c denote respectively the modulus and the frequency at which $G' = G''$ in (a). The blue curves correspond to a Kelvin-Voigt model (see appendix A.5). The grey curves correspond to the master curves obtained for G' (solid line) and G'' (dashed line) by rescaling viscoelastic spectra of CB dispersions in oil for various volume fractions [data extracted from [Trappe, 2000]]. Inset: G_c vs. f_c . The red dotted line is the best linear fit of the data: $G_c = 14.5f_c$. (c) Evolution of G_c (top) and f_c (bottom) vs. $\dot{\gamma}_0$. The red line is the best fit of the data using equation (3.1) and the structural information reported in figure 2.12. The best fit is obtained with a single adjustable parameter, namely the prefactor $G_{CB} = 9\text{ Pa}$	44
2.11	(a) Evolution of G_c as a function of the weight concentration in carbon black particles c_w for various shear rates applied prior to flow cessation: $\dot{\gamma}_0 = 0.1\text{ s}^{-1}$ (circle), 2 s^{-1} (diamond), 100 s^{-1} (triangle) and 1500 s^{-1} (square). Red lines are the best power-law fit of the data $G_c = (c_w/C_1)^\alpha$. Both α and C_1 depend on $\dot{\gamma}_0$. (b) α and C_1 vs. the shear rate $\dot{\gamma}_0$. Red lines are the best logarithmic fit of the data: $\alpha = \log_{10}(\dot{\gamma}_0/\dot{\Gamma}_1)$ with $\dot{\Gamma}_1 = 10^{-3.9}\text{ s}^{-1}$ and $C_1 = C_2 \log_{10}(\dot{\gamma}_0/\dot{\Gamma}_2)$ with $C_2 = 0.7\%$ and $\dot{\Gamma}_2 = 0.015\text{ s}^{-1}$. Dotted lines are the best power law fits. (c) Evolution of G_c as function of the dimensionless concentration and shear rate.	45
2.12	Structure of the gel obtained after flow cessation. The scattering intensity $I(q)$ is measured 360 s after the end of the flow cessation test for different preshear $\dot{\gamma}_0$ in carbon black dispersions at $c_w = 4\%$. (a) The thick lines represent the evolution of $I(q)$ (top) and $I.q^{d_f}$ (bottom) as a function of the wave vector q . Color codes from pink to black for $\dot{\gamma}_0 = 0.1, 2, 20$ and 100 s^{-1} . The dotted line is the form factor obtained at $c_w = 0.1\%$. Red lines are fit to the experimental data by a two-level Beaucage model composed of the CB particles of radius r_0 and clusters of size ξ_c with fractal dimension d_f , modified by an intercluster structure factor that accounts for the center-to-center distance ξ_s between the clusters. The scattering intensity $I(q)$ and $I.q^{d_f}$ are translated along the y-axis for better readability. (b) Evolution of the fit parameters ξ_c (green diamond), ξ_s (pink star), ξ_c/ξ_s (circle) and d_f (square) as a function of $\dot{\gamma}_0$. For the four fits, we obtained radius of gyration $r_0 = 28.5\text{ nm}$. (c) Schematic of the clusters evolution as the preshear $\dot{\gamma}_0$ decreases between the top and bottom panels.	46
3.1	Sketch of the contributions to the gel elasticity associated with the gel hierarchical structure.	51
3.2	Evolution of $\xi_c/\xi_s \mapsto (1 + \xi_s/(2\xi_c))^{d_f/3} (1 - \xi_s/\xi_c)^{2d_f/3}$ for different values of d_f on $[1.2, 1.8]$	53
3.3	Sketch of the double fractal structure transmitting stresses in the system, inside the clusters and between the particles	53
3.4	Sensitivity study of G' , γ_{NL} and σ_y from top to bottom respectively, according to equations (3.13) to (3.15) following the relative variation of the parameters around the value given in table 3.2. The conditions $(d, \delta) \in [1.1, 1.4]^2$, $(D, \mathcal{D}) \in]2, 3[^2$, $\epsilon \in [0, 1]$, $\alpha \in [0, 1]$ and $\text{dim} = 3$ have been implemented.	55
3.5	Example of intensity spectrum extracted from equation (3.16) with $A_\ell = 10^6\text{ a.u.}$, $A_a = 1\text{ a.u.}$, $\ell/a = 400$, $D = 2.6$ and $\mathcal{D} = 2.9$	55

3.6	Carbon black gels properties resulting from flow cessation. (a) Evolution of the gel elasticity G'_{∞} (●) as a function of $\dot{\gamma}_0$ the shear rate intensity before flow cessation. the blue line represents the fits (a) through (d) listed in table 3.3. The fits are indistinguishable. (b) Gel scattered intensity $I(q)$ as a function of the wave vector number q . The colors from light orange to black correspond to a decreasing $\dot{\gamma}_0$. The black dots correspond to the experimental form factor of the carbon black particles and the blue solid line is the fit of this form factor. $I(q)$ resulting from $\dot{\gamma}_0 = 0.1 \text{ s}^{-1}$ is on absolute scale. The rest of the data is translated along the y -axis for better readability. (c) Kratky representation, $I(q) q^2$ versus q , of the data shown in (b). The arrows point to the three bumps at q_0 , q_1 and q_2 , associated respectively to the length scales a , ξ_1 and ξ_2 . The green lines correspond to the two level modified Beaucage model (equation (3.35)) and the red dash lines correspond to three level beaucage model (equation (3.30)). Experimental data are extracted from [Dagès, 2022].	59
3.7	Sketch of the gel hierarchical structures. ϕ -power law models which model the gel elasticity G' are based at the particle scale on the colloid-colloidal interactions, at the meso scale on the aggregated structures and at the macroscopic scale on the network topology. The structural length ξ_s defined at the aggregation scale sets the coarse grain scale for the network scale. In the cluster ϕ -power law model $\xi_s = \xi$, in the clusters of clusters ϕ -power law model $\xi_s = \xi_2$ and in the interpenetration of clusters ϕ -power law model $\xi_s = \xi_1$.	60
3.8	Parameters of the scattering models resulting from fitting the scattering intensity $I(q)$ in figure 3.6, (a) using the cluster interpenetration approach (equation (3.35), green symbols) and (b) using the clusters of the clusters approach (equation (3.30), red symbols). From top to bottom: ξ_1 (◆), ξ_2 (★), ξ_1/ξ_2 (+), d_1 (●), d_2 (■) and ρ (×) as a function of the applied shear rate $\dot{\gamma}_0$ before flow cessation. The carbon black radius a is constant in all the fits and equal to $a = 27 \text{ nm}$.	62
3.9	Evolution of the gel network fractal dimension D as a function of $\dot{\gamma}_0$ for the models (a) through (d) which parameters are listed in table 3.3. The fractal dimension d_1 and d_2 from figure 3.8 are also plotted for comparison. The green data is related to the interpenetrating cluster models whereas the red data is related to the cluster of clusters model.	67
4.1	Streamlines oriented by the direction of the displacement and colored according to the dimensionless norm of the displacement $8\pi \sqrt{G/\rho G} \mathbf{u} / \omega^2 F$ in the xy plane assuming that the point force is in the x direction and applied at the origin (0, 0). The xy plane is actually a radial plane containing the force vector due to symmetry of revolution. The space units are taken as the wavelength. To compare with equation (4.15), $r^2 = x^2 + y^2$ and $\tan(\theta) = y/x$. From top to bottom, ratio of the loss modulus G'' over the storage modulus G' increases from 10^{-6} to 10^6 .	74
4.2	Evolution of the viscoelastic modulus G in the complex plane as a function of the stress intensity σ . The big red dot (●) is a reference point with $\sigma = \sigma_c$.	74
4.3	Evolution of the real part of displacement u_y as a function of the distance x from the application point of ultrasound.	75
4.4	Description of the potential fluidisation process happening in the radioactive sludges	76
A.1	Scattering intensity I vs. scattering wave number q of dilute dispersion of carbon black Vulcan PF nanoparticles in the RTM17 mineral oil ($c_w = 0.01 \%$). The red line is a mass fractal fit of such a form factor using a fractal dimension $d_{f0} = 2.9$ and a Schulz particle radius distribution $P(r)$ centered on a radius of gyration $r_g = 35 \text{ nm}$ (dashed line) with a polydispersity of 20 % as shown in the inset.	84
A.2	Flow curve of the carbon black dispersion at $c_w = 4\%w$ showing the evolution of the measured stress σ as a function of the imposed shear rate $\dot{\gamma}$. $\dot{\gamma}$ is ramped down then up between 1500 s^{-1} to 0.015 s^{-1} with 10 points per decades at a rate of one point every 1 s. The red line is an Herschel-Bulkley fit. Unstationnary flow curve extracted from the preashear at $\dot{\gamma}_0$ in figure 2.9b at $t = 1 \text{ s}$ (×), at the maximum of σ (+) and at the end of the protocol (*).	84
A.3	Evolution of the viscoelastic moduli during the rest just after the flow cessation protocol. The viscoelastic moduli G' (line) and G'' (dash) are measured during 360 s at an oscillation amplitude of $\gamma = 0.1 \%$ and a frequency of $f = 1 \text{ Hz}$.	85
A.4	$\tan(\delta)$ representation of the viscoelastic spectrum measured in figure 2.10a-b. (a) $\tan(\delta)$ as a function of the frequency f . (b) $\tan(\delta)$ as a function of the normalized frequency f/f_c .	85

A.5	Model of the normalized viscoelastic spectrum. Evolution of the normalized elastic G'/G_c (grey line) and viscous G''/G_c (dashed grey line) moduli as a function of the frequency f/f_c , extracted from [Trappe, 2000]. (f_c, G_c) are the coordinates of the crossover between G' and G'' . The Kelvin-Voigt model is pictured in blue and the fractional Kelvin-Voigt model in red.	86
A.6	Evolution of the viscoelastic spectrum for different gel concentration c_w at $\dot{\gamma}_0 = 1500 \text{ s}^{-1}$. (a) G' (line) and G'' (dash) as a function of f . The concentration is varied from $c_w = 2$ (blue) to 8% (green). (b) Rescaled viscoelastic spectrum. The grey curves are taken from [Trappe, 2000] and corresponds to the master curve obtained by scaling a concentration series of carbon black dispersion in oil.	86
A.7	Fractal dimension d_f as a function of the shear step $\dot{\gamma}_0$. Measurements of d_f extracted from the SAXS fits in figure 2.12 (square) and evaluated from figure 2.11 using the weak link model (circle) and the strong link model (diamond) from [Shih, 1990]. The fractal dimension x of the gel backbone has been varied from $x=1.5$ (light blue) to $x=2.5$ (dark blue) in the strong link model.	86
A.8	Comparison of the scattering intensity between the tangential I_{tan} (green) and radial $I_{rad\perp}$ (cyan) $I_{rad\parallel}$ (magenta) configuration.	87
A.9	Decomposition of the modified Beaucage model as written in equation (A.3). Scattering intensity $I(q)$ as a function of q : experimental data (black), I_2 (pink), $I_1 + I_2$ (cyan), $I_1.S_1 + I_2$ (red).	87
A.10	Density of particles per unit cell ρ as the function of the step shear $\dot{\gamma}_0$. ρ is calculated from the values r_0, ξ_c, d_f and ξ_s obtained fitting the scattering intensity $I(q)$ plotted in figure 2.12a with equation (A.3). The dash line is the average.	87
B.1	Evolution of the transient moduli of S_{xy}, S_{yy} and σ_{yy} and the average according to time of transient moduli of σ_{xx} and σ_{xy} , all divided by η/λ as a function $\lambda\omega$ with $\varepsilon_0 = 1$	94
B.2	Evolution of the various moduli of σ_{xy} and σ_{xx} divided by η/λ as a function ωt imposing $\lambda\omega = \varepsilon_0 = 1$	94
B.3	Evolution of the viscous moduli of σ_{xy} and σ_{xx} divided by η/λ as a function of the elastic moduli divided by η/λ imposing $\lambda\omega = \varepsilon_0 = 1$. The purple dotted line corresponds to the first bisector $y = x$	95

List of Tables

1.1	Waste management matrix according to <i>Andra</i> . Extracted from [ANDRA, 2023].	4
1.2	Compilation of various rheological models expressed in one dimension with their sources.	6
1.3	Conversion formulae between the Cauchy stress tensor σ , the Kirchhoff stress tensor τ , the Nominal stress tensor N , the first Piol-Kirchhoff stress tensor P , the second Piola-Kirchhoff stress tensor S and the Biot stress tensor T . $F = RU$ is the displacement gradient with $R^T = R^{-1}$ and U is symmetric, positive definite, right stretch and $J = \det(F)$. Extracted from [Wikipedia contributors, 2022a] and inspired from [Landau, 1959].	10
1.4	Comparison of models relating the storage modulus G' , the limit of linearity strain γ_y and the yield stress σ_y . The exponents reported in the table are the exponent of the $\phi^{\frac{1}{\dim-D}} = \ell/a$ with ϕ the particle volume fraction, \dim the dimension of the euclidean space, D the fractal dimension, ℓ the size of the cluster and a the particle size. Here above, $\epsilon \in [0, 1]$ with $\epsilon = 0$ corresponds to the stretching regime and $\epsilon = 1$ corresponds to the bending regime, then, $\alpha \in [0, 1]$ with $\alpha = 0$ corresponds to the weak-link regime and $\alpha = 1$ corresponds to the strong-link regime. Adapted from [Bouthier, 2022].	18
1.5	Comparison of scaling laws exponent m with previous studies. "E" means experimental, "N" means numerical and "T" means theoretical. Adapted from [Kimbonguila Manounou, 2014; Bouthier, 2023a]	23
2.1	Exponents and prefactors of the power-law fits in figure 2.4 for the different geometries, widths, and sizes ℓ and k_{\min}	36
2.2	Experimental parameters and measurements of the aggregate size from the literature. ℓ_{exp} is the direct measurement of the aggregate size, while ℓ_{th} is the aggregate size estimated using equation (2.23) based on the parameters defined in the text and reported in the references of the first column.	41
3.1	Comparison of the different models of the literature relating rheological quantities to microstructure. One can note that $\phi = \left(\frac{\ell}{a}\right)^{D-\dim}$ in all these models.	56
3.2	Results and parameters to assess the rheological properties in [Gibaud, 2020a; Dagès, 2021]. G'_{exp} , $\gamma_{\text{NL}}^{\text{exp}}$ are the direct measurements of the storage modulus at strain $\gamma \rightarrow 0$ and the limit strain of linearity of the carbon black particle suspension, respectively. Also, $\sigma_y^{\text{exp}} = G'_{\text{exp}} \gamma_{\text{NL}}^{\text{exp}}$. Then, G'_{th} , $\gamma_{\text{NL}}^{\text{th}}$ and σ_y^{th} are the estimated storage modulus according to equation (3.13), the limit strain of linearity according to equation (3.14) and the yield stress according to equation (3.15), respectively, with the other parameters.	57
3.3	Parameters of the models that fit G'_{∞} in figure 3.6. α and ϵ define the models. We set $G_{\text{cc}} = 6 \times 10^7$ Pa as in [Varga, 2019]. ξ_1 , d_1 , ξ_2 and d_2 are determined by the experiments (figure 3.8). \mathfrak{D} , \mathfrak{d}_1 , \mathfrak{d}_2 are kept constant to 1.25. D is the free fit parameter. Its values as a function of $\dot{\gamma}_0$ are displayed in figure 3.9. Model (e) could not fit the data for any D value.	68
4.1	Orders of magnitude for the rheological parameters to evaluate typical length scales. U is the amplitude of displacement imposed by the ultrasound and b is the width of the transducer used to produce the ultrasound.	73

Publications list

Published or accepted articles

Louis-Vincent Bouthier, Romain Castellani, Elie Hachem, Rudy Valette. "*Proposition of extension of models relating rheological quantities and microscopic structure through the use of a double fractal structure*". *Physics of Fluids* 34, 083105, 2022.

DOI: [10.1063/5.0101750](https://doi.org/10.1063/5.0101750)

Noémie Dagès, Louis-Vincent Bouthier, Lauren Matthews, Sébastien Manneville, Thibaut Divoux, Arnaud Poulesquen, Thomas Gibaud. "*Interpenetration of fractal clusters drives elasticity in colloidal gels formed upon flow cessation*". *Soft Matter* 18, 6645-6659, 2022.

DOI: [10.1039/D2SM00481J](https://doi.org/10.1039/D2SM00481J)

Louis-Vincent Bouthier, Francesco Delloro, Elie Hachem. "*Application and assessment of the Improved Delayed Detached Eddy Simulation model to the cold spray process: towards high fidelity Computational Fluid Dynamics simulations*". *Physics of Fluids* 34, 095109, 2022.

DOI: [10.1063/5.0100954](https://doi.org/10.1063/5.0100954)

Louis-Vincent Bouthier, Romain Castellani, Sébastien Manneville, Arnaud Poulesquen, Rudy Valette, Elie Hachem. "*Aggregation and disaggregation processes in clusters of particles: simple numerical and theoretical insights*". *Physical Review Fluids* 8, 023304, 2023.

DOI: [10.1103/PhysRevFluids.8.023304](https://doi.org/10.1103/PhysRevFluids.8.023304)

Louis-Vincent Bouthier, Thomas Gibaud. "*Three length scales colloidal gels: the clusters of clusters versus the interpenetrating clusters approach*". *Journal of Rheology* 67, 621-633, 2023.

DOI: [10.1122/8.0000595](https://doi.org/10.1122/8.0000595)

Articles in preparation

Louis-Vincent Bouthier, Romain Castellani, Rudy Valette, Elie Hachem, Sébastien Manneville, Thomas Gibaud, Arnaud Poulesquen, Bavand Keshavarz, Gareth McKinley. "*Cluster dynamics and rheology review* :

Microscopic and macroscopic coupling". *Reviews of Modern Physics*.

Julien Bauland, Louis-Vincent Bouthier, Arnaud Poulesquen, Thomas Gibaud. "*Structuration of attractive colloidal dispersions under shear*". .

Louis-Vincent Bouthier, Romain Castellani, Rudy Valette, Elie Hachem. "*Extension of Sequence of Physical Processes relating the second Piola-Kirchhoff stress tensor to the Green-Lagrange strain tensor*". *Journal of Rheology*.

International conference as a first author

Louis-Vincent Bouthier, Romain Castellani, Thomas Gibaud. "*Three length scales colloidal gels: the clusters of clusters versus the interpenetrating clusters approach*". 19th World Congress on Rheology (ICR 2023) Athens, Greece, July 29 – August 4, 2023.

Louis-Vincent Bouthier, Romain Castellani, Elie Hachem, Rudy Valette. "*Proposition of extension of models relating rheological quantities and microscopic structure through the use of a double fractal structure*". 19th World Congress on Rheology (ICR 2023) Athens, Greece, July 29 – August 4, 2023.

Bibliography

- [Abolhasani, 2016] Milad Abolhasani and Klavs F. Jensen. “Oscillatory multiphase flow strategy for chemistry and biology”. *Lab on a Chip* 16.15 (2016), pp. 2775–2784. ISSN: 1473-0189. DOI: [10 . 1039 / C6LC00728G](https://doi.org/10.1039/C6LC00728G) (cit. on p. 95).
- [Albert, 2002] Réka Albert and Albert-László Barabási. “Statistical mechanics of complex networks”. *Reviews of Modern Physics* 74.1 (1 2002), pp. 47–97. ISSN: 0034-6861. DOI: [10 . 1103 / RevModPhys . 74 . 47](https://doi.org/10.1103/RevModPhys.74.47) (cit. on p. 13).
- [Alexander, 1998] Shlomo Alexander. “Amorphous solids: their structure, lattice dynamics and elasticity”. *Physics Reports* 296.2 (1998), pp. 65–236. ISSN: 0370-1573. DOI: [10 . 1016 / S0370 - 1573\(97 \) 00069-0](https://doi.org/10.1016/S0370-1573(97)00069-0) (cit. on pp. 21, 40).
- [Alexeev, 2004] Boris V. Alexeev. *Generalized Boltzmann Physical Kinetics*. Elsevier, 2004. ISBN: 0-444-51582-8 (cit. on pp. 14, 36).
- [Algahtani, 2016] Obaid Jefain Julaighim Algahtani. “Comparing the Atangana-Baleanu and Caputo-Fabrizio derivative with fractional order: Allen Cahn model”. *Chaos, Solitons & Fractals* 89 (2016), pp. 552–559. ISSN: 0960-0779. DOI: [10 . 1016 / j . chaos . 2016 . 03 . 026](https://doi.org/10.1016/j.chaos.2016.03.026) (cit. on p. 7).
- [Alhulaifi, 2012] Abdulaziz S. Alhulaifi, Gregory A. Buck, and William J. Abegast. “Numerical and Experimental Investigation of Cold Spray Gas Dynamic Effects for Polymer Coating”. *Journal of Thermal Spray Technology* 21.5 (2012), pp. 852–862. ISSN: 1059-9630. DOI: [10 . 1007 / s11666 - 012 - 9743 - 4](https://doi.org/10.1007/s11666-012-9743-4) (cit. on p. 96).
- [Allen, 2017] Michael P. Allen and Dominic J. Tildesley. *Computer Simulation of Liquids*. 2nd ed. Great Clarendon Street, Oxford, OX2 6DP, United Kingdom: Oxford University Press, 2017. ISBN: 978-0-19-880319-5 (cit. on p. 17).
- [Amaya-Bower, 2010] Luz Amaya-Bower and Taehun Lee. “Single bubble rising dynamics for moderate Reynolds number using Lattice Boltzmann Method”. *Computers & Fluids* 39.7 (2010), pp. 1191–1207. ISSN: 0045-7930. DOI: [10 . 1016 / j . compfluid . 2010 . 03 . 003](https://doi.org/10.1016/j.compfluid.2010.03.003) (cit. on p. 95).
- [Andereck, 1986] C. David Andereck, S. S. Liu, and Harry L. Swinney. “Flow regimes in a circular Couette system with independently rotating cylinders”. *Journal of Fluid Mechanics* 164 (1986), pp. 155–183. ISSN: 0022-1120. DOI: [10 . 1017 / S0022112086002513](https://doi.org/10.1017/S0022112086002513) (cit. on p. 26).
- [ANDRA, 2023] ANDRA. *Inventaire national des matières et déchets radioactifs*. Tech. rep. Agence nationale pour la gestion des déchets radioactifs, 2023 (cit. on pp. 3, 4).
- [Andreotti, 2013] Bruno Andreotti, Yoël Forterre, and Olivier Pouliquen. *Granular media: between fluid and solid*. Cambridge University Press, 2013. ISBN: 9781107034792 (cit. on p. 11).
- [Aranson, 2013] Igor S. Aranson. “Collective behavior in out-of-equilibrium colloidal suspensions”. *Comptes Rendus Physique* 14 (2013), pp. 518–527. ISSN: 1631-0705. DOI: [10 . 1016 / j . crhy . 2013 . 05 . 002](https://doi.org/10.1016/j.crhy.2013.05.002) (cit. on p. 20).
- [Atangana, 2016] Abdon Atangana and Dumitru Baleanu. “New fractional derivatives with non-local and non-singular kernel: Theory and Application Heat Transfer Model”. *Thermal Science* 20.2 (2016), pp. 763–769. DOI: [10 . 2298 / TSCI160111018A](https://doi.org/10.2298/TSCI160111018A) (cit. on p. 7).
- [Atangana, 2017] Abdon Atangana and J. F. Gómez-Aguilar. “Numerical approximation of Riemann-Liouville definition of fractional derivative: From Riemann-Liouville to Atangana-Baleanu”. *Numerical Methods Partial Differential Equations* 34.5 (2017), pp. 1502–1523. DOI: [10 . 1002 / num . 22195](https://doi.org/10.1002/num.22195) (cit. on p. 8).
- [Bahbah, 2019] C. Bahbah, M. Khalloufi, A. Larcher, Y. Mesri, T. Coupeuz, R. Valette, and E. Hachem. “Conservative and adaptive level-set method for the simulation of two-fluid flows”. *Computers and Fluids* 191.104223 (2019), pp. 1–21. ISSN: 0045-7930. DOI: [10 . 1016 / j . compfluid . 2019 . 06 . 022](https://doi.org/10.1016/j.compfluid.2019.06.022) (cit. on pp. 95, 96).
- [Bahbah, 2020] Chahrazade Bahbah. “Méthodes numériques avancées pour la simulation du procédé de trempe industrielle”. PhD thesis. Université Paris sciences et lettres, 2020 (cit. on p. 95).

- [Banasiak, 2020a] Jacek Banasiak, Wilson Lamb, and Philippe Laurençot. *Analytic Methods for Coagulation-Fragmentation Models, Volume I*. Vol. 1. Monographs and Research Notes in Mathematics. CRC PressTaylor & Francis Group6000 Broken Sound Parkway NW, Suite 300Boca Raton, FL 33487-2742: CRC Press, 2020. ISBN: 978-1-4987-7265-5 (cit. on pp. 13, 23, 36, 38, 39, 48).
- [Banasiak, 2020b] Jacek Banasiak, Wilson Lamb, and Philippe Laurençot. *Analytic Methods for Coagulation-Fragmentation Models, Volume II*. Vol. 2. Monographs and Research Notes in Mathematics. CRC PressTaylor & Francis Group6000 Broken Sound Parkway NW, Suite 300Boca Raton, FL 33487-2742: CRC Press, 2020. ISBN: 978-0-367-23548-2 (cit. on pp. 13, 23, 36, 38, 39).
- [Bantawa, 2021a] Minaspi Bantawa. “Microstructure, Dynamics and Rheology of Model Soft Particulate Gels”. PhD thesis. Georgetown University, 2021 (cit. on p. 17).
- [Bantawa, 2021b] Minaspi Bantawa, Wayan A. Fontaine-Seiler, Peter D. Olmsted, and Emanuela Del Gado. “Microscopic interactions and emerging elasticity in model soft particulate gels”. *Journal of Physics: Condensed Matter* 33.414001 (2021), pp. 1–14. ISSN: 1361-648X. DOI: [10.1088/1361-648X/ac14f6](https://doi.org/10.1088/1361-648X/ac14f6) (cit. on p. 17).
- [Barabási, 2003] Albert-László Barabási. “Linked: The New Science of Networks”. *American Journal of Physics* 71.4 (2003), pp. 409–410. ISSN: 0002-9505. DOI: [10.1119/1.1538577](https://doi.org/10.1119/1.1538577) (cit. on p. 13).
- [Barabási, 1999] Albert-László Barabási and Réka Albert. “Emergence of Scaling in Random Networks”. *Science* 286.5439 (1999), pp. 509–512. ISSN: 0036-8075. DOI: [10.1126/science.286.5439.509](https://doi.org/10.1126/science.286.5439.509) (cit. on p. 13).
- [Baravian, 1998] C Baravian and Daniel Quemada. “Using instrumental inertia in controlled stress rheometry”. *Rheologica acta* 37.3 (1998), pp. 223–233 (cit. on p. 43).
- [Barber, 2004] J. R. Barber. *Elasticity*. 3rd ed. Vol. 107. Solid Mechanics and its applications. Springer Dordrecht, 2004. ISBN: 978-94-007-3101-1. DOI: [10.1007/978-90-481-3809-8](https://doi.org/10.1007/978-90-481-3809-8) (cit. on p. 4).
- [Barman, 2016] Sourav Barman and Gordon F. Christopher. “Role of capillarity and microstructure on interfacial viscoelasticity of particle laden interfaces”. *Journal of Rheology* 60.1 (2016), pp. 35–45. ISSN: 0148-6055. DOI: [10.1122/1.4935128](https://doi.org/10.1122/1.4935128) (cit. on p. 20).
- [Barnes, 1993] H. A. Barnes, J. F. Hutton, and K. Walters. *An Introduction to Rheology*. 3rd ed. Elsevier, 1993. ISBN: 0-444-87140-3 (cit. on p. 103).
- [Barnes, 1999] Howard A. Barnes. “The yield stress — a review or “ $\pi\alpha\nu\tau\alpha\ \rho\epsilon\iota$ ” — everything flows?” *Journal of Non-Newtonian Fluid Mechanics* 81 (1999), pp. 133–178. ISSN: 0377-0257. DOI: [10.1016/S0377-0257\(98\)00094-9](https://doi.org/10.1016/S0377-0257(98)00094-9) (cit. on p. 21).
- [Barthel, 2008] E. Barthel. “Adhesive elastic contacts: JKR and more”. *Journal of Physics D: Applied Physics* 41.16 (2008), p. 163001. ISSN: 0022-3727. DOI: [10.1088/0022-3727/41/16/163001](https://doi.org/10.1088/0022-3727/41/16/163001) (cit. on p. 21).
- [Barthelmes, 2003] G. Barthelmes, S. E. Pratsinis, and H. Buggisch. “Particle size distributions and viscosity of suspensions undergoing shear-induced coagulation and fragmentation”. *Chemical Engineering Science* 58.3 (2003), pp. 2893–2902. ISSN: 0009-2509. DOI: [10.1016/S0009-2509\(03\)00133-7](https://doi.org/10.1016/S0009-2509(03)00133-7) (cit. on pp. 23, 39).
- [Bassett, 2015] Danielle S. Bassett, Eli T. Owens, Mason A. Porter, M. Lisa Manning, and Karen E. Daniels. “Extraction of force-chain network architecture in granular materials using community detection”. *Soft Matter* 11.14 (14 2015), pp. 2731–2744. ISSN: 1744-6848. DOI: [10.1039/C4SM01821D](https://doi.org/10.1039/C4SM01821D) (cit. on pp. 11, 12).
- [Bayın, 2016] Selçuk Ş. Bayın. “Definition of the Riesz derivative and its application to space fractional quantum mechanics”. *Journal of Mathematical Physics* 57.12 (2016), p. 123501. ISSN: 0022-2488. DOI: [10.1063/1.4968819](https://doi.org/10.1063/1.4968819) (cit. on p. 8).
- [Beaucage, 1995] G. Beaucage. “Approximations Leading to a Unified Exponential/Power-Law Approach to Small-Angle Scattering”. *Journal of Applied Crystallography* 28.6 (1995), pp. 717–728. ISSN: 0021-8898. DOI: [10.1107/S0021889895005292](https://doi.org/10.1107/S0021889895005292) (cit. on pp. 12, 46, 60, 61, 87).
- [Beaucage, 1996] G. Beaucage. “Small-Angle Scattering from Polymeric Mass Fractals of Arbitrary Mass-Fractal Dimension”. *Journal of Applied Crystallography* 29.2 (1996), pp. 134–146. ISSN: 0021-8898. DOI: [10.1107/S0021889895011605](https://doi.org/10.1107/S0021889895011605) (cit. on pp. 13, 46, 60, 61, 87).
- [Beaucage, 2012] G. Beaucage. “Polymer Science: A Comprehensive Reference”. Vol. 2. Elsevier, 2012. Chap. Combined Small-Angle Scattering for Characterization of Hierarchically Structured Polymer Systems over Nano-to-Micron Meter: Part II Theory, pp. 399–409. ISBN: 978-0-08-087862-1. DOI: [10.1016/B978-0-444-53349-4.00032-7](https://doi.org/10.1016/B978-0-444-53349-4.00032-7) (cit. on p. 61).
- [Ben Messaoud, 2020] Ghazi Ben Messaoud, Patrick Le Griel, Daniel Hermida-Merino, and Niki Baccile. “Effects of pH, temperature and shear on the structure–property relationship of lamellar hydrogels from microbial glucolipids probed by in situ rheo-SAXS”.

- Soft Matter* 16 (10 2020), pp. 2540–2551. issn: 1744-6848. doi: [10.1039/C9SM02494H](https://doi.org/10.1039/C9SM02494H) (cit. on p. 17).
- [Benmouffok-Benbelkacem, 2010] G. Benmouffok-Benbelkacem, F. Caton, C. Baravian, and S. Skali-Lami. “Non-linear viscoelasticity and temporal behavior of typical yield stress fluids: Carbopol, Xanthan and Ketchup”. *Rheol Acta* 49 (2010), pp. 305–314 (cit. on p. 43).
- [Benzi, 2021a] Roberto Benzi, Thibaut Divoux, Catherine Barentin, and Sébastien Manneville. “Stress Overshoots in Simple Yield Stress Fluids”. *Physical Review Letters* 127.14 (2021), p. 148003. issn: 0031-9007. doi: [10.1103/PhysRevLett.127.148003](https://doi.org/10.1103/PhysRevLett.127.148003) (cit. on p. 6).
- [Benzi, 2021b] Roberto Benzi, Thibaut Divoux, Catherine Barentin, Sébastien Manneville, Mauro Sbragaglia, and Federico Toschi. “Continuum modeling of shear startup in soft glassy materials”. *Physical Review E* 104.3 (2021), p. 034612. issn: 2470-0045. doi: [10.1103/PhysRevE.104.034612](https://doi.org/10.1103/PhysRevE.104.034612) (cit. on p. 6).
- [Benzi, 2016] Roberto Benzi, Mauro Sbragaglia, M. Bernaschi, S. Succi, and Federico Toschi. “Cooperativity flows and shear-banding: a statistical field theory approach”. *Soft Matter* 12.2 (2016), pp. 514–530. issn: 1744-6848. doi: [10.1039/c5sm01862e](https://doi.org/10.1039/c5sm01862e) (cit. on p. 6).
- [Bergman, 2011] Theodore L. Bergman, Adrienne S. Lavine, Frank P. Incropera, and David P. Dewitt. *Fundamentals of Heat and Mass Transfer*. 7th ed. John Wiley & Sons, 2011. isbn: 978-0470-50197-9 (cit. on p. 4).
- [Beris, 1994] Antony N. Beris and Brian J. Edwards. *Thermodynamics of Flowing Systems with internal microstructure*. Oxford Engineering Science Series 36. 200 Madison Avenue, New York, New York 10016: Oxford University Press, 1994. isbn: 0-19-507694-X (cit. on p. 9).
- [Berka, 2005] Marta Berka and James A. Rice. “Relation between Aggregation Kinetics and the Structure of Kaolinite Aggregates”. *Langmuir* 21.4 (2005), pp. 1223–1229. issn: 0743-7463. doi: [10.1021/la0478853](https://doi.org/10.1021/la0478853) (cit. on p. 20).
- [Berker, 1963] Ratib Berker. “Intégration des équations du mouvement d’un fluide visqueux incompressible”. *Handbuch der Physik* 3 (1963) (cit. on p. 11).
- [Berker, 1936] Ratib A. Berker. “Sur quelques cas d’intégration des équations du mouvement d’un fluide visqueux incompressible”. PhD thesis. Université de Lille, 1936 (cit. on p. 11).
- [Bertram, 2021] Albrecht Bertram. “Rheology”. *Elasticity and Plasticity of Large Deformations: Including Gradient Materials*. Cham: Springer International Publishing, 2021, pp. 331–343. isbn: 978-3-030-72328-6. doi: [10.1007/978-3-030-72328-6_11](https://doi.org/10.1007/978-3-030-72328-6_11) (cit. on p. 9).
- [Bhatnagar, 1954] P. L. Bhatnagar, E. P. Gross, and M. Krook. “A Model for Collision Processes in Gases. I. Small Amplitude Processes in Charged and Neutral One-Component Systems”. *Physical Review* 94 (3 1954), pp. 511–525. doi: [10.1103/PhysRev.94.511](https://doi.org/10.1103/PhysRev.94.511) (cit. on p. 14).
- [Bhatti, 1987] M. S. Bhatti and R. K. Shah. “Handbook of single-phase convective heat transfer”. Vol. 18. 22. John Wiley & Sons, 1987. Chap. Turbulent and Transition Flow Convective Heat Transfer in Ducts, pp. 1–166. isbn: 0-471-81702-3 (cit. on p. 4).
- [Bianconi, 2001a] G. Bianconi and A.-L. Barabási. “Competition and multiscaling in evolving networks”. *Europhysics Letters (EPL)* 54.4 (2001), pp. 436–442. issn: 0295-5075. doi: [10.1209/epl/i2001-00260-6](https://doi.org/10.1209/epl/i2001-00260-6) (cit. on p. 13).
- [Bianconi, 2001b] Ginestra Bianconi and Albert-László Barabási. “Bose-Einstein Condensation in Complex Networks”. *Physical Review Letters* 86 (24 2001), pp. 5632–5635. issn: 0031-9007. doi: [10.1103/PhysRevLett.86.5632](https://doi.org/10.1103/PhysRevLett.86.5632) (cit. on p. 13).
- [Biggs, 2002] C. A. Biggs and P. A. Lant. “Modelling activated sludge flocculation using population balances”. *Powder Technology* 124.3 (2002), pp. 201–211. issn: 0032-5910. doi: [10.1016/S0032-5910\(02\)00017-7](https://doi.org/10.1016/S0032-5910(02)00017-7) (cit. on p. 16).
- [Bingham, 1922] Eugene C. Bingham. *Fluidity and Plasticity*. First. Anna: McGraw-Hill Book company, 1922 (cit. on pp. 5–7).
- [Bird, 1987] R. Byron Bird, Robert C. Armstrong, and Ole Hassager. *Dynamics of Polymeric Liquids*. 2nd ed. John Wiley & Sons, 1987. isbn: 0-471-80245-X (cit. on p. 103).
- [Bird, 2002] R. Byron Bird, Warren E. Stewart, and Edwin N. Lightfoot. *Transport Phenomena*. Deuxième. Chemical Engineering Department University of Wisconsin-Madison: John Wiley and Sons, 2002. isbn: 0-471-41077-2 (cit. on p. 4).
- [Biroli, 2018] Giulio Biroli, Guy Bunin, and Chiara Cammarota. “Marginally stable equilibria in critical ecosystems”. *New Journal of Physics* 20.8 (2018), p. 083051. issn: 1367-2630. doi: [10.1088/1367-2630/aada58](https://doi.org/10.1088/1367-2630/aada58) (cit. on p. 11).

- [Blanc, 2011] F. Blanc, F. Peters, and E. Lemaire. “Local transient rheological behavior of concentrated suspensions”. *Journal of Rheology* 55.4 (2011), pp. 835–854. issn: 0148-6055. doi: [10 . 1122 / 1 . 3582848](https://doi.org/10.1122/1.3582848) (cit. on p. 12).
- [Blanc, 2013] Frédéric Blanc, Elisabeth Lemaire, Alain Meunier, and François Peters. “Microstructure in sheared non-Brownian concentrated suspensions”. *Journal of Rheology* 57.1 (2013), pp. 273–292. issn: 0148-6055. doi: [10 . 1122 / 1 . 4766597](https://doi.org/10.1122/1.4766597) (cit. on p. 12).
- [Blandin, 2005] A. F. Blandin, D. Mangin, C. Subero-Couroyer, A. Rivoire, J. P. Klein, and J. M. Bous-soutrot. “Modelling of agglomeration in suspension: Application to salicylic acid microparticles”. *Powder Technology* 150 (2005), pp. 19–33. issn: 0032-5910. doi: [10 . 1016 / j . powtec . 2005 . 05 . 049](https://doi.org/10.1016/j.powtec.2005.05.049) (cit. on p. 23).
- [Blasius, 1907] Heinrich Blasius. *Grenzschichten in Flüssigkeiten mit kleiner Reibung*. Druck von BG Teubner, 1907 (cit. on p. 26).
- [Bocquet, 2009] Lydéric Bocquet, Annie Colin, and Armand Ajdari. “Kinetic Theory of Plastic Flow in Soft Glassy Materials”. *Physical Review Letters* 103.036001 (2009), pp. 1–4. issn: 0031-9007. doi: [10 . 1103 / PhysRevLett . 103 . 036001](https://doi.org/10.1103/PhysRevLett.103.036001) (cit. on p. 17).
- [Bonacci, 2022] Francesco Bonacci, Xavier Chateau, Eric M. Furst, Julie Goyon, and Anaël Lemaître. “Yield Stress Aging in Attractive Colloidal Suspensions”. *Physical Review Letters* 128.1 (1 2022), p. 018003. issn: 0031-9007. doi: [10 . 1103 / PhysRevLett . 128 . 018003](https://doi.org/10.1103/PhysRevLett.128.018003) (cit. on p. 6).
- [Bonn, 2017] Daniel Bonn, Morton M. Denn, Ludovic Berthier, Thibaut Divoux, and Sébastien Manneville. “Yield stress materials in soft condensed matter”. *Reviews of Modern Physics* 89.3 (2017), pp. 1–40. issn: 0034-6861. doi: [10 . 1103 / RevModPhys . 89 . 035005](https://doi.org/10.1103/RevModPhys.89.035005) (cit. on pp. 6, 9).
- [Bossler, 2018] Frank Bossler, Johannes Maurath, Katrin Dyhr, Norbert Willenbacher, and Erin Koos. “Fractal approaches to characterize the structure of capillary suspensions using rheology and confocal microscopy”. *Journal of Rheology* 62.1 (2018), pp. 183–196. issn: 0148-6055. doi: [10 . 1122 / 1 . 4997889](https://doi.org/10.1122/1.4997889) (cit. on p. 20).
- [Boussinesq, 1868] Joseph Boussinesq. “Mémoire sur l’influence des Frottements dans les Mouvements Réguliers des Fluides”. *Journal de Mathématiques Pures et Appliquées* 13.2 (1868), pp. 377–424 (cit. on p. 11).
- [Bouthier, 2022] Louis-Vincent Bouthier, Romain Castellani, Elie Hachem, and Rudy Valette. “Proposition of extension of models relating rheological quantities and microscopic structure through the use of a double fractal structure”. *Physics of Fluids* 34.8 (2022), p. 083105. issn: 1070-6631. doi: [10 . 1063 / 5 . 0101750](https://doi.org/10.1063/5.0101750) (cit. on pp. 4, 17, 18, 53, 54, 56, 58, 60, 63, 64, 68, 109).
- [Bouthier, 2023a] Louis-Vincent Bouthier, Romain Castellani, Sébastien Manneville, Arnaud Poulesquen, Rudy Valette, and Elie Hachem. “Aggregation and disaggregation processes in clusters of particles under flow: Simple numerical and theoretical insights”. *Physical Review Fluids* 8.2 (2023), p. 023304. issn: 2469-990X. doi: [10 . 1103 / PhysRevFluids . 8 . 023304](https://doi.org/10.1103/PhysRevFluids.8.023304) (cit. on pp. 4, 22, 23, 30, 32, 34, 36, 38, 40, 97).
- [Bouthier,] Louis-Vincent Bouthier, Romain Castellani, Rudy Valette, Elie Hachem, Sébastien Manneville, Thomas Gibaud, Arnaud Poulesquen, Bavand Keshavarz, and Gareth McKinley. “Cluster dynamics and rheology review: Microscopic and macroscopic coupling”. in preparation () (cit. on pp. 4, 6, 8, 10, 12, 14, 16, 18, 20, 22, 24, 26).
- [Bouthier, 2023b] Louis-Vincent Bouthier and Thomas Gibaud. “Three length-scales colloidal gels: The clusters of clusters versus the interpenetrating clusters approach”. *Journal of Rheology* 67.3 (2023), pp. 621–633. issn: 0148-6055. doi: [10 . 1122 / 8 . 0000595](https://doi.org/10.1122/8.0000595) (cit. on pp. 4, 58, 60, 62, 64, 66, 68).
- [Bouzig, 2017] Mehdi Bouzig, Jader Colombo, Lucas Vieira Barbosa, and Emanuela Del Gado. “Elastically driven intermittent microscopic dynamics in soft solids”. *Nature communications* 8 (2017), p. 15846. issn: 2041-1723. doi: [10 . 1038 / ncomms15846](https://doi.org/10.1038/ncomms15846) (cit. on p. 17).
- [Bouzig, 2018a] Mehdi Bouzig and Emanuela Del Gado. “Network Topology in Soft Gels: Hardening and Softening Materials”. *Langmuir* 34.3 (2018), pp. 773–781. issn: 0743-7463. doi: [10 . 1021 / acs . langmuir . 7b02944](https://doi.org/10.1021/acs.langmuir.7b02944) (cit. on p. 17).
- [Bouzig, 2019] Mehdi Bouzig and Emanuela Del Gado. “Handbook of Materials Modeling”. Springer, 2019. Chap. Mechanics of Soft Gels: Linear and Non-linear Response, pp. 1–29. isbn: 978-3-319-50257-1. doi: [10 . 1007 / 978 - 3 - 319 - 50257 - 1 _ 129 - 2](https://doi.org/10.1007/978-3-319-50257-1_129-2) (cit. on p. 17).
- [Bouzig, 2018b] Mehdi Bouzig, Bavand Keshavarz, Michela Geri, Thibaut Divoux, Emanuela Del Gado, and Gareth H. McKinley. “Computing the linear viscoelastic properties of soft gels using an optimally windowed chirp protocol”. *Journal of Rheology* 62.4

- (2018), pp. 1037–1050. issn: 0148-6055. doi: [10 . 1122/1.5018715](https://doi.org/10.1122/1.5018715) (cit. on pp. 11, 17).
- [Brakalov, 1987] L. B. Brakalov. “Connection between the orthokinetic coagulation capture efficiency of aggregates and their maximum size”. *Chemical Engineering Science* 42.10 (1987), pp. 2373–2383. doi: [10 . 1016/0009 - 2509\(87\) 80111 - 2](https://doi.org/10.1016/0009-2509(87)80111-2) (cit. on pp. 21, 23, 40).
- [Brinkman, 1952] H. C. Brinkman. “The Viscosity of Concentrated Suspensions and Solutions”. *The Journal of Chemical Physics* 20.4 (1952), pp. 571–571. issn: 0021-9606. doi: [10 . 1063/1.1700493](https://doi.org/10.1063/1.1700493) (cit. on p. 7).
- [Broadbent, 1957] S. R. Broadbent and J. M. Hammersley. “Percolation processes: I. Crystals and mazes”. *Mathematical Proceedings of the Cambridge Philosophical Society* 53.3 (1957), pp. 629–641. issn: 0305-0041. doi: [10 . 1017 / S0305004100032680](https://doi.org/10.1017/S0305004100032680) (cit. on p. 12).
- [Broedersz, 2011] Chase P. Broedersz, Xiaoming Mao, Tom C. Lubensky, and Frederick C. MacKintosh. “Criticality and isostaticity in fibre networks”. *Nature Physics* 7 (2011), pp. 983–988. issn: 1745-2481. doi: [10.1038/nphys2127](https://doi.org/10.1038/nphys2127) (cit. on p. 17).
- [Bubakova, 2013] Petra Bubakova, Martin Pivokonsky, and Petr Filip. “Effect of shear rate on aggregate size and structure in the process of aggregation and at steady state”. *Powder Technology* 235 (2013), pp. 540–549. issn: 0032-5910. doi: [10 . 1016 / j . powtec.2012.11.014](https://doi.org/10.1016/j.powtec.2012.11.014) (cit. on p. 67).
- [Buckingham, 1914] E. Buckingham. “On Physically Similar Systems; Illustrations of the Use of Dimensional Equations”. *Physical Review* 4.4 (1914), pp. 345–376. doi: [10 . 1103/PhysRev.4.345](https://doi.org/10.1103/PhysRev.4.345) (cit. on pp. 24, 30, 31, 37, 38).
- [Buckingham, 1915a] E. Buckingham. “Model experiments and the forms of empirical equations”. *Transactions of the American Society of Mechanical Engineers*. Vol. 37. American Society of Mechanical Engineers. American Society of Mechanical Engineers, 1915, pp. 263–296 (cit. on pp. 24, 30, 31, 37, 38).
- [Buckingham, 1915b] E. Buckingham. “The Principle of Similitude”. *Nature* 96 (1915), pp. 396–397. issn: 0028-0836. doi: [10 . 1038/096396d0](https://doi.org/10.1038/096396d0) (cit. on pp. 24, 30, 31, 37, 38).
- [Buliński, 2018] Piotr Buliński, Jacek Smolka, Sławomir Golak, Roman Przyłucki, Michał Palacz, Grzegorz Siwiec, Bartłomiej Melka, and Leszek Blacha. “Numerical modelling of multiphase flow and heat transfer within an induction skull melting furnace”. *International Journal of Heat and Mass Transfer* 126 (2018), pp. 980–992. issn: 0017-9310. doi: [10.1016/j.ijheatmasstransfer.2018.06.074](https://doi.org/10.1016/j.ijheatmasstransfer.2018.06.074) (cit. on p. 95).
- [Burns, 1997] Janine L. Burns, Yao-de Yan, Graeme J. Jameson, and Simon Biggs. “A Light Scattering Study of the Fractal Aggregation Behavior of a Model Colloidal System”. *Langmuir* 13.24 (1997), pp. 6413–6420. issn: 0743-7463. doi: [10 . 1021 / la970303f](https://doi.org/10.1021/la970303f) (cit. on pp. 12, 13).
- [Buscall, 1988] Richard Buscall, Paul DA Mills, James W Goodwin, and DW Lawson. “Scaling behaviour of the rheology of aggregate networks formed from colloidal particles”. *Journal of the Chemical Society, Faraday Transactions 1: Physical Chemistry in Condensed Phases* 84.12 (1988), pp. 4249–4260 (cit. on p. 45).
- [Caggioni, 2020] Marco Caggioni, Veronique Trappe, and Patrick T. Spicer. “Variations of the Herschel–Bulkley exponent reflecting contributions of the viscous continuous phase to the shear rate-dependent stress of soft glassy materials”. *Journal of Rheology* 64.2 (2020), pp. 413–422. issn: 0148-6055. doi: [10 . 1122/1.5120633](https://doi.org/10.1122/1.5120633) (cit. on p. 6).
- [Caputo, 1967] Michele Caputo. “Linear Models of Dissipation whose Q is almost Frequency Independent - II”. *Geophysical Journal International* 13.5 (1967), pp. 529–539. issn: 0956-540X. doi: [10 . 1111 / j . 1365 - 246X . 1967 . tb02303 . x](https://doi.org/10.1111/j.1365-246X.1967.tb02303.x) (cit. on p. 7).
- [Caputo, 2015] Michele Caputo and Mauro Fabrizio. “A new definition of fractional derivative without singular kernel”. *Progress in Fractional Differentiation & Applications* 1.2 (2015), pp. 73–85. doi: [10 . 12785/pfda/010201](https://doi.org/10.12785/pfda/010201) (cit. on p. 7).
- [Carpinetti, 1990] M. Carpinetti, F. Ferri, M. Giglio, E. Paganini, and U. Perini. “Salt-induced fast aggregation of polystyrene latex”. *Physical Review A* 42.12 (1990), pp. 7347–7354. issn: 2469-9926. doi: [10 . 1103/PhysRevA.42.7347](https://doi.org/10.1103/PhysRevA.42.7347) (cit. on p. 20).
- [Carpinetti, 1992] Marina Carpinetti and Marzio Giglio. “Spinodal-type dynamics in fractal aggregation of colloidal clusters”. *Physical Review Letters* 68.22 (1992), pp. 3327–3330. issn: 0031-9007. doi: [10.1103/PhysRevLett.68.3327](https://doi.org/10.1103/PhysRevLett.68.3327) (cit. on p. 20).
- [Çengel, 2006] Yunus A. Çengel and John M. Cimbala. *Fluid Mechanics: Fundamentals and Applications*. McGraw Hill, 2006. isbn: 0-07-247236-7 (cit. on p. 11).
- [Chaikin, 1995] P. M. Chaikin and T. C. Lubensky. *Principles of Condensed Matter Physics*. Cambridge University Press, 1995. isbn: 9780511813467. doi: [10.1017/CB09780511813467](https://doi.org/10.1017/CB09780511813467) (cit. on p. 102).
- [Chandler, 1987] David Chandler. *Introduction to Modern Statistical Mechanics*. 200 Madison Avenue, New York, New York 10016: Oxford University Press, 1987. isbn: 0-19-504277-8 (cit. on p. 17).

- [Cheng, 2010] Ming Cheng, Jinsong Hua, and Jing Lou. “Simulation of bubble–bubble interaction using a lattice Boltzmann method”. *Computers & Fluids* 39.2 (2010), pp. 260–270. ISSN: 0045-7930. DOI: [10.1016/j.compfluid.2009.09.003](https://doi.org/10.1016/j.compfluid.2009.09.003) (cit. on pp. 14, 95).
- [Cloitre, 2017a] Michel Cloitre. “Ideal colloids”. *Soft Matter and Chemistry*. Groupe Français de Rhéologie. Short courses GFR 2017, 2017 (cit. on p. 9).
- [Cloitre, 2017b] Michel Cloitre. “Real Colloids”. *Soft Matter and Chemistry*. Groupe Français de Rhéologie. Short courses GFR 2017, 2017 (cit. on p. 9).
- [Colebrook, 1937] C. F. Colebrook, C. M. White, and Geoffrey Ingram Taylor. “Experiments with fluid friction in roughened pipes”. *Proceedings of the Royal Society of London. Series A - Mathematical and Physical Sciences* 161.906 (1937), pp. 367–381. ISSN: 0954-4062. DOI: [10.1098/rspa.1937.0150](https://doi.org/10.1098/rspa.1937.0150) (cit. on p. 26).
- [Colombo, 2014a] Jader Colombo and Emanuela Del Gado. “Self-assembly and cooperative dynamics of a model colloidal gel network”. *Soft Matter* 10.22 (22 2014), pp. 4003–4015. ISSN: 1744-6848. DOI: [10.1039/C4SM00219A](https://doi.org/10.1039/C4SM00219A) (cit. on pp. 17, 33).
- [Colombo, 2014b] Jader Colombo and Emanuela Del Gado. “Stress localization, stiffening, and yielding in a model colloidal gel”. *Journal of Rheology* 58.5 (2014), pp. 1089–1116. ISSN: 0148-6055. DOI: [10.1122/1.4882021](https://doi.org/10.1122/1.4882021) (cit. on pp. 17, 33).
- [Colombo, 2013] Jader Colombo, Asaph Widmer-Cooper, and Emanuela Del Gado. “Microscopic Picture of Cooperative Processes in Restructuring Gel Networks”. *Physical Review Letters* 110.19 (2013), p. 198301. ISSN: 0031-9007. DOI: [10.1103/PhysRevLett.110.198301](https://doi.org/10.1103/PhysRevLett.110.198301) (cit. on pp. 17, 33).
- [Conchuir, 2014] Breannan O. Conchuir, Yogesh M. Harshe, Marco Lattuada, and Alessio Zaccone. “Analytical Model of Fractal Aggregate Stability and Restructuring in Shear Flows”. *Industrial & Engineering Chemistry Research* 53.22 (2014), pp. 9109–9119. ISSN: 0888-5885. DOI: [10.1021/ie4032605](https://doi.org/10.1021/ie4032605) (cit. on p. 67).
- [Conchúir, 2013] Breannán Ó Conchúir and Alessio Zaccone. “Mechanism of flow-induced biomolecular and colloidal aggregate breakup”. *Physical Review E* 87 (3 2013), p. 032310. ISSN: 1539-3755. DOI: [10.1103/PhysRevE.87.032310](https://doi.org/10.1103/PhysRevE.87.032310) (cit. on pp. 21, 23, 40).
- [Coupez, 2011] T. Coupez. “Metric construction by length distribution tensor and edge based error for anisotropic adaptive meshing”. *Journal of Computational Physics* 230.7 (2011), pp. 2391–2405. ISSN: 0021-9991. DOI: [10.1016/j.jcp.2010.11.041](https://doi.org/10.1016/j.jcp.2010.11.041) (cit. on p. 96).
- [Coupez, 2013] T. Coupez and E. Hachem. “Solution of high-Reynolds incompressible flow with stabilized finite element and adaptive anisotropic meshing”. *Computer Methods in Applied Mechanics and Engineering* 267 (2013), pp. 65–85. ISSN: 0045-7825. DOI: [10.1016/j.cma.2013.08.004](https://doi.org/10.1016/j.cma.2013.08.004) (cit. on p. 96).
- [Courtens, 1987] E. Courtens and R. Vacher. “Structure and dynamics of fractal aerogels”. *Zeitschrift für Physik B Condensed Matter* 68.2 (1987), pp. 355–361 (cit. on pp. 46, 59).
- [Coussot, 2010] P. Coussot and G. Ovarlez. “Physical origin of shear-banding in jammed systems”. *The European Physical Journal E* 33 (2010), pp. 183–188. ISSN: 1292-8941. DOI: [10.1140/epje/i2010-10660-9](https://doi.org/10.1140/epje/i2010-10660-9) (cit. on p. 9).
- [Creton, 2016] Costantino Creton and Matteo Ciccotti. “Fracture and adhesion of soft materials: a review”. *Reports on Progress in Physics* 79.4 (2016), p. 046601. ISSN: 0034-4885. DOI: [10.1088/0034-4885/79/4/046601](https://doi.org/10.1088/0034-4885/79/4/046601) (cit. on pp. 7, 31).
- [Croce, 2010] Roberto Croce, Michael Griebel, and Marc Alexander Schweitzer. “Numerical simulation of bubble and droplet deformation by a level set approach with surface tension in three dimensions”. *International Journal for Numerical Methods in Fluids* 62.9 (2010), pp. 963–993. ISSN: 1097-0363. DOI: [10.1002/flid.2051](https://doi.org/10.1002/flid.2051) (cit. on p. 95).
- [Dagès, 2022] Noémie Dagès, Louis V. Bouthier, Lauren Matthews, Sébastien Manneville, Thibaut Divoux, Arnaud Poulesquen, and Thomas Gibaud. “Interpenetration of fractal clusters drives elasticity in colloidal gels formed upon flow cessation”. *Soft Matter* 18.35 (2022), pp. 6645–6659. ISSN: 1744-6848. DOI: [10.1039/D2SM00481J](https://doi.org/10.1039/D2SM00481J) (cit. on pp. 4, 17, 41, 42, 44, 46, 50, 52, 58, 59, 62, 66, 72, 83, 85, 87).
- [Dagès, 2021] Noémie Dagès, Pierre Lidon, Guillaume Jung, Frédéric Pignon, Sébastien Manneville, and Thomas Gibaud. “Mechanics and structure of carbon black gels under high-power ultrasound”. *Journal of Rheology* 65.3 (2021), pp. 477–490. ISSN: 0148-6055. DOI: [10.1122/8.0000187](https://doi.org/10.1122/8.0000187) (cit. on pp. 2, 12, 17, 20, 41, 42, 54, 56–58, 62).
- [Dalbe, 2011] Marie-Julie Dalbe, Darija Cosic, Michael Berhanu, and Arshad Kudrolli. “Aggregation of frictional particles due to capillary attraction”. *Physical Review E* 83.5 (5 2011), p. 051403. ISSN: 1539-3755. DOI: [10.1103/PhysRevE.83.051403](https://doi.org/10.1103/PhysRevE.83.051403) (cit. on p. 20).
- [Danov, 2010] Krassimir D. Danov and Peter A. Kralchevsky. “Capillary forces between particles at a liquid interface: General theoretical approach and interactions between capillary multipoles”. *Advances in Colloid and Interface Science* 154 (2010), pp. 91–

103. ISSN: 0001-8686. DOI: [10.1016/j.cis.2010.01.010](https://doi.org/10.1016/j.cis.2010.01.010) (cit. on p. 20).
- [Das, 2022] Mohan Das and George Petekidis. “Shear induced tuning and memory effects in colloidal gels of rods and spheres”. *arXiv:2207.05185* (2022) (cit. on pp. 44, 59).
- [De Groot, 2013] S. R. De Groot and P. Mazur. *Non-Equilibrium Thermodynamics*. Dover Books on Physics. Dover Publications, 2013. ISBN: 9780486153506 (cit. on p. 14).
- [Del Gado, 2021] Emanuela Del Gado. “Encyclopedia of Complexity and Systems Science”. Springer, 2021. Chap. Stress Localization in Soft Particulate Gels, pp. 1–15. DOI: [10.1007/978-3-642-27737-5_734-1](https://doi.org/10.1007/978-3-642-27737-5_734-1) (cit. on p. 17).
- [Delichatsios, 1976] Michael A. Delichatsios and Ronald F. Probstein. “The Effect of Coalescence on the Average Drop Size in Liquid-Liquid Dispersions”. *Industrial & Engineering Chemistry Fundamentals* 15.2 (1976), pp. 134–138. DOI: [10.1021/i160058a010](https://doi.org/10.1021/i160058a010) (cit. on pp. 14, 39).
- [Deng, 2010] Youjin Deng, Wei Zhang, Timothy M. Garoni, Alan D. Sokal, and Andrea Sportiello. “Some geometric critical exponents for percolation and the random-cluster model”. *Physical Review E* 81.2 (2010), p. 020102. ISSN: 2470-0045. DOI: [10.1103/PhysRevE.81.020102](https://doi.org/10.1103/PhysRevE.81.020102) (cit. on p. 12).
- [Dienes, 1979] John K. Dienes. “On the analysis of rotation and stress rate in deforming bodies”. *Acta mechanica* 32.4 (1979), pp. 217–232. ISSN: 0001-5970. DOI: [10.1007/BF01379008](https://doi.org/10.1007/BF01379008) (cit. on p. 10).
- [Ding, 2015] Hengfei Ding, Changpin Li, and YangQuan Chen. “High-order algorithms for Riesz derivative and their applications (II)”. *Journal of Computational Physics* 293 (2015), pp. 218–237. ISSN: 0021-9991. DOI: [10.1016/j.jcp.2014.06.007](https://doi.org/10.1016/j.jcp.2014.06.007) (cit. on p. 8).
- [Dinsmore, 2006] A. D. Dinsmore, V. Prasad, I. Y. Wong, and D. A. Weitz. “Microscopic Structure and Elasticity of Weakly Aggregated Colloidal Gels”. *Physical Review Letters* 96.18 (18 2006), p. 185502. ISSN: 0031-9007. DOI: [10.1103/PhysRevLett.96.185502](https://doi.org/10.1103/PhysRevLett.96.185502) (cit. on p. 68).
- [Divoux, 2013] Thibaut Divoux, Vincent Grenard, and Sébastien Manneville. “Rheological Hysteresis in Soft Glassy Materials”. *Physical Review Letters* 110.1 (2013), p. 018304. DOI: [10.1103/PhysRevLett.110.018304](https://doi.org/10.1103/PhysRevLett.110.018304) (cit. on p. 6).
- [Donley, 2019] Gavin J. Donley, John R. de Bruyn, Gareth H. McKinley, and Simon A. Rogers. “Time-resolved dynamics of the yielding transition in soft materials”. *Journal of Non-Newtonian Fluid Mechanics* 264 (2019), pp. 117–134. ISSN: 0377-0257. DOI: [10.1016/j.jnnfm.2018.10.003](https://doi.org/10.1016/j.jnnfm.2018.10.003) (cit. on pp. 11, 89, 90, 93).
- [Drazin, 1970] P. G. Drazin. “Kelvin–Helmholtz instability of finite amplitude”. *Journal of Fluid Mechanics* 42.2 (1970), pp. 321–335. ISSN: 0022-1120. DOI: [10.1017/S0022112070001295](https://doi.org/10.1017/S0022112070001295) (cit. on pp. 11, 97).
- [Ducrot, 2014] Etienne Ducrot, Yulan Chen, Markus Bulters, Rint P. Sijbesma, and Costantino Creton. “Toughening Elastomers with Sacrificial Bonds and Watching Them Break”. *Science* 6180.344 (2014), pp. 186–189. ISSN: 0036-8075. DOI: [10.1126/science.1248494](https://doi.org/10.1126/science.1248494) (cit. on p. 7).
- [Dullaert, 2005] Konraad Dullaert and Jan Mewis. “Thixotropy: Build-up and breakdown curves during flow”. *Journal of Rheology* 49.6 (2005), pp. 1213–1230. ISSN: 0148-6055 (cit. on p. 43).
- [Eggers, 2008] Jens Eggers and Emmanuel Villermaux. “Physics of liquid jets”. *Reports on Progress in Physics* 71.3 (2008), p. 036601. ISSN: 0034-4885. DOI: [10.1088/0034-4885/71/3/036601](https://doi.org/10.1088/0034-4885/71/3/036601) (cit. on p. 14).
- [Eggersdorfer, 2010] M. L. Eggersdorfer, D. Kadau, H. J. Herrmann, and S. E. Pratsinis. “Fragmentation and restructuring of soft-agglomerates under shear”. *Journal of Colloid and Interface Science* 342 (2010), pp. 261–268. ISSN: 0021-9797. DOI: [10.1016/j.jcis.2009.10.062](https://doi.org/10.1016/j.jcis.2009.10.062) (cit. on pp. 21, 23, 37, 38, 40, 48, 54, 67).
- [Einstein, 1911] A. Einstein. “Berichtigung zu meiner Arbeit: “Eine neue Bestimmung der Moleküldimensionen””. *Annalen der Physik* 339.3 (1911), pp. 591–592. DOI: <https://doi.org/10.1002/andp.19113390313> (cit. on pp. 6, 7, 12).
- [Erdős, 1959] P. Erdős and A. Rényi. “On Random Graphs I”. *Publicationes Mathematicae Debrecen* 6 (1959), p. 290 (cit. on p. 13).
- [Ewoldt, 2007] R. H. Ewoldt and G. H. McKinley. “Creep Ringing in Rheometry or How to Deal with Oft-discarded Data in Step Stress Tests!” *Rheology Bulletin* 76 (2007), pp. 4–24 (cit. on p. 43).
- [Fardin, 2014] MA Fardin, C Perge, and N Taberlet. ““The hydrogen atom of fluid dynamics”–introduction to the Taylor–Couette flow for soft matter scientists”. *Soft Matter* 10.20 (2014), pp. 3523–3535. ISSN: 1744-6848 (cit. on p. 42).

- [Fardin, 2012] Marc-Antoine Fardin. “From Shear-Banding to Viscoelastic Turbulence: A Study in Rheology”. PhD thesis. Université Paris-Diderot, 2012 (cit. on p. 9).
- [Fazio, 2008] S. Fazio, J. Guzmán, M. T. Colomer, A. Salomoni, and R. Moreno. “Colloidal stability of nanosized titania aqueous suspensions”. *Journal of the European Ceramic Society* 28 (2008), pp. 2171–2176. ISSN: 0955-2219. DOI: [10.1016/j.jeurceramsoc.2008.02.017](https://doi.org/10.1016/j.jeurceramsoc.2008.02.017) (cit. on p. 12).
- [Feng, 2018] Di Feng, Jacob Notbohm, Ava Benjamin, Shijie He, Minxian Wang, Lay-Hong Ang, Minaspi Bantawa, Mehdi Bouzid, Emanuela Del Gado, Ramaswamy Krishnan, and Martin R. Pollak. “Disease-causing mutation in α -actinin-4 promotes podocyte detachment through maladaptation to periodic stretch”. *Proceedings of the National Academy of Sciences* 115.7 (2018), pp. 1517–1522. ISSN: 1091-6490. DOI: [10.1073/pnas.1717870115](https://doi.org/10.1073/pnas.1717870115) (cit. on p. 17).
- [Ferreiro-Córdova, 2020] Claudia Ferreiro-Córdova, Emanuela Del Gado, Giuseppe Foffi, and Mehdi Bouzid. “Multi-component colloidal gels: interplay between structure and mechanical properties”. *Soft Matter* 16.18 (18 2020), pp. 4414–4421. ISSN: 1744-6848. DOI: [10.1039/C9SM02410G](https://doi.org/10.1039/C9SM02410G) (cit. on p. 17).
- [Fielding, 2020] Suzanne M. Fielding. “Elastoviscoplastic rheology and aging in a simplified soft glassy constitutive model”. *Journal of Rheology* 64.3 (2020), pp. 723–738. ISSN: 0148-6055. DOI: [10.1122/1.5140465](https://doi.org/10.1122/1.5140465) (cit. on pp. 6, 17).
- [Flory, 1941] Paul J. Flory. “Molecular Size Distribution in Three Dimensional Polymers. I. Gelation¹”. *Journal of the American Chemical Society* 63.11 (1941), pp. 3083–3090. ISSN: 0002-7863. DOI: [10.1021/ja01856a061](https://doi.org/10.1021/ja01856a061) (cit. on p. 13).
- [Foderà, 2013] Vito Foderà, Alessio Zaccane, Marco Lattuada, and Athene M. Donald. “Electrostatics Controls the Formation of Amyloid Superstructures in Protein Aggregation”. *Physical Review Letters* 111 (10 2013), p. 108105. ISSN: 0031-9007. DOI: [10.1103/PhysRevLett.111.108105](https://doi.org/10.1103/PhysRevLett.111.108105) (cit. on p. 57).
- [Fornari, 2020] Sveva Fornari, Amelie Schäfer, Ellen Kuhl, and Alain Goriely. “Spatially-extended nucleation-aggregation-fragmentation models for the dynamics of prion-like neurodegenerative protein-spreading in the brain and its connectome”. *Journal of Theoretical Biology* 486.110102 (2020), pp. 1–17. ISSN: 0022-5193. DOI: [10.1016/j.jtbi.2019.110102](https://doi.org/10.1016/j.jtbi.2019.110102) (cit. on p. 23).
- [Fortuin, 1972] C. M. Fortuin and P. W. Kasteleyn. “On the random-cluster model: I. Introduction and relation to other models”. *Physica* 57.4 (1972), pp. 536–564. ISSN: 0031-8914. DOI: [10.1016/0031-8914\(72\)90045-6](https://doi.org/10.1016/0031-8914(72)90045-6) (cit. on p. 13).
- [Franceschini, 2012] Emilie Franceschini and Régine Guillermin. “Experimental assessment of four ultrasound scattering models for characterizing concentrated tissue-mimicking phantoms”. *The Journal of the Acoustical Society of America* 132.6 (2012), pp. 3735–3747. ISSN: 0001-4966. DOI: [10.1121/1.4765072](https://doi.org/10.1121/1.4765072) (cit. on p. 12).
- [Franceschini, 2011] Emilie Franceschini, Bloen Metzger, and Guy Cloutier. “Forward Problem Study of an Effective Medium Model for Ultrasound Blood Characterization”. *IEEE Transactions on Ultrasonics, Ferroelectrics, and Frequency Control* 58.12 (2011), pp. 2668–2679. ISSN: 0885-3010. DOI: [10.1109/TUFFC.2011.2129](https://doi.org/10.1109/TUFFC.2011.2129) (cit. on p. 12).
- [Franceschini, 2010] Emilie Franceschini, François T. H. Yu, François Destrempe, and Guy Cloutier. “Ultrasound characterization of red blood cell aggregation with intervening attenuating tissue-mimicking phantoms”. *The Journal of the Acoustical Society of America* 127.2 (2010), pp. 1104–1115. ISSN: 0001-4966. DOI: [10.1121/1.3277200](https://doi.org/10.1121/1.3277200) (cit. on p. 12).
- [Freltoft, 1986] T. Freltoft, J. K. Kjems, and S. K. Sinha. “Power-law correlations and finite-size effects in silica particle aggregates studied by small-angle neutron scattering”. *Physical Review B* 33.1 (1 1986), pp. 269–275. ISSN: 2469-9950. DOI: [10.1103/PhysRevB.33.269](https://doi.org/10.1103/PhysRevB.33.269) (cit. on p. 13).
- [Frenkel, 2002] Daan Frenkel and Berend Smit. *Understanding Molecular Simulation*. 2nd ed. Academic Press, 2002. ISBN: 978-0-12-267351-1. DOI: [10.1016/B978-0-12-267351-1.X5000-7](https://doi.org/10.1016/B978-0-12-267351-1.X5000-7) (cit. on p. 17).
- [Fuchs, 2003] Matthias Fuchs and Michael E. Cates. “Schematic models for dynamic yielding of sheared colloidal glasses”. *Faraday Discussions* 123 (0 2003), pp. 267–286. ISSN: 1359-6640. DOI: [10.1039/B205629A](https://doi.org/10.1039/B205629A) (cit. on p. 25).
- [Furukawa, 1985] Hiroshi Furukawa. “A dynamic scaling assumption for phase separation”. *Advances in Physics* 34.6 (1985), pp. 703–750. ISSN: 0001-8732. DOI: [10.1080/00018738500101841](https://doi.org/10.1080/00018738500101841) (cit. on p. 12).
- [Galvan-Miyoshi, 2008] J. Galvan-Miyoshi, J. Delgado, and R. Castillo. “Diffusing wave spectroscopy in Maxwellian fluids”. *The European Physical Journal E* 26 (2008), pp. 369–377. DOI: [10.1140/epje/i2007-10335-8](https://doi.org/10.1140/epje/i2007-10335-8) (cit. on p. 12).

- [García Daza, 2022] Fabián A. García Daza, Antonio M. Puertas, Alejandro Cuetos, and Alessandro Patti. “Microrheology of colloidal suspensions via dynamic Monte Carlo simulations”. *Journal of Colloid and Interface Science* 605 (2022), pp. 182–192. issn: 0021-9797. doi: [10.1016/j.jcis.2021.07.088](https://doi.org/10.1016/j.jcis.2021.07.088) (cit. on p. 14).
- [Gauer, 2009] Cornelius Gauer, Hua Wu, and Massimo Morbidelli. “Effect of Surface Properties of Elastomer Colloids on Their Coalescence and Aggregation Kinetics”. *Langmuir* 25.20 (2009), pp. 12073–12083. issn: 0743-7463. doi: [10.1021/la901702s](https://doi.org/10.1021/la901702s) (cit. on p. 20).
- [Genovese, 2012] Diego B. Genovese. “Shear rheology of hard-sphere, dispersed, and aggregated suspensions, and filler-matrix composites”. *Advances in Colloid and Interface Science* 171-172 (2012), pp. 1–16. issn: 0001-8686. doi: [10.1016/j.cis.2011.12.005](https://doi.org/10.1016/j.cis.2011.12.005) (cit. on p. 17).
- [Geri, 2018] Michela Geri, Bavand Keshavarz, Thibaut Divoux, Christian Clasen, Daniel J. Curtis, and Gareth H. McKinley. “Time-Resolved Mechanical Spectroscopy of Soft Materials via Optimally Windowed Chirps”. *Physical Review X* 8 (4 2018), p. 041042. issn: 2160-3308. doi: [10.1103/PhysRevX.8.041042](https://doi.org/10.1103/PhysRevX.8.041042) (cit. on p. 11).
- [Geri, 2017] Michela Geri, Ramachandran Venkatesan, Krishnaraj Sambath, and Gareth H. McKinley. “Thermokinematic memory and the thixotropic elasto-viscoplasticity of waxycrude oils”. *Journal of Rheology* 61.3 (2017), pp. 427–454. issn: 0148-6055. doi: [10.1122/1.4978259](https://doi.org/10.1122/1.4978259) (cit. on p. 7).
- [Gibaud, 2020a] Thomas Gibaud, Noémie Dagès, Pierre Lidon, Guillaume Jung, L. Christian Houré, Michael Sztucki, Arnaud Poulesquen, Nicolas Hengl, Frédéric Pignon, and Sébastien Manneville. “Rheoacoustic Gels: Tuning Mechanical and Flow Properties of Colloidal Gels with Ultrasonic Vibrations”. *Physical Review X* 10.1 (2020), pp. 1–21. issn: 2160-3308. doi: [10.1103/PhysRevX.10.011028](https://doi.org/10.1103/PhysRevX.10.011028) (cit. on pp. 2, 11, 12, 14, 17, 20, 41, 54, 56–58).
- [Gibaud, 2020b] Thomas Gibaud, Thibaut Divoux, and Sébastien Manneville. “Encyclopedia of Complexity and Systems Science”. Springer, 2020. Chap. Nonlinear mechanics of colloidal gels: creep, fatigue and shear-induced yielding, pp. 1–24. isbn: 978-3-642-27737-5. doi: [10.1007/978-3-642-27737-5_743-1](https://doi.org/10.1007/978-3-642-27737-5_743-1) (cit. on pp. 9, 41, 58).
- [Gibaud, 2010] Thomas Gibaud, Damien Frelat, and Sébastien Manneville. “Heterogeneous yielding dynamics in a colloidal gel”. *Soft Matter* 6.15 (2010), pp. 3482–3488. issn: 1744-6848 (cit. on pp. 48, 58).
- [Gibaud, 2016] Thomas Gibaud, Christophe Perge, Stefan B. Lindström, Nicolas Taberlet, and Sébastien Manneville. “Multiple yielding processes in a colloidal gel under large amplitude oscillatory stress”. *Soft Matter* 12.6 (6 2016), pp. 1701–1712. issn: 1744-6848. doi: [10.1039/C5SM02587G](https://doi.org/10.1039/C5SM02587G) (cit. on p. 58).
- [Gibaud, 2013] Thomas Gibaud, Alessio Zaccone, Emanuela Del Gado, Véronique Trappe, and Peter Schurtenberger. “Unexpected decoupling of stretching and bending modes in protein gels”. *Physical review letters* 110.5 (2013), p. 058303. issn: 0031-9007 (cit. on p. 68).
- [Gilbert, 2021] Duncan Gilbert. “Rôle des contacts adhésifs et frottants dans la rhéologie des suspensions non-browniennes”. PhD thesis. Université Côte d’Azur, 2021 (cit. on p. 21).
- [Gils, 2011] Dennis P. M. van Gils, Sander G. Huisman, Gert-Wim Bruggert, Chao Sun, and Detlef Lohse. “Torque Scaling in Turbulent Taylor-Couette Flow with Co- and Counterrotating Cylinders”. *Physical Review Letters* 106 (2 2011), p. 024502. issn: 0031-9007. doi: [10.1103/PhysRevLett.106.024502](https://doi.org/10.1103/PhysRevLett.106.024502) (cit. on p. 26).
- [Giordano, 2006] Nicholas J. Giordano and Hisao Nakanishi. *Computational Physics*. 2nd ed. Upper Saddle River, NJ 0745: Pearson, 2006. isbn: 0-13-146990-8 (cit. on p. 17).
- [Gisler, 1999] T. Gisler, R. C. Ball, and D. A. Weitz. “Strain Hardening of Fractal Colloidal Gels”. *Physical Review Letters* 5.82 (1999), pp. 1064–1067. doi: [10.1103/PhysRevLett.82.1064](https://doi.org/10.1103/PhysRevLett.82.1064) (cit. on p. 17).
- [Giusti, 2016] Chad Giusti, Lia Papadopoulos, Eli T. Owens, Karen E. Daniels, and Danielle S. Bassett. “Topological and geometric measurements of force-chain structure”. *Physical Review E* 94.3 (3 2016), p. 032909. issn: 2470-0045. doi: [10.1103/PhysRevE.94.032909](https://doi.org/10.1103/PhysRevE.94.032909) (cit. on p. 13).
- [Golse, 2005] François Golse. “Handbook of Differential Equations: Evolutionary Equations”. Vol. II. Elsevier-North-Holland, 2005. Chap. The Boltzmann Equation and Its Hydrodynamic Limits, pp. 159–301. isbn: 978-0-444-52048-7 (cit. on p. 36).
- [Gong, 2010] Jian Ping Gong. “Why are double network hydrogels so tough?” *Soft Matter* 6 (2010), pp. 2583–2590. issn: 1744-6848. doi: [10.1039/b924290b](https://doi.org/10.1039/b924290b) (cit. on p. 7).
- [Gong, 2003] Jian Ping Gong, Yoshinori Katsuyama, Takayuki Kurokawa, and Yoshito Osada. “Double-Network Hydrogels with Extremely High Mechanical Strength”. *Advanced Materials* 15.14 (2003), pp. 1155–1158. issn: 0935-9648. doi: [10.1002/adma.200304907](https://doi.org/10.1002/adma.200304907) (cit. on p. 7).

- [Goodeve, 1938] C. F. Goodeve and G. W. Whitfield. “The measurement of thixotropy in absolute units”. *Transactions of the Faraday Society* 34 (0 1938), pp. 511–520. issn: 0956-5000. doi: [10.1039/TF9383400511](https://doi.org/10.1039/TF9383400511) (cit. on p. 6).
- [Grassberger, 1985] P. Grassberger. “On the spreading of two-dimensional percolation”. *Journal of Physics A: Mathematical and General* 18.4 (1985), pp. L215–L219. issn: 0305-4470. doi: [10.1088/0305-4470/18/4/005](https://doi.org/10.1088/0305-4470/18/4/005) (cit. on pp. 12, 63, 64, 67).
- [Grassberger, 1992a] P. Grassberger. “Numerical studies of critical percolation in three dimensions”. *Journal of Physics A: Mathematical and General* 25.22 (1992), pp. 5867–5888. issn: 0305-4470. doi: [10.1088/0305-4470/25/22/015](https://doi.org/10.1088/0305-4470/25/22/015) (cit. on pp. 12, 63, 64, 67).
- [Grassberger, 1992b] P. Grassberger. “Spreading and backbone dimensions of 2D percolation”. *Journal of Physics A: Mathematical and General* 25.21 (1992), pp. 5475–5484. issn: 0305-4470. doi: [10.1088/0305-4470/25/21/009](https://doi.org/10.1088/0305-4470/25/21/009) (cit. on pp. 12, 54, 63, 64, 67).
- [Gravelle, 2021] Andrew J. Gravelle and Alejandro G. Marangoni. “A new fractal structural-mechanical theory of particle-filled colloidal networks with heterogeneous stress translation”. *Journal of Colloid and Interface Science* 598 (2021), pp. 56–68. issn: 0021-9797. doi: [10.1016/j.jcis.2021.03.180](https://doi.org/10.1016/j.jcis.2021.03.180) (cit. on pp. 17, 50, 62).
- [Green, 2009] Micah J. Green, Robert A. Brown, and Robert C. Armstrong. “Rheological phase diagrams for nonhomogeneous flows of rodlike liquid crystalline polymers”. *Journal of Non-Newtonian Fluid Mechanics* 157.1 (2009), pp. 34–43. issn: 0377-0257. doi: [10.1016/j.jnnfm.2008.09.004](https://doi.org/10.1016/j.jnnfm.2008.09.004) (cit. on p. 25).
- [Grenard, 2014] Vincent Grenard, Thibaut Divoux, Nicolas Taberlet, and Sébastien Manneville. “Timescales in creep and yielding of attractive gels”. *Soft matter* 10.10 (2014), pp. 1555–1571. issn: 1744-6848 (cit. on pp. 48, 58).
- [Grenier, 2013] N. Grenier, D. Le Touzé, A. Colagrossi, M. Antuono, and G. Colicchio. “Viscous bubble flows simulation with an interface SPH model”. *Ocean Engineering* 69 (2013), pp. 88–102. issn: 0029-8018. doi: [10.1016/j.oceaneng.2013.05.010](https://doi.org/10.1016/j.oceaneng.2013.05.010) (cit. on p. 95).
- [Griffith, 1921] Alan Arnold Griffith. “VI. The phenomena of rupture and flow in solids”. *Philosophical Transactions of the Royal Society A* 221 (1921), pp. 582–593. issn: 0264-3952. doi: [10.1098/rsta.1921.0006](https://doi.org/10.1098/rsta.1921.0006) (cit. on pp. 7, 31).
- [Guazzelli, 2018] Élisabeth Guazzelli and Olivier Pouliquen. “Rheology of dense granular suspensions”. *Journal of Fluid Mechanics* 852.P1 (2018), pp. 1–73. doi: [10.1017/jfm.2018.548](https://doi.org/10.1017/jfm.2018.548) (cit. on pp. 11, 12).
- [Gurtin, 2010] M. E. Gurtin, E. Fried, and L. Anand. *The Mechanics and Thermodynamics of Continua*. Cambridge University Press, 2010. isbn: 9781139482158 (cit. on p. 9).
- [Hachem, 2010] E. Hachem, B. Rivaux, T. Kloczko, H. Dignonnet, and T. Coupez. “Stabilized finite element method for incompressible flows with high Reynolds number”. *Journal of Computational Physics* 229 (2010), pp. 8643–8665. issn: 0021-9991. doi: [10.1016/j.jcp.2010.07.030](https://doi.org/10.1016/j.jcp.2010.07.030) (cit. on p. 96).
- [Halphen, 1975] Bernard Halphen and Quoc Son Nguyen. “Sur les matériaux standards généralisés”. *Journal de Mécanique* 14.1 (1975), pp. 39–63 (cit. on pp. 5–7, 9, 79).
- [Hammouda, 2010] Boualem Hammouda. “Analysis of the Beaucage model”. *Journal of Applied Crystallography* 43.6 (2010), pp. 1474–1478. issn: 0021-8898. doi: [10.1107/S0021889810033856](https://doi.org/10.1107/S0021889810033856) (cit. on pp. 12, 56, 60).
- [Hanotin, 2012] C. Hanotin, S. Kiesgen de Richter, P. Marchal, L. J. Michot, and C. Baravian. “Vibration-induced Liquefaction of Granular Suspensions”. *Physical Review Letters* 108.198301 (2012), pp. 1–5. issn: 0031-9007. doi: [10.1103/PhysRevLett.108.198301](https://doi.org/10.1103/PhysRevLett.108.198301) (cit. on pp. 11, 12).
- [Hanotin, 2015] C. Hanotin, S. Kriesgen de Richter, L. J. Michot, and Ph. Marchal. “Viscoelasticity of vibrated granular suspensions”. *Journal of Rheology* 59.1 (2015), pp. 253–273. issn: 0148-6055. doi: [10.1122/1.4904421](https://doi.org/10.1122/1.4904421) (cit. on pp. 11, 12).
- [Harshe, 2011] Yogesh M. Harshe, Marco Lattuada, and Miroslav Soos. “Experimental and Modeling Study of Breakage and Restructuring of Open and Dense Colloidal Aggregates”. *Langmuir* 27 (2011), pp. 5739–5752. issn: 0743-7463. doi: [10.1021/la104658](https://doi.org/10.1021/la104658) (cit. on pp. 21, 23, 40).
- [Hartley, 1985] P. A. Hartley and G. D. Parfitt. “Dispersion of Powders in Liquids. 1. The Contribution of the van der Waals Force to the Cohesiveness of Carbon Black Powders”. *Langmuir* 1.6 (1985), pp. 651–657. issn: 0743-7463. doi: [10.1021/la00066a003](https://doi.org/10.1021/la00066a003) (cit. on p. 12).
- [He, 2020] Qiyang He, Huanxiong Xia, Jianhua Liu, Xiaohui Ao, and Shengxiang Lin. “Modeling and numerical studies of selective laser melting: Multiphase flow, solidification and heat transfer”. *Materials & Design* 196 (2020), p. 109115. issn: 0264-1275. doi: [10.1016/j.matdes.2020.109115](https://doi.org/10.1016/j.matdes.2020.109115) (cit. on p. 95).

- [He, 2015] Wei He, Nesrin Şenbil, and A. D. Dinsmore. “Measured capillary forces on spheres at particle-laden interfaces”. *Soft Matter* 11.25 (2015), pp. 5087–5094. ISSN: 1744-6848. DOI: [10.1039/C5SM00245A](https://doi.org/10.1039/C5SM00245A) (cit. on p. 12).
- [Hébraud, 1998] P. Hébraud and F. Lequeux. “Mode-Coupling Theory for the Pasty Rheology of Soft Glassy Materials”. *Physical Review Letters* 81.14 (1998), pp. 2934–2937. ISSN: 0031-9007. DOI: [10.1103/physrevlett.81.2934](https://doi.org/10.1103/physrevlett.81.2934) (cit. on p. 17).
- [Helal, 2016] Ahmed Helal, Thibaut Divoux, and Gareth H McKinley. “Simultaneous rheoelectric measurements of strongly conductive complex fluids”. *Physical Review Applied* 6.6 (2016), p. 064004 (cit. on pp. 41, 58, 59).
- [Hengl, 2014] N. Hengl, Y. Jin, F. Pignon, S. Baup, R. Mollard, N. Gondrexon, A. Magnin, L. Michot, and E. Paineau. “A new way to apply ultrasound in cross-flow ultrafiltration: Application to colloidal suspensions”. *Ultrasonics Sonochemistry* 21 (2014), pp. 1018–1025. ISSN: 1350-4177. DOI: [10.1016/j.ultsonch.2013.11.008](https://doi.org/10.1016/j.ultsonch.2013.11.008) (cit. on p. 20).
- [Herd, 1992] Charles R Herd, Gerard C McDonald, and William M Hess. “Morphology of carbon-black aggregates: fractal versus euclidean geometry”. *Rubber chemistry and technology* 65.1 (1992), pp. 107–129 (cit. on p. 42).
- [Herminghaus, 2000] S. Herminghaus. “Roughness-induced non-wetting”. *Europhysics Letters (EPL)* 52.2 (2000), pp. 165–170. ISSN: 0295-5075. DOI: [10.1209/epl/i2000-00418-8](https://doi.org/10.1209/epl/i2000-00418-8) (cit. on p. 12).
- [Herrmann, 1984] H. J. Herrmann, D. C. Hong, and H. E. Stanley. “Backbone and elastic backbone of percolation clusters obtained by the new method of ‘burning’”. *Journal of Physics A: Mathematical and General* 17.5 (1984), pp. L261–L266. ISSN: 0305-4470. DOI: [10.1088/0305-4470/17/5/008](https://doi.org/10.1088/0305-4470/17/5/008) (cit. on pp. 15, 54).
- [Herrmann, 1988] H. J. Herrmann and H. E. Stanley. “The fractal dimension of the minimum path in two- and three-dimensional percolation”. *Journal of Physics A: Mathematical and General* 21.17 (1988), pp. L829–L833. ISSN: 0305-4470. DOI: [10.1088/0305-4470/21/17/003](https://doi.org/10.1088/0305-4470/21/17/003) (cit. on p. 15).
- [Herrmann, 2018] Richard Herrmann. *Fractional Calculus*. 3rd ed. WORLD SCIENTIFIC, 2018. DOI: [10.1142/111107](https://doi.org/10.1142/111107) (cit. on p. 7).
- [Herschel, 1926a] Von Winslow H. Herschel and Ronald Bulkley. “Ronsistenzmessungen von Gummi-Benzollösungen”. *Kolloid-Zeitschrift* 39.291 (1926), pp. 291–300. DOI: [10.1007/BF01432034](https://doi.org/10.1007/BF01432034) (cit. on pp. 5, 6, 105).
- [Herschel, 1926b] W. H. Herschel and Ronald Bulkley. “Measurement of consistency as applied to rubber-benzene solutions”. *Am. Soc. Test Proc.* Vol. 26. 1926, pp. 621–633 (cit. on pp. 42, 105).
- [Higashitani, 1998] Ko Higashitani and Kenji Iimura. “Two-Dimensional Simulation of the Breakup Process of Aggregates in Shear and Elongational Flows”. *Journal of Colloid and Interface Science* 204 (1998), pp. 320–327. ISSN: 0021-9797. DOI: [10.1006/jcis.1998.5561](https://doi.org/10.1006/jcis.1998.5561) (cit. on pp. 21, 23, 40).
- [Higashitani, 2001] Ko Higashitani, Kenji Iimura, and Hiroko Sanda. “Simulation of deformation and breakup of large aggregates in Flows of viscous Fluids”. *Chemical Engineering Science* 56 (2001), pp. 2927–2938. ISSN: 0009-2509. DOI: [10.1016/S0009-2509\(00\)00477-2](https://doi.org/10.1016/S0009-2509(00)00477-2) (cit. on pp. 21, 23, 40).
- [Hipp, 2019] Julie B. Hipp, Jeffrey J. Richards, and Norman J. Wagner. “Structure-property relationships of sheared carbon black suspensions determined by simultaneous rheological and neutron scattering measurements”. *Journal of Rheology* 63.3 (2019), pp. 423–436. ISSN: 0148-6055. DOI: [10.1122/1.5071470](https://doi.org/10.1122/1.5071470) (cit. on p. 58).
- [Hipp, 2021] Julie B. Hipp, Jeffrey J. Richards, and Norman J. Wagner. “Direct measurements of the microstructural origin of shear-thinning in carbon black suspensions”. *Journal of Rheology* 65.2 (2021), pp. 145–157. ISSN: 0148-6055. DOI: [10.1122/8.0000089](https://doi.org/10.1122/8.0000089) (cit. on pp. 17, 42, 47).
- [Hoekstra, 2005] H. Hoekstra, J. Mewis, T. Narayanan, and J. Vermant. “Multi Length Scale Analysis of the Microstructure in Sticky Sphere Dispersions during Shear Flow”. *Langmuir* 21.24 (2005), pp. 11017–11025. ISSN: 0743-7463. DOI: [10.1021/la051488q](https://doi.org/10.1021/la051488q) (cit. on p. 20).
- [Hoekstra, 2003] H. Hoekstra, J. Vermant, J. Mewis, and G. G. Fuller. “Flow-Induced Anisotropy and Reversible Aggregation in Two-Dimensional Suspensions”. *Langmuir* 19.22 (2003), pp. 9134–9141. ISSN: 0743-7463. DOI: [10.1021/la034582k](https://doi.org/10.1021/la034582k) (cit. on p. 20).
- [Hosseini, 2021] Seyyed Ahmad Hosseini, Paolo Moretti, Dimitrios Konstantinidis, and Michael Zaiser. “Beam network model for fracture of materials with hierarchical microstructure”. *International Journal of Fracture* 227.2 (2021), pp. 243–257. ISSN: 0376-9429. DOI: [10.1007/s10704-020-00511-w](https://doi.org/10.1007/s10704-020-00511-w) (cit. on p. 17).
- [Hua, 2007] Jinsong Hua and Jing Lou. “Numerical simulation of bubble rising in viscous liquid”. *Journal of Computational Physics* 222.2 (2007), pp. 769–795. ISSN: 0021-9991. DOI: [10.1016/j.jcp.2006.08.008](https://doi.org/10.1016/j.jcp.2006.08.008) (cit. on p. 95).

- [Hua, 2008] Jinsong Hua, Jan F. Stene, and Ping Lin. “Numerical simulation of 3D bubbles rising in viscous liquids using a front tracking method”. *Journal of Computational Physics* 227.6 (2008), pp. 3358–3382. ISSN: 0021-9991. DOI: [10.1016/j.jcp.2007.12.002](https://doi.org/10.1016/j.jcp.2007.12.002) (cit. on p. 95).
- [Huang, 2021] Ssu-Ting Huang, Cheng-Hao Yang, Peng-Ju Lin, Chien-You Su, and Chi-Chung Hua. “Multiscale structural and rheological features of colloidal low-methoxyl pectin solutions and calcium-induced sol–gel transition”. *Physical Chemistry Chemical Physics* 23.35 (2021), pp. 19269–19279 (cit. on p. 47).
- [Huber, 2015] Patrick Huber. “Soft matter in hard confinement: phase transition thermodynamics, structure, texture, diffusion and flow in nanoporous media”. *Journal of Physics: Condensed Matter* 27.10 (2015), p. 103102. ISSN: 0953-8984. DOI: [10.1088/0953-8984/27/10/103102](https://doi.org/10.1088/0953-8984/27/10/103102) (cit. on p. 103).
- [Hunter, 1980] Robert John Hunter and John Frayne. “Flow Behavior of Coagulated Colloidal Sols”. *Journal of Colloid and Interface Science* 76.1 (1980), pp. 107–115. ISSN: 0021-9797. DOI: [10.1016/0021-9797\(80\)90275-1](https://doi.org/10.1016/0021-9797(80)90275-1) (cit. on pp. 21, 23, 40).
- [Hurd, 1988] Alan J. Hurd and William L. Flower. “In situ growth and structure of fractal silica aggregates in a flame”. *Journal of Colloid and Interface Science* 122.1 (1988), pp. 178–192. ISSN: 0021-9797. DOI: [10.1016/0021-9797\(88\)90301-3](https://doi.org/10.1016/0021-9797(88)90301-3) (cit. on p. 20).
- [Hwang, 2016] Hyun Joo Hwang, Robert A. Riggleman, and John C. Crocker. “Understanding soft glassy materials using an energy landscape approach”. *Nature Materials* 15 (2016), pp. 1031–1036. ISSN: 1476-1122. DOI: [10.1038/nmat4663](https://doi.org/10.1038/nmat4663) (cit. on p. 11).
- [Irwin, 1957] G. R. Irwin. “Analysis of Stresses and Strains Near the End of a Crack Traversing a Plate”. *Journal of Applied Mechanics* 24.3 (1957), pp. 361–364. DOI: [10.1115/1.4011547](https://doi.org/10.1115/1.4011547) (cit. on pp. 7, 31).
- [Itou, 2020] Hiromichi Itou, Victor A. Kovtunenkov, and Kumbakonam R. Rajagopal. “The Boussinesq flat-punch indentation problem within the context of linearized viscoelasticity”. *International Journal of Engineering Science* 151 (2020), p. 103272. ISSN: 0020-7225. DOI: [10.1016/j.ijengsci.2020.103272](https://doi.org/10.1016/j.ijengsci.2020.103272) (cit. on pp. 71–73).
- [Jacquin, 2018] Laurent Jacquin. *Mécanique des fluides*. École Polytechnique, 2018 (cit. on p. 67).
- [Jaishankar, 2012] Aditya Jaishankar and Gareth H. McKinley. “Power-law rheology in the bulk and at the interface: quasi-properties and fractional constitutive equations”. *Proceedings of the Royal Society A*. Vol. 20120284. Royal Society. Royal Society, 2012, pp. 1–18. DOI: [10.1098/rspa.2012.0284](https://doi.org/10.1098/rspa.2012.0284) (cit. on pp. 6, 7).
- [Jaishankar, 2014] Aditya Jaishankar and Gareth H. McKinley. “A fractional K-BKZ constitutive formulation for describing the nonlinear rheology of multiscale complex fluids”. *Journal of Rheology* 58.6 (2014), pp. 1751–1788. ISSN: 0148-6055. DOI: [10.1122/1.4892114](https://doi.org/10.1122/1.4892114) (cit. on pp. 6, 7).
- [Jamali, 2019a] Safa Jamali, Robert C. Armstrong, and Gareth H. McKinley. “Multiscale Nature of Thixotropy and Rheological Hysteresis in Attractive Colloidal Suspensions under Shear”. *Physical Review Letters* 123.24 (2019), p. 248003. ISSN: 0031-9007. DOI: [10.1103/PhysRevLett.123.248003](https://doi.org/10.1103/PhysRevLett.123.248003) (cit. on pp. 21, 48, 67).
- [Jamali, 2020] Safa Jamali, Robert C. Armstrong, and Gareth H. McKinley. “Time-rate-transformation framework for targeted assembly of short-range attractive colloidal suspensions”. *Materials Today Advances* 5 (2020), p. 100026. ISSN: 2590-0498. DOI: [10.1016/j.mtadv.2019.100026](https://doi.org/10.1016/j.mtadv.2019.100026) (cit. on pp. 21, 31, 48, 67).
- [Jamali, 2019b] Safa Jamali and John F. Brady. “Alternative Frictional Model for Discontinuous Shear Thickening of Dense Suspensions: Hydrodynamics”. *Physical Review Letters* 123.13 (13 2019), p. 138002. ISSN: 0031-9007. DOI: [10.1103/PhysRevLett.123.138002](https://doi.org/10.1103/PhysRevLett.123.138002) (cit. on p. 67).
- [Jarvis, 2005] P. Jarvis, B. Jefferson, J. Gregory, and S. A. Parsons. “A review of floc strength and breakage”. *Water Research* 39.14 (2005), pp. 3121–3137. ISSN: 0043-1354. DOI: [10.1016/j.watres.2005.05.022](https://doi.org/10.1016/j.watres.2005.05.022) (cit. on p. 23).
- [Jawerth, 2020] Louise Jawerth, Elisabeth Fischer-Friedrich, Suropriya Saha, Jie Wang, Titus Franzmann, Xiaojie Zhang, Jenny Sachweh, Martine Ruer, Mahdiye Ijavi, Shambaditya Saha, et al. “Protein condensates as aging Maxwell fluids”. *Science* 370.6522 (2020), pp. 1317–1323 (cit. on p. 47).
- [Jeldres, 2018] Ricardo I. Jeldres, Phillip D. Fawell, and Brendan J. Florio. “Population balance modelling to describe the particle aggregation process: A review”. *Powder Technology* 326 (2018), pp. 190–207. ISSN: 0032-5910. DOI: [10.1016/j.powtec.2017.12.033](https://doi.org/10.1016/j.powtec.2017.12.033) (cit. on p. 16).
- [Jiang, 2020] Li Jiang, Mohammad Rahnema, Biao Zhang, Xun Zhu, Pang-Chieh Sui, Ding-Ding Ye, and Ned Djilali. “Predicting the interaction between nanoparticles in shear flow using lattice Boltzmann method and Derjaguin-Landau-Verwey-Overbeek (DLVO) theory”. *Physics of Fluids* 32.4 (2020), p. 043302. ISSN: 1070-6631. DOI: [10.1063/1.5142669](https://doi.org/10.1063/1.5142669) (cit. on p. 14).

- [Johnson, 2016] Richard W. Johnson. *Handbook of Fluid Dynamics*. 2nd ed. CRC Press/Taylor & Francis Group 6000 Broken Sound Parkway NW, Suite 300 Boca Raton, FL 33487-2742: CRC Press, 2016. ISBN: 978-1-4398-4955-2 (cit. on p. 11).
- [Joshi, 2014] Yogesh M. Joshi. “Dynamics of Colloidal Glasses and Gels”. *Annual Review of Chemical and Biomolecular Engineering* 5.1 (2014), pp. 181–202. ISSN: 1947-5446. DOI: [10 . 1146 / annurev - chembioeng - 060713 - 040230](https://doi.org/10.1146/annurev-chembioeng-060713-040230) (cit. on p. 11).
- [Jungblut, 2019] Swetalan Jungblut, Jan-Ole Joswig, and Alexander Eychmüller. “Diffusion- and reaction-limited cluster aggregation revisited”. *Physical Chemistry Chemical Physics* 21 (2019), pp. 5723–5729. ISSN: 1463-9084. DOI: [10 . 1039 / C9CP00549H](https://doi.org/10.1039/C9CP00549H) (cit. on p. 20).
- [Kádár, 2021] Roland Kádár, Stefan Spirk, and Tina Nypelö. “Cellulose Nanocrystal Liquid Crystal Phases: Progress and Challenges in Characterization Using Rheology Coupled to Optics, Scattering, and Spectroscopy”. *ACS Nano* 15.5 (2021), pp. 7931–7945. ISSN: 1936-0851. DOI: [10 . 1021 / acsnano . 0c09829](https://doi.org/10.1021/acsnano.0c09829) (cit. on p. 17).
- [Kammler, 2005] Hendrik K. Kammler, Gregory Beaucage, Douglas J. Kohls, Nikhil Agashe, and Jan Ilavsky. “Monitoring simultaneously the growth of nanoparticles and aggregates by in situ ultra-small-angle x-ray scattering”. *Journal of Applied Physics* 97.5 (2005), p. 054309. ISSN: 0021-8979. DOI: [10 . 1063 / 1 . 1855391](https://doi.org/10.1063/1.1855391) (cit. on p. 61).
- [Kantor, 1984a] Y. Kantor and T. A. Witten. “Mechanical stability of tenuous objects”. *Journal de Physique Lettres* 45.13 (1984), pp. 675–679. ISSN: 2777-3434. DOI: [10 . 1051 / jphyslet : 019840045013067500](https://doi.org/10.1051/jphyslet:019840045013067500) (cit. on pp. 12, 15, 50–52, 66).
- [Kantor, 1984b] Yacov Kantor and Itzhak Webman. “Elastic Properties of Random Percolating Systems”. *Physical Review Letters* 52.21 (1984), pp. 1891–1894. ISSN: 0031-9007. DOI: [10 . 1103 / PhysRevLett . 52 . 1891](https://doi.org/10.1103/PhysRevLett.52.1891) (cit. on pp. 12, 15, 50–52, 66).
- [Keim, 2019] Nathan C Keim, Joseph D Paulsen, Zorana Zeravcic, Srikanth Sastry, and Sidney R Nagel. “Memory formation in matter”. *Reviews of Modern Physics* 91.3 (2019), p. 035002 (cit. on p. 47).
- [Kelly, 2009] James F. Kelly and Robert J. McGough. “Fractal ladder models and power law wave equations”. *Journal of the Acoustical Society of America* 126.4 (2009), pp. 2072–2081. ISSN: 0001-4966. DOI: [10 . 1121 / 1 . 3204304](https://doi.org/10.1121/1.3204304) (cit. on p. 8).
- [Kelvin, 1890] W. T. B. Kelvin, J. Larmor, and J. P. Joule. *Mathematical and Physical Papers: Elasticity, heat, electro-magnetism*. Mathematical and Physical Papers. University Press, 1890 (cit. on pp. 6, 7, 104).
- [Kern, 1967] Kern and Bland. *Solid Mensuration*. 2nd ed. John Wiley & Sons, 1967. ISBN: 971-587-010-4 (cit. on pp. 51, 65).
- [Keshavarz, 2021] Bavand Keshavarz, Donatien Gomes Rodrigues, Jean-Baptiste Champenois, Matthew G. Frith, Jan Ilavsky, Michela Geri, Thibaut Divoux, Gareth H. McKinley, and Arnaud Poulèsquen. “Time-connectivity superposition and the gel/glass duality of weak colloidal gels”. *Proceedings of the National Academy of Sciences of the United States of America* 118.15 (2021), pp. 1–9. DOI: [10 . 1073 / pnas . 2022339118](https://doi.org/10.1073/pnas.2022339118) (cit. on pp. 17, 61, 87).
- [Khanwale, 2020] Makrand A. Khanwale, Alec D. Lofquist, Hari Sundar, James A. Rossmann, and Baskar Ganapathysubramanian. “Simulating two-phase flows with thermodynamically consistent energy stable Cahn-Hilliard Navier-Stokes equations on parallel adaptive octree based meshes”. *Journal of Computational Physics* 419 (2020), p. 109674. ISSN: 0021-9991. DOI: [10 . 1016 / j . jcp . 2020 . 109674](https://doi.org/10.1016/j.jcp.2020.109674) (cit. on p. 95).
- [Kim, 2020] Dokyung Kim and Sangkyun Koo. “Rheological estimation of aggregate size for a colloidal suspension of carbon black particles”. *Korea-Australian Rheology Journal* 32.4 (2020), pp. 301–308. ISSN: 1226-119X. DOI: [10 . 1007 / s13367 - 020 - 0028 - z](https://doi.org/10.1007/s13367-020-0028-z) (cit. on p. 17).
- [Kim, 2018] Noori Kim and Sangkyun Koo. “Rheological analysis of particle aggregation in a colloidal suspension of carbon black particles”. *Korea-Australian Rheology Journal* 30.3 (2018), pp. 189–197. ISSN: 1226-119X. DOI: [10 . 1007 / s13367 - 018 - 0019 - 5](https://doi.org/10.1007/s13367-018-0019-5) (cit. on p. 17).
- [Kim, 1991] Sangtae Kim and Seppo J. Karrila. *Microhydrodynamics: principles and selected applications*. Butterworth - Heinemann series in chemical engineering. Butterworth - Heinemann, 1991. ISBN: 0-7506-9173-5 (cit. on p. 71).
- [Kim, 2004] W. Kim, C. M. Sorensen, and A. Chakrabarti. “Universal Occurrence of Soot Superaggregates with a Fractal Dimension of 2.6 in Heavily Sooting Laminar Diffusion Flames”. *Langmuir* 20.10 (2004), pp. 3969–3973. ISSN: 0743-7463. DOI: [10 . 1021 / la036085 +](https://doi.org/10.1021/la036085+) (cit. on pp. 20, 60).
- [Kimbonguila Manounou, 2014] A. Kimbonguila Manounou and S. Rémond. “Discrete element modeling of the microstructure of fine particle agglomerates in sheared dilute suspension”. *Physica A* 412 (2014), pp. 66–83. ISSN: 0378-4371. DOI: [10 . 1016 / j . physa . 2014 . 06 . 023](https://doi.org/10.1016/j.physa.2014.06.023) (cit. on pp. 21, 23, 30, 40, 48, 54, 67).

- [Klimchitskaya, 2000] G. L. Klimchitskaya, U. Mohideen, and V. M. Mostepanenko. “Casimir and Van der Waals force between two plates or a sphere (lens) above a plate made of real metals”. *Physical Review A* 61.6 (2000), p. 062107. ISSN: 2469-9926. DOI: [10.1103/PhysRevA.61.062107](https://doi.org/10.1103/PhysRevA.61.062107) (cit. on pp. 12, 41).
- [Knoll, 2018] Pamela Knoll and Oliver Steinbock. “Particle Aggregation Modifies Crystallization: Extending the Hierarchical Order of a Polycrystalline Material to the Macroscale”. *Journal of Physical Chemistry C* 122.41 (2018), pp. 23554–23563. ISSN: 1932-7447. DOI: [10.1021/acs.jpcc.8b07212](https://doi.org/10.1021/acs.jpcc.8b07212) (cit. on pp. 12, 20).
- [Kolev, 2012] Nikolay Ivanov Kolev. *Multiphase Flow Dynamics 4 : Turbulence, Gas Adsorption and Release, Diesel Fuel Properties*. 2nd ed. Springer Berlin, Heidelberg, 2012. ISBN: 978-3-642-20748-8. DOI: [10.1007/978-3-642-20749-5](https://doi.org/10.1007/978-3-642-20749-5) (cit. on p. 95).
- [Kolev, 2015] Nikolay Ivanov Kolev. *Multiphase Flow Dynamics 5 : Nuclear Thermal Hydraulics*. 3rd ed. Springer Cham, 2015. ISBN: 978-3-319-15155-7. DOI: [10.1007/978-3-319-15156-4](https://doi.org/10.1007/978-3-319-15156-4) (cit. on p. 95).
- [Kolmogorov, 1991] A. N. Kolmogorov. “The Local Structure of Turbulence in Incompressible Viscous Fluid for Very Large Reynolds Numbers”. *Proceedings: Mathematical and Physical Sciences*. Vol. 434. Turbulence and Stochastic Process: Kolmogorov’s Ideas 50 Years 1890. The Royal Society, 1991, pp. 9–13 (cit. on pp. 30, 67, 79).
- [Koumakis, 2015] Nick Koumakis, Esmael Moghimi, Rut Besseling, Wilson C. K. Poon, John F. Brady, and George Petekidis. “Tuning colloidal gels by shear”. *Soft Matter* 11 (2015), pp. 4640–4648. ISSN: 1744-6848. DOI: [10.1039/C5SM00411J](https://doi.org/10.1039/C5SM00411J) (cit. on pp. 20, 45, 47, 59).
- [Kralchevsky, 2001a] Peter A. Kralchevsky and Nikolai D. Denkov. “Capillary forces and structuring in layers of colloid particles”. *Current Opinion in Colloid & Interface Science* 6 (2001), pp. 383–401. ISSN: 1359-0294. DOI: [10.1016/S1359-0294\(01\)00105-4](https://doi.org/10.1016/S1359-0294(01)00105-4) (cit. on p. 20).
- [Kralchevsky, 2001b] Peter A. Kralchevsky, Nikolai D. Denkov, and Krassimir D. Danov. “Particles with an Undulated Contact Line at a Fluid Interface: Interaction between Capillary Quadrupoles and Rheology of Particulate Monolayers”. *Langmuir* 17.24 (2001), pp. 7694–7705. ISSN: 0743-7463. DOI: [10.1021/la0109359](https://doi.org/10.1021/la0109359) (cit. on p. 20).
- [Kralchevsky, 2001c] Peter A. Kralchevsky and Kuniki Nagayama. *Particles at Fluid Interfaces and Membranes: Attachment of Colloid Particles and Proteins to Intercalated and Formation of Two-Dimensional Arrays*. Vol. 10. Studies in Interface Science. Elsevier, 2001. ISBN: 0-444-50234-3 (cit. on p. 20).
- [Krieger, 1972] Irvin M. Krieger. “Rheology of monodisperse latices”. *Advances In Colloid and Interface Science* 3 (1972), pp. 111–136. DOI: [10.1016/0001-8686\(72\)80001-0](https://doi.org/10.1016/0001-8686(72)80001-0) (cit. on pp. 6, 7, 12, 17).
- [Krieger, 1959] Irvin M. Krieger and Thomas J. Dougherty. “A Mechanism for Non-Newtonian Flow in Suspensions of Rigid Spheres”. *Transactions of the Society of Rheology* 3.1 (1959), pp. 137–152. ISSN: 0148-6055. DOI: [10.1122/1.548848](https://doi.org/10.1122/1.548848) (cit. on pp. 6, 7, 12, 17).
- [Krijt, 2014] S. Krijt, C. Dominik, and A. G. G. M. Tielens. “Rolling friction of adhesive microspheres”. *Journal of Physics D: Applied Physics* 47.17 (2014), p. 175302. ISSN: 0022-3727. DOI: [10.1088/0022-3727/47/17/175302](https://doi.org/10.1088/0022-3727/47/17/175302) (cit. on p. 21).
- [Krishnan, 2010] Arjun S Krishnan, Sönke Seifert, Byeongdu Lee, Saad A Khan, and Richard J Spontak. “Cosolvent-regulated time–composition rheological equivalence in block copolymer solutions”. *Soft Matter* 6.18 (2010), pp. 4331–4334. ISSN: 1744-6848 (cit. on p. 47).
- [Kryven, 2014] Ivan Kryven, Stefano Lazzari, and Giuseppe Storti. “Population Balance Modeling of Aggregation and Coalescence in Colloidal Systems”. *Macromolecular Theory and Simulations* 23.3 (2014), pp. 170–181. ISSN: 1521-3919. DOI: [10.1002/mats.201300140](https://doi.org/10.1002/mats.201300140) (cit. on pp. 13, 39).
- [Krzysko, 2020] Anthony J. Krzysko, Elias Nakouzi, Xin Zhang, Trent R. Graham, Kevin M. Rosso, Gregory K. Schenter, Jan Ilavsky, Ivan Kuzmenko, Matthew G. Frith, Cornelius F. Ivory, Sue B. Clark, Javen S. Weston, Katie M. Weigandt, James J. De Yoreo, Jaehun Chun, and Lawrence M. Anovitz. “Correlating inter-particle forces and particle shape to shear-induced aggregation/fragmentation and rheology for dilute anisotropic particle suspensions: A complementary study via capillary rheometry and in-situ small and ultra-small angle X-ray scattering”. *Journal of Colloid and Interface Science* 576 (2020), pp. 47–58. ISSN: 0021-9797. DOI: [10.1016/j.jcis.2020.04.016](https://doi.org/10.1016/j.jcis.2020.04.016) (cit. on p. 20).
- [Kusters, 1991] K. A. Kusters. “The influence of turbulence on aggregation of small particles in agitated vessels”. PhD thesis. Chemical Engineering and Chemistry, 1991. DOI: [10.6100/IR362582](https://doi.org/10.6100/IR362582) (cit. on pp. 20, 39).
- [Lahaye, 1994] J Lahaye and F Ehrburger-Dolle. “Mechanisms of carbon black formation. Correlation with the morphology of aggregates”. *Carbon* 32.7 (1994), pp. 1319–1324 (cit. on pp. 42, 58).

- [Landau, 1959] L. D. Landau and E. M. Lifshitz. *Theory of Elasticity*. 1st ed. Vol. 7. Pergamon Press LTD., 4 and 5 Fitzroy Square, London W.1: Pergamon Press, 1959. ISBN: 978-0-7506-2633-0 (cit. on pp. 4–6, 9, 10).
- [Landau, 1987] L. D. Landau and E. M. Lifshitz. *Fluid Mechanics*. Deuxième. Vol. 6. Course of Theoretical Physics. Institute of Physical Problems, U.S.S.R. Academy of Sciences: Pergamon Press, 1987. ISBN: 0-08-033932-8 (cit. on pp. 4–6).
- [Larson, 1999] Ronald G. Larson. *The Structure and Rheology of Complex Fluids*. Oxford University press, 1999. ISBN: 0-19-512197-X (cit. on p. 102).
- [Larson, 2019] Ronald G. Larson and Yufei Wei. “A review of thixotropy and its rheological modeling”. *Journal of Rheology* 63.3 (2019), pp. 477–501. ISSN: 0148-6055. DOI: [10.1122/1.5055031](https://doi.org/10.1122/1.5055031) (cit. on p. 6).
- [Lattuada, 2003] Marco Lattuada, Hua Wu, and Massimo Morbidelli. “Hydrodynamic radius of fractal clusters”. *Journal of Colloid and Interface Science* 268.1 (2003), pp. 96–105. ISSN: 0021-9797. DOI: [10.1016/j.jcis.2003.07.028](https://doi.org/10.1016/j.jcis.2003.07.028) (cit. on p. 12).
- [Lattuada, 2016] Marco Lattuada, Alessio Zaccone, Hua Wu, and Massimo Morbidelli. “Population-balance description of shear-induced clustering, gelation and suspension viscosity in sheared DLVO colloids”. *Soft Matter* 12.24 (2016), pp. 5313–5324. ISSN: 1744-6848. DOI: [10.1039/C6SM01097K](https://doi.org/10.1039/C6SM01097K) (cit. on pp. 13, 35, 38, 39).
- [Le Tallec, 2019] Patrick Le Tallec. *Mécanique des milieux continus II*. École Polytechnique, 2019 (cit. on p. 90).
- [Lees, 1972] A. W. Lees and S. F. Edwards. “The computer study of transport processes under extreme conditions”. *Journal of Physics C: Solid State Physics* 5.15 (1972), pp. 1921–1929. ISSN: 0022-3719. DOI: [10.1088/0022-3719/5/15/006](https://doi.org/10.1088/0022-3719/5/15/006) (cit. on p. 17).
- [Levitz, 1992] P. Levitz and D. Tchoubar. “Disordered porous solids : from chord distributions to small angle scattering”. *Journal de Physique I France* 2.6 (1992), pp. 771–790. DOI: [10.1051/jp1:1992174](https://doi.org/10.1051/jp1:1992174) (cit. on p. 12).
- [Lin, 1990a] M. Y. Lin, R. Klein, H. M. Lindsay, D. A. Weitz, R. C. Ball, and P. Meakin. “The Structure of Fractal Colloidal Aggregates of Finite Extent”. *Journal of Colloid and Interface Science* 137.1 (1990), pp. 263–280. ISSN: 0021-9797. DOI: [10.1016/0021-9797\(90\)90061-R](https://doi.org/10.1016/0021-9797(90)90061-R) (cit. on p. 20).
- [Lin, 1989] M. Y. Lin, H. M. Lindsay, D. A. Weitz, R. C. Ball, R. Klein, and P. Meakin. “Universality in colloid aggregation”. *Nature* 339 (1989), pp. 360–362. ISSN: 0028-0836. DOI: [10.1038/339360a0](https://doi.org/10.1038/339360a0) (cit. on pp. 12, 20).
- [Lin, 1990b] M. Y. Lin, H. M. Lindsay, D. A. Weitz, R. Klein, R. C. Ball, and P. Meakin. “Universal diffusion-limited colloid aggregation”. *Journal of Physics: Condensed Matter* 2.3 (1990), pp. 3093–3113. ISSN: 0953-8984. DOI: [10.1088/0953-8984/2/13/019](https://doi.org/10.1088/0953-8984/2/13/019) (cit. on p. 20).
- [Lin, 2016] Neil Y. C. Lin, Christopher Ness, Michael E. Cates, Jin Sun, and Itai Cohen. “Tunable shear thickening in suspensions”. *Proceedings of the National Academy of Sciences of the United States of America* 113.39 (2016), pp. 10774–10778. DOI: [10.1073/pnas.1608348113](https://doi.org/10.1073/pnas.1608348113) (cit. on p. 20).
- [Lobry, 2019] Laurent Lobry, Elisabeth Lemaire, Frédéric Blanc, Stany Gallier, and François Peters. “Shear thinning in non-Brownian suspensions explained by variable friction between particles”. *Journal of Fluid Mechanics* 860 (2019), pp. 682–710. ISSN: 0022-1120. DOI: [10.1017/jfm.2018.881](https://doi.org/10.1017/jfm.2018.881) (cit. on p. 12).
- [Lorenzo, 2022] Turetta Lorenzo and Lattuada Marco. “Brownian Dynamics simulations of shear-induced aggregation of charged colloidal particles in the presence of hydrodynamic interactions”. *Journal of Colloid and Interface Science* (2022). ISSN: 0021-9797. DOI: [10.1016/j.jcis.2022.05.047](https://doi.org/10.1016/j.jcis.2022.05.047) (cit. on p. 20).
- [Lu, 2008] Peter James Lu. *Gelation and phase separation of attractive colloids*. Harvard University, 2008. ISBN: 978-0-549-61762-4 (cit. on p. 12).
- [Lubensky, 1993] T. C. Lubensky and F. C. MacKintosh. “Theory of “Ripple” Phases of Lipid Bilayers”. *Physical Review Letters* 71.10 (10 1993), pp. 1565–1568. ISSN: 0031-9007. DOI: [10.1103/PhysRevLett.71.1565](https://doi.org/10.1103/PhysRevLett.71.1565) (cit. on p. 17).
- [MacKintosh, 1991] F. C. MacKintosh and T. C. Lubensky. “Orientational order, topology, and vesicle shapes”. *Physical Review Letters* 67.9 (9 1991), pp. 1169–1172. ISSN: 0031-9007. DOI: [10.1103/PhysRevLett.67.1169](https://doi.org/10.1103/PhysRevLett.67.1169) (cit. on p. 17).
- [Macosko, 1994] Christopher W. Macosko. *Rheology : Principles, Measurements and Applications*. John Wiley and Sons, 1994. ISBN: 1-56081-579-5 (cit. on pp. 6, 9, 11).
- [Madivala, 2009] Basavaraj Madivala, Jan Fransaer, and Jan Vermant. “Self-Assembly and Rheology of Ellipsoidal Particles at Interfaces”. *Langmuir* 25.5 (2009), pp. 2718–2728. ISSN: 0743-7463. DOI: [10.1021/la803554u](https://doi.org/10.1021/la803554u) (cit. on p. 20).
- [Madraki, 2017] Yasaman Madraki, Sarah Hormozi, Guillaume Ovarlez, Élisabeth Guazzelli, and Olivier Pouliquen. “Enhancing shear thickening”. *Physical Review Fluids* 2 (3 2017), p. 033301. ISSN: 2469-990X. DOI: [10.1103/PhysRevFluids.2.033301](https://doi.org/10.1103/PhysRevFluids.2.033301) (cit. on p. 5).

- [Mahbubul, 2014] I. M. Mahbubul, Tet Hien Chong, S. S. Khaleduzzaman, I. M. Shahrul, R. Saidur, B. D. Long, and M. A. Amalina. “Effect of Ultrasonication Duration on Colloidal Structure and Viscosity of Alumina-Water Nanofluid”. *Industrial & Engineering Chemistry Research* 53 (2014), pp. 6677–6684. doi: [10.1021/ie500705j](https://doi.org/10.1021/ie500705j) (cit. on p. 12).
- [Mahbubul, 2012] I. M. Mahbubul, R. Saidur, and M. A. Amalina. “Latest developments on the viscosity of nanofluids”. *International Journal of Heat and Mass Transfer* 55 (2012), pp. 874–885. ISSN: 0017-9310. doi: [10.1016/j.ijheatmasstransfer.2011.10.021](https://doi.org/10.1016/j.ijheatmasstransfer.2011.10.021) (cit. on p. 9).
- [Mandelbrot, 1983] B. B. Mandelbrot. *The Fractal Geometry of Nature*. Einaudi paperbacks. Henry Holt and Company, 1983. ISBN: 9780716711865 (cit. on p. 12).
- [Mansard, 2011] Vincent Mansard, Annie Colin, Pinaki Chaudhuri, and Lydéric Bocquet. “A kinetic elasto-plastic model exhibiting viscosity bifurcation in soft glassy materials”. *Soft Matter* 7 (2011), pp. 5524–5527. doi: [10.1039/c1sm05229b](https://doi.org/10.1039/c1sm05229b) (cit. on p. 17).
- [Marangoni, 2000] Alejandro G. Marangoni. “Elasticity of high-volume-fraction fractal aggregate networks: A thermodynamic approach”. *Physical Review B* 62.21 (2000), pp. 13951–13955. ISSN: 2469-9950. doi: [10.1103/PhysRevB.62.13951](https://doi.org/10.1103/PhysRevB.62.13951) (cit. on pp. 17, 50, 54, 55).
- [Marioni, 2017] Luca Marioni. “Computational Modelling and Electromagnetic-CFD Coupling in Casting Processes.” Theses. Université Paris sciences et lettres, 2017 (cit. on pp. 95, 96).
- [Marmottant, 2004] P. Marmottant and E. Villermaux. “On spray formation”. *Journal of Fluid Mechanics* 498 (2004), pp. 73–111. ISSN: 0022-1120. doi: [10.1017/S0022112003006529](https://doi.org/10.1017/S0022112003006529) (cit. on p. 14).
- [Marshall, 2014] Jeffery S. Marshall and Shuiqing Li. *Adhesive Particle Flow: A Discrete-Element Approach*. 1st ed. 32 Avenue of the Americas, NY 10013-2473, USA: Cambridge University Press, 2014. ISBN: 978-1-107-03207-1. doi: [10.1017/CB09781139424547](https://doi.org/10.1017/CB09781139424547) (cit. on pp. 21, 30, 31, 37, 48, 54).
- [Martinez, 2017] Roberto Fernandez Martinez, Maider Iturrondobeitia, Julen Ibarretxe, and Teresa Guraya. “Methodology to classify the shape of reinforcement fillers: optimization, evaluation, comparison, and selection of models”. *Journal of Materials Science* 52.1 (2017), pp. 569–580 (cit. on pp. 42, 83).
- [Masoero, 2014] Enrico Masoero, Emanuela Del Gado, Roland J.-M. Pellenq, Sidney Yip, and Franz-Josef Ulm. “Nano-scale mechanics of colloidal C-S-H gels”. *Soft Matter* 10.3 (2014), pp. 491–499. ISSN: 1744-6848. doi: [10.1039/C3SM51815A](https://doi.org/10.1039/C3SM51815A) (cit. on p. 14).
- [Massaro, 2020] Roberta Massaro, Gabriele Colombo, Peter Van Puyvelde, and Jan Vermant. “Viscoelastic cluster densification in sheared colloidal gels”. *Soft Matter* 16.10 (2020), pp. 2437–2447. ISSN: 1744-6848. doi: [10.1039/C9SM02368B](https://doi.org/10.1039/C9SM02368B) (cit. on p. 20).
- [Masschaele, 2009] Kasper Masschaele, Jan Fransaer, and Jan Vermant. “Direct visualization of yielding in model two-dimensional colloidal gels subjected to shear flow”. *Journal of Rheology* 53.6 (2009), pp. 1437–1460. ISSN: 0148-6055. doi: [10.1122/1.3237154](https://doi.org/10.1122/1.3237154) (cit. on pp. 20, 22).
- [Maxwell, 1867] James Clerk Maxwell. “IV. On the dynamical theory of gases”. *Philosophical Transactions of the Royal Society of London* 157 (1867), pp. 49–88. doi: [10.1098/rstl.1867.0004](https://doi.org/10.1098/rstl.1867.0004) (cit. on pp. 6, 7, 9, 72).
- [Meakin, 1992] Paul Meakin. “Aggregation kinetics”. *Physica Scripta* 46.4 (1992), pp. 295–331. ISSN: 0031-8949. doi: [10.1088/0031-8949/46/4/002](https://doi.org/10.1088/0031-8949/46/4/002) (cit. on p. 20).
- [Meeker, 2004] Steven P Meeker, Roger T Boncacez, and Michel Cloitre. “Slip and flow in pastes of soft particles: Direct observation and rheology”. *Journal of Rheology* 48.6 (2004), pp. 1295–1320. ISSN: 0148-6055 (cit. on p. 43).
- [Mellema, 2002] M. Mellema, J. H. J. van Opheusde, and T. van Vliet. “Categorization of rheological scaling models for particle gels applied to casein gels”. *Journal of Rheology* 46.1 (2002), pp. 11–29. ISSN: 0148-6055. doi: [10.1122/1.1423311](https://doi.org/10.1122/1.1423311) (cit. on pp. 17, 18, 50–52, 54–56, 62–64, 66, 79, 109).
- [Mewis, 2009] Jan Mewis and Norman J. Wagner. “Thixotropy”. *Advances in Colloid and Interface Science* 147-148 (2009), pp. 214–227. ISSN: 0001-8686. doi: [10.1016/j.cis.2008.09.005](https://doi.org/10.1016/j.cis.2008.09.005) (cit. on p. 6).
- [Mewis, 2012] Jan Mewis and Norman J. Wagner. *Colloidal Suspension Rheology*. Cambridge University Press, 2012. ISBN: 978-0-521-51599-3. doi: [10.1017/CB09780511977978](https://doi.org/10.1017/CB09780511977978) (cit. on pp. 9, 17, 50, 102).
- [Mises, 1913] R. von Mises. “Mechanik der festen Körper im plastisch-deformablen Zustand”. *Nachrichten von der Gesellschaft der Wissenschaften zu Göttingen* 1 (1913), pp. 582–592 (cit. on pp. 5, 6, 31).

- [Mohraz, 2005] Ali Mohraz and Michael J. Solomon. “Orientation and rupture of fractal colloidal gels during start-up of steady shear flow”. *Journal of Rheology* 49.3 (2005), pp. 657–681. issn: 0148-6055. doi: [10.1122/1.1895799](https://doi.org/10.1122/1.1895799) (cit. on p. 20).
- [Møller, 2008] P. C. F. Møller, S. Rodts, M. A. J. Michels, and Daniel Bonn. “Shear banding and yield stress in soft glassy materials”. *Physical Review E* 77.041507 (2008), pp. 1–5. issn: 1539-3755. doi: [10.1103/PhysRevE.77.041507](https://doi.org/10.1103/PhysRevE.77.041507) (cit. on p. 17).
- [Monchy, 2016] Romain de Monchy, François Destrempes, Ratan K. Saha, Guy Cloutier, and Emilie Franceschini. “Coherent and incoherent ultrasound backscatter from cell aggregates”. *The Journal of the Acoustical Society of America* 140.3 (2016), pp. 2173–2184. issn: 0001-4966. doi: [10.1121/1.4962502](https://doi.org/10.1121/1.4962502) (cit. on pp. 12, 13).
- [Monchy, 2018] Romain de Monchy, Julien Rouyer, François Destrempes, Boris Chayer, Guy Cloutier, and Emilie Franceschini. “Estimation of polydispersity in aggregating red blood cells by quantitative ultrasound backscatter analysis”. *Journal of the Acoustical Society of America* 143.4 (2018), pp. 2207–2216. issn: 0001-4966. doi: [10.1121/1.5031121](https://doi.org/10.1121/1.5031121) (cit. on pp. 12, 13).
- [Mondragon, 2012] Rosa Mondragon, J. Enrique Julia, Antonio Barba, and Juan Carlos Jarque. “Characterization of silica–water nanofluids dispersed with an ultrasound probe: A study of their physical properties and stability”. *Powder Technology* 224 (2012), pp. 138–146. issn: 0032-5910. doi: [10.1016/j.powtec.2012.02.043](https://doi.org/10.1016/j.powtec.2012.02.043) (cit. on pp. 12, 20).
- [Morbideilli,] Massimo Morbidelli. “Kinetics and Structure of Colloidal Aggregates” (cit. on p. 23).
- [Mosayebi, 2014] Majid Mosayebi, Patrick Ilg, Asaph Widmer-Cooper, and Emanuela Del Gado. “Soft Modes and Nonaffine Rearrangements in the Inherent Structures of Supercooled Liquids”. *Physical Review Letters* 112.10 (10 2014), p. 105503. issn: 0031-9007. doi: [10.1103/PhysRevLett.112.105503](https://doi.org/10.1103/PhysRevLett.112.105503) (cit. on p. 17).
- [Mullineux, 2008] Glen Mullineux. “Non-linear least squares fitting of coefficients in the Herschel–Bulkley model”. *Applied Mathematical Modelling* 32.12 (2008), pp. 2538–2551. issn: 0307-904X. doi: [10.1016/j.apm.2007.09.010](https://doi.org/10.1016/j.apm.2007.09.010) (cit. on p. 5).
- [Mwasame, 2016] Paul M. Mwasame, Norman J. Wagner, and Antony N. Beris. “Modeling the viscosity of polydisperse suspensions: Improvements in prediction of limiting behavior”. *Physics of Fluids* 28.6 (2016), p. 061701. issn: 1070-6631. doi: [10.1063/1.4953407](https://doi.org/10.1063/1.4953407) (cit. on p. 12).
- [Nabizadeh, 2021] Mohammad Nabizadeh and Safa Jamali. “Life and death of colloidal bonds control the rate-dependent rheology of gels”. *Nature Communications* 12.1 (2021), pp. 1–9. issn: 2041-1723. doi: [10.1038/s41467-021-24416-x](https://doi.org/10.1038/s41467-021-24416-x) (cit. on pp. 31, 47).
- [Nampoothiri, 2020] Jishnu N. Nampoothiri, Yinqiao Wang, Kabir Ramola, Jie Zhang, Subhro Bhattacharjee, and Bulbul Chakraborty. “Emergent Elasticity in Amorphous Solids”. *Physical Review Letters* 125.11 (11 2020), p. 118002. issn: 0031-9007. doi: [10.1103/PhysRevLett.125.118002](https://doi.org/10.1103/PhysRevLett.125.118002) (cit. on p. 6).
- [Narayanan, 2022] Theyencheri Narayanan, Michael Sztucki, Thomas Zinn, Jérôme Kieffer, Alejandro Homs-Puron, Jacques Gorini, Pierre Van Vaerenbergh, and Peter Boesecke. “Performance of the time-resolved ultra-small-angle X-ray scattering beamline with the Extremely Brilliant Source”. *Journal of Applied Crystallography* 55.1 (2022), pp. 98–111 (cit. on p. 42).
- [Nedderman, 1992] Ronald Midgley Nedderman. *Statics and kinematics of granular materials*. 1st ed. Vol. 352. Cambridge University Press, The Edinburgh Building, Cambridge CB2 2RU, UK: Cambridge University Press Cambridge, 1992. isbn: 978-0-521-01907-1 (cit. on p. 11).
- [Nguyen, 2011] Van Son Nguyen, Didier Rouxel, Rachid Hadji, Brice Vincent, and Yves Fort. “Effect of ultrasonication and dispersion stability on the cluster size of alumina nanoscale particles in aqueous solutions”. *Ultrasonics Sonochemistry* 18 (2011), pp. 382–388. issn: 1350-4177. doi: [10.1016/j.ultsonch.2010.07.003](https://doi.org/10.1016/j.ultsonch.2010.07.003) (cit. on pp. 12, 20, 41).
- [Okubo, 1995] T. Okubo. “Surface Tension of Structured Colloidal Suspensions of Polystyrene and Silica Spheres at the Air–Water Interface”. *Journal of Colloid and Interface Science* 171 (1995), pp. 55–62. issn: 0021-9797. doi: [10.1006/jcis.1995.1150](https://doi.org/10.1006/jcis.1995.1150) (cit. on pp. 12, 20).
- [Ostwald, 1925] Wolfgang Ostwald. “Ueber die Geschwindigkeitsfunktion der Viskosität disperser Systeme. I”. *Kolloid-Zeitschrift* 36 (1925), pp. 99–117. issn: 0303-402X. doi: [10.1007/BF01431449](https://doi.org/10.1007/BF01431449) (cit. on pp. 5, 6).
- [Ovarlez, 2013] Guillaume Ovarlez, Laurent Tocquer, François Bertrand, and Philippe Coussot. “Rheopexy and tunable yield stress of carbon black suspensions”. *Soft Matter* 9.23 (2013), pp. 5540–5549. issn: 1744-6848 (cit. on pp. 41, 58, 59).
- [Ozenda, 2018] Olivier Ozenda, Pierre Saramito, and Guillaume Chambon. “A new non-colloidal suspension model A new rate-independent tensorial model for suspensions of non-colloidal rigid particles in Newtonian fluids”. 2018 (cit. on pp. 6, 7).

- [Palierne, 1990] J. F. Palierne. “Linear rheology of viscoelastic emulsions with interfacial tension”. *Rheologica Acta* 29 (1990), pp. 204–214. issn: 0035-4511. doi: [10.1007/BF01331356](https://doi.org/10.1007/BF01331356) (cit. on p. 15).
- [Panigrahy, 2019] Chinmaya Panigrahy, Ayan Seal, Nihar Kumar Mahato, and Debotosh Bhattacharjee. “Differential box counting methods for estimating fractal dimension of gray-scale images: A survey”. *Chaos, Solitons & Fractals* 126 (2019), pp. 178–202. issn: 0960-0779. doi: [10.1016/j.chaos.2019.06.007](https://doi.org/10.1016/j.chaos.2019.06.007) (cit. on p. 12).
- [Panine, 2003] P Panine, M Gradzielski, and T Narayanan. “Combined rheometry and small-angle x-ray scattering”. *Review of Scientific Instruments* 74.4 (2003), pp. 2451–2455 (cit. on p. 42).
- [Pantina, 2005] John P. Pantina and Eric M. Furst. “Elasticity and Critical Bending Moment of Model Colloidal Aggregates”. *Physical Review Letters* 94.13 (13 2005), p. 138301. issn: 0031-9007. doi: [10.1103/PhysRevLett.94.138301](https://doi.org/10.1103/PhysRevLett.94.138301) (cit. on p. 6).
- [Pantina, 2006] John P. Pantina and Eric M. Furst. “Colloidal Aggregate Micromechanics in the Presence of Divalent Ions”. *Langmuir* 22.12 (2006), pp. 5282–5288. issn: 0743-7463. doi: [10.1021/la0534120](https://doi.org/10.1021/la0534120) (cit. on p. 68).
- [Papanastasiou, 1987] Tasos C. Papanastasiou. “Flows of Materials with Yield”. *Journal of Rheology* 31.5 (1987), pp. 385–404. issn: 0148-6055. doi: [10.1122/1.549926](https://doi.org/10.1122/1.549926) (cit. on pp. 6, 7).
- [Pastor-Satorras, 2001] Romualdo Pastor-Satorras and Alessandro Vespignani. “Epidemic Spreading in Scale-Free Networks”. *Physical Review Letters* 86.14 (14 2001), pp. 3200–3203. issn: 0031-9007. doi: [10.1103/PhysRevLett.86.3200](https://doi.org/10.1103/PhysRevLett.86.3200) (cit. on p. 13).
- [Patel, 2022] Panchami Patel and Prachi Thareja. “Hydrogels differentiated by length scales: A review of biopolymer-based hydrogel preparation methods, characterization techniques, and targeted applications”. *European Polymer Journal* 163 (2022), p. 110935. issn: 0014-3057. doi: [10.1016/j.eurpolymj.2021.110935](https://doi.org/10.1016/j.eurpolymj.2021.110935) (cit. on p. 17).
- [Pearce, 2005] David J. Pearce. *An improved algorithm for finding the strongly connected components of a directed graph*. Tech. rep. Victoria University, 2005 (cit. on p. 33).
- [Perge, 2014] Christophe Perge, Nicolas Taberlet, Thomas Gibaud, and Sébastien Manneville. “Time dependence in large amplitude oscillatory shear: A rheo-ultrasonic study of fatigue dynamics in a colloidal gel”. *Journal of Rheology* 58.5 (2014), pp. 1331–1357. issn: 0148-6055. doi: [10.1122/1.4887081](https://doi.org/10.1122/1.4887081) (cit. on p. 58).
- [Peuvrel-Disdier, 2012] Edith Peuvrel-Disdier, Sébastien Manneville, Guillaume Ovarlez, Frédéric Pignon, and Stéphane Rodts. “Apport de techniques couplées (diffusion de rayonnements, résonance magnétique, vélocimétrie ultrasonore) à la rhéologie”. *Rhéologie* 21 (2012), pp. 36–67 (cit. on p. 11).
- [Picu, 2011] R. C. Picu. “Mechanics of random fiber networks — a review”. *Soft Matter* 7.15 (15 2011), pp. 6768–6785. issn: 1744-6848. doi: [10.1039/C1SM05022B](https://doi.org/10.1039/C1SM05022B) (cit. on p. 17).
- [Pierce, 2019] Allan D. Pierce. *Acoustics : An Introduction to Its Physical Principles and Applications*. 3rd ed. East SandwichMA, USA: Springer, 2019. isbn: 978-3-030-11213-4. doi: [10.1007/978-3-030-11214-1](https://doi.org/10.1007/978-3-030-11214-1).
- [Polyanin, 2007] Andrei D. Polyanin and Alexander V. Manzhirov. *Handbook of Mathematics for Engineers and Scientists*. Chapman & Hall/CRC Taylor & Francis Group 6000 Broken Sound Parkway NW, Suite 300 Boca Raton, FL 33487-2742: Chapman & Hall, 2007. isbn: 978-1-58488-502-3 (cit. on pp. 51, 65).
- [Pooseh, 2012] Shakoore Pooseh, Ricardo Almeida, and Delfim F. M. Torres. “Numerical Approximations of Fractional Derivatives with Applications”. *Asian Journal of Control* 15.5 (2012), pp. 1–15. doi: [10.1002/asjc.617](https://doi.org/10.1002/asjc.617) (cit. on p. 8).
- [Potanin, 1995] A. A. Potanin, R. De Rooij, D. Van den Ende, and J. Mellema. “Microrheological modeling of weakly aggregated dispersions”. *The Journal of Chemical Physics* 102.14 (1995), pp. 5845–5853. issn: 0021-9606. doi: [10.1063/1.469317](https://doi.org/10.1063/1.469317) (cit. on p. 17).
- [Potanin, 1996] A. A. Potanin and W. B. Russel. “Fractal model of consolidation of weakly aggregated colloidal dispersions”. *Physical Review E* 53.4 (1996), pp. 3702–3709. issn: 1063-651X. doi: [10.1103/PhysRevE.53.3702](https://doi.org/10.1103/PhysRevE.53.3702) (cit. on pp. 21, 23, 40).
- [Potanin, 1991] Andrew A. Potanin. “On the Mechanism of Aggregation in the Shear Flow of Suspensions”. *Journal of Colloid and Interface Science* 145.1 (1991), pp. 140–157. issn: 0021-9797. doi: [10.1016/0021-9797\(91\)90107-J](https://doi.org/10.1016/0021-9797(91)90107-J) (cit. on pp. 21, 23, 40).
- [Potanin, 1992] Andrew A. Potanin. “On the model of colloid aggregates and aggregating colloids”. *Journal of Chemical Physics* 96.12 (1992), pp. 9191–9200. issn: 0021-9606. doi: [10.1063/1.462229](https://doi.org/10.1063/1.462229) (cit. on pp. 21, 23, 40).
- [Prandtl, 1904] Ludwig Prandtl. “Über Flüssigkeitsbewegung bei sehr kleiner Reibung”. *Verhandl. III, Internat. Math.-Kong., Heidelberg, Teubner, Leipzig, 1904* (1904), pp. 484–491 (cit. on p. 26).

- [Prasad, 2003] V. Prasad, V. Trappe, A. D. Dinsmore, P. N. Segre, L. Cipelletti, and D. A. Weitz. “Rideal Lecture Universal features of the fluid to solid transition for attractive colloidal particles”. *Faraday Discussions* 123 (0 2003), pp. 1–12. issn: 1359-6640. doi: [10.1039/B211107C](https://doi.org/10.1039/B211107C) (cit. on pp. 11, 42, 44, 45).
- [Pratsinis, 1998] Sotiris E. Pratsinis. “Flame aerosol synthesis of ceramic powders”. *Progress in Energy and Combustion Science* 24.3 (1998), pp. 197–219. issn: 0360-1285. doi: [10.1016/S0360-1285\(97\)00028-2](https://doi.org/10.1016/S0360-1285(97)00028-2) (cit. on pp. 14, 23).
- [Press, 2007] William H. Press, Saul A. Teukolsky, William T. Vetterling, and Brian P. Flannery. *Numerical Recipes: The Art of Scientific Computing*. 3rd ed. The Edinburgh Building, Cambridge CB2 8RU, UK: Cambridge University Press, 2007. isbn: 978-0-521-88068-8 (cit. on p. 17).
- [Puisto, 2012] A. Puisto, X. Illa, M. Mohtaschemi, and M. J. Alava. “Modeling the viscosity and aggregation of suspensions of highly anisotropic nanoparticles”. *The European Physical Journal E* 35.1 (2012), pp. 1–7. issn: 1292-8941. doi: [10.1140/epje/i2012-12006-1](https://doi.org/10.1140/epje/i2012-12006-1) (cit. on pp. 13, 38, 39).
- [Qian, 2022] Yunzhou Qian, Shane P. Usher, Peter J. Scales, Anthony D. Stickland, and Alessio Alexiadis. “Agglomeration Regimes of Particles under a Linear Laminar Flow: A Numerical Study”. *Mathematics* 10.11 (2022). issn: 2227-7390. doi: [10.3390/math10111931](https://doi.org/10.3390/math10111931) (cit. on pp. 24, 26).
- [Quezada de Luna, 2020] Manuel Quezada de Luna, J. Haydel Collins, and Christopher E. Kees. “An unstructured finite element model for incompressible two-phase flow based on a monolithic conservative level set method”. *International Journal for Numerical Methods in Fluids* 92.9 (2020), pp. 1058–1080. issn: 1097-0363. doi: [10.1002/flid.4817](https://doi.org/10.1002/flid.4817) (cit. on p. 95).
- [Radhakrishnan, 2017] Rangarajan Radhakrishnan, Thibaut Divoux, Sébastien Manneville, and Suzanne M. Fielding. “Understanding rheological hysteresis in soft glassy materials”. *Soft Matter* 13.9 (2017), pp. 1834–1852. issn: 1744-6848 (cit. on p. 43).
- [Rahman, 2019] Syed Ehsanur Rahman, Nader Laal-Dehghani, Sourav Barman, and Gordon F. Christopher. “Modifying interfacial interparticle forces to alter microstructure and viscoelasticity of densely packed particle laden interfaces”. *Journal of Colloid and Interface Science* 536 (2019), pp. 30–41. issn: 0021-9797. doi: [10.1016/j.jcis.2018.10.028](https://doi.org/10.1016/j.jcis.2018.10.028) (cit. on p. 12).
- [Raney, 2018] Jordan R Raney, Brett G Compton, Jochen Mueller, Thomas J Ober, Kristina Shea, and Jennifer A Lewis. “Rotational 3D printing of damage-tolerant composites with programmable mechanics”. *Proceedings of the National Academy of Sciences* 115.6 (2018), pp. 1198–1203 (cit. on p. 59).
- [Räntzsch, 2019] Volker Röntzsch, Mürüvvet Begüm Özen, Karl-Friedrich Rätzsch, Eric Stellamanns, Michael Sprung, Gisela Guthausen, and Manfred Wilhelm. “Polymer Crystallization Studied by Hyphenated Rheology Techniques: Rheo-NMR, Rheo-SAXS, and Rheo-Microscopy”. *Macromolecular Materials and Engineering* 304.2 (2019), p. 1800586. issn: 1439-2054. doi: [10.1002/mame.201800586](https://doi.org/10.1002/mame.201800586) (cit. on p. 17).
- [Raelison, 2020] R. N. Raelison, L. L. Koithara, S. Costil, and C. Langlade. “Turbulences of the supersonic gas flow during cold spraying and their negative effects: A DNS CFD analysis coupled with experimental observation and laser impulse high-speed shadowgraphs of the particles in-flight flow”. *International Journal of Heat and Mass Transfer* 147 (2020), pp. 118894–118912. issn: 0017-9310. doi: [10.1016/j.ijheatmasstransfer.2019.118894](https://doi.org/10.1016/j.ijheatmasstransfer.2019.118894) (cit. on p. 96).
- [Rehage, 1988] H. Rehage and H. Hoffmann. “Rheological Properties of Viscoelastic Surfactant Systems”. *Journal of Physical Chemistry* 92.16 (1988), pp. 4712–4719. issn: 0022-3654. doi: [10.1021/j100327a031](https://doi.org/10.1021/j100327a031) (cit. on p. 11).
- [Richards, 2017] Jeffrey J. Richards, Julie B. Hipp, John K. Riley, Norman J. Wagner, and Paul D. Butler. “Clustering and Percolation in Suspensions of Carbon Black”. *Langmuir* 33.43 (2017), pp. 12260–12266. issn: 0743-7463. doi: [10.1021/acs.langmuir.7b02538](https://doi.org/10.1021/acs.langmuir.7b02538) (cit. on pp. 17, 42).
- [Rogers, 2012a] Simon A. Rogers. “A sequence of physical processes determined and quantified in LAOS: An instantaneous local 2D/3D approach”. *Journal of Rheology* 56.5 (2012), pp. 1129–1151. issn: 0148-6055. doi: [10.1122/1.4726083](https://doi.org/10.1122/1.4726083) (cit. on pp. 11, 89, 93).
- [Rogers, 2017] Simon A. Rogers. “In search of physical meaning: defining transient parameters for nonlinear viscoelasticity”. *Rheology Acta* 56 (2017), pp. 501–525. issn: 0035-4511. doi: [10.1007/s00397-017-1008-1](https://doi.org/10.1007/s00397-017-1008-1) (cit. on pp. 11, 89, 90, 93).
- [Rogers, 2011] Simon A. Rogers, Brian M. Erwin, Dimitris Vlassopoulos, and Michel Cloitre. “A sequence of physical processes determined and quantified in LAOS: Application to a yield stress fluid”. *Journal of Rheology* 55.2 (2011), pp. 435–458. issn: 0148-6055. doi: [10.1122/1.3544591](https://doi.org/10.1122/1.3544591) (cit. on pp. 11, 89, 93).

- [Rogers, 2012b] Simon A. Rogers and M. Paul Lettinga. “A sequence of physical processes determined and quantified in large-amplitude oscillatory shear (LAOS): Application to theoretical nonlinear models”. *Journal of Rheology* 56.1 (2012), pp. 1–25. ISSN: 0148-6055. doi: [10.1122/1.3662962](https://doi.org/10.1122/1.3662962) (cit. on pp. 11, 89, 93).
- [Roldughin, 2003] V. I. Roldughin. “The characteristics of fractal disperse systems”. *Russian Chemical Reviews* 72.11 (2003), pp. 913–937. doi: [10.1070/RC2003v072n11ABEH000829](https://doi.org/10.1070/RC2003v072n11ABEH000829) (cit. on pp. 17, 50).
- [Rooij, 1993] R. de Rooij, A. A. Potanin, D. van den Ende, and J. Mellema. “Steady shear viscosity of weakly aggregating polystyrene latex dispersions”. *The Journal of Chemical Physics* 99.11 (1993), pp. 9213–9223. ISSN: 0021-9606. doi: [10.1063/1.465537](https://doi.org/10.1063/1.465537) (cit. on p. 17).
- [Rotstein, 2015] Horacio G. Rotstein. “Cluster-size dynamics: A phenomenological model for the interaction between coagulation and fragmentation processes”. *The Journal of Chemical Physics* 142.22 (2015), p. 224101. ISSN: 0021-9606. doi: [10.1063/1.4922113](https://doi.org/10.1063/1.4922113) (cit. on p. 23).
- [RTE, 2023] RTE. *Bilan électrique 2022 : Principaux résultats*. Tech. rep. Le réseau de transport d’électricité, 2023 (cit. on pp. 1, 2).
- [Ruan, 2020] Xuan Ruan, Sheng Chen, and Shuiqing Li. “Structural evolution and breakage of dense agglomerates in shear flow and Taylor-Green vortex”. *Chemical Engineering Science* 211 (2020), pp. 115261–115273. ISSN: 0009-2509. doi: [10.1016/j.ces.2019.115261](https://doi.org/10.1016/j.ces.2019.115261) (cit. on pp. 21, 23, 39, 40, 54, 67).
- [Ruan, 2021] Xuan Ruan, Sheng Chen, and Shuiqing Li. “Effect of long-range Coulomb repulsion on adhesive particle agglomeration in homogeneous isotropic turbulence”. *Journal of Fluid Mechanics* 915.A131 (2021), pp. 1–27. ISSN: 0022-1120. doi: [10.1017/jfm.2021.127](https://doi.org/10.1017/jfm.2021.127) (cit. on p. 21).
- [Russel, 1989] W. B. Russel, D. A. Saville, and W. R. Schowalter. *Colloidal Dispersions*. Cambridge Monographs on Mechanics. Cambridge University Press, 1989. ISBN: 9780511608810. doi: [10.1017/CB09780511608810](https://doi.org/10.1017/CB09780511608810) (cit. on p. 102).
- [Saramito, 2007] Pierre Saramito. “A new constitutive equation for elastoviscoplastic fluid flows”. *Journal of Non-Newtonian Fluid Mechanics* 145 (2007), pp. 1–14. ISSN: 0377-0257. doi: [10.1016/j.jnnfm.2007.04.004](https://doi.org/10.1016/j.jnnfm.2007.04.004) (cit. on pp. 6, 7, 25, 79).
- [Saramito, 2009] Pierre Saramito. “A new elastoviscoplastic model based on the Herschel-Bulkley viscoplastic model”. *Journal of Non-Newtonian Fluid Mechanics* 158.1 (2009), pp. 154–161. ISSN: 0377-0257. doi: [10.1016/j.jnnfm.2008.12.001](https://doi.org/10.1016/j.jnnfm.2008.12.001) (cit. on pp. 6, 7).
- [Sauter, 2008] C. Sauter, M. A. Emin, H. P. Schuchmann, and S. Tavman. “Influence of hydrostatic pressure and sound amplitude on the ultrasound induced dispersion and de-agglomeration of nanoparticles”. *Ultrasonics Sonochemistry* 15 (2008), pp. 517–523. ISSN: 1350-4177. doi: [10.1016/j.ultsonch.2007.08.010](https://doi.org/10.1016/j.ultsonch.2007.08.010) (cit. on pp. 12, 20).
- [Saxena, 2022] Akash Saxena, Jean-Sébastien Kroll-Rabotin, and R. Sean Sanders. “Numerical investigation of the respective roles of cohesive and hydrodynamic forces in aggregate restructuring under shear flow”. *Journal of Colloid and Interface Science* 608.1 (2022), pp. 355–365. ISSN: 0021-9797. doi: [10.1016/j.jcis.2021.08.208](https://doi.org/10.1016/j.jcis.2021.08.208) (cit. on p. 21).
- [Schaefer, 1984] Dale W Schaefer, James E Martin, Pierre Wiltzius, and David S Cannell. “Fractal geometry of colloidal aggregates”. *Physical Review Letters* 52.26 (1984), p. 2371. ISSN: 0031-9007 (cit. on p. 47).
- [Schiessel, 1993] H. Schiessel and A. Blumen. “Hierarchical analogues to fractional relaxation equations”. *Journal of Physics A: Mathematical and General* 26 (1993), pp. 5057–5069. ISSN: 0305-4470. doi: [10.1088/0305-4470/26/19/034](https://doi.org/10.1088/0305-4470/26/19/034) (cit. on pp. 7, 8).
- [Schiessel, 1995a] H. Schiessel and A. Blumen. “Mesoscopic Pictures of the Sol-Gel Transition: Ladder Models and Fractal Networks”. *Macromolecules* 28.11 (1995), pp. 4013–4019. ISSN: 0024-9297. doi: [10.1021/ma00115a038](https://doi.org/10.1021/ma00115a038) (cit. on p. 8).
- [Schiessel, 2000] H. Schiessel, C. Friedrich, and A. Blumen. “Applications of Fractional Calculus in Physics”. World Scientific, 2000. Chap. Applications to problems in polymer physics and rheology, pp. 331–376. doi: [10.1142/9789812817747_0007](https://doi.org/10.1142/9789812817747_0007) (cit. on p. 7).
- [Schiessel, 1995b] H. Schiessel, R. Metzler, A. Blumen, and T. F. Nonnenmacher. “Generalized viscoelastic models: their fractional equations with solutions”. *Journal of Physics A: Mathematical and General* 28 (1995), pp. 6567–6584. ISSN: 0305-4470. doi: [10.1088/0305-4470/28/23/012](https://doi.org/10.1088/0305-4470/28/23/012) (cit. on pp. 7, 85).
- [Schilde, 2011] Carsten Schilde, Caroline Mages-Sauter, Arno Kwade, and H. P. Schuchmann. “Efficiency of different dispersing devices for dispersing nanosized silica and alumina”. *Powder Technology* 207 (2011), pp. 353–361. ISSN: 0032-5910. doi: [10.1016/j.powtec.2010.11.019](https://doi.org/10.1016/j.powtec.2010.11.019) (cit. on pp. 12, 20).

- [Schoenholz, 2016] S. S. Schoenholz, E. D. Cubuk, D. M. Sussman, E. Kaxiras, and A. J. Liu. “A structural approach to relaxation in glassy liquids”. *Nature Physics* 12 (2016), pp. 469–471. issn: 1745-2473. doi: [10.1038/nphys3644](https://doi.org/10.1038/nphys3644) (cit. on p. 11).
- [Sciortino, 2002] Francesco Sciortino. “One liquid, two glasses”. *Nature materials* 1.3 (2002), pp. 145–146. issn: 1476-1122. doi: [10.1038/nmat752](https://doi.org/10.1038/nmat752) (cit. on pp. 11, 12).
- [Seemann, 2011] Ralf Seemann, Martin Brinkmann, Thomas Pfohl, and Stephan Herminghaus. “Droplet based microfluidics”. *Reports on Progress in Physics* 75.1 (2011), p. 016601. issn: 0034-4885. doi: [10.1088/0034-4885/75/1/016601](https://doi.org/10.1088/0034-4885/75/1/016601) (cit. on p. 12).
- [Sehgal, 2019] Prateek Sehgal, Meera Ramaswamy, Itai Cohen, and Brian J. Kirby. “Using Acoustic Perturbations to Dynamically Tune Shear Thickening in Colloidal Suspensions”. *Physical Review Letters* 123.12 (2019), p. 128001. issn: 0031-9007. doi: [10.1103/PhysRevLett.123.128001](https://doi.org/10.1103/PhysRevLett.123.128001) (cit. on p. 20).
- [Selomulya, 2002] C. Selomulya, G. Bushell, R. Amal, and T. D. Waite. “Aggregation Mechanisms of Latex of Different Particle Sizes in a Controlled Shear Environment”. *Langmuir* 18.6 (2002), pp. 1974–1984. issn: 0743-7463. doi: [10.1021/la010702h](https://doi.org/10.1021/la010702h) (cit. on p. 20).
- [Selomulya, 2001] Cordelia Selomulya, Rose Amal, Graeme Bushell, and T. David Waite. “Evidence of Shear Rate Dependence on Restructuring and Breakup of Latex Aggregates”. *Journal of Colloid and Interface Science* 236.1 (2001), pp. 67–77. issn: 0021-9797. doi: [10.1006/jcis.2000.7372](https://doi.org/10.1006/jcis.2000.7372) (cit. on p. 20).
- [Selvadurai, 2001] A. P. S. Selvadurai. “On Boussinesq’s problem”. *International Journal of Engineering Science* 39.3 (2001), pp. 317–322. issn: 0020-7225. doi: [10.1016/S0020-7225\(00\)00043-4](https://doi.org/10.1016/S0020-7225(00)00043-4) (cit. on pp. 71, 72).
- [Shah, 2003] S. A. Shah, Y.-L. Chen, K. S. Schweizer, and C. F. Zukoski. “Viscoelasticity and rheology of depletion flocculated gels and fluids”. *The Journal of Chemical Physics* 119.16 (2003), pp. 8747–8760. issn: 0021-9606. doi: [10.1063/1.1598192](https://doi.org/10.1063/1.1598192) (cit. on p. 15).
- [Shih, 1990] Wei-Heng Shih, Wan Y. Shih, Seong-II Kim, Jun Liu, and Ilhan A. Aksay. “Scaling behavior of the elastic properties of colloidal gels”. *Physical Review A* 42.8 (1990), pp. 4772–4779. issn: 2469-9926. doi: [10.1103/PhysRevA.42.4772](https://doi.org/10.1103/PhysRevA.42.4772) (cit. on pp. 14–16, 18, 19, 45, 50–52, 54–56, 62–64, 66, 68, 79, 86, 109).
- [Shivers, 2020] Jordan L. Shivers, Jingchen Feng, Anne S. G. van Oosten, Herbert Levine, Paul A. Janmey, and Fred C. MacKintosh. “Compression stiffening of fibrous networks with stiff inclusions”. *Proceedings of the National Academy of Sciences* 117.35 (2020), pp. 21037–21044. issn: 1091-6490. doi: [10.1073/pnas.2003037117](https://doi.org/10.1073/pnas.2003037117) (cit. on p. 17).
- [Singhal, 2018] Chirag Singhal, Qasim Murtaza, and Parvej. “Simulation of Critical Velocity of Cold Spray Process with Different Turbulence Models”. *Materials Today: Proceedings* 5.9, Part 1 (2018), pp. 17371–17379. issn: 2214-7853. doi: [10.1016/j.matpr.2018.04.150](https://doi.org/10.1016/j.matpr.2018.04.150) (cit. on p. 96).
- [Sint Annaland, 2006] M. van Sint Annaland, W. Dijkhuizen, N. G. Deen, and J. A. M. Kuipers. “Numerical simulation of behavior of gas bubbles using a 3-D front-tracking method”. *AIChE Journal* 52.1 (2006), pp. 99–110. issn: 1547-5905. doi: [10.1002/aic.10607](https://doi.org/10.1002/aic.10607) (cit. on p. 95).
- [Snabre, 1996] P. Snabre and P. Mills. “I. Rheology of Weakly Flocculated Suspensions of Rigid Particles”. *Journal de Physique III* 6.12 (1996), pp. 1811–1834. doi: [10.1051/jp3:1996215](https://doi.org/10.1051/jp3:1996215) (cit. on pp. 6, 21).
- [Sollich, 1998] Peter Sollich. “Rheological constitutive equation for a model of soft glassy materials”. *Physical Review E* 58.1 (1998), pp. 738–759. issn: 1063-651X. doi: [10.1103/PhysRevE.58.738](https://doi.org/10.1103/PhysRevE.58.738) (cit. on pp. 6, 17, 72, 105).
- [Sollich, 1997] Peter Sollich, François Lecqueux, Pascal Hébraud, and Michael E. Cates. “Rheology of Soft Glassy Materials”. *Physical Review Letters* 78.10 (1997), pp. 2020–2023. issn: 0031-9007. doi: [10.1103/PhysRevLett.78.2020](https://doi.org/10.1103/PhysRevLett.78.2020) (cit. on pp. 6, 17, 72, 105).
- [Sonntag, 1986] Richard C. Sonntag and William B. Russel. “Structure and Breakup of Floccs Subjected to Fluid Stresses: I. Shear Experiments”. *Journal of Colloid and Interface Science* 115.2 (1986), pp. 390–395. issn: 0021-9797. doi: [10.1016/0021-9797\(87\)90054-3](https://doi.org/10.1016/0021-9797(87)90054-3) (cit. on pp. 21, 23, 40).
- [Sonntag, 1987a] Richard C. Sonntag and William B. Russel. “Structure and Breakup of Floccs Subjected to Fluid Stresses: II. Theory”. *Journal of Colloid and Interface Science* 115.2 (1987), pp. 378–389. issn: 0021-9797. doi: [10.1016/0021-9797\(87\)90053-1](https://doi.org/10.1016/0021-9797(87)90053-1) (cit. on pp. 21, 23, 40).
- [Sonntag, 1987b] Richard C. Sonntag and William B. Russel. “Structure and Breakup of Floccs Subjected to Fluid Stresses: III. Converging Flow”. *Journal of Colloid and Interface Science* 113.2 (1987), pp. 399–413. issn: 0021-9797. doi: [10.1016/0021-9797\(86\)90175-X](https://doi.org/10.1016/0021-9797(86)90175-X) (cit. on pp. 21, 23, 40).

- [Sorensen, 2001] C. M. Sorensen. “Light Scattering by Fractal Aggregates: A Review”. *Aerosol Science Technology* 35 (2001), pp. 648–687. issn: 0278-6826. doi: [10.1080/02786820117868](https://doi.org/10.1080/02786820117868) (cit. on pp. 12, 15, 56).
- [Sorensen, 1987] C. M. Sorensen, H. X. Zhang, and T. W. Taylor. “Cluster-size evolution in a coagulation-fragmentation system”. *Physical Review Letters* 59.3 (1987), pp. 363–366. issn: 0031-9007. doi: [10.1103/PhysRevLett.59.363](https://doi.org/10.1103/PhysRevLett.59.363) (cit. on pp. 13, 21, 38, 48, 54).
- [Spicer, 1996] Patrick T. Spicer and Sotiris E. Pratsinis. “Coagulation and fragmentation: Universal steady-state particle-size distribution”. *AIChE Journal* 42.6 (1996), pp. 1612–1620. issn: 1547-5905. doi: [10.1002/aic.690420612](https://doi.org/10.1002/aic.690420612) (cit. on pp. 23, 39).
- [Spicer, 1998] Patrick T. Spicer, Sotiris E. Pratsinis, Judy Raper, Rose Amal, Graeme Bushell, and Gabriele Meesters. “Effect of shear schedule on particle size, density, and structure during flocculation in stirred tanks”. *Powder Technology* 97.1 (1998), pp. 26–34. issn: 0032-5910. doi: [10.1016/S0032-5910\(97\)03389-5](https://doi.org/10.1016/S0032-5910(97)03389-5) (cit. on p. 67).
- [Sprakel, 2011] Joris Sprakel, Stefan B Lindström, Thomas E Kodger, and David A Weitz. “Stress enhancement in the delayed yielding of colloidal gels”. *Physical review letters* 106.24 (2011), p. 248303. issn: 0031-9007 (cit. on p. 48).
- [Stadnichuk, 2015] Vladimir Stadnichuk, Anna Bodrova, and Nikolai Brilliantov. “Smoluchowski aggregation fragmentation equations: Fast numerical method to find steady-state solutions”. *International Journal of Modern Physics B* 29.1550208 (2015), pp. 1–10. doi: [10.1142/S0217979215502082](https://doi.org/10.1142/S0217979215502082) (cit. on pp. 14, 23, 36, 48).
- [Stamou, 2000] Dimitris Stamou, Clus Duschl, and Diethelm Johannsmann. “Long-range attraction between colloidal spheres at the air-water interface: The consequence of an irregular meniscus”. *Physica Review E* 62.4 (2000), pp. 5263–5272. issn: 1063-651X. doi: [10.1103/PhysRevE.62.5263](https://doi.org/10.1103/PhysRevE.62.5263) (cit. on p. 20).
- [Stauffer, 2003] Dietrich Stauffer and Amnon Aharony. *Introduction to Percolation Theory*. 2nd ed. 325 Chestnut Street 8th Floor Philadelphia: Taylor & Francis, 2003. isbn: 0-7484-0253-5. doi: [10.1201/9781315274386](https://doi.org/10.1201/9781315274386) (cit. on p. 17).
- [Stockmayer, 1944] Walter H. Stockmayer. “Theory of Molecular Size Distribution and Gel Formation in Branched Polymers II. General Cross Linking”. *The Journal of Chemical Physics* 12.4 (1944), pp. 125–131. issn: 0021-9606. doi: [10.1063/1.1723922](https://doi.org/10.1063/1.1723922) (cit. on p. 13).
- [Stokes, 1901] George Gabriel Stokes. “On the Effect of the Internal Friction of Fluids on the Motion of Pendulums”. *Mathematical and Physical Papers*. Vol. 3. Cambridge Library Collection - Mathematics. Cambridge University Press, 1901, pp. 1–10. doi: [10.1017/CB09780511702266.002](https://doi.org/10.1017/CB09780511702266.002) (cit. on p. 26).
- [Storm, 2005] Cornelis Storm, Jennifer J. Pastore, F. C. MacKintosh, T. C. Lubensky, and Paul A. Janmey. “Nonlinear elasticity in biological gels”. *Nature* 435 (2005), pp. 191–194. issn: 0028-0836. doi: [10.1038/nature03521](https://doi.org/10.1038/nature03521) (cit. on p. 79).
- [Stranne, 2016] C. Stranne, M. O’Regan, and M. Jakobsson. “Overestimating climate warming-induced methane gas escape from the seafloor by neglecting multiphase flow dynamics”. *Geophysical Research Letters* 43.16 (2016), pp. 8703–8712. issn: 1944-8007. doi: [10.1002/2016GL070049](https://doi.org/10.1002/2016GL070049) (cit. on p. 95).
- [Stukowski, 2010] Alexander Stukowski. “Visualization and analysis of atomistic simulation data with OVITO—the Open Visualization Tool”. *Modelling and Simulation in Materials Science and Engineering* 18.1 (2010), p. 015012. issn: 0965-0393. doi: [10.1088/0965-0393/18/1/015012](https://doi.org/10.1088/0965-0393/18/1/015012) (cit. on p. 34).
- [Stumpf, 2000] Andrew J. Stumpf, Bruce E. Broster, and Victor M. Levson. “Multiphase flow of the late Wisconsinan Cordilleran ice sheet in western Canada”. *GSA Bulletin* 112.12 (2000), pp. 1850–1863. issn: 0016-7606. doi: [10.1130/0016-7606\(2000\)112<1850:MFOTLW>2.0.CO;2](https://doi.org/10.1130/0016-7606(2000)112<1850:MFOTLW>2.0.CO;2) (cit. on p. 95).
- [Suarez, 2018] Andres Suarez. “Numerical simulation of multi-dimensional fractal soot aggregates”. MA thesis. Royal Institute of Technology, 2018 (cit. on p. 14).
- [Sudreau, 2022] Iana Sudreau, Sébastien Manneville, Marion Servel, and Thibaut Divoux. “Shear-induced memory effects in boehmite gels”. *Journal of Rheology* 66.1 (2022), pp. 91–104. issn: 0148-6055. doi: [10.1122/8.0000282](https://doi.org/10.1122/8.0000282) (cit. on p. 44).
- [Sugimoto, 2019] Tadao Sugimoto. “Monodispersed Particles”. Second. Elsevier, 2019. Chap. Application to Fundamental Studies, pp. 545–592. isbn: 978-0-444-62749-0. doi: [10.1016/C2012-0-02740-8](https://doi.org/10.1016/C2012-0-02740-8) (cit. on p. 9).
- [Sussman, 1994] Mark Sussman, Peter Smereka, and Stanley Osher. “A Level Set Approach for Computing Solutions to Incompressible Two-Phase Flow”. *Journal of Computational Physics* 114.1 (1994), pp. 146–159. issn: 0021-9991. doi: [10.1006/jcph.1994.1155](https://doi.org/10.1006/jcph.1994.1155) (cit. on p. 96).

- [Swope, 1982] William C. Swope, Hans C. Andersen, Peter H. Berens, and Kent R. Wilson. “A computer simulation method for the calculation of equilibrium constants for the formation of physical clusters of molecules: Application to small water clusters”. *The Journal of Chemical Physics* 76.1 (1982), pp. 637–649. ISSN: 0021-9606. DOI: [10.1063/1.442716](https://doi.org/10.1063/1.442716) (cit. on pp. 14, 33).
- [Szewc, 2013] K. Szewc, J. Pozorski, and J.-P. Minier. “Simulations of single bubbles rising through viscous liquids using Smoothed Particle Hydrodynamics”. *International Journal of Multiphase Flow* 50 (2013), pp. 98–105. ISSN: 0301-9322. DOI: [10.1016/j.ijmultiphaseflow.2012.11.004](https://doi.org/10.1016/j.ijmultiphaseflow.2012.11.004) (cit. on p. 95).
- [Sztucki, 2007] M. Sztucki, T. Narayanan, and G. Beaucage. “In situ study of aggregation of soot particles in an acetylene flame by small-angle x-ray scattering”. *Journal of Applied Physics* 101.11 (2007), p. 114304. ISSN: 0021-8979. DOI: [10.1063/1.2740341](https://doi.org/10.1063/1.2740341) (cit. on pp. 20, 42, 58, 60, 83).
- [Tang, 2006] Dongming Tang and Alejandro G. Marangoni. “Microstructure and Fractal Analysis of Fat Crystal Networks”. *Journal of the American Oil Chemists’ Society* 83.5 (2006), pp. 377–388. ISSN: 0003-021X. DOI: [10.1007/s11746-006-1216-9](https://doi.org/10.1007/s11746-006-1216-9) (cit. on p. 17).
- [Tang, 2008] Dongming Tang and Alejandro G. Marangoni. “Modified fractal model and rheological properties of colloidal networks”. *Journal of Colloid and Interface Science* 318.2 (2008), pp. 202–209. ISSN: 0021-9797. DOI: [10.1016/j.jcis.2007.09.062](https://doi.org/10.1016/j.jcis.2007.09.062) (cit. on pp. 17, 62).
- [Tanner, 2018] Roger I. Tanner. “Review Article: Aspects of non-colloidal suspension rheology”. *Physics of Fluids* 30.10 (2018), p. 101301. ISSN: 1070-6631. DOI: [10.1063/1.5047535](https://doi.org/10.1063/1.5047535) (cit. on p. 9).
- [Tapia, 2019] Franco Tapia, Olivier Pouliquen, and Élisabeth Guazzelli. “Influence of surface roughness on the rheology of immersed and dry frictional spheres”. *Physical Review Fluids* 4 (10 2019), p. 104302. ISSN: 2469-990X. DOI: [10.1103/PhysRevFluids.4.104302](https://doi.org/10.1103/PhysRevFluids.4.104302) (cit. on p. 12).
- [Tavares, 2016] Dina Tavares, Ricardo Almeida, and Delfim F. M. Torres. “Caputo derivatives of fractional variable order: Numerical approximations”. *Communications Nonlinear Sciences and Numerical Simulation* 35 (2016), pp. 69–87. ISSN: 1007-5704. DOI: [10.1016/j.cnsns.2015.10.027](https://doi.org/10.1016/j.cnsns.2015.10.027) (cit. on p. 8).
- [Teixeira, 1988] J. Teixeira. “Small-angle scattering by fractal systems”. *Journal of Applied Crystallography* 21.6 (1988), pp. 781–785. ISSN: 0021-8898. DOI: [10.1107/S0021889888000263](https://doi.org/10.1107/S0021889888000263) (cit. on pp. 13, 83).
- [Tennekes, 1972] H. Tennekes and J. L. Lumley. *A First Course in Turbulence*. MIT Press, 1972. ISBN: 0262200198 (cit. on p. 11).
- [Thomas, 1999] D. N. Thomas, S. J. Judd, and N. Fawcett. “Flocculation modelling: a review”. *Water Research* 33.7 (1999), pp. 1579–1592. ISSN: 0043-1354. DOI: [10.1016/S0043-1354\(98\)00392-3](https://doi.org/10.1016/S0043-1354(98)00392-3) (cit. on p. 23).
- [Thompson, 2022] A. P. Thompson, H. M. Aktulga, R. Berger, D. S. Bolintineanu, W. M. Brown, P. S. Crozier, P. J. in ’t Veld, A. Kohlmeyer, S. G. Moore, T. D. Nguyen, R. Shan, M. J. Stevens, J. Tranchida, C. Trott, and S. J. Plimpton. “LAMMPS - a flexible simulation tool for particle-based materials modeling at the atomic, meso, and continuum scales”. *Computer Physics Communications* 271 (2022), p. 108171. ISSN: 0010-4655. DOI: [10.1016/j.cpc.2021.108171](https://doi.org/10.1016/j.cpc.2021.108171) (cit. on p. 32).
- [Tine, 2011] Léon Matar S. Tine. “Analyse mathématique et numérique de modèles de coagulation-fragmentation”. PhD thesis. Université Lille 1, 2011 (cit. on p. 14).
- [Tirado-Miranda, 1999] M. Tirado-Miranda, A. Schmitt, J. Callejas-Fernández, and A. Fernández-Barbero. “Colloidal Clusters with Finite Binding Energies: Fractal Structure and Growth Mechanism”. *Langmuir* 15.10 (1999), pp. 3437–3444. ISSN: 0743-7463. DOI: [10.1021/la981233v](https://doi.org/10.1021/la981233v) (cit. on p. 20).
- [Torres, 1991a] Francisco E. Torres, William B. Russel, and William R. Schowalter. “Floc Structure and Growth Kinetics for Rapid Shear Coagulation of Polystyrene Colloids”. *Journal of Colloid and Interface Science* 142.2 (1991), pp. 554–574. ISSN: 0021-9797. DOI: [10.1016/0021-9797\(91\)90086-N](https://doi.org/10.1016/0021-9797(91)90086-N) (cit. on pp. 21, 23, 40).
- [Torres, 1991b] Francisco E. Torres, William B. Russel, and William R. Schowalter. “Simulation of Coagulation in Viscous Flows”. *Journal of Colloid and Interface Science* 145.1 (1991), pp. 51–73. ISSN: 0021-9797. DOI: [10.1016/0021-9797\(91\)90099-T](https://doi.org/10.1016/0021-9797(91)90099-T) (cit. on pp. 21, 23, 40).
- [Trappe, 2000] V Trappe and DA Weitz. “Scaling of the viscoelasticity of weakly attractive particles”. *Physical review letters* 85.2 (2000), p. 449. ISSN: 0031-9007 (cit. on pp. 44, 58, 86).
- [Trappe, 2001] V. Trappe, V. Prasad, Luca Cipelletti, P. N. Segre, and D. A. Weitz. “Jamming phase diagram for attractive particles”. *Nature* 411 (2001), pp. 772–775. ISSN: 0028-0836. DOI: [10.1038/35081021](https://doi.org/10.1038/35081021) (cit. on pp. 11, 45).

- [Trappe, 2007] Veronique Trappe, Estelle Pitard, Laurence Ramos, Aymeric Robert, Hugo Bissig, and Luca Cipelletti. “Investigation of q-dependent dynamical heterogeneity in a colloidal gel by x-ray photon correlation spectroscopy”. *Physical Review E* 76.5 (2007), p. 051404 (cit. on p. 42).
- [Tresca, 1864] Henri Tresca. “Mémoires sur l’écoulement des corps solides soumis à de fortes pressions”. *Compte Rendus à l’Académie des Sciences de Paris* 59 (1864), p. 754 (cit. on pp. 5, 6).
- [van Dillen, 2008] T. van Dillen, P. R. Onck, and E. Van der Giessen. “Models for stiffening in cross-linked biopolymer networks: A comparative study”. *Journal of the Mechanics and Physics of Solids* 56.6 (2008), pp. 2240–2264. issn: 0022-5096. doi: [10 . 1016/j . jmps . 2008 . 01 . 007](https://doi.org/10.1016/j.jmps.2008.01.007) (cit. on p. 17).
- [Van Gorp, 1998] Marnix Van Gorp and Jo Palmen. “Time-temperature superposition for polymeric blends”. *Rheol. Bull* 67.1 (1998), pp. 5–8 (cit. on p. 47).
- [van Sint Annaland, 2005] M. van Sint Annaland, N. G. Deen, and J. A. M. Kuipers. “Numerical simulation of gas bubbles behaviour using a three-dimensional volume of fluid method”. *Chemical Engineering Science* 60.11 (2005), pp. 2999–3011. issn: 0009-2509. doi: [10 . 1016/j . ces . 2005 . 01 . 031](https://doi.org/10.1016/j.ces.2005.01.031) (cit. on p. 95).
- [Varga, 2019] Zsigmond Varga, Vincent Grenard, Stefano Pecorario, Nicolas Taberlet, Vincent Dolique, Sébastien Manneville, Thibaut Divoux, Gareth H. McKinley, and James W. Swan. “Hydrodynamics control shear-induced pattern formation in attractive suspensions”. *Proceedings of the National Academy of Sciences* 116.25 (2019), pp. 12193–12198. doi: [10 . 1073 / pnas . 1901370116](https://doi.org/10.1073/pnas.1901370116) (cit. on pp. 11, 21, 31, 41, 66–68).
- [Varga, 2018] Zsigmond Varga and James W. Swan. “Large scale anisotropies in sheared colloidal gels”. *Journal of Rheology* 62.2 (2018), pp. 405–418. issn: 0148-6055. doi: [10 . 1122/1 . 5003364](https://doi.org/10.1122/1.5003364) (cit. on p. 48).
- [Varrato, 2012] Francesco Varrato, Lorenzo Di Michele, Maxim Belushkin, Nicolas Dorsaz, Simon H. Nathan, Erika Eiser, and Giuseppe Foffi. “Arrested demixing opens route to bigels”. *Proceedings of the National Academy of Sciences* 109.47 (2012), pp. 19155–19160. issn: 0027-8424. doi: [10 . 1073 / pnas . 1214971109](https://doi.org/10.1073/pnas.1214971109) (cit. on p. 17).
- [Vassileva, 2005] Nikolina D. Vassileva, Dirk van den Ende, Frieder Mugele, and Jorrit Mellema. “Capillary Forces between spherical Particles Floating at a Liquid-Liquid Interface”. *Langmuir* 21.24 (2005), pp. 11190–11200. issn: 0743-7463. doi: [10 . 1021 / la051186o](https://doi.org/10.1021/la051186o) (cit. on pp. 12, 20).
- [Vella, 2005] Dominic Vella and L. Mahadevar. “The “Cheerios effect””. *American Journal of Physics* 73.9 (2005), pp. 817–825. doi: [10 . 1119/1 . 1898523](https://doi.org/10.1119/1.1898523) (cit. on p. 20).
- [Ven, 1977] T. G. M. van de Ven and S. G. Mason. “The microrheology of colloidal dispersions VII. Orthokinetic doublet formation of spheres”. *Colloid & Polymer Sciences* 255 (1977), pp. 468–479. issn: 0303-402X. doi: [10 . 1007 / BF01536463](https://doi.org/10.1007/BF01536463) (cit. on p. 12).
- [Vereroudakis, 2020] Emmanouil Vereroudakis, Minaspi Bantawa, René P. M. Lafleur, Daniele Parisi, Nicholas M. Matsumoto, Joris W. Peeters, Emanuela Del Gado, E. W. Meijer, and Dimitris Vlassopoulos. “Competitive Supramolecular Associations Mediate the Viscoelasticity of Binary Hydrogels”. *ACS Central Science* 6.8 (2020), pp. 1401–1411. issn: 2374-7951. doi: [10 . 1021 / acscentsci . 0c00279](https://doi.org/10.1021/acscentsci.0c00279) (cit. on p. 17).
- [Vernerey, 2021] Franck J. Vernerey, Shankar Lalitha Sridhar, Archish Muralidharan, and Stephanie J. Bryant. “Mechanics of 3D Cell-Hydrogel Interactions: Experiments, Models, and Mechanisms”. *Chemical Reviews* 121.18 (2021), pp. 11085–11148. issn: 0009-2665. doi: [10 . 1021 / acs . chemrev . 1c00046](https://doi.org/10.1021/acs.chemrev.1c00046) (cit. on p. 17).
- [Vilensky, 2012] G. Vilensky, G. ter Haar, and N. Safari. “A model of acoustic absorption in fluids based on a continuous distribution of relaxation times”. *Wave Motion* 49 (2012), pp. 93–108. issn: 0165-2125. doi: [10 . 1016/j . wavemoti . 2011 . 07 . 005](https://doi.org/10.1016/j.wavemoti.2011.07.005) (cit. on p. 8).
- [Villa, 2018] Stefano Villa. “Behaviour of a Colloid close to an Air-Water Interface: Interactions and Dynamics”. PhD thesis. Université de Montpellier, 2018 (cit. on p. 20).
- [Visser, 1972] J. Visser. “On Hamaker constants: A comparison between Hamaker constants and Lifshitz-Van der Waals constants”. *Advances in Colloid and Interface Science* 3 (1972), pp. 331–363. doi: [10 . 1016/0001 - 8686 \(72\) 85001 - 2](https://doi.org/10.1016/0001-8686(72)85001-2) (cit. on pp. 12, 41).
- [Voigt, 1890] W. Voigt. “Ueber die innere Reibung der festen Körper, insbesondere der Krystalle”. *Abhandlungen der Königlichen Gesellschaft der Wissenschaften in Göttingen* 36 (1890), pp. 3–48 (cit. on pp. 6, 7, 104).
- [Wagner, 2021] Norman J. Wagner and Jan Mewis. *Theory and Applications of Colloidal Suspension Rheology*. Cambridge University Press, 2021. isbn: 978-1-108-42303-8. doi: [10 . 1017 / 9781108394826](https://doi.org/10.1017/9781108394826) (cit. on p. 17).

- [Wagner, 1990] Norman J. Wagner and William B. Russel. “Light scattering measurements of a hard-sphere suspension under shear”. *Physics of Fluids A: Fluid Dynamics* 2.4 (1990), pp. 491–502. issn: 0899-8213. doi: [10.1063/1.857749](https://doi.org/10.1063/1.857749) (cit. on p. 13).
- [Waite, 2001] T. D. Waite, J. K. Cleaver, and J. K. Beattie. “Aggregation Kinetics and Fractal Structure of γ -Alumina Assemblages”. *Journal of Colloid and Interface Science* 241 (2001), pp. 333–339. issn: 0021-9797. doi: [10.1006/jcis.2001.769](https://doi.org/10.1006/jcis.2001.769) (cit. on pp. 12, 20, 41).
- [Wallace, 2017] J. B. Wallace, L. B. Bayu Aji, L. Shao, and S. O. Kucheyev. “Fractal analysis of collision cascades in pulsed-ion-beam-irradiated solids”. *Scientific Reports* 7.17574 (2017), pp. 1–11. doi: [10.1038/s41598-017-17781-5](https://doi.org/10.1038/s41598-017-17781-5) (cit. on p. 20).
- [Wang, 2013] Junfeng Wang, Zongzheng Zhou, Wei Zhang, Timothy M. Garoni, and Youjin Deng. “Bond and site percolation in three dimensions”. *Physical Review E* 87.5 (2013), p. 052107. issn: 1539-3755. doi: [10.1103/PhysRevE.87.052107](https://doi.org/10.1103/PhysRevE.87.052107) (cit. on p. 12).
- [Wang, 2018] Meng-Jiao Wang. *Carbon Black: Science and Technology*. Routledge, 2018 (cit. on pp. 42, 58).
- [Wang, 2022] Yilin Wang and Randy H. Ewoldt. *New insights on carbon black suspension rheology – anisotropic thixotropy and anti-thixotropy*. 2022. doi: [10.48550/ARXIV.2202.05772](https://doi.org/10.48550/ARXIV.2202.05772) (cit. on pp. 17, 47).
- [Wattis, 2006] Jonathan A. D. Wattis. “An introduction to mathematical models of coagulation–fragmentation processes: A discrete deterministic mean-field approach”. *Physica D* 222 (2006), pp. 1–20. issn: 0167-2789. doi: [10.1016/j.physd.2006.07.024](https://doi.org/10.1016/j.physd.2006.07.024) (cit. on pp. 13, 23, 39).
- [Webber, 2007] Rebecca E. Webber, Constantino Creton, Hugh R. Brown, and Jian Ping Gong. “Large Strain Hysteresis and Mullins Effect of Tough Double-Network Hydrogels”. *Macromolecules* 40.8 (2007), pp. 2919–2927. issn: 0024-9297. doi: [10.1021/ma062924y](https://doi.org/10.1021/ma062924y) (cit. on p. 7).
- [Weitz, 1985] D. A. Weitz, J. S. Huang, M. Y. Lin, and J. Sung. “Limits of the Fractal Dimension for Irreversible Kinetic Aggregation of Gold Colloids”. *Physical Review Letters* 54.13 (1985), pp. 1416–1419. issn: 0031-9007. doi: [10.1103/PhysRevLett.54.1416](https://doi.org/10.1103/PhysRevLett.54.1416) (cit. on pp. 12, 54).
- [Weitz, 1984] D. A. Weitz and M. Oliveria. “Fractal Structures Formed by Kinetic Aggregation of Aqueous Gold Colloids”. *Physical Review Letters* 52.16 (1984), pp. 1433–1436. issn: 0031-9007. doi: [10.1103/PhysRevLett.52.1433](https://doi.org/10.1103/PhysRevLett.52.1433) (cit. on pp. 12, 47, 54).
- [Wen, 2014] Yu Ho Wen, Yingying Lu, Kerianne M Dobosz, and Lynden A Archer. “Structure, ion transport, and rheology of nanoparticle salts”. *Macromolecules* 47.13 (2014), pp. 4479–4492 (cit. on p. 47).
- [Wen, 2015] Yu Ho Wen, Jennifer L Schaefer, and Lynden A Archer. “Dynamics and rheology of soft colloidal glassestrappe2007”. *Acs Macro Letters* 4.1 (2015), pp. 119–123 (cit. on p. 47).
- [Wessel, 1992] R. Wessel and R. C. Ball. “Fractal aggregates and gels in shear flow”. *Physical Review A* 46.6 (1992), R3008–R3011. issn: 2469-9926. doi: [10.1103/PhysRevA.46.R3008](https://doi.org/10.1103/PhysRevA.46.R3008) (cit. on pp. 21, 23, 40, 47, 50, 52, 66, 67).
- [Whitaker, 2019] Kathryn A. Whitaker, Zsigmond Varga, Lilian C. Hsiao, Michael J. Solomon, James W. Swan, and Eric M. Furst. “Colloidal gel elasticity arises from the packing of locally glassy clusters”. *Nature Communications* 10.2237 (2019), pp. 1–8. issn: 2041-1723. doi: [10.1038/s41467-019-10039-w](https://doi.org/10.1038/s41467-019-10039-w) (cit. on p. 17).
- [Wikipedia contributors, 2022a] Wikipedia contributors. *Alternative stress measures — Wikipedia, The Free Encyclopedia*. [Online; accessed 19-August-2022]. 2022 (cit. on pp. 9, 10).
- [Wikipedia contributors, 2022b] Wikipedia contributors. *Objective stress rate — Wikipedia, The Free Encyclopedia*. [Online; accessed 19-August-2022]. 2022 (cit. on p. 10).
- [Williams, 1985] Forman A. Williams. *Combustion Theory: The Fundamental Theory of Chemically Reacting Flow Systems*. Second. Benjamin-Cummings Publishing Company, 1985. isbn: 0-8053-9801-5 (cit. on pp. 14, 16).
- [Won, 2005] You-Yeon Won, Steve P Meeker, Veronique Trappe, David A Weitz, Nancy Z Diggs, and Jacob I Emert. “Effect of temperature on carbon-black agglomeration in hydrocarbon liquid with adsorbed dispersant”. *Langmuir* 21.3 (2005), pp. 924–932. issn: 0743-7463 (cit. on p. 44).
- [Wu, 2013] Hua Wu, Marco Lattuada, and Massimo Morbidelli. “Dependence of fractal dimension of DLCA clusters on size of primary particles”. *Advances in Colloid and Interface Science* 195-196 (2013), pp. 41–49. issn: 0001-8686. doi: [10.1016/j.cis.2013.04.001](https://doi.org/10.1016/j.cis.2013.04.001) (cit. on p. 20).
- [Wu, 2003] Hua Wu, Marco Lattuada, Peter Sandkühler, Jan Sefcik, and Massimo Morbidelli. “Role of Sedimentation and Buoyancy on the Kinetics of Diffusion Limited Colloidal Aggregation”. *Langmuir* 19.26 (2003), pp. 10710–10718. issn: 0743-7463. doi: [10.1021/la034970m](https://doi.org/10.1021/la034970m) (cit. on p. 13).

- [Wu, 2001] Hua Wu and Massimo Morbidelli. “Model Relating Structure of Colloidal Gels to Their Elastic Properties”. *Langmuir* 17.4 (2001), pp. 1030–1036. ISSN: 0743-7463. DOI: [10.1021/1a001121f](https://doi.org/10.1021/1a001121f) (cit. on pp. 15, 17, 18, 50–52, 54–56, 62–66, 79, 109).
- [Xi, 2006] Jun Xi and B-J Zhong. “Soot in diesel combustion systems”. *Chemical Engineering & Technology: Industrial Chemistry-Plant Equipment-Process Engineering-Biotechnology* 29.6 (2006), pp. 665–673 (cit. on pp. 42, 58).
- [Xie, 2010] Delong Xie, Hua Wu, Alessio Zaccone, Leonie Braun, Huanqin Chen, and Massimo Morbidelli. “Criticality for shear-induced gelation of charge-stabilized colloids”. *Soft Matter* 6 (12 2010), pp. 2692–2698. ISSN: 1744-6848. DOI: [10.1039/C002043E](https://doi.org/10.1039/C002043E) (cit. on pp. 21, 23, 31, 40).
- [Xie, 2016] Zhihua Xie, Dimitrios Pavlidis, Pablo Salinas, James R. Percival, Christopher C. Pain, and Omar K. Matar. “A balanced-force control volume finite element method for interfacial flows with surface tension using adaptive anisotropic unstructured meshes”. *Computers & Fluids* 138 (2016), pp. 38–50. ISSN: 0045-7930. DOI: [10.1016/j.compfluid.2016.08.005](https://doi.org/10.1016/j.compfluid.2016.08.005) (cit. on p. 95).
- [Xu, 2014] Xiao Xu, Junfeng Wang, Jian-Ping Lv, and Youjin Deng. “Simultaneous analysis of three-dimensional percolation models”. *Frontier of Physics* 9.1 (2014), pp. 113–119. ISSN: 2095-0462. DOI: [10.1007/s11467-013-0403-z](https://doi.org/10.1007/s11467-013-0403-z) (cit. on p. 12).
- [Xue, 1992] J.-Z. Xue, E. Herbolzheimer, M. A. Rutgers, W. B. Russel, and P. M. Chaikin. “Diffusion, Dispersion, and Settling of Hard Spheres”. *Physical Review Letters* 69.11 (1992), pp. 1715–1718. DOI: [10.1103/PhysRevLett.69.1715](https://doi.org/10.1103/PhysRevLett.69.1715) (cit. on p. 12).
- [Yamamoto, 2017] Takuya Yamamoto, Yasunori Okano, and Sadik Dost. “Validation of the S-CLSVOF method with the density-scaled balanced continuum surface force model in multiphase systems coupled with thermocapillary flows”. *International Journal for Numerical Methods in Fluids* 83.3 (2017), pp. 223–244. ISSN: 1097-0363. DOI: [10.1002/flid.4267](https://doi.org/10.1002/flid.4267) (cit. on p. 97).
- [Yao, 2021] Yuan Yao and Jesse Capecelatro. “Deagglomeration of cohesive particles by turbulence”. *Journal of Fluid Mechanics* 911.A10 (2021), pp. 1–26. ISSN: 0022-1120. DOI: [10.1017/jfm.2020.1020](https://doi.org/10.1017/jfm.2020.1020) (cit. on p. 21).
- [Yin, 2016] Shuo Yin, Morten Meyer, Wenya Li, Hanlin Liao, and Rocco Lupoi. “Gas Flow, Particle Acceleration, and Heat Transfer in Cold Spray: A review”. *Journal of Thermal Spray Technology* 25.5 (2016), pp. 874–896. ISSN: 1059-9630. DOI: [10.1007/s11666-016-0406-8](https://doi.org/10.1007/s11666-016-0406-8) (cit. on pp. 95, 96).
- [Yokoi, 2014] Kensuke Yokoi. “A density-scaled continuum surface force model within a balanced force formulation”. *Journal of Computational Physics* 278 (2014), pp. 221–228. ISSN: 0021-9991. DOI: [10.1016/j.jcp.2014.08.034](https://doi.org/10.1016/j.jcp.2014.08.034) (cit. on p. 97).
- [Yokoi, 2016] Kensuke Yokoi, Ryo Onishi, Xiao-Long Deng, and Mark Sussman. “Density-Scaled Balanced Continuum Surface Force Model with a Level Set Based Curvature Interpolation Technique”. *International Journal of Computational Methods* 13.04 (2016), p. 1641004. ISSN: 0219-8762. DOI: [10.1142/S0219876216410048](https://doi.org/10.1142/S0219876216410048) (cit. on p. 97).
- [Yu, 2009] Zhao Yu and Liang-Shih Fan. “An interaction potential based lattice Boltzmann method with adaptive mesh refinement (AMR) for two-phase flow simulation”. *Journal of Computational Physics* 228.17 (2009), pp. 6456–6478. ISSN: 0021-9991. DOI: [10.1016/j.jcp.2009.05.034](https://doi.org/10.1016/j.jcp.2009.05.034) (cit. on pp. 14, 95).
- [Yu, 2011] Zhao Yu, Hui Yang, and Liang-Shih Fan. “Numerical simulation of bubble interactions using an adaptive lattice Boltzmann method”. *Chemical Engineering Science* 66.14 (2011), pp. 3441–3451. ISSN: 0009-2509. DOI: [10.1016/j.ces.2011.01.019](https://doi.org/10.1016/j.ces.2011.01.019) (cit. on p. 95).
- [Yuan, 2016] Wen-Jie Yuan, Qing Huang, Cheng-Ji Deng, and Hong-Xi Zhu. “Effects of Powder Characteristics on Rheological Properties of Alumina Slurries”. *2nd Annual International Conference on Advanced Material Engineering*. Atlantis Press, 2016, pp. 665–669. DOI: [10.2991/ame-16.2016.111](https://doi.org/10.2991/ame-16.2016.111) (cit. on p. 12).
- [Zaccone, 2010] Alessio Zaccone, Daniele Gentili, Hua Wu, and Massimo Morbidelli. “Shear-induced reaction-limited aggregation kinetics of Brownian particles at arbitrary concentrations”. *The Journal of Chemical Physics* 132.13 (2010), pp. 134903–1–7. ISSN: 0021-9606. DOI: [10.1063/1.3361665](https://doi.org/10.1063/1.3361665) (cit. on p. 13).
- [Zaccone, 2009a] Alessio Zaccone, Miroslav Soos, Marco Lattuada, Hua Wu, Matthäus U. Bäbler, and Massimo Morbidelli. “Breakup of dense colloidal aggregates under hydrodynamic stresses”. *Physical Review E* 79 (6 2009), p. 061401. ISSN: 2470-0045. DOI: [10.1103/PhysRevE.79.061401](https://doi.org/10.1103/PhysRevE.79.061401) (cit. on pp. 21, 23, 40).
- [Zaccone, 2009b] Alessio Zaccone, Hua Wu, and Emanuela Del Gado. “Elasticity of Arrested Short-Range Attractive Colloids: Homogeneous and Heterogeneous Glasses”. *Physical Review Letters* 103.20 (2009), p. 208301. ISSN: 0031-9007. DOI: [10.1103/PhysRevLett.103.208301](https://doi.org/10.1103/PhysRevLett.103.208301) (cit. on p. 23).

- [Zaccone, 2009c] Alessio Zaccone, Hua Wu, Daniele Gentili, and Massimo Morbidelli. “Theory of activated-rate processes under shear with application to shear-induced aggregation of colloids”. *Physical Review E* 80 (5 2009), p. 051404. issn: 2470-0045. doi: [10.1103/PhysRevE.80.051404](https://doi.org/10.1103/PhysRevE.80.051404) (cit. on p. 67).
- [Zhang, 2015] Aman Zhang, Pengnan Sun, and Furen Ming. “An SPH modeling of bubble rising and coalescing in three dimensions”. *Computer Methods in Applied Mechanics and Engineering* 294 (2015), pp. 189–209. issn: 0045-7825. doi: [10.1016/j.cma.2015.05.014](https://doi.org/10.1016/j.cma.2015.05.014) (cit. on p. 95).
- [Zhang, 1996] Jingwu Zhang and Jacques Buffle. “Multi-method determination of the fractal dimension of hematite aggregates”. *Colloids and Surfaces A: Physicochemical and Engineering Aspects* 107 (1996), pp. 175–187. issn: 0927-7757. doi: [10.1016/0927-7757\(95\)03344-0](https://doi.org/10.1016/0927-7757(95)03344-0) (cit. on pp. 12, 13).
- [Zhang, 2021] Shang Zhang, Ethan Stanifer, Vishwas Vasisht, Leyou Zhang, Emanuela Del Gado, and Xiaoming Mao. *Prestressed elasticity of amorphous solids*. 2021 (cit. on p. 6).
- [Zhou, 2012] Zongzheng Zhou, Ji Yang, Youjin Deng, and Robert M. Ziff. “Shortest-path fractal dimension for percolation in two and three dimensions”. *Physical Review E* 86.6 (2012), p. 061101. issn: 2470-0045. doi: [10.1103/PhysRevE.86.061101](https://doi.org/10.1103/PhysRevE.86.061101) (cit. on p. 12).
- [Zhou, 1991] Zukang Zhou and Benjamin Chu. “Light-scattering study on the fractal aggregates of polystyrene spheres: Kinetic and structural approaches”. *Journal of Colloid and Interface Science* 143.2 (1991), pp. 356–365. issn: 0021-9797. doi: [10.1016/0021-9797\(91\)90269-E](https://doi.org/10.1016/0021-9797(91)90269-E) (cit. on p. 12).
- [Zölzer, 1993] U Zölzer and H-F Eicke. “Free oscillatory shear measurements—An interesting application of constant stress rheometers in the creep mode”. *Rheol. acta* 32.1 (1993), pp. 104–107 (cit. on p. 43).

RÉSUMÉ

Les suspensions colloïdales, le couplage entre l'environnement, la structure microscopique et la rhéologie sont étudiées dans ce manuscrit. Ce travail utilisera majoritairement un point de vue théorique mais fera intervenir aussi des approches expérimentales et numériques. Caractérisées par des agrégats de particules formés grâce à un potentiel d'interaction attractif, ces suspensions peuvent être soumises à une sollicitation externe sous forme d'ultrasons, de cisaillement ou tout autre forme mécanique. Les agrégats répondent à cette sollicitation en adaptant leur microstructure, notamment en taille.

Par ailleurs, cette même microstructure est la brique élémentaire transmettant les efforts de part et d'autre d'un gel colloïdal, ce qui peut se traduire par des lois d'échelles entre la microstructure et la rhéologie macroscopique.

Par conséquent, on observe un couplage fort entre l'échelle macroscopique, composée de l'environnement extérieur et la réponse rhéologique, et l'échelle microscopique, avec la structure microscopique s'adaptant et influençant l'échelle précédente. C'est ainsi qu'il est possible de construire un outil d'application industriel incorporant cette description physique afin de prédire les effets d'une sollicitation externe sur un matériau la vérifiant.

MOTS CLÉS

Suspension colloïdale, Rhéologie, Aggrégats fractales

ABSTRACT

Colloidal suspensions, the coupling between environment, microscopic structure and rheology are studied in this manuscript. This work will mainly use a theoretical point of view but will also involve experimental and numerical approaches. Characterized by aggregates of particles formed thanks to an attractive interaction potential, these suspensions can be subjected to an external solicitation in the form of ultrasound, shear or any other mechanical form. The aggregates respond to this solicitation by adapting their microstructure, especially in size.

Moreover, this same microstructure is the elementary brick transmitting the efforts on both sides of a colloidal gel, which can be recovered by laws of scale between the microstructure and the macroscopic rheology.

Therefore, we observe a strong coupling between the macroscopic scale, composed of the external environment and the rheological response, and the microscopic scale, with the microscopic structure adapting and influencing the previous scale. It is thus possible to build an industrial application tool incorporating this physical description in order to predict the effects of an external stress on a material verifying it.

KEYWORDS

Colloidal suspension, Rheology, Fractal clusters